UNIVERSITY OF NIŠ

ISSN 0354-804X (Print)
ISSN 2406-0534 (Online)
COBISS.SR-ID 72210956
UDC 502/504

FACTA UNIVERSITATIS

Series
WORKING AND LIVING ENVIRONMENTAL PROTECTION
Vol. 21, N° 4, Special Issue, 2024

Scientific Journal **FACTA UNIVERSITATIS**
UNIVERSITY OF NIŠ
Univerzitetski trg 2, 18000 Niš, Republic of Serbia
Phone: +381 18 257 095 Telefax: +381 18 257 950
e-mail: facta@ni.ac.rs http://casopisi.junis.ni.ac.rs/

Scientific Journal FACTA UNIVERSITATIS publishes original high scientific level works in the fields classified accordingly into the following periodical and independent series:

Architecture and Civil Engineering
Automatic Control and Robotics
Economics and Organization
Electronics and Energetics
Law and Politics
Linguistics and Literature
Mathematics and Informatics
Mechanical Engineering
Medicine and Biology
Philosophy, Sociology, Psychology and History
Physical Education and Sport
Physics, Chemistry and Technology
Teaching, Learning and Teacher Education
Visual Arts and Music
Working and Living Environmental Protection

SERIES **WORKING AND LIVING ENVIRONMENTAL PROTECTION**

Editor-in-Chief: **Nenad Živković**, e-mail: *fuwaleped@junis.ni.ac.rs*
University of Niš, Faculty of Occupational Safety
Republic of Serbia, 18000 Niš, Čarnojevića 10a
Phone: +381 18 529 705, Fax: +381 18 249 962

Technical Assistance: **Aca Božilov**, e-mail: *fuwalepts@junis.ni.ac.rs*
University of Niš, Faculty of Occupational Safety

UDC Classification Associate: **Sanja Vučković**, Library of Faculty of Occupational Safety, Niš
English Proofreader: **Aleksandra Petković**, University of Niš, Faculty of Occupational Safety
The authors themselves are responsible for the correctness of the English language in the body of papers.
Computer support: **Mile Ž. Ranđelović**, Head of Publishing Department, University of Niš, e-mail: *mile@ni.ac.rs*
Secretary: **Aleksandra Golubović**, University of Niš, e-mail: *saska@ni.ac.rs*
The cover image design: **Rodoljub Avramović**
Publication frequency – one volume, three issues per year.
Published by the University of Niš, Republic of Serbia

Printed by ATLANTIS DOO, Niš, Republic of Serbia
Circulation 80

ISSN 0354 – 804X (Print)
ISSN 2406 – 0534 (Online)
COBISS.SR-ID 72210956
UDC 502/504

FACTA UNIVERSITATIS

SERIES **WORKING AND LIVING ENVIRONMENTAL PROTECTION**
Vol. 21, N° 4, Special Issue, 2024

28th International Conference "Noise and Vibration"
Conference Proceedings

UNIVERSITY OF NIŠ

INSTRUCTIONS FOR CONTRIBUTORS

Contributions should be (preferably) in English, French or German.
Under the paper title, the name(s) of the author(s) should be given while the full name, official title, institute or company affiliation and the like should be placed at the end of the paper together with the exact mail and e-mail address, as well as short (running) title of paper.
Manuscript format. A brief abstract of approximately 100 to 150 words in the same language and a list of up to six key words should precede the text body of the manuscript. All the authors apart from foreign ones should also submit a complete manuscript in Serbian. Manuscript should be prepared using a Word template, downloaded from web address: http://casopisi.junis.ni.ac.rs/index.php/FUWorkLivEnvProt/about/submissions#authorGuidelines
Manuscript length. Brief articles and discussions (10 pages or less) are encouraged. Otherwise, papers should present well-focused arguments of approximately 16 pages.
Style requirements. **Letters, figures and symbols** should be clearly denoted.
Equations should be typewritten and, with the number, placed in parentheses at the right margin. References to equations should be in the form "Eq. (2)" or simply (2). For equations that cannot be entered in a single line, use the Equation Editor in MS Word. In equations and in the text, *italicize* symbols that are used to represent variables or parameters, including subscripts and superscripts. Only use characters and symbols that are available in the Equation Editor, in the *Symbol font* or in *Times New Roman*.
All illustrations (figures, photographs, line drawings, graphs) should be numbered in series and all legends should be included at the bottom of each illustration. All figures, photographs, line drawings and graphs, should be prepared in electronic form and converted in TIFF or JPG (max quality) file types, in 300 dpi resolution, for superior reproduction. Figures, line drawings and graphs prepared using elements of MS Drawing or MS Graph must be converted in form of pictures and unchangeable. All illustrations should be planned in advance so as to allow reduction to 12.75 cm in column width. Please review all illustrations to ensure that they are readable.
All **tables** should be numbered with consecutive Arabic numbers. They should have descriptive captions at the top of each table and should be mentioned in the text.
References should be listed alphabetically at the end of the manuscript, in the same way as the following examples (for a paper in a journal, a book, paper in a contributed volume and for an unpublished paper):

1. Connor, J. J., Logcher, R. D. and Shing-Ching, C.: *Nonlinear Analysis of Elastic Framed Structures*, J. Struct. Div., ASCE Vol. **ST** 6, pp. 1525-1547, 1968.
2. Arriaga F. and others: *Grading and load carrying capacity determination of old timber beams*, American Society for Agricultural Engineers, paper No 92-4068, 1992.
3. J. N. Reddy: *A refined nonlinear theory of plates with transverse shear deformation*, J. Solids and Struct., Vol bf 20, pp. 881-896, 1984, Comput. Struct., Vol. **5**, pp. 257-260, 1975.

References should be quoted in the text by the corresponding number in square brackets.

Electronic submission. Papers for consideration should be submitted to the Series Editor in electronic form via the Journal's home page: http://casopisi.junis.ni.ac.rs/index.php/FUWorkLivEnvProt.

FACTA UNIVERSITATIS

Series

Working and Living Environmental Protection

Vol. 21, N° 4, Special Issue, 2024

Contents

FACTA UNIVERSITATIS
Series: **Working and Living Environmental Protection** Vol. 21, Nº 4, Special Issue, 2024, pp. 191 - 199
https://doi.org/10.22190/FUWLEP241104018M

Original scientific paper

SOUND INSULATION PARADOX OF MASSIVE CAVITY WALLS IN BUILDINGS

UDC 692.21:699.844

Miomir Mijić, Dragana Šumarac Pavlović

University of Belgrade, School of Electrical Engineering, Belgrade, Serbia

ORCID iDs: Miomir Mijić https://orcid.org/0000-0002-3474-0897
Dragana Šumarac Pavlović https://orcid.org/0000-0002-4173-8832

Abstract. *In literature, the "box-in-box" system is described as a solution for achieving the highest possible sound insulation in a room. The system involves double walls separating a room from the surroundings in all directions, without any lateral pass for sound. This approach doubles the number of discontinuities in the material through which sound energy travels, thus providing higher sound insulation. Based on such an idea, some dwelling houses were designed with massive cavity walls between apartments with the expectation of better sound insulation. The concept was further motivated by the need to achieve adequate thermal insulation between apartments using insulation material in the cavity. However, in buildings where this was implemented, residents complained about inadequate sound insulation. Measurements showed that the sound reduction index of the double brick wall was lower than expected, even less than that of a wall where the two thinner layers were combined into a single thicker brick wall without an internal cavity. This was surprising, leading to research aimed at finding an explanation. It was concluded that in buildings there is the influence of sound paths through the wall's lateral junctions, which is more pronounced with two thinner layers. With a cavity wall, the transmission of sound energy through lateral junctions and further by flanking transmission is more pronounced than with a single wall of the same surface mass. Additionally, the high seismic zone in Serbia requires certain adjustments in construction, invisible in architectural drawings, that further diminish the effect of the increased number of discontinuities in the wall. All of this makes the massive cavity wall in the building, contrary to expectations, less effective than a single wall made of the same quantity of material, making it acoustically and financially unreasonable. Research also revealed that material in the cavity has no influence on the sound reduction index value of the wall.*

Key words: *flanking transmission, massive cavity wall, sound insulation, sound reduction index, vibration reduction index*

Received November 4, 2024 / Accepted November 7, 2024
Corresponding author: Miomir Mijić
University of Belgrade, School of Electrical Engineering, Bul. kralja Aleksandra 73, 11120 Belgrade, Serbia.
E-mail: emijic@etf.rs

1. INTRODUCTION

The concept of sound insulation between rooms in buildings is based on the appropriate application of partitions with different physical properties. Partitions differ from each other in the mechanisms of sound transmission, and their combinations are used to adjust the processes for stopping sound propagation. In design practice, this involves using elements of the building's concrete structure, massive walls made of various construction materials, typically brick or different types of blocks, and lightweight flexible partitions in the form of drywall and lining, usually made of gypsum boards of different densities.

In literature addressing sound insulation in buildings, the concept referred to as the "box within a box" or "room within a room" is highlighted as a solution for achieving the highest level of insulation. Many studio spaces, where the goal is always to maximize sound isolation from the surroundings, are constructed with this concept. The image of two massive walls at a certain distance from each other, surrounding a room on all sides, can be seen in manuals for designing studio spaces for sound recording. The partition made of two massive walls positioned at a small distance apart is described in DIN 4109 [1]. It is noted that this construction provides an improvement of approximately 12 dB compared to a single wall of the same mass.

What happens when the concept of sound insulation with double massive walls is applied in the construction of typical residential buildings? This idea appeared in Serbia during the last 10 years. It involves dividing a thicker massive wall into two slightly spaced thinner walls and placing them between concrete ceilings, as illustrated in Figure 1. It is not entirely clear, but it seems that the idea of splitting a massive wall into two parts arose from the demands for energy efficiency and the need to achieve adequate thermal insulation between apartments. The aim was to meet the minimum thermal insulation requirements with a material inserted between the two massive layers. The thermal behaviour of such partitions has been thoroughly analysed in various literature (e.g., [2]). It is likely assumed that this approach also improved sound insulation between apartments.

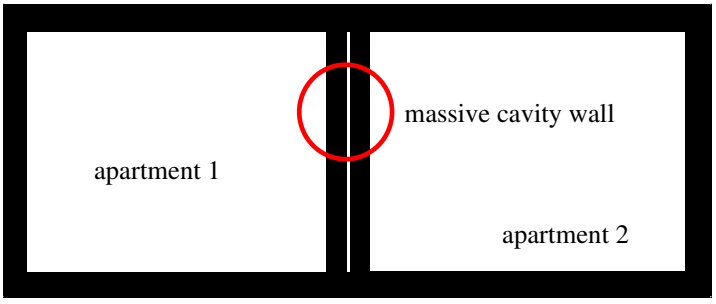

Fig. 1 Concept of a double massive wall (“cavity wall”) between rooms in a building

However, in the buildings where this was implemented, residents began to complain about the inadequate sound insulation. It is well known that sound insulation problems in buildings can be quickly identified, immediately upon moving in, unlike thermal insulation issues, which require time and suitable conditions to reveal potential problems. The residents' complaints, followed by the confusion of architects due to the unexpected results, initiated research that included laboratory measurements of the sound insulation capabilities of

certain configurations of massive cavity walls, along with theoretical analysis and simulations based on known calculation algorithms. This paper attempts to synthesize the results of that research and draw conclusions that can assist architects in making decisions regarding wall selection in the future.

2. Experimental Analysis of Massive Cavity Walls in Buildings

The concept of a double massive wall is illustrated in Fig. 2. A single partition made of a massive material is "split" into two parts and spaced apart to create room for thermal insulation material, typically mineral wool. It is reasonable to assume that there was also an intention for the wool to contribute to the sound insulation of such a wall. The size of the gap between the two layers of the wall is dictated by the minimum required thickness of the thermal insulation material to meet energy efficiency requirements, as well as various practical considerations (minimizing wall thickness to avoid losing space in the rooms, the practical feasibility of the partition structure under given conditions, and so on).

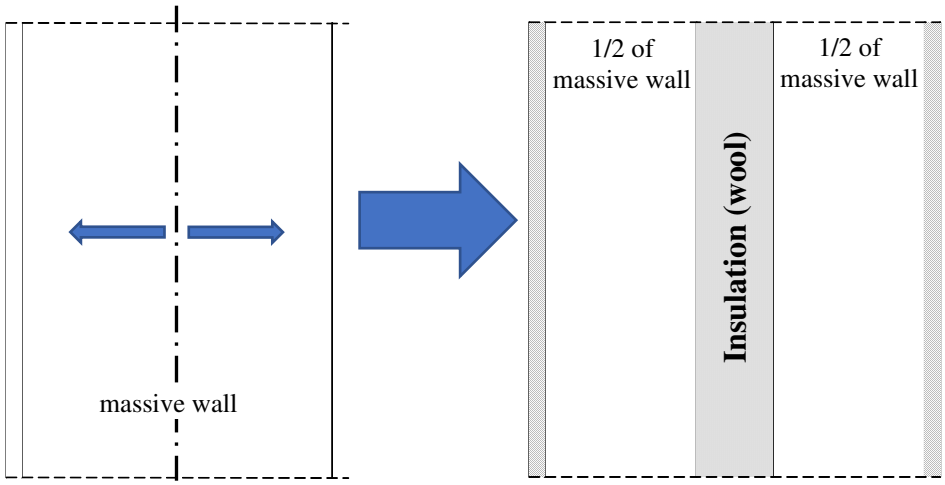

Fig. 2 Concept of idea about massive cavity wall

To explain the unexpected sound insulation measurement results achieved with cavity walls in several buildings, an investigation was initiated. Some of the results have been previously published [3,4]. The research included laboratory measurements of a cavity wall and a single wall made of nearly the same mass of material. Silicate brick as the material was selected for the tested wall, which has a density of about 1,800 kg/m³. This material was chosen because it has been used in buildings where unsatisfactory sound insulation was measured.

The results of the laboratory measurements are shown in Fig. 3 [3]. The diagram presents the measured sound reduction index values of a cavity wall with a width of 2x115 mm and a single wall with a width of 175 mm, both made of the same material (silicate bricks). Although these walls do not have equal surface masses to correspond to the situation in Fig. 2, they are close enough to qualitatively illustrate the principle of the

processes occurring when a massive wall is split into two thinner layers. Both walls were plastered on both sides with the same type of mortar. Glass wool was installed in the cavity of the wall.

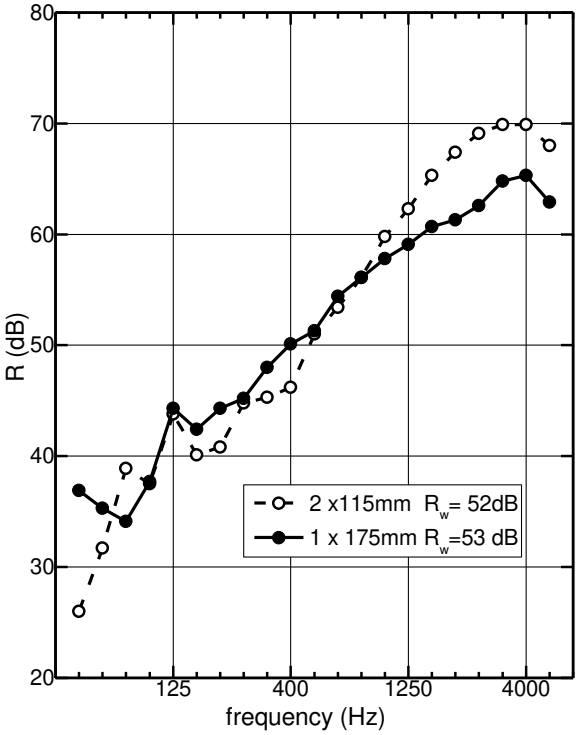

Fig. 3 Comparison of the sound reduction index of a single and double wall made of the same material**:** 1 – Double wall made of solid silicate bricks, 2x115 mm, with a 50 mm gap filled with wool, plastered on both sides**;** 2 – Single wall made of solid silicate bricks, 175 mm wide, plastered on both sides [3]

In this experimental analysis, the single wall is slightly thinner in terms of the total thickness of the massive material, measuring 175 mm compared to 225 mm of the double wall. That fact actually provided a slight advantage to the double wall in terms of total surface mass. Nevertheless, the measured sound reduction index *R* for the single wall was 1 dB higher. Only at the highest frequencies, the sound reduction index of the double wall exceeds that of the single wall, but due to the shape of the standard curve, this did not affect the single-number, apparent value of the sound reduction index.

In an effort to discover the reason behind the result achieved by the cavity wall, various modifications were tested by changing the material, its thickness, and density, in the cavity. The idea was to reveal the possible influence of cavity content on the sound reduction index. The result of those measurements is shown in Fig. 4 [3]. The most drastic option was the addition of gypsum board in the cavity along with the glass wool. The idea behind

this modification was the potential contribution of the gypsum board, by analogy with the contribution it provides by typical wall lining in rooms. It can be seen that with all the described changes, the sound reduction index value varied by only 1 dB. That is negligible considering measurement uncertainty and the fact that minor details in the wall construction might have such an effect.

Therefore, the conclusions obtained from laboratory tests of various configurations are:

- A massive cavity wall applied in buildings between two rooms does not provide an improvement in sound insulation compared to a single wall made of the same quantity of massive material;
- The material in the cavity of the double wall has no practical effect on the wall's sound reduction index.

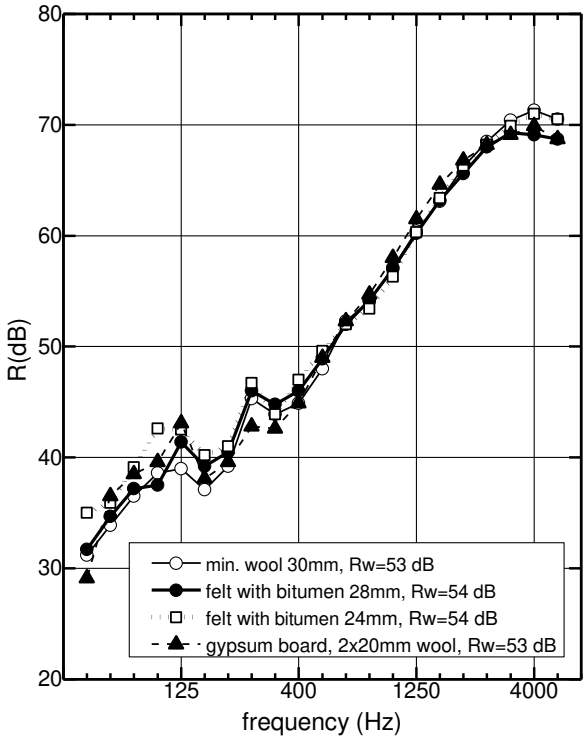

Fig. 4 The laboratory measurement of the massive cavity wall sound reduction index with various materials applied in the cavity [3]

3. Further Analysis of the Massive Cavity Wall

The measurement results in the laboratory showed that the double massive wall does not exhibit the expected improvement in sound insulation compared to a single wall, even though some additional discontinuities appear inside the partition affecting the sound energy propagation. After the experimental analysis performed in the laboratory, the reasons for the

phenomenon that negates the theoretically expected improvement remained unclear. Therefore, explanations were sought in the theory of sound propagation through the complex structure of the buildings and in constructive details of the cavity wall.

Factors influencing the sound propagation between two adjacent rooms in a building separated by a partition are marked in Fig. 5 [5]. It is well known that there is flanking sound transmission between neighbouring rooms involving all lateral partitions, walls, and ceilings. Flanking transmission makes the difference between laboratory results and apparent sound reduction index in buildings. The transmission paths are indicated in the figure with red arrows. The drawing presented in Fig. 5 is simplified to a two-dimensional representation of the rooms, where lateral transmission is shown within the four represented partitions. However, in three-dimensional reality, eight lateral partitions are involved in sound energy traffic between rooms.

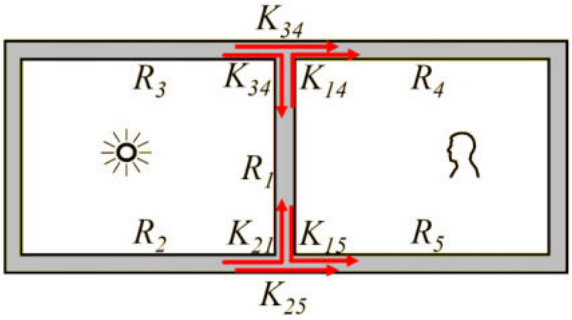

Fig. 5 Paths of sound energy transmission between rooms with identified factors affecting its attenuation [5].

Figure 5 reveals that the sound insulation is determined not only by the sound reduction index of the partition directly separating the rooms, marked as R_1, but also by the sound reduction index of the sideways partitions along which sound energy also travels between the rooms. Their sound reduction index marked from R_2 to R_5 is indicated in the figure (but the total of eight in three-dimensional space).

When propagating through a partition, wall or ceiling, the attenuation of sound energy with distance is relatively small compared to that in free space. This is because there is no wavefront spreading out inside the partitions, unlike in three-dimensional open space where a phenomenon of energy density, known as the "6 dB law", occurs. Significant attenuation of sound energy appears only at the partition's junctions. At those points, attenuation occurs due to material discontinuities at junctions, as well as because at junctions, energy is splitting into multiple paths. The attenuation at junctions is described by a parameter called the vibration reduction index K_{ij}.

The value of the vibration reduction index K_{ij} is expressed in decibels and depends on two factors: the ratio of the surface masses of the partitions connected at a junction and the type of their joint (rigid or flexible). In the case of massive cavity walls, the connection of the wall falls into the category of rigid joints, meaning that the energy transfer processes are determined by the masses of the connected partitions. The values of the index K_{ij} for rigid joints of massive partitions are defined by a diagram shown in standard EN 12354-1, which is also presented here in Fig. 6 [5]. The diagram illustrates the parameter's changes

as a function of the surface mass ratio of the connecting partitions. Splitting a single massive partition into two lighter ones, affects the reduction of sound energy that passes through the joints. This means that such changes alter the conditions on the paths of lateral transmission. The diagram presented in Fig. 6 should be understood as an illustration of the trends in these changes.

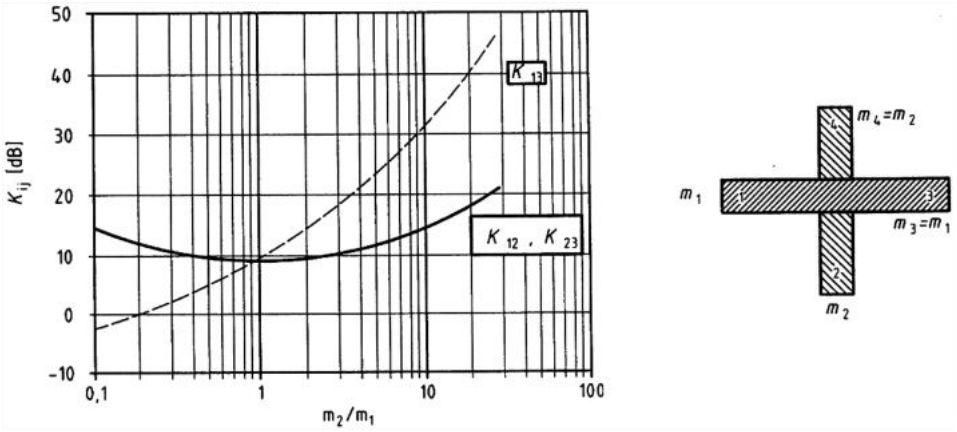

Fig. 6 Vibration reduction index K_{ij} at the joints of partitions as a function of their mass per unit area (according to document EN 12354-1) [5]

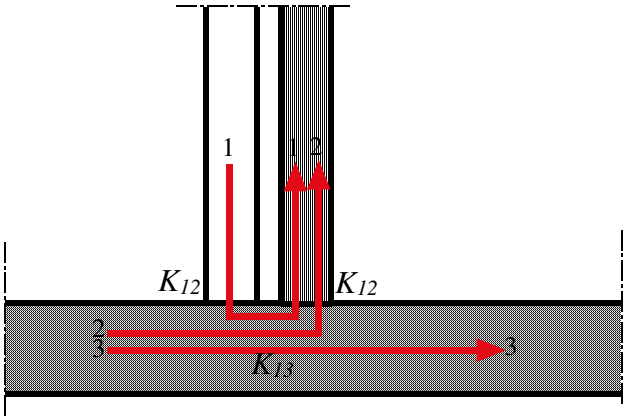

Fig. 7 Sound energy flow along a flanking path with the cavity wall; numbers in the index of vibration reduction index K_{ij} correspond to those in Fig. 6

At the joint of a massive cavity wall with lateral partitions, there are sound energy pathways illustrated in Fig. 7. When the layers' mass is reduced in a double partition, the values of the vibration reduction index at all joints change when compared to a single massive wall (diagram K_{12} in Fig. 6). There is now an additional pathway between two partitions, marked as 1 in Fig. 7. This is a parallel pathway introducing a by-pass for the transmission of sound energy through the cavity. Such a pathway is formed around the entire perimeter of

the wall, which means its impact is certainly not negligible in a quantitative sense for the sound isolation between rooms. That path is present in the laboratory, too.

In laboratory environments, the measurement of the sound reduction index, by definition, does not include flanking transmission paths between the transmitting and receiving rooms. However, in the case of cavity walls, there are important additional paths illustrated in Fig. 7 and marked as 2. That is an indirect path for the transmission of sound energy between flanking partitions in the source room and the cavity wall thin layer on the receiving room side. The diagram in Fig. 6 illustrates that with reduced wall mass connected with very massive ceilings, the value of vibration reduction index K_{12} is lower. Furthermore, in buildings, there is a flanking path marked as 3. Due to the change in wall mass ratio when the cavity wall is between rooms, there will be increased transmission of sound energy through the flanking paths [6,7].

Alongside all the changes that occur in the transmission of sound energy between adjacent rooms when a massive cavity wall is installed instead of a single wall, there are also some effects that are not visible in architectural drawings but contribute to the reduction of the apparent sound reduction index in buildings. Specifically, when cavity partitions are organized as a 'box within a box' system, the statics of such a construction are also somehow addressed. The inner 'box' is designed as a rigid form resting on specific supports, which means that the contact between the layers is limited to the supports of the inner 'box.' However, when a standalone double massive wall is placed between two concrete ceilings, as shown in Figure 1, new issues arise independent of acoustics, such as the statics of the wall and its seismic stability. Thus, massive cavity walls require secure connections between layers, meaning there needs to be a certain number of solid connections between them. Some manufacturers of clay and similar blocks have even provided accessories for such purposes. This means that additional paths will appear between the two wall layers due to the inserted solid connections, making it so that the partition no longer consists of two completely separate layers with insulation material in between, but rather two point-connected masses.

4. CONCLUSION

Double massive walls, typically made of clay blocks or bricks, with thermal insulation material in the cavity did not exhibit the expected sound insulation properties in residential buildings. Moreover, the results in some buildings were below the established minimum criteria for acoustic comfort. All expectations regarding massive cavity walls are based on the elementary theory of sound propagation. In these walls, the discontinuities of the medium that cause attenuation of transparent sound energy are effectively doubled, which would imply an increased value of the sound reduction index. Such expectations are further supported by literature that contains statements about the double walls applied in various music studios, as by information generated in some European countries regarding insulation in residential buildings constructed in a row.

None of this is incorrect; however, the physical conditions in buildings built in a conventional manner, with reinforced concrete structures, in general, do not provide the necessary conditions for massive cavity walls to demonstrate their theoretically expected properties. The physical explanation for the somewhat unexpected outcome lies in the complexity of sound paths between adjacent rooms with lighter partitions that are rigidly connected to the surroundings. In the case of massive cavity walls, the mass of the layers

connected to the side partitions is smaller than a single monolithic wall made from the same amount of building material. As the surface mass of the wall layers decreases, the value of the vibration transmission reduction index K_{ij} at the junctions changes when compared to the state with a single massive wall at the same position. As a result, in massive cavity walls, the influence of sound energy paths through their lateral connections is amplified.

In short, the sound insulation effectiveness of double massive walls in buildings will significantly depend on the physical context in which they are placed. To reach a theoretical limit of their sound reduction index value it is necessary to place them along a dilation in construction. In standard residential buildings, it is hardly possible to provide such conditions, or can be unreasonable. Such walls have increased thickness, but slightly lower or, at best, the same insulation effectiveness as single walls made with the same quantity of massive material. When examples from the literature concerned with the application of massive cavity walls are presented, it becomes evident that they are always placed at the dilation in the structure [1]. Thus, any connection for lateral sound transmission is destroyed. In literature was shown that a single wall with a gypsum board lining provides higher sound insulation effectiveness than a wall with a doubled massive layer and some infill in the cavity [8].

What is particularly significant in the topic addressed in this paper regarding massive cavity walls is the demonstration of complexity in sound insulation issues inside buildings. The case of cavity walls shows that details, such as changes in physical processes at the partitions junctions can affect the sound insulation. This further implies that for a quality design of buildings, it is essential to systematically consider the physical characteristics of building constructions, rather than just selecting walls based on their data from a catalogue or database.

REFERENCES

1. DIN 4109 Supplement 1 - Sound control in buildings, Design examples and calculation procedure
2. Hens H., Janssens A., Depraetere W., Carmeliet J., Brick Cavity Walls: A Performance Analysis Based on Measurements and Simulations, *Journal of Building Physics*, Vol 31, No 2, 2007. 95-124
3. Šumarac Pavlović D., Dinić M., Bezbradica V.., Bjelić M., Analiza izolacionih moći dvostrukih pregrada - laboratorijska merenja, ETRAN 2017, Proceedings, AK1.3.1-6, ISBN 978-86-7466-692-0
4. Dinić M., Šumarac Pavlović D., Bjelić M., Ristanović I., Dileme u proceni izolacionih osobina dvostrukih masivnih prerada prema standardu SRPS EN12354-1
5. SRPS EN 12354-1 Akustika u građevinarstvu — Ocena zvučne zaštite zgrada na osnovu akustičkih performansi građevinskih elemenata — Deo 1: Zvučna izolacija između prostorija
6. Gerretsen E., The effects of the element damping in sound insulation predictions following EN12354, Proc. Mtgs. Acoust. **30**, 015003 (2017); doi: 10.1121/2.0000537
7. Schiavi A., Astolfi A., The prediction of the vibration reduction index *Kij* for brick and concrete rigid junctions, Applied Acoustics 71 (2010) 523–530
8. Milenković A., Boljević D., Doprinos upotrebe izolacionih materijala kod zidova od opeke i bloka na zvučnu izolaciju, VIII Kongres savremene industrije glinenih proizvoda Srbije, 2018.

FACTA UNIVERSITATIS
Series: **Working and Living Environmental Protection** Vol. 21, Nº 4, Special Issue, 2024, pp. 201 - 211
https://doi.org/10.22190/FUWLEP240929019K

Original scientific paper

VIBRATION MITIGATION-BASED MACHINE LEARNING-DRIVEN DESIGN OF METASTRUCTURES

UDC 621.373:004.85:534

Ivana Kovačić[1], Željko Kanović[2], Ljiljana Teofanov[2], Vladimir Rajs[2]

[1]University of Novi Sad, Faculty of Technical Sciences, Centre of Excellence for Vibro-Acoustic Systems and Signal Processing CEVAS, Novi Sad, Serbia
[2] University of Novi Sad, Faculty of Technical Sciences, Novi Sad, Serbia

ORCID iDs:	Ivana Kovačić	https://orcid.org/0000-0002-0433-1953
	Željko Kanović	https://orcid.org/0000-0003-1456-1135
	Ljiljana Teofanov	https://orcid.org/0000-0002-0302-1830
	Vladimir Rajs	https://orcid.org/0000-0003-4357-770X

Abstract. *This research is concerned with the development of a longitudinally excited metastructure, featuring periodically distributed external units, each equipped with internal oscillators functioning as vibration absorbers. Initially, the metastructure designed for vibration attenuation around the first structural resonance, is characterized by uniformity, with all absorbers being identical and consisting of cantilevers integrated into the external components, each cantilever terminating in a concentrated mass block. This study employs a machine learning approach to maximize vibration attenuation efficiency around the second resonance, as well as concurrently at the first and second resonant frequencies in two associated optimality criteria related to the width of the attenuation region and the amplitude reduction, respectively. The new metastructures redesigned based on these criteria are fabricated by 3D printing, and their enhanced vibration mitigation capabilities are verified experimentally.*

Key words: *metastructure, vibration mitigation, auxiliary oscillators, machine learning.*

1. INTRODUCTION

The concept of 'metastructures' has recently emerged in the field of vibration control, evolving from the framework of the concept of metamaterials [1–3]. This approach entails the integration of a series of internal, distributed, and tuned auxiliary oscillators within the external components of a structure, aimed at controlling its vibrational response. Despite its recent introduction, the fundamental principle is rooted in the enhancement of Den

Received September 29, 2024 / Accepted October 10, 2024
Corresponding author: Ivana Kovacic
University of Novi Sad, Faculty of Technical Sciences, CEVAS, Trg D. Obradovica 6, 21000 Novi Sad, Serbia
E-mail: ivanakov@uns.ac.rs

Hartog's methodology [4], which focuses on managing the response of a main vibrating structure, subjected to external excitation, modelled as a one-degree-of-freedom linear mechanical oscillator. This is achieved by incorporating an auxiliary oscillator that matches the frequencies of the main structure, the external harmonic excitation, and the natural frequency of the auxiliary oscillator itself. Consequently, the auxiliary oscillator must be meticulously designed (tuned) to align with such frequency. As a result, rather than exhibiting resonance characterized by an infinite response at this specific frequency, the undamped main structure, when externally excited, will instead exhibit antiresonance, resulting in a zero-amplitude response [4–6]. The auxiliary oscillator functions as a vibration absorber [4–6], which is, in the context of damping, referred to as a tuned-mass damper [7, 8].

The application of data science and machine learning (ML) has significantly broadened the scope for numerical development and optimization of engineering structures, including vibration absorbers. Nevertheless, this methodology has not been widely adopted in the design of metastructures that exhibit effective vibration control through specifically calibrated auxiliary oscillators. In [9], an Archimedean spiral metastructure was introduced to manage low-frequency flexural waves. The inverse design process, which targeted specific bandgap widths and central frequencies, was successfully executed using ML techniques. The efficacy of this method was substantiated through Finite Element Method (FEM) analysis and experimental validation. The research detailed in [10] utilized numerical simulations alongside ML strategies to implement both forward and inverse design methodologies for a composite metastructure, with the goal of achieving subwavelength and ultrawide bandgaps. The outcomes of the ML approach were corroborated through numerical assessments and experimental tests on 3D-printed prototypes, with distinct excitations applied in both longitudinal and transversal orientations. To derive an optimal metastructure model that incorporates considerations of structural integrity and quasi-zero stiffness properties, a recent study employed a combination of deep reinforcement learning and FEM within an optimization framework [11]. Following this, 3D printing was utilized, and experimental results indicated that the produced metastructures demonstrated exceptional capabilities in vibration reduction, particularly in the low-frequency spectrum. Additionally, hull grillage metastructures were noted for their significant isolation properties concerning low-frequency flexural vibrations [12]. A dataset was generated using the theoretical wave mechanics model of hull grillage metastructures, and a forward prediction neural network model was subsequently applied to assess the vibration transmission characteristics. In [13], a metastructure grounded in phononic crystal principles was examined, and an innovative deep learning approach was proposed to facilitate its optimization through both qualitative and quantitative analyses, thereby reducing the likelihood of errors in judgment. Furthermore, the optimization procedure encompassed metastructures characterized by different periodic constants and filling fractions, yielding significant insights into the equilibrium between spatial efficiency, material usage, and vibration mitigation. The efficiency of the optimized configurations regarding vibration performance was validated through FEM analysis. The recent review article concerning ML-assisted intelligent design of metastructures [14] indicated that while ML has the potential to yield outstanding design outcomes for a range of acoustic or mechanical specifications, the majority of existing studies fell short in terms of manufacturing and experimental validation following the design phase.

The primary aim of this research is to enhance the application of data science, specifically ML, within the domain of the design of metastructures that would yield their desirable

behaviour when exposed to an external vibration source. Additionally, the study seeks to qualitatively validate the design through both manufacturing processes and experimental analyses, which is the shortcoming pointed out in [14].

This study is organized as follows. Section 2 elaborates on the primary structure and its structural characteristics. The ML methodology employed, and the results achieved are discussed in Section 3. In Section 4, the vibration responses of the newly developed metastructures are validated through experimental data. Lastly, Section 5 encapsulates the key findings and articulates the relevant conclusions.

2. On the Primary Metastructure

The primary metastructure, labelled herein as MS0, consists of both external units and internal oscillators. This metastructure was first introduced in reference [15] and is also described in detail in [16]. Their basic units are shown in Figure 1.

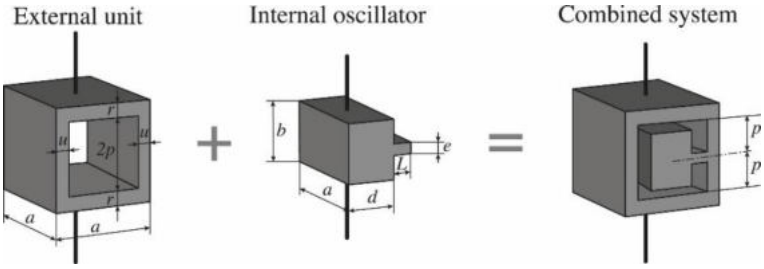

Fig. 1 Units of a metastructure under consideration

The external unit features a hollow square cross-section part, with its essential attributes depicted in Figure 1. In particular, the external dimensions are specified as a for both width and length, the wall length is indicated as u, and the height of the transverse components, namely the floor and ceiling, is marked as r. The internal oscillator depicted in Figure 1 consists of a cantilever characterized by its length L and height e, with a concentrated mass positioned at its tip, forming a discrete block. The dimensions of the internal oscillator, specifically the length d, the width a, and the height b, are noted in Figure 1. The internal oscillator is symmetrically integrated into the wall of the external unit at a specific location defined by parameter p in relation to both the ceiling and the floor, as seen in the combined system in Figure 1. Further, these units can be arranged to get a multi-level structure, which is done in this study to realize a cohesive 10-unit metastructure, achieved by replicating the combined units while excluding the floors. Each absorber within this metastructure is numbered from 1 to 10, beginning from the bottom. Detailed geometric parameters are listed in Table 1, while the MS0 itself is shown in Figure 2a, and its internal oscillators are labelled as the absorber type TA0. To reduce bending, pairs of internal oscillators are attached to the opposing internal walls of the external units, as seen in Figure 2a. The odd-numbered oscillators are secured to one side of the wall, while the even-numbered oscillators are integrated on the opposite side. The internal oscillators exhibit transversal oscillations whose basic axis is aligned with the basic axis of longitudinal oscillations of each individual unit and the overall metastructure, as illustrated by the black tick solid line in Figure 1. This

metastructure has demonstrated suitability for 3D printing due to its homogeneous and uniform characteristics, allowing for scalability to a desired number of units while effectively achieving vibration attenuation near the first structural resonance [17]. Nevertheless, the design of absorbers warrants further investigation, particularly in optimizing efficiency for vibration attenuation in the vicinity of the second resonance region, as well as concurrently addressing the first and second resonant response while maintaining a consistent shape. This raises the question of how to redesign MS0 to incorporate such vibration attenuations, which is addressed in the following section.

Table 1 Parameters of MS0

Part	Parameter	Value [mm]
External unit	u	6.5
	r	6.5
	p	14
Internal oscillator	L	6.5
	e	4
	d	17
	b	20
External unit & Internal Oscillator	a	40

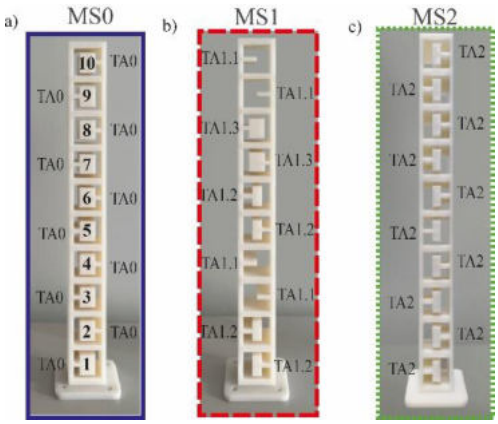

Fig. 2 Metastructures MS with distinct types of absorbers TA: a) MS0; b) MS1; c) MS2.

3. MACHINE LEARNING-DRIVEN REDESIGN

The fundamental redesign of the metastructure focuses on the internal oscillators, which influences the dimensions of both the mass block and the cantilever, specifically the parameters d and L. There are two physics-based conditions set for the redesign. First, to maintain the integrity of the longitudinal axis and prevent potential bending, it is essential that the combined lengths adhere to the constraint $L + d/2 = \text{constant}$. This condition ensures that the vertical symmetry axis of the structure remains unchanged. The parameter d is evaluated in three distinct scenarios: in the initial configuration of MS0, it serves as

the baseline variation; the second scenario features *d* at half its original value; and the third scenario sets *d* to zero, indicating the absence of mass at the cantilever's end. To further mitigate bending, the second condition for redesign necessitates the modification of internal oscillators 1-10 in pairs, with the stipulation that each consecutive pair must be geometrically equivalent (1=2, 3=4, 5=6, 7=8, 9=10). This results in five pairs of internal oscillators that require redesign. By incorporating three variations of parameter d across these pairs, an initial consideration of 3^5=243 unique metastructures is conducted.

The redesigning process encompasses three primary steps, which collectively outline a general methodology for formulating the ML problem, as defined in [16]:

Step 1: Employ simulation software that integrates both geometrical and physical modelling capabilities, along with results assessment, to conduct a comprehensive numerical vibration analysis across all variations of the metastructures. Herein, all 243 parameter variations of the metastructure are generated using Excel. Following this, the variations are imported into the COMSOL Multiphysics software, where the associated metastructures are visualized according to the imported geometrical parameters. More importantly, this step should yield a dataset that encapsulates the Amplitude-Frequency Response Curves (AFRCs) and the associated numerical data for the frequency and the associated amplitude for the point situated on the top of each metastructure for all variations of the metastructure, as being of interest from the viewpoint of further minimization of its amplitude.

Step 2: The discrete numerical dataset generated in Step 1 is used and ML techniques are applied to derive a continuous model of the metastructure, which will serve as the foundation for optimizing the geometry of the absorbers. It is essential to explore multiple ML techniques and select the one that delivers the highest accuracy. Two particular ML techniques, specifically Support Vector Regression (SVR) and Artificial Neural Networks (ANN), are examined in this study. In both methodologies, the numerical dataset generated is utilized to train the metastructure model. This process involves the application of various combinations of geometric parameters corresponding to different metastructure configurations as input data, while the output data is represented by the width of the corresponding attenuation regions. The model incorporates a total of ten input variables, which correspond to the dimensions *d* and *L* for each pair of internal oscillators within the metastructure, while the output consists of four variables. Two of them are linked to the width of the attenuation regions surrounding the first and second modal frequencies, and the other two represent the total 'amount' of vibration attenuation in attenuation regions, defined as:

$$I_i = \int_{B_1}^{B_2} (A_{MS} - A_{MS0})^2 df \ , \ \ i = 1,2 \tag{1}$$

where B_1 and B_2 denote the boundaries of the attenuation region, A_{MS} and A_{MS0} are amplitudes of vibration of the metastructure defined by input geometry parameters and basic metastructure MS0, respectively, and *f* is the frequency.

Although this model interpretation includes redundant features, due to the constraint $L + d/2$ = constant, this representation is adopted to enhance the clarity of the input features. Generally, while the model with redundant features may not be optimal in terms of size and efficiency, it does not compromise the accuracy of the results. The performance and precision of both ML models developed in this manner were evaluated using Root Mean Square Error (RMSE) and Mean Absolute Error (MAE) metrics. Observing the values of these evaluation criteria, it has been concluded that the SVR model outperforms the ANN model significantly. Therefore, only the SVR model is used in further analyses.

Step 3: With the continuous ML model developed in *Step 2*, initiate the optimization process aimed at determining the most effective geometry for the absorbers, while defining precisely the optimality criteria. Two optimality criteria are defined in this study, and both of them are described subsequently.

3.1. First optimality criterion

The first optimality criterion regards the width of a vibration attenuation region. The attenuation region is characterized as the frequency range in which the displacement amplitude of the new metastructure is less than that of MS0, as defined in [17]. Two distinct formulations of the first Optimality Criterion OC1 are introduced:

OC1.1. The extent of the frequency range in which vibration attenuation occurs around the second modal frequency, and

OC1.2. The cumulative width of the frequency ranges exhibiting vibration reduction around both the first and the second modal frequencies.

For both formulations, a singular optimized metastructure is identified, herein referred to as MS1. This metastructure MS1 is shown in Figure 2b. It is evident that it incorporates an original configuration of absorbers, but their arrangement is neither straightforward nor anticipated. In fact, there are three categories of absorbers (TA1) in MS1:

TA1.1: A cantilever-type absorber characterized by its maximum length (specifically absorbers 3, 4, 9, and 10);

TA1.2: An absorber featuring a longer cantilever with a shorter tip mass than in MS0 (absorbers 1, 2, 5, and 6);

TA1.3: An absorber that includes a slightly longer cantilever paired with a slightly shorter tip mass than in MS0 (absorbers 7 and 8).

The specifications for TA1 in terms of their dimensions are detailed in Table 2.

Table 2 Parameters of the metastructure MS1

Parameter of MS1	Internal oscillator number				
	1, 2	3, 4	5, 6	7, 8	9, 10
Types of absorbers (TA1)	TA1.2	TA1.1	TA1.2	TA1.3	TA1.1
L [mm]	9.895	15	9.895	6.6	15
d [mm]	10.21	0	10.21	16.8	0

3.2. Second optimality criterion

Unlike OC1, which regards only the width of the vibration attenuation region, the second optimality criterion OC2 is defined to take into account the amplitude reduction. This criterion is defined as the sum of the integrals of the AFRC around the first and second modal frequency, and it is equal to the sum of the model output parameters I_1 and I_2 defined in Eq. (1).

In this case, the metastructure labelled as MS2 (Figure 2c) is obtained as the optimal one for the maximal reduction of the amplitude in the integral sense described above. MS2 is shown in Figure 2c next to MS0 and MS1 for the sake of their mutual comparison. It is evident that MS2 incorporates uniformly distributed absorbers as in MS0. However, the dimensions of these absorbers (TA2) are different from TA0. Their specification is given in Table 3.

Table 3 Parameters of the metastructure MS2

Parameter of MS1	Internal oscillator number
	1-10
Types of absorbers (TA2)	TA2
L [mm]	9.922
d [mm]	10.156

4. Experimental Results

The original metastructure MS0, along with its redesigned counterparts MS1 and MS2, were produced utilizing Fused Filament Fabrication (FFF) technology, a specific form of 3D printing characterized by a resolution ranging from 0.1 to 0.3 mm (Figure 1). The material employed in this process was Acrylonitrile Butadiene Styrene (ABS), the properties of which are: a Young's modulus of elasticity E=1900 MN/m^2 and a density ρ=1.015 g/cm^3 (these values are obtained from the manufacturer for the metastructures produced). These structures were exposed to base excitation in an experimental setup the details of which are presented in Figure 3. The driving signal was generated using a computer equipped with the SCO-107 software package, designed for sine sweep operations, with the base acceleration amplitude set to 1g, where g represents gravitational acceleration. This signal is initially routed to an LAS200 controller, then to an LPA100 amplifier, and finally to an LDS V408 vibration shaker. The frequency and amplitude of the driving signal are regulated by a lower accelerometer model 4534-B, which has a sensitivity of 10 mV/g. The output from this accelerometer is also sent back to the controller for feedback. Additionally, a second accelerometer of the same model is affixed to the center of the uppermost horizontal plane of the metastructure to measure the response in the vertical direction. This signal is connected to both the controller and the computer for subsequent processing and analysis.

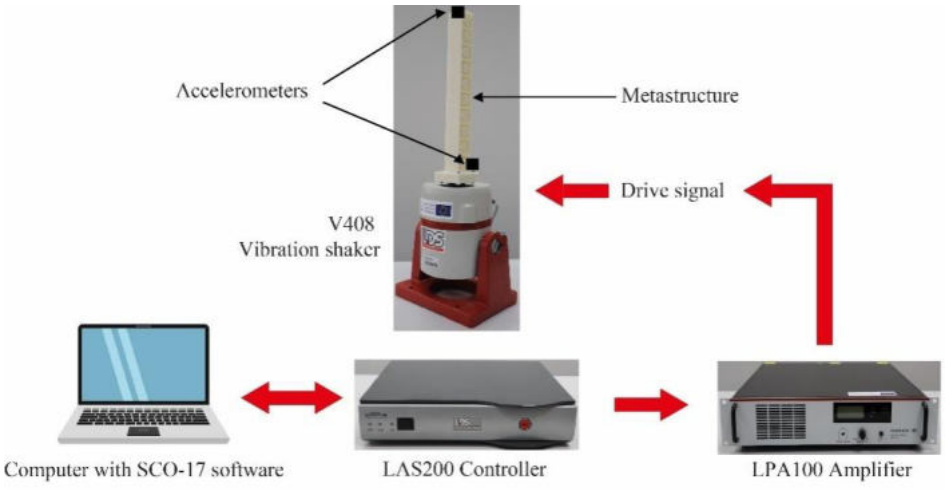

Fig. 3 Experimental setup

The recorded AFRCs for the top of the original metastructure MS0 and the modified metastructure MS1 are presented in Figure 4. The frequency was considered within the frequency range of 400 Hz to 1100 Hz, which is identified as the target frequency band encompassing two significant resonances of MS0 pertinent to this investigation. It is important to note that the subsequent diagrams depict non-dimensional frequency and non-dimensional displacement amplitudes. The non-dimensional frequency is determined by the ratio of the excitation frequency to the frequency of the metastructure MS0 with blocked TA0 absorbers, which is 588 Hz [18]. Meanwhile, the non-dimensional displacement amplitude is calculated as the ratio of the displacement amplitude on the top to the total height of the metastructure, measured at 358 mm. The attenuation region achieved by MS1, which exhibits a reduced amplitude response compared to MS0, is highlighted in grey in this figure, a representation that is consistent across the subsequent figure as well. For comparative purposes, photos of both the original metastructure MS0 and the redesigned metastructure MS1 are displayed on the left and right sides of this figure, respectively, along with the legend for the AFRCs presented. It is seen that the response of both metastructures is similar around the first resonance and that the values of the first antiresonance are close to each other. However, MS1 has more dense resonance frequencies in the frequency region of interest (three of them), while MS0 has two of them. The appearance of the second antiresonance of MS1 decreases the amplitude response and makes it smaller than the one of MS0, which is seen as the second attenuation region starting at the nondimensional frequency of 1.07. It is also seen that the response of MS0 around the second resonance and the response of MS1 around the third resonance are alike, but the one of MS1 is always smaller than the amplitude of MS0.

Analogously, Figure 5 shows the AFRCs for the top of the original metastructure MS0 and the modified metastructure MS2. Their comparison reveals completely distinctive characteristics of the dynamic behaviour of MS2 with respect to MS1 shown in Figure 4. It is seen that the first two resonance peaks of MS2 are shifted to the left, toward higher frequencies. The appearance of the first antiresonance of MS2 is actually the region when its response is of a smaller amplitude than the one of MS0.

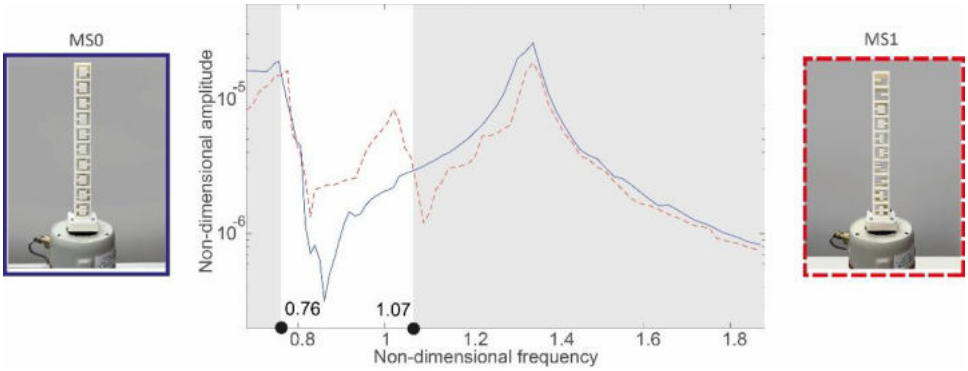

Fig. 4 Measured AFRCs of the point on the top of the redesigned metastructure MS1 compared to the original one MS0 with the attenuation region shaded in grey.

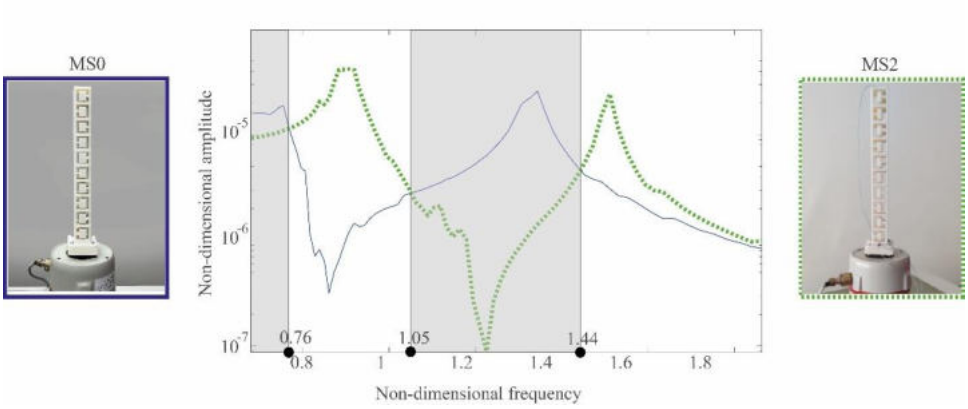

Fig. 5 Measured AFRCs of the point on the top of the redesigned metastructure MS2 compared to the original one MS0 with the attenuation region shaded in grey.

5. Conclusions

This study has focused on the reconfiguration of integrated internal oscillators within a metastructure composed of ten units that exhibit longitudinal vibrations. The objective has been to attain efficient vibration attenuation at designated resonance frequencies, specifically targeting either the second frequency or both the first and second frequencies concurrently. The initial design of the metastructure MS0 was homogeneous, incorporating uniform absorbers across all units. These absorbers were originally designed as cantilevers that are embedded in the external units of the metastructure, each equipped with a block mass positioned at the end of the cantilever.

The process of redesigning integrated internal oscillators has consisted of three fundamental steps, which together delineate a comprehensive approach to defining the machine learning problem. The initial phase has involved the development of a distinct numerical dataset comprising frequency-displacement amplitude pairs within simulation software that encompasses both geometric and physical modelling functionalities. This dataset has subsequently been utilised, and machine learning techniques have been employed to formulate a continuous model of the metastructure. In this investigation, two specific machine learning techniques, namely Support Vector Regression and Artificial Neural Networks, have been analysed. The efficacy and accuracy of the machine learning models created through this approach have been assessed utilizing the Root Mean Square Error and Mean Absolute Error metrics. Analyzing the results from these evaluation metrics has led to the conclusion that the Support Vector Regression model has significantly surpassed the Artificial Neural Network model in performance. Consequently, only the Support Vector Regression model has been employed in subsequent analyses. In the third phase, utilizing the continuous machine learning model established in the previous step, the optimization process has been initiated to identify the most effective geometry for the absorbers, with a clear definition of the optimality criteria.

This study has delineated two optimality criteria. The first optimality criterion has pertained to the region of vibration attenuation, which has been defined as the frequency spectrum where the displacement amplitude of the newly designed metastructure is lower than that of the original one, surrounding the second modal frequency, as well as the total width of the frequency ranges that demonstrate vibration reduction around both the first and second frequencies. In both cases, a unique optimized metastructure MS1 has been identified, featuring an innovative configuration of three types of absorbers, whose arrangement is neither simple nor predictable. The second optimality criterion has been articulated so that the new metastructure MS2 emerges as the optimal configuration for achieving maximal amplitude reduction in the integral sense. MS2 has been obtained to feature uniformly distributed absorbers of the same shape as those in MS0 but characterised by different dimensions.

The experiments conducted have shown that the newly developed metastructures demonstrate superior vibration attenuation properties in comparison to the original metastructure, as per the established criteria and within the specified frequency range. Thus, it has been confirmed that this study has successfully developed sophisticated and original metastructures through the application of a machine learning approach, which underscores the effectiveness of the data science methodology employed in this research.

Acknowledgement: *This study has been realised during the NOLIMAST research project funded by the Ministry of Science, Technological Development and Innovation of the Republic of Serbia.*

REFERENCES

1. Ji J.C., Luo Q.T., Ye K., (2021), Vibration control based metamaterials and origami structures: a state-of-the-art review, *Mechanical Systems and Signal Processing*, 161, Art. No. 107945.
2. Dalela S., Balaji P. S., Jena D. P., (2022), A review on application of mechanical metamaterials for vibration control, *Mechanics of Advanced Materials and Structures*, 29, pp. 3237–3262.
3. Contreras N., Zhang X.H., Hao H., Hernandez F., (2024), Application of elastic metamaterials/meta-structures in civil engineering: A review, *Composite Structures*, 327, Art. No. 117663.
4. Den Hartog J.P., (1934), *Mechanical Vibrations*, McGraw-Hill, New York, (reprinted by Dover, 1985).
5. Rao S., (2011), *Mechanical Vibrations* (5th Edition), Prentice Hall, ISBN-10: 9810687125, ISBN-13: 978-9810687120, p. 1112.
6. Kovacic I., Radomirovic D., (2017), *Mechanical Vibrations: Fundamentals with Solved Examples,* John Willey & Sons, ISBN: 978-1-118-67515-1, p. 280.
7. Steffen Jr. V., Rade D., (2001), Dynamic vibration absorber, in *Encyclopedia of Vibration*, Accademic Press, pp. 9–26.
8. Yang F., Sedaghati R., Esmailzadeh E., (2022), Vibration suppression of structures using tuned mass damper technology: A state-of-the-art review, *Journal of Vibration and Control*, 28, pp. 812–836.
9. Jin Y.B., Zeng S.X., Wen Z.H., He L.S., Li Y., Li Y., (2022), Deep-subwavelength lightweight metastructures for low-frequency vibration isolation, *Materials & Design*, 215, Art. No. 110499.
10. Muhammad J.K., Ogun O. (2023), Design and fabrication of 3D-printed composite metastructure with subwavelength and ultrawide bandgaps, *New Journal of Physics,* 25, Art. No. 053015.
11. Hong H.S., Kim W., Kim W.V., Jeong J.-M., Kim S., Kim S.S., (2024), Machine learning-driven design optimization of buckling-induced quasi-zero stiffness metastructures for low-frequency vibration isolation, *ACS Applies Materials & Interfaces*, 16(14), pp. 17965 – 17972.
12. Chen D.K., Li Y.G., Gong Y.F., Li X.Y., Ouyang W., Li X.B., (2024), Low frequency vibration isolation characteristics and intelligent design method of hull grillage metastructures, *Marine Structure*s, 94, Art. No. 103572.

13. Liu C.-X., Yu G.-L., Liu Z., Liu C.-X., Yu G.-L., Liu Z., Liu C.-X., Yu G.-L., Liu Z., (2024), Fast topology optimization of phononic crystal-based metastructures for vibration isolation by deep learning, *Computer-Aided Civil and Infrastructure Engineering*, 39(5), pp. 776 – 790.
14. He L.S., Li Y., Torrent D., Zhuang X.Y., Rabczuk T., Jin Y.B., (2023), Machine learning assisted intelligent design of meta structures: a review, *Microstructures*, 3, Art. No. 2023037.
15. Hobeck J.D., Laurent C.M.V., Inman D.J., (2015), 3D Printing of metastructures for passive broadband vibration suppression, *Proceedings of the 20th International Conference on Composite Materials*, Copenhagen, 19–24 July 2015.
16. Kovacic I., Kanovic Z., Rajs V., Teofanov Lj., Zhu R., (2024), Reaching a desirable metastructures for passive vibration attenuation by using a machine learning approach, *Nonlinear Dynamics*, 12(17), 2709; https://doi.org/10.1007/s11071-024-10058-3
17. Kovacic I., Teofanov Lj., Kanovic Z., Zhao J., Zhu R., Rajs V., (2023), On the influence of internal oscillators on the performance of metastructures: Modelling and tuning conditions, *Mechanical Systems and Signal Processing*, 205, Art. No. 110861, https://doi.org/10.1016/j.ymssp.2023.110861
18. Kovacic I., Rakaric Z., Kanovic Z., Rajs V. (2022), Metastructure with integrated oscillators of constant, linearly and nonlinearly varying natural frequency, *Frontiers in Physics,* 10, Art. No. 934998, https://doi.org/10.3389/fphy.2022.934998

FACTA UNIVERSITATIS
Series: **Working and Living Environmental Protection** Vol. 21, Nº 4, Special Issue, 2024, pp. 213 - 223
https://doi.org/10.22190/FUWLEP241023020R

Review paper

MODELS FOR PREDICTING SOUND ABSORPTION OF POROUS MATERIALS

UDC 534.822:66.017

Branko Radičević

University of Kragujevac, Faculty of Mechanical and Civil Engineering, Kraljevo, Serbia

ORCID iDs: Branko Radičević https://orcid.org/0000-0002-4182-4095

Abstract. *Porous materials are widely used in the field of noise control. The acoustic properties of these materials are best characterized by the sound absorption coefficient, which can be predicted using different mathematical models presented in this paper: empirical, phenomenological, and statistical. Optimization models based on biologically inspired algorithms were used to determine the non-acoustic parameters of the acoustic models. In addition to mathematical models for predicting acoustic parameters of porous materials, the paper also presents models for identifying non-acoustic parameters that are input parameters of empirical and phenomenological models. Air flow resistance is one of the most significant non-acoustic parameters of porous materials, and its values shown in this paper were measured according to the SRPS EN ISO 9053-1:2019 method. In empirical models, resistance to airflow is the only input parameter, while in phenomenological and optimization models it is one of several input parameters that establish a connection between microstructure and acoustic properties of porous materials. Based on the experimental values of the sound absorption coefficient, the non-acoustic parameters of the phenomenological models were determined using biologically inspired optimization algorithms. Statistical models are based on ANOVA analysis and determination of the sound absorption coefficient's dependence on the material layer's thickness and frequency. Predictions of the sound absorption coefficient of open-cell polyurethane foam were determined using the above models and are compared with pipe impedance measurements. In this way, the accuracy of the prediction of mathematical models for determining sound absorption was established. In addition, this research shows that low-density open-cell polyurethane foams have good sound absorption performance over a wide frequency range, and as such can be used for noise protection.*

Key words: *porous materials, acoustic models, sound absorption coefficient*

Received October 23, 2024 / Accepted November 25, 2024
Corresponding author: Branko Radičević
University of Kragujevac, Faculty of Mechanical and Civil Engineering, 36000 Kraljevo, Serbia
E-mail: radicevic.b@mfkv.kg.ac.rs

1. INTRODUCTION

Many scientific and professional papers, books, and other literature talk about acoustic materials for sound absorption. The basis of these publications is empirical, stating the acoustic properties of various materials that have been experimentally determined and proposing design methods based on the analysis of empirical data. These methods of designing sound-absorbing materials were the only ones used until recently when materials designed by theoretical analysis of the physical principles of wave mechanics began to appear.

1.1. Porous materials

Porous materials are those materials in which the solid mass is permeated with canals, i.e. pores, interconnected in a continuous network. The sound penetrates deep into the pores of these materials, where, due to high friction, the acoustic energy is converted into heat [1].

Ayub et al. [2] analyzed sound absorption from natural coconut fiber, using the Delany-Bazley model [29]. Navacerrada et al. [3] presented natural fibrous material from tree leaves as an ecological alternative that can be used in construction for noise protection. AL-Rahman et al. [4] studied fibers of natural materials in the direction of sound absorption and environmental pollution protection. It has been proven that the mixture of palm and coconut fibers can replace synthetic fiber materials, such as glass wool, rock wool, and asbestos.

Porous foams can be produced from a large number of different materials. Therefore, it is difficult to give a general approach to studying the acoustic properties of foams and fibrous materials [5]. Polyurethane foams are available in a wide range of densities and thicknesses, so as such they have found wide application in the automotive industry, furniture production, textile, footwear, packaging, and construction [6]. PU foams are increasingly a substitute for mineral and stone wool, which are harmful to human health [7]. Kino et al. [8] presented the acoustic and non-acoustic properties of cross-linked and partially cross-linked polyurethane foams. Pompoli and Bonfiglio [9] conducted an experimental study of polyurethane foams with open cells. Vuković et al. in their work [10] state that changing the composition of the reactants and the conditions of polymer synthesis enables obtaining PU for different purposes.

Research by various authors has shown that materials with the desired acoustic properties can be made from recycled rubber. Pfretzschner and Rodríguez [11], proved that rubber granules can be a good sound absorber, for broadband absorption, which is very suitable for protection against traffic noise. Swift et al. [12] found that these materials can effectively absorb sound if the size of the rubber aggregate granules and the binder content are carefully selected. Han et al. [13] found that recycled rubber granules are an excellent material for combining with concrete to create sound barriers next to high-frequency roads, in places where they pass through residential areas. In the work of Radičević and Ristanović [14], the results of research into the acoustic properties of materials based on recycled rubber are presented.

Composite materials are increasingly used for sound insulation. Composites that can be characterized as "green" are especially important. Zainulabidin et al. [15] studied the acoustic properties of a mixture of rubber sponges and glass wool fibers. Theophilus et al. [16] examined and analyzed the absorption properties of a mixture of sawdust, gypsum,

mud, and sand, mixed in different amounts. Mahzan et al. [17] studied a mixture of natural rice husk fibers with polyurethane foam that serves as a binder.

1.2. Some methods for determining acoustic properties

1.2.1. Determination of resistance to airflow

Air flow resistance is a basic non-acoustic parameter that affects the sound absorption of porous materials [18]. Certain authors [9,19,20] pointed to the problem of excessive errors when determining the resistance to airflow, which is primarily due to the inhomogeneity of the samples. Dragonetti et al. [18] developed a method for measuring resistance to airflow, based on alternating airflow, which does not require calibration, so it can be implemented in most acoustic laboratories. Ingard and Dear [21] proposed measuring the resistance to airflow in a pipe with a sound source. In the scientific literature, there are few works devoted to predicting the resistance to airflow of porous materials [22]. Bies and Hansen [23] presented a model that allows calculating the resistance to airflow starting from the density and diameter of the fiber of the porous material. Kino and Ueno [24] developed a new relationship between the longitudinal resistance to flow and the density of melamine foam, using the equivalent fiber diameter. Garai and Pompoli [22] presented a simple model that allows the calculation of flow resistance depending on the density of the polyester fiber material. Vigo Tarnow [25] presented a new way of calculating the longitudinal resistance to airflow for a set of randomly placed parallel cylinders.

1.2.2. Measurement of the coefficient of sound absorption in an impedance tube

The measurement of the normal acoustic impedance of a porous material is standardized by the EN ISO 10534-2 method [26]. Janiv [27] proposed a method for deriving the propagation constant and characteristic impedance. Utsuno et al. [28] proposed a new method with two cavities. Using propagation constant and characteristic impedance data, the normal incidence absorption coefficient can be predicted for different sample thicknesses. Predictions of absorption coefficients at normal incidence with different thicknesses of air layers located in front of the rigid substrate are also possible.

1.3. Models for predicting the acoustic properties of porous materials

In the scientific literature, there are many works dedicated to predicting the characteristic acoustic impedance and expansion constant of porous materials. By introducing the hypothesis of plane progressive wave propagation, the sound absorption coefficient can be easily determined. Those models can be classified according to Garai and Pompoli [22], as empirical, phenomenological, or microstructural.

1.3.1. Empirical models

Among the empirical models, the most famous is the one defined by Delany and Bazley [29], in which they presented simple expressions for complex functions of acoustic impedance and wave number, obtained by regression analysis of a large number of experimental samples. In the mentioned model, only one input parameter appears, the airflow resistance, which is relatively easy to measure. Due to its simplicity, this model is probably the most well-known, considering its citations. Delany and Bazley defined diagrams for evaluating the airflow

resistance of fibrous materials as a function of their density. Dunn and Davern [30] kept the same form of the model, but for polyurethane foams they determined new values of regression constants in characteristic impedance and propagation constant, using experimental samples of polyurethane foams with low values of resistance to airflow. Using essentially the same methodology, the works of Voronina [31,32] show the characteristic impedance and expansion constants as a function of fiber diameter and porosity. Gardner et al. [33] used a neural network to implement an empirical model, using airflow resistance as the only input parameter in the model.

1.3.2. Theoretical models

The sound absorption of porous materials can be studied using "equivalent fluids", characterized by two macroscopic dynamic properties, bulk density and bulk modulus of elasticity, which take into account viscous and thermal effects between the porous structure and the interstitial fluid. Hammet [34] took thermal and viscous dissipation into account in his extended phenomenological model. Significant progress in the development of theoretical models was made by Biot [35], who developed a general theory of the propagation of elastic waves in a fluid saturated with a porous rigid, and elastic frame. Using Biot's results, Lambert [36] developed an analytical model for highly porous polyurethane foams, whose verification he confirmed by measuring some structural parameters.

An approach of a more general nature, known as the microstructural approach, consists of performing wave propagation within individual pores, and thus generalizing the results at the macroscopic level. Zwikker and Kosten [37] applied this procedure for unconnected circular pipes. Allard et al. [38] formed a model using the dynamic density function given by Biot [35], the expression for the dynamic bulk modulus of elasticity presented in the work of Zwikker and Kosten [37], and the frequency-independent shape factor. Champoux and Stinson [39] proposed another model with 5 parameters, including two different shape factors that take into account viscous and thermal effects. The model has been validated on porous materials that have exactly the specified geometry of the structure.

1.3.3. Statistical models

To determine the sound absorption coefficient using statistical models [40], it is necessary to carry out a regression analysis procedure and select an adequate model after choosing an experimental plan and conducting experimental measurements.

1.3.4. Optimization models

Many optimization techniques have been adopted to perform inverse acoustic characterization in recent years.

Atalla and Panneton [41] found the non-acoustic parameters for the porous material of a rigid frame using the Johnson–Champoux–Allard model [42] using the genetic algorithm optimization method. They also extended this to a multi-layer material configuration. Based on the differential evolution algorithm, Atalla and Panneton [43] solved the inverse problem of characterizing three input parameters in the JCA model. Pelegrins [44] solved the error minimization problem using the simplex optimization method. Cobo et al. [45] used a simulated annealing algorithm for determining non-acoustic parameters of granular acoustic absorption materials. Bonfiglio and Pompoli [46] gave a comparative account of

the different methods used to determine the physical parameters of porous materials. The research results from the literature [46] show that the analytical method and the iterative method are difficult to deal with nonlinear constraints and that the optimization solution time of the iterative method is relatively long. The local search ability of the genetic algorithm is relatively weak, and the encoding and decoding process is quite complex.

The measuring devices listed in [47] are not a common part of acoustic laboratories, so the use of the inverse acoustic characterization method helps a lot in determining these parameters. In inverse characterization methods, the main focus is on reducing the error between experimental data and theoretical data that are the result of the prediction of different analytical models.

Multi-criteria optimization for the selection of absorption materials is very rarely represented in the scientific literature. The basic problem consists of the impossibility of reliably generating a large number of alternatives that meet specific acoustic requirements for specific cases of noise protection.

The paper [48] shows the application of the Taguchi method in the optimization of sound transmission losses through sandwich plaster constructions and those consisting of concrete masonry blocks and plasterboards. Using the Taguchi method, the relative influence of various parameters affecting sound transmission losses was investigated. Analytical predictions of the "Insul" software were used in the paper for different sandwich materials. The authors point out that the application of the Taguchi method for the optimization of sound transmission losses has rarely been published in scientific papers. Statistical analysis of variance (ANOVA) was conducted to determine significant parameters. The paper presents two case studies related to the optimization of sound insulation using the Taguchi method for multi-layered building elements, using the analytical results of the "Insul" software.

2. Examples of Acoustic Models from the Literature

2.1. Delany-Bazley model

In 1970, Delany and Bazley [29] presented a model for determining the characteristic impedance, Z_0, and the expansion coefficient γ, depending on the longitudinal resistance to airflow of the porous material.

$$Z_0 = R + jX \tag{1}$$

$$\gamma = \alpha + j\beta \tag{2}$$

After a large number of measurements in the impedance tube for materials with different resistance to airflow and a specific frequency range, Delany and Bazley [29] established the laws of change in impedance and coefficient of propagation as complex quantities as a function of the ratio of frequency and longitudinal resistance to airflow.

These regularities can be written as a function of a dimensionless term, which is obtained when the ratio of frequency and longitudinal resistance to airflow is multiplied by the density of the fluid, $\rho_0 f/\sigma$, which Delany and Bazley [29] call the normalized dimensionless parameter. Laws established by Delany and Bazley [29], taking into account the international system of units, can be expressed in the form:

$$Z_c = \rho_0 c\left[1+0.0571\left(\frac{\rho_0 f}{\sigma}\right)^{-0.574} - j0.087\left(\frac{\rho_0 f}{\sigma}\right)^{-0.732}\right] \tag{3}$$

$$k_c = \frac{\omega}{c}\left[1+0.0978\left(\frac{\rho_0 f}{\sigma}\right)^{-0.7} - j0.189\left(\frac{\rho_0 f}{\sigma}\right)^{-0.595}\right] \tag{4}$$

The model assumes that the absorbent material is fibrous and that the fibers are uniformly distributed. Delany and Bazley [29] defined the domain of functions in their empirical model:

$$10 \le f/\sigma \le 1000 \tag{5}$$

where the frequency f is expressed in Hz and the longitudinal resistance to airflow, σ, in kg/m^{3}s.

The validity range of the model can be expressed through a dimensionless parameter in the form: $0.01 \le \rho_0 f/\sigma \le 1$.

It should be noted that all fibrous materials considered in this model have porosity close to unity.

2.2. Johnson – Champoux – Allard (JCA) model

As a semi-empirical model, the JCA model [42] is the most commonly used sound absorption model. It contains five physical parameters, namely porosity ϕ, airflow resistance σ, tortuosity α, viscous characteristic length Λ, and thermal characteristic length Λ'. Porosity is the percentage of pore volume occupied by a saturated medium (usually air) compared to the total volume of the material in its natural state. Airflow resistance has an important effect on the sound absorption performance of porous materials. It is usually defined as the resistance of air flowing through a porous material of a certain thickness. The tortuosity of porous materials is the deviation between the actual path and the true path of sound waves in the materials, which represents the complexity of the pores of the material. Both porosity and tortuosity are dimensionless quantities. The viscous characteristic length represents the size of the viscous force, and the thermal characteristic length describes the degree of heat exchange between the saturated medium in the pore and the solid frame at high frequencies [49].

According to the JCA model, the effective density $\rho e(\omega)$ and bulk modulus K(ω) of porous materials can be calculated using the following expressions:

$$\rho_e(\omega) = \alpha_\infty \rho_0\left[1 - j\frac{\sigma\phi}{\alpha_\infty \rho_0 \omega}\sqrt{1+j\frac{4\alpha_\infty^2 \eta \rho_0 \omega}{\sigma^2 \Lambda^2 \phi^2}}\right] \tag{6}$$

$$K_e(\omega) = \gamma P_0\left[\gamma - \frac{\gamma-1}{1-j\frac{8\eta}{\rho_0 \omega N_{pr}\Lambda'^2}\left(1+\sqrt{1+j\frac{\rho_0 \omega N_{pr}\Lambda'^2}{16\eta}}\right)^{\frac{1}{2}}}\right]^{-1} \tag{7}$$

where ω is the angular frequency of the incident wave, j is an imaginary unit, ρ_0 is the air density, N_{pr} is the Prandtl number of the air, η is the dynamic viscosity of the air, γ is the specific heat ratio related to the state of the air, and P_0 is the ambient atmospheric pressure. It should be noted that Λ and Λ' are related to some other physical parameters of the material and can be written as:

$$\Lambda = \frac{1}{c}\left(\frac{8\alpha_\infty \eta}{\sigma\phi}\right)^{\frac{1}{2}}$$
$$\Lambda' = \frac{1}{c'}\left(\frac{8\alpha_\infty \eta}{\sigma\phi}\right)^{\frac{1}{2}} \tag{8}$$

where c and c' are the shape factor and the scale factor of the pore cross-section, respectively.

The characteristic impedance $Z_c(\omega)$ and the complex expansion constant $k(\omega)$ of porous materials can be deduced from Eqs. (3) and (4), and can be expressed as Eqs. (9) and (10).

$$Z_c(\omega) = \sqrt{K_e(\omega)\rho_e(\omega)} \tag{9}$$

$$k_e(\omega) = \omega\sqrt{\frac{\rho_e(\omega)}{K_e(\omega)}} \tag{10}$$

Considering that the porous material of thickness d is covered by a rigid boundary, the sound absorption coefficient (SAC) α of the porous material can be denoted by the following equations:

$$Z_s(\omega) = -j\frac{Z_c(\omega)}{\phi}\cot(k_e(\omega)d) \tag{11}$$

$$R = \frac{Z_s(\omega) - Z_o}{Z_s(\omega) + Z_o} \tag{12}$$

$$\alpha = 1 - R^2 \tag{13}$$

where $Z_s(\omega)$ is the surface characteristic impedance, Z_0 is the air characteristic impedance, and is equal to $\rho_0 c_0$ where c_0 is the sound speed and R is the sound reflection coefficient.

To determine the impedance of the finite thickness of the material Z_l, in front of the rigid wall, knowing the values of the estimated surface impedance using different models, the following expression is used:

$$Z_l = Z_c \coth(jk_c d) \tag{14}$$

where d is the sample thickness.

Estimates of impedance and absorption coefficient calculated according to different empirical models are compared with the values of these quantities measured in the impedance tube.

2.3. Methodology of forming stochastic models

The software package Design Expert v.9.0.6.2 was used to create and analyze stochastic models. The choice of the regression model depends, first of all, on the available number of experimental points. However, even when there is a sufficient number of experimental points, it does not mean that the model of the highest degree will be the best. Models are formed in the form of polynomials of the nth degree. For experiments with mixtures, polynomials up to the fourth degree are used, and for other experiments polynomials up to the sixth degree.

To select a stochastic model, a summary statistical analysis is used, which compares possible models based on: standard deviation (Standard Deviation), coefficient of determination (R-squared), adjusted coefficient of determination (Adjusted R-squared), assumed coefficient of determination (Predicted R-squared) and PRESS statistics (Prediction Sum of Squares Statistic).

The sound absorption coefficient can be expressed by a polynomial function, as given in the expression [41] for open and partially open-cell polyurethane foams:

$$\begin{aligned} Ln(\alpha) = & -2.15980 - 51.64481 * d - 3.46202E - 003 * f + \\ & +0.28361 * d * f + 1164.37919 * d \wedge 2 + 3.54443E - 006 * f \wedge 2 - \\ & -2.87696 * d \wedge 2 * f - 1.56509E - 004 * d * f \wedge 2 - 6589.93271 * d \wedge 3 - \\ & -1.19549E - 009 * f \wedge 3 + 3.58649E - 004 * d \wedge 2 * f \wedge 2 + 11.80043 * \\ & * d \wedge 3 * f + 3.97690E - 008 * d * f \wedge 3 \end{aligned} \tag{15}$$

where d is the thickness of the material in m, and f is the frequency in Hz.

2.4. Non-acoustic parameter identification models

In the JCA model, there are five non-acoustic parameters to be identified: porosity, airflow resistance, tortuosity, viscous characteristic length, and thermal characteristic length. Often this problem boils down to finding four unknown parameters, as porosity can be determined with high accuracy from measured density. In this way, the dimension of the vector $x = [\sigma, \alpha_\infty, c, c']$ is reduced by one.

The viscous characteristic length Λ and the thermal characteristic length Λ' are functions of the shape factor c and the scale factor c' of the pore cross-section, respectively. The range of values of characteristic length is usually from 1 to 3000, while the value of shape factor c or scale factor c' generally ranges from 0.3 to 3.3. Shape factor c and scale factor c' were chosen as design variables instead of viscous characteristic length and thermal characteristic length because narrowing the solution space helps to arrive at a reasonable solution [49].

Non-acoustic parameter identification is essentially a constrained multidimensional parameter optimization problem. According to the principle of the least square method, the objective function and the constraints can be given by Eq. (16):

$$\begin{aligned} & \min f_{obj}(f_i, \mathbf{x}) = \sum_{i=1}^{T} \left[\alpha_{EXP}(f_i) - \alpha_{JCA}(f_i, \mathbf{x}) \right]^2 \\ & s.t. \begin{cases} 1000 \le \sigma \le 20000 \\ 1 \le \alpha_\infty \le 4 \\ 0.3 \le (c, c') \le 3.3 \\ c \ge c' \end{cases} \end{aligned} \tag{16}$$

where T is the number of sampling frequency points in the test frequency range, f_i is the ith frequency point sampled in the experiment, α_{EXP} denotes the sound absorption coefficient measured at the frequency f_i, and α_{JCA} denotes the sound absorption coefficient predicted by the JCA model at the same frequency.

3. CONCLUSIONS

Empirical models are characterized by their simplicity since they depend on only one input parameter, the resistance to airflow, which can be measured relatively easily. Precisely because of this, the resistance to airflow must be determined by applying valid methods, which enable the calculation of the sound absorption coefficient in a wide frequency spectrum. The disadvantage of these models in terms of the breadth of application is that they were developed for a specific material or a specific group of similar materials. Precisely because of this, empirical models sometimes do not give good predictions in certain frequency ranges, and most often these are low frequencies. Given that these models are most often obtained by applying regression analysis and the method of least squares, often for a certain type of material the regression constants cannot be more accurately determined by applying optimization techniques.

Theoretical models or phenomenological as they are also called, which are used to determine sound absorption, are much more complex compared to empirical models. Theoretical models penetrate the physicality of the process, most often through the determination of bulk density and bulk modulus of elasticity, which take into account viscous and thermal effects between the porous structure and the interstitial fluid. The advantage of such models is that optimal process parameters can be indirectly determined in the phase of making porous materials, to achieve the desired acoustic properties. The shortcoming of theoretical models is that the most frequently used five parameters of different models cannot be determined within the model, but additional measurements are required using expensive and specialized measuring equipment.

Statistical models that are primarily based on ANOVA analysis can be very useful when solving the problem of applying absorption materials in noise protection systems. They can be useful when it is necessary to determine the optimal thickness of absorption material for a certain frequency range, or for a given thickness to determine the type of material that will achieve a given level of sound protection. Considering that they are polynomial functions of a higher order, these models give a very precise match of the sound absorption coefficient with the experimental values. The disadvantage of these models is that they are not reliable for frequency ranges for which there are no experimental sound absorption results.

Models based on the application of genetically inspired algorithms for determining the sound absorption of porous materials are more recent. By solving the optimization problem of multidimensional parameters, non-acoustic identification of parameters is performed, which is very important considering the problems during their determination. Solving optimization problems requires an enviable programming experience, which can be considered a shortcoming of these models. Applying optimization algorithms to models that have one input parameter often does not give satisfactory results. By applying optimization techniques, phenomenological models for determining the sound absorption of porous materials are becoming more widely represented.

Acknowledgement: *The author would like to thank the Ministry of Science, Technological Development and Innovation of the Republic of Serbia for the support during this research (contract no. 451-03-65/2024-03/200108).*

REFERENCES

1. Kurtović H., (1990), *Osnovi tehničke akustike*, Naučna knjiga, Beograd
2. Ayub M., Nor M.J.M., Amin N., Zulkifli R., Fouladi M.H., Ismail A.R., (2009), Analysis on sound absorption of natural coir fiber using Delany-Bazley model, P*roceedings of the International Conference on Mechanical Engineering*, Dhaka, Bangladesh, December 26-28, 2009. pp. 1-6.
3. Navacerrada M.Á., Díaz C., Fernández P., Characterization of a Material Based on Short Natural Fique Fibers, *BioResources*, Vol. 9, No. 2, 2014., pp. 3480–3496.
4. AL-Rahman A.L., Raja R.I., Rahman R.A., Experimental Study on Natural Fibres for Green Acoustic Absorption Materials, *American Journal of Applied Sciences,* Vol. 10, No. 10, 2013., pp. 1307–1314.
5. Wang C.-N., Torng J.-H., Experimental study of the absorption characteristics of some porous fibrous materials, *Applied Acoustics*, Vol. 62, No. 4, 2001., pp. 447–459.
6. Eaves D., (2004), *Handbook of Polymer Foams*, Rapra Technology Limited, Shawbury
7. Yamashita T., Suzuki K., Adachi H., Nishino S., Tomota Y., Effect of Microscopic Internal Structure on Sound Absorption Properties of Polyurethane Foam by X-ray Computed Tomography Observations, *Materials Transactions*, Vol. 50, No. 2, 2009., pp. 373–380.
8. Kino N., Nakano G., Suzuki Y., Non-acoustical and acoustical properties of reticulated and partially reticulated polyurethane foams, Applied Acoustics, Elsevier Ltd, Vol. 73, No. 2, 2012., pp. 95–108.
9. Pompoli F., Bonfiglio P., (2007), Acoustical properties of polyurethane open cells materials: Experimental investigation and theoretical models, *Proceedings of the 14th International Congres of Sound and Vibration - ICSV14*, Cairns, Australia, July 9-12, 2007.
10. Vuković J., Pergal M., Jovanović S., Vodnik V., Umreženi poliuretani na bazi hiperrazgranatih polimera, Hemijska Industrija, Vol. 62, No. 6, 2008., pp. 353–359.
11. Pfretzschner, J. and Rodriquez, R.M. (1999) Acoust Properties of Rubber Crumbs. Polymer Testing, 18, 81-92. http://dx.doi.org/10.1016/S0142-9418(98)00009-9
12. Swift M.J., Bris P., Horoshenkov K. V., Acoustic absorption in re-cycled rubber granulate, *Applied Acoustics*, Vol. 57, No. 3, 1999., pp. 203–212.
13. Han Z., Chunsheng L., Kombe T., Thong-On N., Crumb rubber blends in noise absorption study, *Materials, and Structures*, Vol. 41, No. 2, 2008., p. 383–390.
14. Radičević B., Ristanović I., (2014), Koeficijent apsorpcije materijala od recikliranog gumenog otpada, *Zbornik 58. konferencije za elektroniku, telekomunikacije, računarstvo, automatiku i nuklearnu tehniku - ETRAN*, Vrnjačka Banja, Srbija, Jun 2-5, 2014.
15. Zainulabidin M.H., Abdul Rani M.H., Nezere N., Mohd Tobi A.L., Optimum Sound Absorption by Materials Fraction Combination, International Journal of Mechanical and Mechatronics Engineering, Vol. 14, No. 2, 2014., pp. 118–121.
16. Theophilus E.O., Febresima R.C., Mbaka K.V., Analysis of sound absorbing properties of different density local acoustic materials, *International Journal of Educational Research and Reviews*, Vol. 3, No. 4, 2015., pp. 180–182.
17. Mahzan S., Ahmad Zaidi A.M., Ghazali M.I., Yahya M.N., Ismail M., (2009), Investigation on Sound Absorption of Rice-Husk Reinforced Composite, *Proceedings of MUCEET*, 2009.
18. Dragonetti R., Ianniello C., Romano R.A., Measurement of the resistivity of porous materials with an alternating air-flow method, *The Journal of the Acoustical Society of America*, Vol. 129, No. 2, 2011., pp. 753–764.
19. Joshi M.P., Shravage P., Jain S.K., Karanth N. V., A Comparative Study on Flow Resistivity for Different Polyurethane Foam Samples, *Journal of Acoustical Society of India*, Vol. 38, No. 4, 2011., pp. 153–157.
20. Garai M., Pompoli F., (2001), An Intercomparison of Laboratory Measurements of Flow Resistance, *International Congres on Acoustics*, Rome, Italy, 2001.
21. Ingard K.U., Dear T.A., Measurement of acoustic flow resistance, *Journal of Sound and Vibration*, Vol. 103, No. 4, 1985., pp. 567–572.
22. Garai M., Pompoli F., A simple empirical model of polyester fiber materials for acoustical applications, *Applied Acoustics*, Vol. 66, No. 12, 2005., pp. 1383–1398.
23. Bies D.A., Hansen C.H., Flow Resistance Information for Acoustical Design, *Applied Acoustics*, Vol. 13, No. 5, 1980., pp. 357–391.

24. Kino N., Ueno T., Comparisons between characteristic lengths and fiber equivalent diameters in glass fiber and melamine foam materials of similar flow resistivity, *Applied Acoustics*, Vol. 69, No. 4, 2008., pp. 325–331.
25. Tarnow V., Airflow resistivity of models of fibrous acoustic materials, *The Journal of the Acoustical Society of America*, Vol. 100, No. 6, 1996., pp. 3706–3713.
26. EN ISO 10534-2:2001, Determination of sound absorption coefficient and impedance in impedance tubes - Part 2: Transfer - function method
27. Yaniv SL., Impedance measurement of propagation constant and characteristic impedance of porous acoustical material, *The Journal of the Acoustical Society of America*, Vol. 54, 1973., pp. 1138–1142.
28. Utsuno H, Tanaka T, Fujikawa T, Seybert AF., Transfer function method for measuring characteristic impedance and propagation constant of porous materials, *The Journal of the Acoustical Society of America*, Vol. 86, 1989., pp. 637–643.
29. Delany M.E., Bazley E.N., Acoustical properties of fibrous absorbent materials, *Applied Acoustics*, Vol. 3, No. 2, 1970., pp. 105–116.
30. Dunn I.P., Davern W.A., Calculation of acoustic impedance of multi-layer absorbers, *Applied Acoustics*, Vol. 19, No. 5, 1986., pp. 321–334.
31. Voronina N., Acoustic properties of fibrous materials, *Applied Acoustics*, Vol. 42, No. 2, 1994., pp. 165–174.
32. Voronina N., Improved Empirical Model of Sound Propagation Through a Fibrous Material, *Applied Acoustics*, Vol. 48, No. 2, 1996., pp. 121–132.
33. Gardner G.C., O'Leary M.E., Hansen S., Sun J.Q., Neural networks for prediction of acoustical properties of polyurethane foams, *Applied Acoustics*, Vol. 64, No. 2, 2003., pp. 229–242.
34. Hamet JF., Mode´lisation Acoustique dÕun enrobe´ Drainant, Bron: Rapport INRETS, 1992.
35. Biot MA., Theory of propagation of elastic waves in a fluid-saturated porous solid. I. Low-frequency range. II. Higher frequency range., *The Journal of the Acoustical Society of America*, Vol. 28, 1956., pp.168–191.
36. Lambert RF., The acoustical structure of highly porous open-cell foams. *The Journal of the Acoustical Society of America,* Vol. 72, No. 3, 1982., pp. 879–887.
37. Zwikker C, Kosten CW., (1949), *Sound Absorbing Materials*, Elsevier, New York
38. Allard JF, Depollier C, Nicolas J, Lauriks W., Cops A., Proprie´te´s acoustiques des mate´riaux poreux sature´s dÕair et the´orie de Biot, *Journal of Acoustics*, Vol. 3, 1990., pp. 29–38.
39. Champoux Y, Stinson MR., On acoustical models for sound propagation in rigid frame porous materials and the influence of shape factors. *The Journal of the Acoustical Society of America*, Vol. 92, No. 2, 1992., pp. 1120–1131.
40. Radičević B., Development of a decision-making model for the selection of the optimal mixture of sound absorbing materials, Faculty of Mechanical and Civil Engineering in Kraljevo, University of Kragujevac, PhD Dissertation, 2016.
41. Atalla Y. Paneton R., Inverse characterization of the geometrical macroscopic parameters of porous materials, *Canadian Acoustics*, Vol. 33, 2005., pp. 11-24.
42. Allard JF, Champoux Y., New empirical equations for sound propagation in rigid frame Fibrous materials, *The Journal of the Acoustical Society of America,* Vol. 91, 1992., pp. 3346-3353.
43. Atalla Y, Panneton R., Inverse acoustical characterization of open cell porous media using impedance tube materials, *Canadian Acoustics*, Vol. 33, No. 1, 2005., pp. 11-24.
44. Pelegrins MT, Horoshenkov KV, Burnett A., An application of Kozeny-Carman flow resistivity model to predict the acoustical properties of polyester fiber, *Applied Acoustics*, Vol. 101, 2016., pp. 1-4.
45. Cobo P, Simon F., A comparison of impedance models for the inverse estimation of the npn-acoustical parameters of granular absorbers, *Applied Acoustics*, Vol. 104, 2015., pp. 119-126.
46. Bonfiglio P, Pompoli F., Inversion problems for determining physical parameters of porous materials: Overview and Comparison Between Different Methods, *Acta Acustica United with Acustica*, Vol. 99, No. 3, 2013., pp. 341-351.
47. Kino N., Further investigations of empirical improvements to the Johnson-Champoux-Allard model, *Applied Acoustics*, Vol. 96, 2015., pp 153-170.
48. Garg N., Kumar A., Maji S., Parametric Sensitivity Analysis of Factors Affecting Sound Transmission Loss of Multi-Layered Building Elements Using Taguchi Method, *Archives of Acoustics*, Vol. 39, No. 2, 2014., pp. 165–176.
49. Xiaomei X., Ping L., Parameter identification of sound absorption model of porous materials based on modified particle swarm optimization algorithm, *Plos One*, Vol. 16, No. 5, 2021.

FACTA UNIVERSITATIS
Series: **Working and Living Environmental Protection** Vol. 21, Nº 4, Special Issue, 2024, pp. 225 - 235
https://doi.org/10.22190/FUWLEP240920021C

Original scientific paper

THE CONTRIBUTION OF STANDARDS AND STANDARDIZATION IN ACHIEVING ACOUSTIC COMFORT

UDC 534:614

Dragan S. Cvetković

University of Niš, Faculty of Occupational Safety in Niš, Serbia

ORCID iDs: Dragan S. Cvetković N/A

Abstract. *Acoustic comfort in the context of the harmful effect of noise on human health in the living space of a residential building can be viewed based on the definition of the World Health Organization (WHO), according to which health is "a state of complete physical, spiritual and social comfort". According to this definition, health action includes both increased subjective comfort and physical health damage, which over time may result in physical health damage. This paper offers one point of view in an attempt to improve the process of establishing evidence of exposure to noise in the living space of a residential building and to support a more impartial presentation of data regarding the negative effects of disrupting acoustic comfort with contents that violate privacy and human health. The growing influx of complaints about the phenomenon of noise in the environment, as well as its impact on mental and physical health, requires a higher level of professional attitude towards a complex-multidimensional problem and a layered analysis of the spectrum of negative effects that imply sleep disturbance, auditory and extra auditory disturbances. Achieving acoustic comfort is a complex, multi-functional problem, which includes numerous external and architectural factors such as: the purpose of living space, the nature of noise in the environment, and acoustic values of building structures and materials. Unfortunately, numerous examples of "bad practice" are known, where the owners-buyers noticed all construction defects hidden under the luxurious surface only after moving in, and the largest number of customer complaints is related to acoustic comfort.*

Key words: *noise, acoustic comfort, customer satisfaction, public health*

Received September 20, 2024 / Accepted October 21, 2024
Corresponding author: Dragan S. Cvetković
University of Niš, Faculty of Occupational Safety in Niš, Ĉarnojevića 10a, 18000 Niš, Serbia
E-mail: dragan.cvetkovic@znrfak.ni.ac.rs; dcdbest@gmail.com

1. INTRODUCTION

We have witnessed more intensive construction of residential buildings in the last two decades. Construction is particularly intensive in large cities, and in addition, the price per square meter of residential space is constantly increasing, and real estate sales are booming. Buyers are ready to pay significant amounts of money for their "four walls" and rightfully expect high quality in return. Unfortunately, buyers of new apartments complain most frequently about acoustic comfort. What should you do if you've already moved into a noisy apartment and how can you stop this behavior? Objectively, numerous examples of "bad practice" are known where buyers only notice all construction defects hidden under the luxurious surface after moving in. People keep commenting: "I paid thousands of euros for a square meter and I hear my neighbor talking on the phone, snoring while sleeping, how many times he uses the toilet during the night, etc." The explanation of the term "acoustic comfort" is based on the meaning of the term "comfort", which implies comfort, ease, as well as everything that makes life comfortable and pleasant. However, if we ask ourselves what kind of comforts there are when it comes to housing and what is actually "acoustic comfort"? The answer could be derived from the Rulebook on Buildings Energy Efficiency, which considers potential comfort conditions necessary for living comfort, consisting of four basic prerequisites: thermal, air, visual and acoustic comfort. According to the aforementioned viewpoint, acoustic comfort represents conditions in which the level of noise in the living space is such that it does not cause a feeling of discomfort. Good acoustic comfort does not mean achieving complete silence in the housing unit, which in itself can often be unpleasant, but achieving an acceptable level of noise from the outside environment and the immediate environment. In other words, the sounds coming from the hallway, neighboring apartments, or the outside environment must be reduced to a level that in no way disturbs privacy and the daily rhythm of life.

The quality of sound insulation in the "living space" is becoming a more frequently asked question as a result of the growing demands of real estate buyers and users, both in terms of lowering noise levels from the surroundings and from installations within the building. Achieving the required level of acoustic comfort is a technologically complex task, which includes numerous external and architectural factors: the purpose of the building, the acoustic zone of the location, the spectral content of noise in the environment, the use of building systems and materials, the design skills in the materialization of these requirements, the implementation and compliance with standards in order to meet the needs for the comfort of residential space users.

Buyers who spend more and more money on real estate are likely to have higher expectations and demands in terms of sound comfort given the upward trend in the price of square footage of residential space on the domestic real estate market. In practice, unfortunately, providing adequate acoustic comfort is not in the interest of those who define construction conditions; however, it should be in the investor's interest. In the case of the former, the reason is a lack of expertise and insufficient knowledge of the problem, and in the case of others, it is material interest, because acoustic quality costs money.

Acoustic comfort is defined as a psychophysical state where an individual feels good about a particular activity in a particular setting, which implies:

- Protection against noise, because noise is defined as any unwanted sound, so acoustic comfort means providing protection against sound disturbance originating from sources outside the building and inside the building;

- Protection of privacy, because it implies the provision of protection against eavesdropping between rooms, that is, spaces; and
- Adequate quality of the desired sound content, which means ensuring adequate acoustic quality of rooms or spaces in accordance with the requirements of the quality of the sound image (intelligibility and aesthetics).

Unfortunately, in reality, acoustic defect solutions are typically only sought after after the object is completed and the acoustic defects are felt during the use phase of the space in public places like offices, meeting rooms, hospitals, schools, children's institutions, etc.

2. WHY ACOUSTIC COMFORT IS IMPORTANT

Noise as a phenomenon of acoustic activity unequivocally has a negative impact on human health and well-being, and at the same time, it encourages the scientific and professional public to be more and more concerned in the search for acceptable solutions in protection. The latest report from the European Environment Agency (EEA) [1] confirms that exposure to noise has an important impact on people's mental and physical well-being. It is estimated that noise pollution affects at least 20 % of the European population living in urban areas where the level of noise generated by traffic (road, rail and airplane) is harmful to people's health. It is also estimated that in Europe over 113 million people are exposed to long-term noise levels from road traffic during the day and night period (L_{den}), with a value of at least 55 dB. To this data should be added the fact that in Europe, according to estimates from 2020, 80 % of citizens live in or near cities. [2] with increased demand for road, rail and air transport. Simultaneously with the increase in noise sources, one can expect increased exposure and associated adverse health effects. Noise was found to be the cause of 48,000 cases of chemical heart disease, and 12,000 cases of premature death. According to estimates from the EEA – European Environment Agency report, 12,500 European students suffer from learning disabilities resulting from noise generated by air traffic. Seen through the prism of time and the activities undertaken, the number of people exposed to noise sources has been stable from 2012 to the present day, which can be assessed as not achieving the main goal of the vision of the Environmental Noise Directive 2002/49/EC for the year 2020, "that not a single person should be exposed to a level of noise that can endanger health and quality of life".

According to the literature reviewed for this study, there are four key non-physical factors that influence the perception of noise in the environment: work activity; context and attitude; perceived control and predictability; personality and mood [3].

The interpretation of the sound that has taken on the phenomenon of "noise" depends on the personality and a number of other dependent factors and circumstances. This means that individual people will react differently to the same acoustic challenges in their environment, which is another reason for layered consideration of noise disturbance and valuing individual differences in the context of acoustic content in order to reach the required level of "acoustic comfort".

Making a conclusion about the harmfulness of noise to human health must first take into account noise sensitivity, which is based on general attitudes about noise [4,5] and is an important variable for explaining the discrepancy between exposure and individual anxiety response. This fact raises the question of whether individuals who are sensitive to noise are simply those who complain more about their environment.

Health, as a valuable asset, deserves legal protection, and that is why national legislation has a responsibility to regulate the requirements related to sound insulation, which is a prerequisite for acceptable "acoustic comfort", by law and under legal regulations. In the comments of the legal doctrine, it is stated, among other things:

- that the intimate area is specially protected, which includes the sphere of human life characterized by great isolation from the engagement of other people (with the exception of the family).
- that the apartment in the narrower sense is part of the private, intimate sphere. Bearing this in mind, the need for the inviolability of the home to be a right that aims to guarantee the individual the "elementary quality of living space", the right "to enjoy peace", in terms of his human dignity and in the interest of personal free development, is strengthened.

When it comes to ambient comfort: "The building must be designed and built so that the noise felt by the occupants or people nearby is kept at a level that is not dangerous to health and in which satisfactory conditions are provided for night rest, leisure and work." Acoustic comfort in buildings is achieved if unwanted sounds (noise) are not noticed, if people's privacy is ensured, which means that their activities cannot be heard by the environment, and if everything that is wanted to be heard, for example, speech, is recognized and understood without effort (when desired) [6, 7]. In order to achieve this, the construction facilities must provide:

- adequate sound insulation from airborne and structural sound inside the building,
- adequate insulation of the facade, which ensures an acceptable level of ambient noise coming from the outside environment,
- a system of installations in the building that does not produce noise and does not impair other measures to achieve sound comfort,
- privacy in areas where it is necessary,
- adequate acoustic response of interior spaces that determines the sensibility and quality of useful sounds.

To increase satisfaction, classifying "acoustic comfort", which is a very pronounced subjective component, must rely on standards and respect for construction technology (selection of location, purpose of the building, materialization of the architectural project, control over construction processes) in order to increase the level of satisfaction.

3. STANDARDS AS A PREREQUISITE FOR ACOUSTIC COMFORT

In today's living conditions and associated risks, as discussed in the introduction to this paper, "acoustic comfort" has become an unavoidable segment of our reality, especially in the spaces where we spend the most time, the place where we live or work (apartment or office). It is not a rare case that being in an office, restaurant, hospital, hotel, industrial plant, cinema, swimming pool, kindergarten or your child's school is a place where the acoustic content in the environment did not please you and you experienced it as noise [8].

Acoustic comfort is a concept that refers to the quality of sound in a certain space and its impact on the subjective experience of people staying in that space. This concept includes various factors, such as the noise level, the type of sounds present in the environment, the acoustic properties of the materials in the space, and the ability of the space to absorb, reflect or isolate sound.

Ideally, an ambient space is expected to have an optimal acoustic quality that allows people to communicate effortlessly, to relax and concentrate without distraction and to have a pleasant experience of being in that space. This can be especially important in different environments such as offices, classrooms, restaurants, concert halls, hospitals or homes. Maintaining acoustic comfort can involve the application of various techniques such as the use of acoustic materials, designing spaces with optimal acoustic properties, using sound insulation systems, or implementing noise reduction strategies.

Sound insulation standardization is a key element in ensuring "acoustic comfort" - sound quality in construction projects. International organizations for standardization (ISO, EN) as well as national institutions of the most developed countries in Europe create the necessary but not sufficient conditions for achieving the final goal of complete acoustic comfort:

- German Institute for Standardization DIN – "Deutsches Institut für Normung"; Sound insulation is considered in DIN standards through various aspects to ensure that buildings and construction materials meet certain standards for noise protection. The first version of the standard sheet DIN 4109 "Sound insulation in construction", which is still valid today, was published in 1944. DIN 4109 provides the basis for the calculation and gives the minimum specifications for sound insulation. The main goal is to protect health [9]. The minimum sound insulation provided by the DIN 4109 standard has always been considered a way to prevent unreasonable noise during normal life habits. However, this is often not enough in terms of today's user requirements, user behavior, and lifestyle. In order to meet the demands of planners and users who want more than minimum sound insulation, recommendations for increased sound insulation were already included through the 1962 version of DIN 4109, and DIN 4109 from 1989, which is valid today, in the supplementary sheet contains and 2 recommendations for increased sound insulation. However, the values there are so strongly characterized by compromises that the recommendations for increased sound insulation sometimes differ only slightly from the requirements of DIN 4109, and therefore there is no subjectively significant improvement. DIN 52210: "Testing of sound insulation in construction – Testing at the place of application." It provides guidelines and procedures for measuring the sound insulation of materials and structures in real buildings to verify compliance with the specifications in DIN 4109.
- The VDI (Verein Deutscher Ingenieure) is an association of German engineers that also develops technical guidelines and standards, similar to the German Institute for Standardization (DIN). When it comes to acoustics in buildings, VDI also has relevant standards and guidelines. One of the most important VDI standards related to acoustics in buildings is VDI 4100. This standard covers various aspects of acoustics in buildings, including the design and measurement of sound insulation, noise control in interior spaces, as well as criteria for assessing acoustic comfort. The VDI 4100 provides guidance on how to achieve an appropriate level of acoustic comfort in different types of rooms, such as offices, schools, hospitals, hotel rooms and the like. It also provides guidance on materials and constructions used to improve sound insulation and absorption within buildings.
- DEGA – The German Society for Acoustics, "Deutsche Gesellschaft für Akustik", carries out accreditation or certification that confirms that a product or service meets certain standards in the field of acoustics. DEGA is a renowned organization in the field of acoustics, engaged in research, development and promotion of acoustic sciences and technologies. Their standards and guidelines are often used in the

industry to ensure acoustic quality in various environments, such as music rooms, concert halls, offices, or industrial spaces. However, in the field of acoustics, there are different approaches and classifications that can be used to categorize objects according to their acoustic properties. For example, buildings can often be classified according to their purpose and specific requirements for acoustic comfort. This may include the classification of facilities such as concert halls, cinemas, offices, schools, hospitals and the like, with each type of facility having its own specific acoustic needs.

- The French Institute for Standardization "AFNOR – Association Française de Normalisation" publishes the French standards "Normes Françaises NF", One of the most famous French standards related to sound insulation is NF S 31-080: This standard specifies methods for measuring the sound insulation of walls, of floors and ceilings in buildings. It also provides guidelines for the design and installation of sound insulation in buildings with ISO international standards and is often used in French construction projects. These standards specify how to measure a building's acoustic performance and assess its sound insulation through acoustic tests on building components and structures, including sound insulation measurement.
- In Great Britain, "British Standards Institution – BSI" is the institution from which the most famous standards for sound insulation originate. Several key British Standards relate to sound insulation: BS 8233: a standard that provides guidance on the design of sound insulation in buildings to provide a comfortable environment for occupants. It includes factors such as external noise, internal noise, vibration and acoustic comfort. BS 4142: standard which defines procedures for measuring noise from industrial, commercial and recreational sources, and their impact on surrounding buildings and residents. Although it does not focus exclusively on sound insulation, it provides guidelines for assessing noise levels and their impact. BS 6472: standard specifies procedures for measuring vibrations transmitted through ground and structures in buildings. Vibrations can be a source of discomfort and disturbance, so their measurement and control are important for maintaining acoustic comfort. BS EN ISO 717: a series of standards defining procedures for measuring the sound insulation of walls, floors, and ceilings in buildings. All of the standards listed are aligned with international ISO standards and are often used in UK construction projects.

  BREEAM (Building Research Establishment Environmental Assessment Method) is a building sustainability rating system used worldwide to assess the environmental performance of construction projects. This rating system was developed in the UK by the Building Research Establishment - BRE to promote sustainability in the construction industry. BREEAM, as a building sustainability rating system, also considers acoustic comfort as part of its rating criteria. Acoustic comfort plays an important role in the quality of life of building users, so it is important to take this area into account during the design, construction and management of buildings. As part of the BREEAM assessment, acoustic comfort usually includes the following aspects:
  - Sound proofing: This refers to the ability of a building to prevent the transmission of sound between rooms or between the interior and the exterior. BREEAM assesses the sound insulation quality of materials, structures and installations to ensure that privacy is maintained and disturbance from outside noise is reduced.
  - Sound absorption: This aspect refers to the building's ability to absorb sound inside the premises, thereby reducing reverberation and improving acoustic

comfort. This may include the use of acoustic materials and room design that reduces echoes and noise.

- Room acoustic design: BREEAM also assesses the planning and design of rooms to ensure that optimal acoustic comfort is achieved for building users. This may include strategies such as proper speaker positioning, reverberation and noise control, and the use of acoustic screens or baffles.

In our country, the Institute for Standardization of Serbia is a national standardization body, which, among other things, adopts, develops, reviews, changes, supplements and withdraws Serbian standards and related documents; ensures compliance of Serbian standards and related documents with European and international standards and related documents.

In the field U 043 "acoustics in construction", the current number of standards that are available to the public is 151, (published standards, standards for which the review procedure has been completed, and standards for which the review procedure has begun), and the number of new projects is eight.

The existence of standards has created conditions for design, construction and control processes to be carried out without restrictions, for sound insulation to be performed in compliance with accepted construction technology guidelines and in a manner that ensures "air and structural" sound insulation in and around buildings is a reliable guarantee "acoustic comfort" for the benefit of the tenants' health. Unfortunately, one gets the impression that listening to the ambience of significant architectural achievements, the materialization of the space was realized without a sense of how that space will sound and how many chances it will give us to enjoy it with all our senses.

By definition, a standard is a document that provides conditions, specifications, guidelines, or characteristics that can be used to ensure that materials, products, processes and services are fit for purpose. Standards are established by consensus and approved by recognized bodies. The application of Serbian standards is voluntary, which means that there is no automatic legal obligation to apply them. However, laws and technical regulations may refer to standards, making compliance with them mandatory.

Disputes over acoustic comfort and sound insulation as disputed facts demonstrate that the standard is necessary but not decisive in achieving the goal. In the country where the first DIN standard was published in 1938 and determined the minimum level of sound insulation required by construction legislation, it has no influence on current judicial practice. The current version of DIN 4109 from 2018 does not contain any requirements for increased sound insulation. In Part 5 - DIN 4109, increased noise insulation was developed as a continuation of Appendix 2 and published in 2020. Market acceptance will become evident in the coming years. The update of DIN 4109, from a legal point of view, has no impact on current court practice. This is because the Federal Court of Justice (BGH – Bundesgerichtshof), in its judgment of June 14, 2007 - VII ZR 45/06, BG HZ 172, 346, does not base its judgment on the requirements for sound insulation according to DIN standards, but on what are noise insulation level agreed by the contracting parties. In the verdict BGH VII ZR 45/06 of 14.06.2007. the position of the court is that:

- Requirements for sound insulation are subject to dynamic changes. On the one hand, they are based on people's current needs for peace and individual isolation in their own living space.
- On the other hand, they depend on the ability of construction and the construction industry to provide the widest possible noise protection, taking into account the economic interests of both contracting parties.

- Dimensions of sound insulation specified in private technical regulations cannot be used as recognized rules of technology if there are economically acceptable construction methods that comply with recognized rules of technology and which easily achieve greater dimensions of sound insulation.

4. How to Achieve Satisfaction and Acoustic Comfort

The fact that the national legislation, as well as the technical regulations, do not recognize the concept of "acoustic comfort", does not mean that it is less important and that it cannot be the subject of consideration and dispute, because the threat of noise in the living-residence area is an undeniable fact, which is easily proven, and derives from the END - Environmental noise directive 2002/49/EC, Serbian Law on Environmental Noise Protection and other positive laws that address noise as a phenomenon, particularly its subjective aspect.

Scientific experts emphasize the existence of four key non-physical factors that influence the perception of noise in the environment: - work activity; context and attitude; perceived control and predictability; personality and mood. The interpretation of a sound as "noise" depends on personality and a number of other factors and circumstances. This means that individual people will react differently to the same acoustic challenges in their environment [10]. This is another reason for layered consideration of noise disturbance and valuing individual differences, through the context of acoustic content.

On the basis of their personal, scientifically professional knowledge and skills in relation to noise in the environment, after studying the contents of documents from the literature [11,12], the experience achieved in improving acoustic comfort in accordance with the explicit request of the civilized needs of the users of the residential space in relation to the existing practice, they impose directions thoughts:

- The expected level of acoustic comfort depends on the precision of the agreed level of sound insulation from noise between the designer-contractor and the client.
- Compliance with the minimum sound insulation standards is not sufficient in the civil law sense, but only the construction works performed at the time of acceptance, which corresponds to judicial practice.
- Responsibility for an inadequate level of acoustic comfort cannot be avoided, regardless of the fact that in the chain from the purchase contract to the handover of the real estate, omissions are made in the interest of the investor, and to the detriment of the buyer.

The only question is, which mechanisms in construction have lost their function and how to assign them a management structure in order to transform an inert system from a "pathological" into a proactive construction system, which seeks the interests of the customer.

It is difficult to explain why, in reality, the contract for buying apartment defines the purchase of an "area in m^2" of residential space without providing any information regarding the structure's acoustic performance, despite the fact that Article 3a of the Law on Planning and Construction mandates: "Technical documentation ensures that the building as a whole, i.e. individual component, should be suitable for the intended use, and that the building satisfies the following fundamental requirements during an economically viable period of use: point 5 noise protection", but with details about the choice of ceramics, parquet, side of the world, etc. The sales contract is usually prepared by the investor and offered to the buyer on a "take it or leave it" basis.

It is difficult to explain that in the first step of the project implementation, known as "Information on the location for the cadastral plot", the investor is not informed in which acoustic zone the cadastral plot is located, despite the fact that every local community is required to implement environmental protection measures against noise: acoustic zoning, determine quiet zones, as well as prohibit and limit measures on its territory and that by the decision of the competent authority, in accordance with the Law;

Also, it is difficult to explain the fact that the project for obtaining a building permit does not contain a Study on the sound protection of the building, even though it may be a school, kindergarten, senior living facility, hospital, etc., and can be located in one of the five acoustic zones, which is clearly not in accordance with the Law on Planning and Construction.

Furthermore, it is hard to explain that the same object is subject to acoustic tests even though there isn't a single detail in the documentation from the conceptual project to the completed project that takes into account any acoustic issues. On the other hand, it is a problem to prove that the noise issues have been dealt with, if there are no valid records in the project and construction documentation.

There is a question of how to explain the fact that the noise phenomenon mentioned in the Rulebook of requirements and standards for residential building and apartment design ("Official Gazette of RS", no. 58/2012, 74/2015 and 82/2015) is considered only in relation to the provisions of Article 30 "All rooms in which noisy facilities are located (diesel generators, boiler rooms, hydropower stations, heat transfer stations, machine room, driving shaft, ventilation drive equipment, etc.) cannot border residential premises and must be isolated from the structure buildings".

What kind of acoustic comfort can be expected in an expensively paid square meter of an apartment, if the investor appoints the committee for technical inspection? It is important that the members of the committee are persons who have design licenses, and that no examination of the acoustic values of the constructed structures is carried out and that proof of the soundproofing of partition walls, between floor structures, windows and entrance doors is not presented.

It is difficult to accept the fact that all the windows in the building are of the same construction and with the same glazing, regardless of the orientation of the facade and sources of noise from the environment. Also, the entrance door is of the same construction regardless of whether the entrance to the apartment is next to the elevator or next to the entrance to the building. Usually, during the handover of the residential space, the Apartment Condition Report is signed, without a single record of issues that need to be fixed and refers to electrical installations; water installations; sewerage, sound insulation of the facade; windows; partition; energy efficiency passport.

The legalization of the JUS standard in J6 201 in the Rulebook on technical norms for the design and execution of final works in construction ("Sl. list SFRJ", no. 21/90) created catches that the subject of the standard: "This standard establishes the technical conditions that must be met: a) during design, b) during construction or reconstruction, c) when testing sound protection during the reception of buildings intended for human habitation". The provisions of this standard are also applied to the reconstructed parts of the building, as well as to rooms whose purpose has been changed") be mandatory. Realistically, today, after 34 years, there is no trace of such an obligation in Serbian construction.

This situation dissuaded many institutions from giving up the accreditation of the method for field measurement of sound insulation, although they invested significant funds for the purchase of rather expensive equipment, for personnel training and accreditation.

And that's not the end, on August 25, 2015, the Deputy Prime Minister signed the Decision stating that "A working group is being formed to draft a proposal for a regulation on sound comfort in buildings"; however, there is no Regulation. Given that trust is gained through long-term results as evidence of dedication to work, and distrust does not require proof, only suspicion is sufficient. There remains a doubt that some interest has overcome the need, so pleasure and acoustic comfort will have to wait until a new century.

5. CONCLUSION

It stands to reason that the investor should assess the degree of construction from the standpoint of sound comfort in the same manner that the buyer chooses the size of the apartment or the quality of the bathroom ceramics. This statement is supported by the consequences of mass housing construction in Serbia in the last ten years, as well as the way of life; therefore, sound comfort has become a serious design, engineering-scientific, economic and sociological challenge. Acoustics, as one of the engineering disciplines in the design and construction of buildings, has the task of ensuring the expected level of sound comfort in the built space. That specific type of comfort has several dimensions:

- That the person in the apartment is not disturbed by sounds coming from the outside environment and from neighboring rooms, as well as that the sounds produced do not disturb other people in and around the building. In this way, the desired and necessary privacy is ensured.
- To enable quality sound communication in rooms where necessary, which implies good intelligibility and audibility of speech and music.

Unlike other engineering disciplines in the design process, regulations based on standards cannot be an absolute guide for all details important for sound comfort. It is expected that the customer has the right to demand a sound comfort level higher than the minimum prescribed by the regulation. This naturally follows the task of the designer to seek the help of an acoustic consultant to consolidate and optimize the requirements in the initial design phase in order to achieve a successful design outcome, to the satisfaction of users and investors.

REFERENCES

1. Environmental noise in Europe – 2020; European Environment Agency, 2020; Luxembourg: Publications Office of the European Union, 2020 ISBN 978-92-9480-209-5 ISSN 1977-8449 doi:10.2800/686249
2. Eurostat. Urban Europe – Statistics on Cities, Towns and Suburbs. 2016 ed. Publications Office of the European Union; Luxembourg: 2017.
3. Anderson CMB (1971). The measurement of attitude to noise and noises, National Physical Laboratory Acoustics Report, AC 52, Teddington, Middlesex; Stansfeld SA (1992). Noise, noise sensitivity and psychiatric disorder: epidemiological and psychophysiological studies. Psychological Medicine Monograph Supplement 22, Cambridge University Press, Cambridge
4. Nigel Oseland PhD CPsychol: Planning for Psychoacoustics: A Psychological Approach to Resolving Office Noise Distraction; Research Report, April 2015.
5. European Commission. EU Reference Scenario 2016 – Energy, Transport and GHG Emissions: Trends to 2050. European Commission; Brussels, Belgium: 2016.
6. Gupta, A., Gupta, A., Jain, K., & Gupta, S. (2018). Noise pollution and impact on children health. The Indian Journal of Pediatrics, 85(4), 300-306. https://doi.org/10.1007/s12098-01 7-2579-7.
7. Seidman, M. D., & Standring, R. T. (2010). Noise and quality of life. International journal of environmental research and public health, 7(10), 3730-3738. https://doi.org/10.3390/ijerph7103730.

8. US Department of Labor, O.S.a.H.A.U.O. *Noise and Hearing Conservation.* Available online: http://www.osha.gov/SLTC/noise hearing conservation/index.html (Site reviewed on 24 Septembar 2007, accessed on 2 August 2010)
9. Sven Petersen: Floor Heating and Impact Sound Insulation in Solid Construction; Marketing DACH, in Uponor GMBH, SBZ 07/2023.
10. European Commission . *EU Reference Scenario 2016—Energy, Transport and GHG Emissions: Trends to 2050.* European Commission; Brussels, Belgium: 2016.
11. World Health Organization . *Hearing Loss due to Recreational Exposure to Loud Sounds: A Review.* WHO; Geneva, Switzerland: 2015
12. Scientific Committee on Emerging and Newly Identified Health Risks (SCENIHR) Potential Health Risks of Exposure to Noise from Personal Music Players and Mobile Phones Including a Music Playing Function. European Commission; Brussels, Belgium: 2008

FACTA UNIVERSITATIS
Series: **Working and Living Environmental Protection** Vol. 21, N° 4, Special Issue, 2024, pp. 237 - 241
https://doi.org/10.22190/FUWLEP241002022I

Original scientific paper

FINITE ELEMENT MODELLING OF IMPEDANCE TUBE TEST

UDC 621.3.011.21:534.115

Roumen Iankov[1], Momir Praščević[2], Milan Rashevski[1], Abed Nodira[3]

[1]Institute of Mechanics, Bulgarian Academy of Sciences, Sofia, Bulgaria
[2]University of Niš, Faculty of Occupational Safety in Niš, Serbia
[3]Tashkent State Technical University, Tashkent, Uzbekistan

ORCID iDs: Roumen Iankov https://orcid.org/0000-0003-1621-9325
Momir Praščević https://orcid.org/0000-0002-7017-1038
Milan Rashevski https://orcid.org/0000-0001-5535-2482
Abed Nodira https://orcid.org/0000-0002-5020-0903

Abstract. *Impedance tubes are used to characterize porous acoustic materials. The report proposes a suitable model for numerical simulations of the test of materials in an impedance tube. Numerical simulations make it possible to generate synthetic data on the acoustic characteristics of the material when varying the parameters in the material model. These data are suitable for using machine learning algorithms as well as for solving inverse problems for identifying the material parameters in the mathematical model. The Johnson-Champoux-Allard model is used in the work, which is suitable for a wide class of porous acoustic materials.*

Key words: *impedance tube, finite element, acoustic parameters, Johnson-Champoux-Allard model*

1. INTRODUCTION

The creation of new materials intended for sound insulation and noise reduction is connected with their characterization. An impedance tube test can be used to determine the main acoustic material parameters. Usually, these materials are porous. Their characterization is related to the determination of specific material parameters. One possible way to determine these is to use impedance tube test results and numerical simulation of this test. The aim of the present work is to propose an adequate model for numerical simulation with the finite element method.

Received October 2, 2024 / Accepted October 21, 2024
Corresponding author: Momir Praščević
University of Niš, Faculty of Occupational Safety in Niš, Čarnojevića 10a, 18000 Niš, Serbia
E-mail: momir.prascevic@znrfak.ni.ac.rs

2. MATHEMATICAL MODEL

The fluid-structure interaction mathematical model is used to model the impedance tube experiment. In acoustic fluid-structure interaction problems, both the acoustic wave equation and the structural equation need to be coupled to each other [1]. For fluid structure interaction problems, the acoustic and structural matrices are coupled using the following equations.

The load acting on the surface of the fluid cavity by motion of structure is given by:

$$\left[F_f\right] = \rho\left[R\right]\{\ddot{u}\} \tag{1}$$

where subscripts s, f are denote structure and fluid, ρ is a density and u displacement vector. The coupling matrix is denoted as:

$$\left[R\right] = \oint_S \left[N_f\right]^T \left[N_S\right] dS \tag{2}$$

where N_f , N_s are shape functions for fluid and the structural surface of the coupled interface.

The coupled acoustic equation is:

$$\left[M_f\right]\{\ddot{p}\} + \left[C_f\right]\{\dot{p}\} + \left[K_f\right]\{p\} = -\rho\left[R\right]\{\ddot{u}\} \tag{3}$$

The load applied to the structure surface by the fluid is given by

$$\left[F_S\right] = \left[R\right]^T \{p\} \tag{4}$$

Dynamic equation of structure becomes,

$$\left[M_S\right]\{\ddot{u}\} + \left[C_S\right]\{\dot{u}\} + \left[K_S\right]\{u\} = \{R_S\} + \left[R\right]^T \{p\} \tag{5}$$

Thus, the coupled equation is:

$$\begin{bmatrix} M_S & 0 \\ \rho\left[R\right] & M_f \end{bmatrix} \begin{Bmatrix} \ddot{u} \\ \ddot{p} \end{Bmatrix} + \begin{bmatrix} C_S & 0 \\ 0 & C_f \end{bmatrix} \begin{Bmatrix} \dot{u} \\ \dot{p} \end{Bmatrix} + \begin{bmatrix} K_S & \left[R\right]^T \\ 0 & K_f \end{bmatrix} \begin{Bmatrix} u \\ p \end{Bmatrix} = \begin{Bmatrix} F_S \\ 0 \end{Bmatrix} \tag{6}$$

where:

p is pressure;
$\left[M_f\right]$ is the mass matrix for fluid;
$\left[C_f\right]$ is the damping matrix for fluid;
$\left[K_f\right]$ is the stiffness matrix for fluid;
$\left\{F_f\right\}$ is the acoustic load vector;
$\left[N_f\right]$shape function related to the fluid;
$[R]$ is the coupling matrix;
$[M_c]$ is the mass matrix for the structure;
$[C_s]$ is the damping matrix for structure;
$[K_s]$ is the stiffness matrix for structure;
$\{F_s\}$ is the structural load vector.

3. Finite Element Simulation of Impedance Tube Test

The Finite element model is based on fluid-structure interaction problem [2]. The matrix formulation is given in section 2.

3.1. Geometry model

The geometric mode ANSYS software [3] based on the finite element method has been used to develop the numerical simulation. In ANSYS there are two specific acoustic elements that correspond to the impedance of the tube with which the test of the acoustic material is carried out. The acoustic material is modeled as a disk with a diameter of 100 mm and a thickness of 10 mm. The wedge between the eastern sample and the source of sound impact is a cylinder with a diameter of 100mm and a height of 500mm. The geometry model of the boundary value problem is shown in Fig. 1.

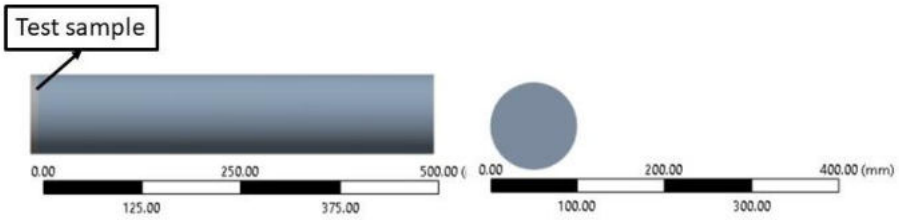

Fig. 1 The geometry model of the boundary value problem

In a vibro-acoustic analysis, typically are used two main physics regions:

- Structural Region: This region involves solid structures that can vibrate. It includes the material properties, boundary conditions, and any external forces or excitations applied to the structure. The structural region is responsible for capturing the mechanical vibrations of the solid components.
- Acoustic Region: This region involves the fluid medium (usually air) through which sound waves propagate. It includes the acoustic properties of the fluid, such as density and speed of sound, as well as boundary conditions like impedance or radiation boundaries. The acoustic region captures the propagation of sound waves generated by the vibrating structure. The interaction between these two regions is crucial in vibroacoustic analysis. The vibrations from the structural region generate sound waves in the acoustic region, and these sound waves can, in turn, affect the vibrations of the structure.

3.2. Material model

The material porous acoustic sample is based on The Johnson-Champoux-Allard (JCA) [4] The Johnson-Champoux-Allard (JCA) model is a mathematical model that describes the acoustical properties of **air-filled porous materials** using parameters such as flow resistivity, porosity, tortuosity, and two characteristic lengths. The JCA model uses the following five parameters to describe the sound propagation through a porous sound

absorbing material: the flow resistivity Ξ ; the porosity Φ ; ,the tortuosity $\alpha\infty$; the thermal and viscous characteristic lengths Λ,Λ'.

ANSYS software based on the finite element method has been used to develop the numerical simulation. In ANSYS there are two specific acoustic elements are used.

The boundary value problem is modeled with 73190 nodes and 18262 elements. (Fig. 2). The governing equation for acoustics, namely the 3-D wave equation, has been discretized taking into account the coupling of acoustic pressure and structural motion at the interface. The element node has four degrees of freedom per node: translations in the nodal x, y and z directions, and pressure.

The FLUID220 FE is used. The FLUID220 is a higher-order 3-D 20-node solid element that exhibits quadratic pressure behavior. The frequency interval was prescribed [0 – 1600 Hz].

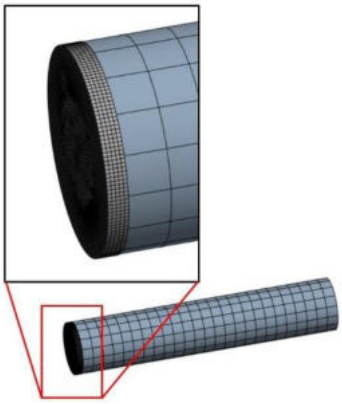

Fig. 2 The FE model of boundary value problem for impedance tube

Boundary conditions are shown in Fig. 3.

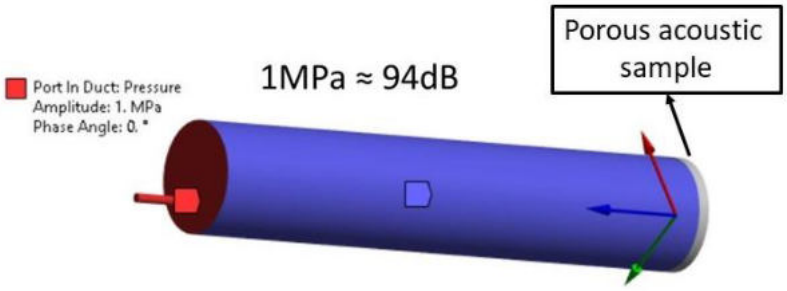

Fig. 3 Boundary conditions prescribed on boundary value problem for impedance tube

3.4. Numerical results

An acoustic analysis calculates either the propagation properties of pure acoustic waves in the given environment or the coupled acoustic structural interaction (FSI) As a result of the numerical solution the sound absorption coefficient can be obtained (Fig. 4).

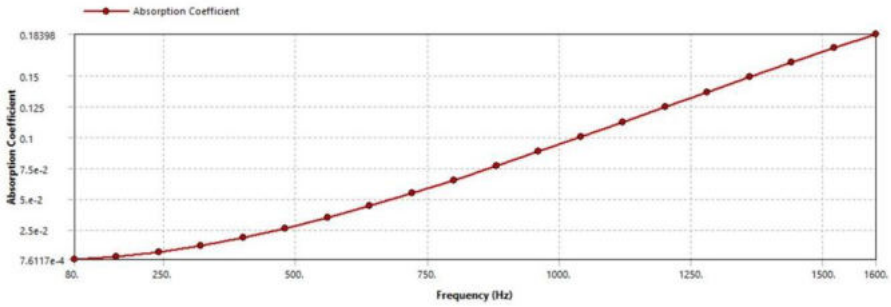

Fig. 4 Absorption coefficient in frequency interval [0 – 1600 Hz]

4. Conclusion

A finite element computational model was proposed for the numerical simulation of the impedance tube experiment. The model can be parameterized both in terms of material parameters and also in terms of geometric parameters. This makes it possible to obtain a series of numerical results for the acoustic parameters of the model. These solutions will be used within the G6006 project for the development of machine learning algorithms designed for the identification of model parameters describing the created acoustic porous materials.

Acknowledgement: *The paper is a part of the research done within the project NATO SPS MYP G6006. The authors express their gratitude for the financial support.*

References

1. Cook R. D., Malkus D.s, Plescha M.E, Eitt R.J, Concepts and applications of finite element analysis, Fourth edition, John Wiley & Sons, 2001, p. 736, ISBN: 978-0-471-35605-9
2. Howard C.Q., Benjamin S. C., Acoustic Analyses using MATLAB® and ANSYS®, CRC press, Inc, 2014, p. 708, ISBN: 978-1-4822-2325-5
3. ANSYS, 2022
4. Allard J. F., Atalla N., Propagation of Sound in Porous Media: Modelling Absorbing materials, Second Edition, John Wiley & Sons, Ltd, p. 358, ISBN:9780470746615, 2009

FACTA UNIVERSITATIS
Series: **Working and Living Environmental Protection** Vol. 21, Nº 4, Special Issue, 2024, pp. 243 - 254
https://doi.org/10.22190/FUWLEP240906023H

Original scientific paper

A CASE STUDY OF LOW-FREQUENCY NOISE

UDC 534.61

Nikola Holeček

University in Ljubljana. Faculty of Chemistry and Chemical Technology,
The Faculty of Environmental Protection, Velenje, Slovenia

ORCID iD: Nikola Holeček N/A

Abstract. *Sound waves below 20 Hz, which are generally inaudible to humans, are called infrasound. When infrasound and the less audible sound of the lowest frequencies (10 to 200Hz) appear as an element that disturbs people and is harmful to health, it is low-frequency noise (LFN). This air-borne noise has a much greater range than normal audible frequency sound and LFN travels much further on the ground. Stronger or longer-lasting infrasound around 7-20 Hz directly affects the human central nervous system and can cause disorientation, anxiety, panic, depression, nausea, discomfort, vomiting, etc. Sooner or later, the waves can lead to damage to the nervous and/or cardiovascular system. It is estimated that about 2.5% of the population may have a low-frequency threshold that is at least 12 dB more sensitive than the average threshold, which corresponds to almost 1,000,000 persons in the age group 50 to 59 years in the EU-15 countries. LFN is recognized as a particular environmental noise problem, especially for sensitive people in their homes. Conventional noise assessment methods are not suitable for LFN and lead to wrong conclusions and consequently to wrong decisions. An LFN source is more difficult to localize, difficult to suppress, and spreads rapidly in all directions so that it can be heard over great distances. All existing sound field visualization methods have a lower frequency limit of 125 HZ. Low-frequency waves surround the noise source and such a source is practically "undirected". In the paper, we described the LFN assessment carried out, which we identified in a commercial/residential building. The measurements were carried out in the immediate vicinity (3-4 km as the crow flies) of the object in question, at the site of industrial facilities (V1 and OM2), the pond complex, and the gas and transformer station. The LFN in the facility was initially unidentified, and the source search diagnostics were based on the method of comparing the generic spectral distributions of the LFN in the facility with other selected measurement positions.*

Key words: *low frequency noise, low frequency noise identification method*

Received September 6, 2024 / Accepted October 9, 2024
Corresponding author: Nikola Holeček
University in Ljubljana. Faculty of Chemistry and Chemical Technology, The Faculty of Environmental Protection, Trg mladosti 7, 3320 Velenje, Slovenia
E-mail: nikola.holecek@fkkt.uni-lj

1. INTRODUCTION

Usually, we use the word sound to denote only the human-audible part of this wave with frequencies in the range between 20 Hz and 20,000 Hz. Sound waves below 20 oscillations per second, which are generally inaudible to humans, are called infrasound, also low-frequency sound (LFS). When infrasound and less audible sound of the lowest frequencies (10 to 200 Hz) appear as an element disturbing and harmful to human health, it is low-frequency noise (LFN). The greatest and most harmful effect on the brain is the sound frequency of 7-8 Hz. (Novak, 2021). In the LFN region, hollow structures in the body are affected: 5 Hz for the chest, 20 Hz for the head, and 80 Hz for the eye cavity.

About 2.5% of the population with a low-frequency threshold that is at least 12 dB more sensitive than the average threshold corresponds to almost 1,000,000 people in the 50-59 age group in the EU-15 countries. This is a group for whom low-frequency noise causes special problems. (Leventhal, 2004).

LFN spreads both by land and by air. LFN traveling through the air has a much greater range than the sound of normal audible frequencies, and LFN travels much further through the ground. Due to its long wavelengths, LFN is very penetrating and reaches large distances, even 5 kilometres.

Research has shown that the perception and effects of sounds at low frequencies are quite different compared to mid or high frequencies. The main reasons for these differences are as follows:

- weakening of the sense of pitch when the sound frequency falls below 60 Hz;
- detecting sounds such as pulsations and oscillations;
- a significantly faster increase in loudness and interference with increasing sound pressure levels at low frequencies than at medium or high frequencies;
- complaints related to a feeling of pressure in the ears;
- disturbances caused by secondary effects, such as the rattling of building elements, windows, and doors or the clinking of objects;
- lower sound transmission losses in buildings at low frequencies than at medium or high frequencies.

Evaluation procedures should be modified to evaluate sounds with a strong representation of low-frequency components (LFCs). The measurement site can be changed and the frequency evaluation is irrelevant because sound with strong low-frequency content causes greater disturbances than predicted by the A-weighted sound pressure level. (ISO 1996-1, 2011).

2. LONG-DISTANCE NOISE TRANSMISSION

The environment in which noise propagates is called the sound field, which includes the sound source, the propagation pathway and the receiver (emission, transmission and immission). For immission, we can take the equivalent level of sound pressure in the octave band at the receiving point in the direction of the wind (Wind Direction) L_{fT} (DW) is calculated for eight octave bands with a rated mean frequency from 63 Hz to 8 kHz according to the equation (1) (SIST ISO 9613-2, 2012):

$$L_{fT}(DW) = L_W + D_C - A \tag{1}$$

where

L_W is the sound power per octave band, in decibels, relative to the reference sound power 10^{-12} W (1 pW), D_C directivity correction, in decibels, describing the degree of deviation of the equivalent continuous level of the point source in a given direction relative to the level of the undirected point sound source radiating the sound power L_W; D_C is equal to the sum of the D_I directivity index, the point source, and the D_Ω index, which takes into account the propagation of sound to a spatial angle of less than 4π steradians; for an undirected point sound source radiating into unobstructed space, $D_C = 0$ dB. An attenuation in octave bands, in decibels, occurs during propagation from the point source to the receiver. The attenuation of A in equation (1) is given by equation (2):

$$A = A_{div} + A_{atm} + A_{gr} + A_{bar} + A_{misc} \tag{2}$$

In transmission, there is a sound attenuation effect caused by the following physical effects:

- geometric divergence, A_{div}
- atmospheric absorption, A_{atm}
- ground effect, A_{gr} sound attenuation due to soil effect (solid, porous or mixed soil)
- reflection from the surface, A_{bar} attenuation of sound due to obstacles
- sound attenuation due to various other effects of A_{misc}, e.g. obstacle diffraction: attenuation of sound when propagating through overgrowth, through industrial areas, and when propagating through built-up areas, (SIST ISO 9613-2, 2012).

2.1. Geometric divergence

The geometric divergence Adiv takes into account the spherical propagation from a point sound source in a free field; the corresponding attenuation in decibels is the same (Equation 3).

$$A_{div} = \left[20lg\left(\frac{r}{r_0}\right) + 11\right] dB \tag{3}$$

where d is the distance from the source to the receiver, in meters, d_0 is the reference distance (= 1 m)

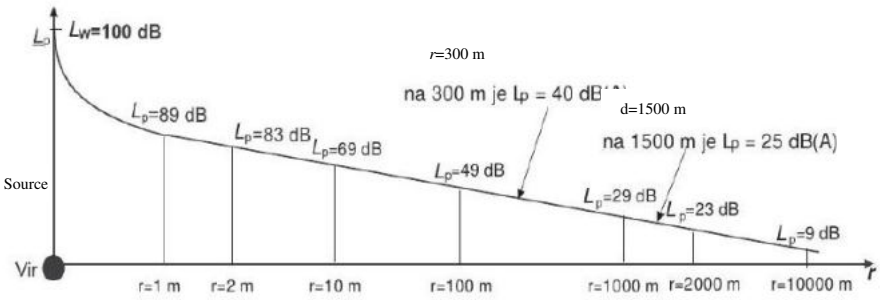

Fig. 1 Noise attenuation due to geometric divergence (Čudina, 2020)

2.2. Atmospheric absorption

The attenuation due to atmospheric absorption A_{atm}, in decibels, during the propagation of sound at a distance r in meters, is given by equation (4):

$$A_{atm} = \frac{\alpha\, r}{1000} \tag{4}$$

where α is the atmospheric attenuation coefficient of sound in the atmosphere, in decibels per kilometre, for each octave band at the mean frequency of the band (see Table 1). The coefficient of atmospheric attenuation in the atmosphere is highly dependent on the frequency of sound, ambient temperature and relative humidity, but significantly less on the ambient pressure. It is evident that at low frequencies, atmospheric dissipation up to 1000 is less than that at higher frequencies 8000 Hz.

Table 1 Coefficient of atmospheric attenuation of sound due to atmosphere α for octave noise bands (ISO 9613-2, 2012)

Tempera-ture	Relative Humidity	Atmospheric attenuation coefficient α, dB/km							
		Nominal midband frequency, Hz							
^{0}C	%	63	125	250	500	1000	2000	4000	8000
10	70	0.1	0.4	1.0	1.9	3.7	9.7	32.8	117
20	70	0.1	0.3	1.1	2.8	5.0	9.0	22.9	76.6
30	70	0.1	0.3	1.0	3.1	7.4	12.7	23.1	59.3
15	20	0.3	0.6	1.2	2.7	8.2	28.2	88.8	202
15	50	0.1	0.5	1.2	2.2	4.2	10.8	36.2	129
15	80	0.1	0.3	1.1	2.4	4.1	8.3	23.7	82.8

2.3. Amplification of low frequencies in rooms due to interference

The ripples of sound in an enclosed space excite modal frequencies, which are the resonant frequencies of a specific space. If the geometry of the room is square, and the dimensions of the room are comparable to the wavelength of sound, there may be marked fluctuations in sound pressure in it. Comparison of annoyances of different types of noise sources at otherwise equal levels of room noise and shorter wavelengths, such modes of oscillation are not pronounced, due to other effects, e.g. diffusion (Deželak, 2020).

Changes in indoor sound pressure levels can be significant, and in contrast to high frequencies, they exceed 20 dB. Also, the subjective sense of loudness, and especially its variations, are significantly greater at low frequencies than at high frequencies. For example, an increment of 5 dB at 30 Hz is equivalent to an increment of 10 dB at 1 kHz, depending on changes in the subjective sense of volume. So once a low-frequency sound is detected, it quickly becomes extremely unfavourable.

In closed spaces, there are different ways of sound fluctuation, which is the result of the formation of standing waves, which occur with the interference between incident and reflected sound waves from individual walls or various obstacles in the room. As a result, the noise level as a result of such a standing wave can be strongly dependent on the location in the room. Modes of such oscillation occur at certain frequencies called resonant frequencies (eigenfrequencies), in which the distance between individual amplitudes is determined by a multiple of the corresponding wavelength. The resonant frequencies f_0 of a square room can be calculated using equation (4) (Deželak, 2020):

$$f_0 = \frac{c_0}{2}\sqrt{(\frac{l}{L_x})^2 + (\frac{m}{L_y})^2 + (\frac{n}{L_z})^2} \quad (4)$$

where f_0 = frequency of natural oscillation Hz c_0 = speed of sound, l = mode of oscillation along the length of the room m = mode of oscillation over the width of the room n = mode of oscillation over the height of the room L_x, L_y, L_z = length, width and height of the room in meters (Larsen, 1972).

3 Noise Assessment with Strong LFCs Representation

LFN is recognized as a particular environmental noise problem and research has shown that A-weighted alone is not sufficient to evaluate sounds with characteristic tonality, impulsiveness, or a strong representation of low-frequency components. To estimate the long-term response of the community to sound disturbance with some of these specific characteristics, a decibel correction shall be added to the A-weighted sound exposure level or to the A-weighted equivalent continuous sound pressure level. Research has also shown that the sounds of different means of transportation or industrial noises elicit different community responses to a disturbance at an otherwise equal A-weighted equivalent continuous sound pressure level.

3.1. Basic Physical Indicators for Sound

In acoustics, there are several different physical indicators that describe sound expressed in decibels (e.g. sound pressure level, maximum sound pressure level, equivalent continuous sound pressure level). The levels corresponding to these physical indicators usually differ for the same type of sound. This often leads to confusion. It is therefore necessary to define basic physical quantities (e.g. sound pressure level, maximum sound pressure level, equivalent continuous sound pressure level). A - weighted is generally used to evaluate all sound sources, except for high-energy impulse sounds and sounds with a strong representation of low-frequency components. A - weighted should not be used to measure peak sound pressure and LFN.

4 Identification of Low-frequency Noise Using a Practical Example

We conducted an LFN assessment that disturbs residents in a commercial/residential building. Measurements were continued in the vicinity (3-4 km as the crow flies) from the object under consideration, where industrial facilities (Vand OM), a complex of ponds (P), a gas and transformer station are located. The LFN in the facility is unidentified, the source search diagnostics was based on the method of comparing the generic spectral distributions of the LFN in the facility with the other selected measurement positions described in Table 2.

Measurement equipment is used: Sound analyser, microphone and preamplifier and handheld acoustic calibrator: NTI AUDIO, XL2-TA. Handheld acoustic calibrator: Bruel & Kjaer 1256. Software used, data transfer: XL2 Projector PRO Display & Remote-Control Tool for the XL2 Sound Level Meter.

Table 2 Description of measuring positions 1 - 12.

Measuring position MP	Description of the measuring point
1.	Interior of the building at 9:00 p.m.
2.	Exterior of the facility at 9:15 p.m.
3.	Transformer station
4.	P (Peer ponds complex with a pump system)
5.	B
6.	In front of the V1 factory
7.	OM1
8.	OM2
9.	G
10.	Gas Plant
11.	J
12.	Interior of the building at 11:00 p.m.

Conventional noise assessment methods are based on A-weighted L_A sound, which greatly reduces the emphasis on low and high frequencies. A - weighted can lower the amplitude too much at low frequencies and their impact can be ignored too quickly. Many countries already have standards for the measurement and characterisation of low-frequency noise. An example of such a standard in Germany is DIN 45680: Measurement and evaluation of low-frequency environmental noise. The recommendation in the standard is that measurements should be made without weighting/evaluation. Table 3 therefore shows the measured unweighted/linear values of the L_z , Z- weighting sound pressure level (SPL) at 1/3 octaves (One-Third-Octave bands). These results are graphically illustrated in Figure 3.

Table 3 SPL as $L_{z\,max}$ in dB in the frequency interval from 6.3 Hz to 250 Hz

MP	6.3 Hz	8 Hz	10 Hz	12.5 Hz	16 Hz	20 Hz	25 Hz	40 Hz	50 Hz	63 Hz	80 Hz	100 Hz	125 Hz	160 Hz	200 Hz	250 Hz
1	39.1	42.9	44.9	44.2	45.5	48.8	49.0	53.1	49.4	60.7	57.2	61.0	61.7	64.5	68.7	59.0
2	39.9	38.1	34.9	39.7	33.1	35.2	33.3	43.4	46.1	42.7	45.3	41.3	37.7	28.8	30.3	30.7
3	47.0	48.1	52.0	45.2	41.5	48.3	42.5	40.7	34.5	31.0	29.0	37.3	28.1	28.7	32.1	29.2
4	39.4	38.6	39.1	37.0	36.6	36.1	34.3	34.5	39.0	41.8	40.0	42.9	40.5	37.5	32.1	34.8
5	34.8	37.2	31.2	36.7	34.1	33.3	32.7	36.9	48.4	52.2	60.0	53.7	45.6	36.7	37.7	36.5
6	44.6	47.0	44.7	47.5	57.5	48.1	63.4	54.8	55.4	45.9	45.9	50.1	42.9	39.6	36.9	33.8
7	38.3	38.3	40.4	43.6	53.0	56.0	53.9	69.0	62.6	64.8	61.3	55.9	57.9	50.7	53.5	50.7
8	44.2	48.2	46.1	44.6	44.2	46.5	45.5	47.9	49.1	43.5	46.7	40.2	37.0	40.0	36.0	34.3
9	52.5	53.0	53.0	52.9	67.5	55.7	66.4	55.6	56.9	50.8	51.1	53.3	48.1	45.3	44.5	42.9
10	42.9	46.5	47.0	47.3	49.9	49.3	46.5	43.0	53.2	43.7	43.1	43.6	43.9	40.2	33.2	29.9
11	53.3	53.1	50.7	43.7	41.5	38.3	38.7	37.5	32.3	31.1	29.0	40.3	36.7	30.8	28.7	31.7
12	36.5	36.2	34.6	33.2	33.8	33.9	32.5	27.3	29.2	33.6	32.2	30.5	27.0	29.9	26.9	29.0

We were interested in whether LFN limit values were exceeded inside the building (Table 4). Graph 2 shows that they are vastly exceeded in the range of 40 Hz upwards (Figures 2 & 3).

Table 4 LFN limit values at night in accordance with DIN 45680

f (Hz)	10	12,5	16	20	25	31,5	40	50	63	80	100
L_z (dB)	95	86.5	79	71	63	55.5	48	40	33.5	33	33.5

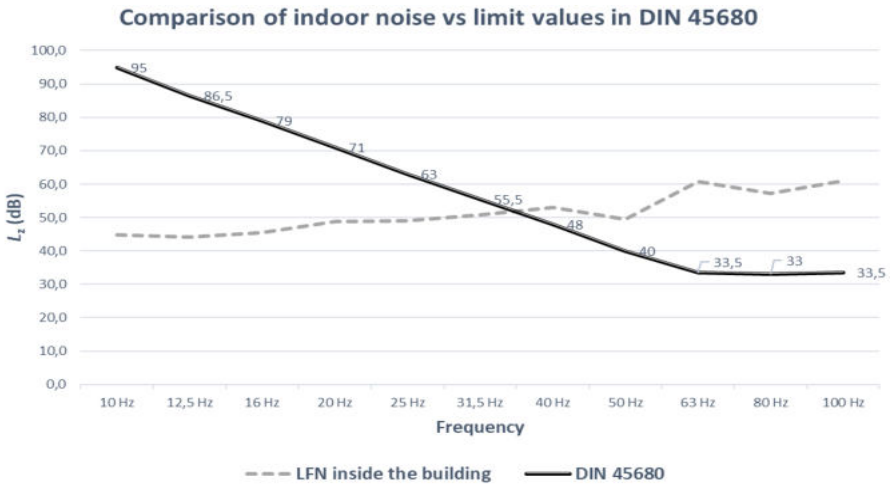

Fig. 2 Comparison of indoor noise with limit values in DIN 45 680.

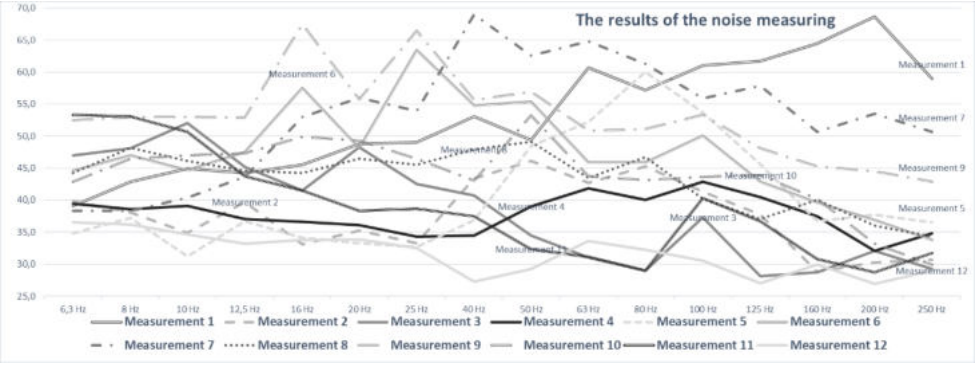

Fig. 3 LFH expressed as $L_{z\,max}$ at One-Third-Octave bands in the interval 6.3 – 250 Hz, all measurement positions 1 to 12.

4.1. Measurement results

Figures 4 – 9 compare the results of the measurements.

In Figure 4, the spectral distribution of LFN in the interior of the facility is measured at different times: at 9 p.m. and 11 p.m., as shown in Table 2. The frequency of 63 Hz stands out. The frequency of 200 Hz is the result of an event in the object itself, it is not present in the second measurement in the building.

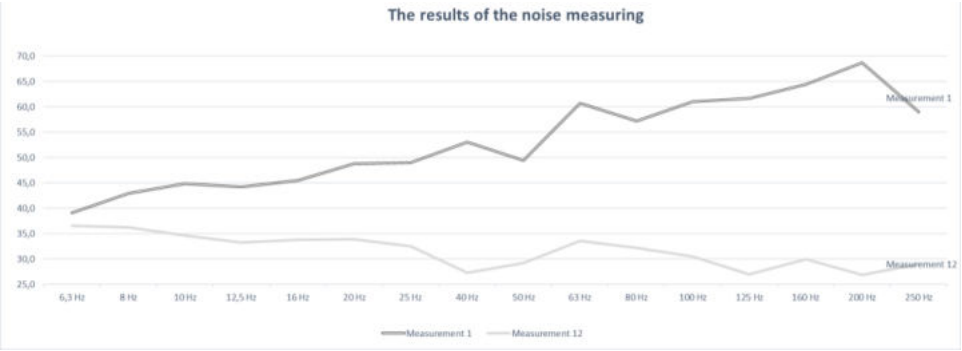

Fig. 4 Measurement 1 and 12 (Table 2). LFN expressed as $L_{z\,max}$ on One-Third-Octave bands in the interval 6.3 – 250 Hz, measurements made at different time intervals.

Figure 5 provides a graphical representation of the measurements 1, 2, 3 in 12 (see Table 2). Measurement 2 taken in front of the house itself shows the same generic spectrum as in the house itself. Measurement 3 in front of the transformer station shows a typical 100 Hz, which is not detected in the house. The transformer station can be ruled out as the dominant cause of LFN in the house.

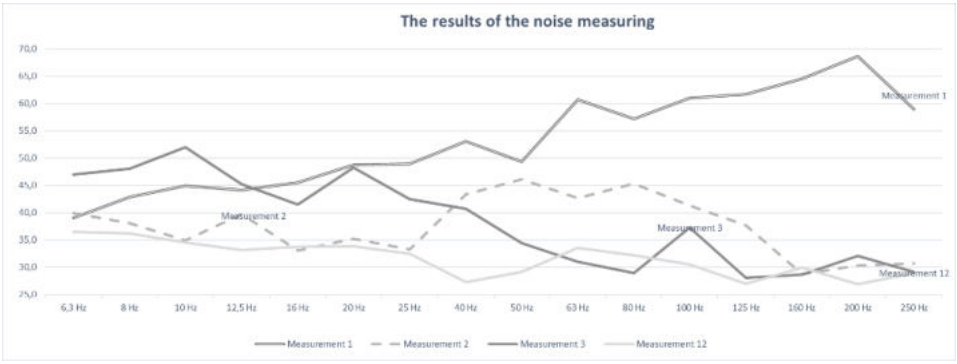

Fig. 5 Measurement 1, 2, 3 and 12 (Table 2). LFN is expressed as $L_{z\,max}$ on One-Third-Octave bands in the range of 6.3 – 250 Hz.

Figure 6 provides a graphical representation of the measurements 1, 4, 5 in 12 (see Table 2). Measurement 4 shows the same generic spectrum as in the house. It is necessary to investigate why this occurs, so what is the P (Peer -house connection? Measurement 5 before measurement point B shows 80 Hz, which is detected at measurement point O.

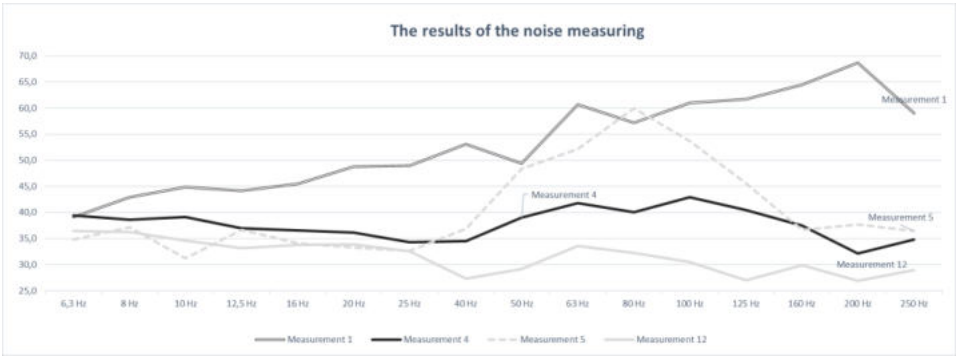

Fig 6. Measurement 1, 4, 5 and 12 (see Table 2). LFN is expressed as $L_{z\,max}$ at One-Third-Octave bands in the interval 6.3 – 250 Hz.

Figure 7 provides a graphical representation of the measurements 1, 6, 7 in 12 (see Table 2). Measurement 6 shows the expressed LFN at 16 and 25 Hz, which are not detected in the house itself. Measurement 7 shows a distinct 40 Hz, which is not typical of a house, so O can also be ruled out with a high degree of probability.

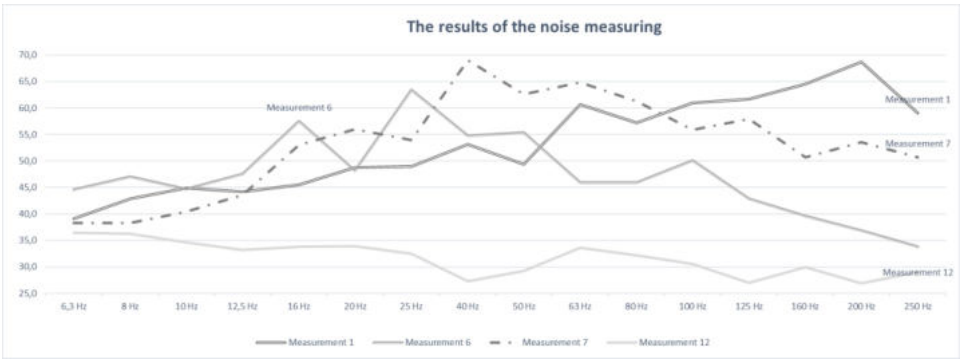

Fig. 7 Measurement 1, 6, 7 and 12 (see Table 2). LFN is expressed as $L_{z\,max}$ at One-Third-Octave bands in the range of 6.3 – 250 Hz.

Figure 8 provides a graphical representation of the measurements 1, 8, 9 in 12 (see Table 2). Measurement 8 shows LFN, which is not typical for the generic spectrum in the house! Measurement 9 shows prominent 16 and 25 Hz, which are not characteristic of the house, so V can also be ruled out.

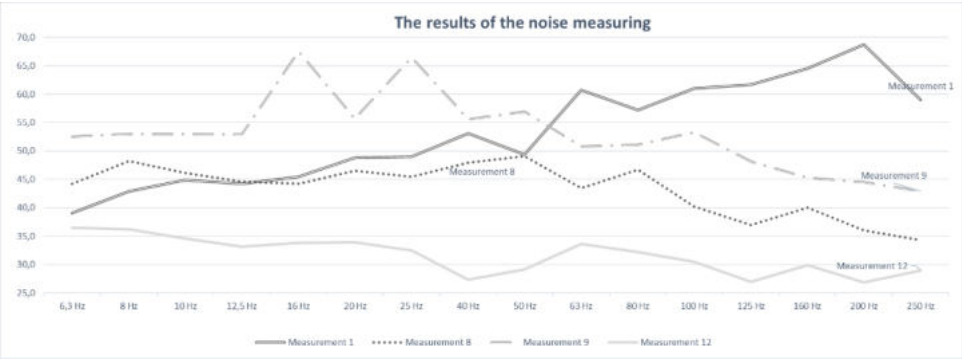

Fig. 8 Measurement 1, 8, 9 and 12 (see Table 2). LFN is expressed as $L_{z\,max}$ One-Third-Octave bands in the interval 6.3 – 250 Hz.

Figure 9 provides a graphical representation of the measurements 1, 10, 11 in 12 (see Table 2). Measurement 10 performed at the gas plant shows LFN, which is partially similar to the generic spectrum in the house in terms of the LFN P (Peer) form.

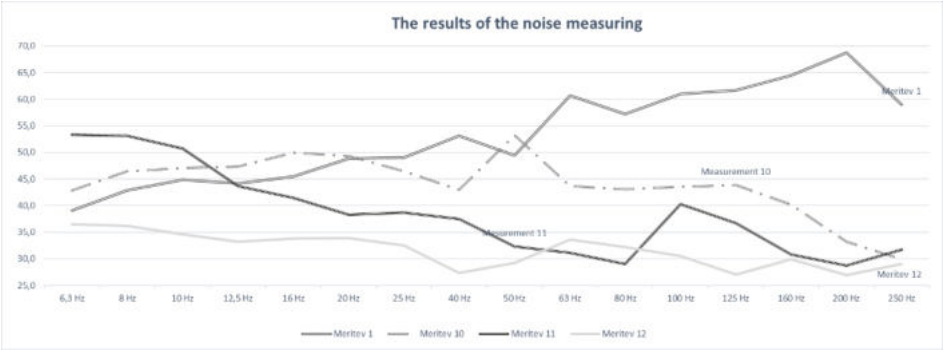

Fig. 9 Measurement 1, 10, 11 and 12 (see Table 2). LFN is expressed as $L_{z\,max}$ at One-Third-Octave bands in the range of 6.3 – 250 Hz.

4.2. Comment Measurements

The threshold of harmfulness of low-frequency noise is not sufficiently defined by the general noise determination and assessment procedure, which refers to certain relevant standards (A-weighted sound level). Since LFN is generally inaudible or poorly audible to humans, we considered it as a separate category of environmental pollution and looked at specific international standards such as DIN 45680 and ISO 7196.

On the basis of the measurements carried out, we excluded the transformer station and both industrial facilities as the cause of LFN in the facility in question and estimated that the pond system was in the first place and the gas station was a possible source in the second place.

5. CONCLUSION

Methods of describing, measuring, and estimating environmental noise are used to characterize LFN and are related to the human response to noise. The increase in LFN brings a number of adverse consequences to the environment, but the exact relationship between response and dose still remains a subject of scientific debate. In addition, it is important that all the methods used are practically feasible in the social, economic, and political environment in which they are used. For these reasons, there is a very wide range of different methods currently used around the world for different types of noise, which causes great problems for international comparison and understanding. If we analyse the recommendations for conducting LFN measurements, we can highlight the following facts:

- The usable frequency range is from about 5 Hz to about 100 Hz. In the range below about 20 Hz, some countries use G-weighted to evaluate sound. Above about 15 Hz, several countries use Octave or One-Third-Octave bands analysis in the range of about 16 Hz to 100 Hz. (G-weighted is specified in ISO 7196).
- States with special procedures for assessing LFN do not use A- weighted in the same way that it is used to evaluate medium and high-frequency sound. LFN is only rated in a limited frequency range as noted above.
- A number of states have set criteria for LFN based on indoor sound measurements rather than outdoors. Others use indoor and outdoor measurements in their national standards.
- One of the questions in estimating LFN is whether room resonances at low frequencies can create conditions that are difficult to predict based on outdoor measurements. This can be especially important when evaluating specific dwellings. However, outdoor measurements may be sufficient to estimate the prevalence of severe disturbance in the population environment.
- LFN-induced rusting in building elements is an important factor in the disruption it causes. The methods in Appendix B of ISO 1996-1 specifically take into account the factor of this roaring associated with high-energy pulsed sound. Some countries have set indoor criteria for continuous sound, which include both audible sound and roaring sound. Others have established separate boundaries for enclosed spaces when assessing sound-induced buzzing.

In this paper, we described the LFN assessment that we identified in the commercial/residential facility. Measurements were carried out up to 3-4 km as the crow flies from the object under consideration, on the site of industrial facilities, pond complexes, gas and transformer stations. The cause of LFN in the facility was initially unidentified, but the source search diagnostics was based on the method of comparing the generic spectral distributions (Z – weighting) of LFN inside and outside the facility with other selected measurement positions. Based on the analysis shown, the actual source of LFN is recognized with a high degree of probability.

Acknowledgement: *The author of the research publicly thanks the client for the research on noise recognition on private property.*

REFERENCES

1. Novak, B. (2021). Nizkofrekvenčni hrup je zdravju nevarno valovanje. 10. februar 2021 http://nf-hrup.si/2
2. Leventhall, H. G. (2004). Low frequency noise and annoyance. *Noise Health*; volume 6; issue 23, 59-72. https://www.noiseandhealth.org/article.asp?issn=1463_741
3. Deželak, Vetrne elektrarne in motenost okolja z njihovim hrupom, Zavod za varstvo pri delu (ZVD), Ljubljana 2020, »International scientific consultation on wind turbine noise and possible impacts on living environment«
4. Larsen, Reverberation Process at Low Frequencies, Bruel&Kjaer , Technical Review No. 4, 1978
5. SIST ISO 1996, 2011, Acoustics – Description, measurement and assessment of environmental noise Part 1: Basic quantities and assessment procedures
6. SIST ISO 9613, 2012, Acoustics –Attenuation of sound during propagation outdoors – Part 2: General method of calculation
7. Čudina, Vpliv hrupa vetrnih elektraran, Ljubljana 2020, »International scientific consultation on wind turbine noise and possible impacts on living environment«
8. Persson, K., (1997): 'Estimation of Environmental Low Frequency Noise – a Comparison of Previous Suggestions and the New Swedish Recommendation', *Proceedings of the 8th International Meeting on Low Frequency Noise and Vibration*, Gothenburg (pp. 135-141).
9. Piorr, D. and Wietlake, K., (1990): 'Assessment of Low Frequency Noise in the Vicinity of Industrial Noise Sources', *Journal of Low Frequency Noise and Vibration*, Volume 9 (3:116-119).
10. Cocchi, A., Fausti, P. and Piva, S., (1992): 'Experimental Characterisation of the Low Frequency Noise Annoyance Arising from Industrial Plants', *Journal of Low Frequency Noise and Vibration*, Volume 11(4:124-132).
11. Vercammen, M.L.S., (1989): 'Setting Limits for Low Frequency Noise', *Journal of Low Frequency Noise and Vibration*, Volume 8(4:105-109).
12. German Standard DlN 45680 (1997): 'Messung und Bewertung tieffrequenter Gerauschimmissionen in der Nachbarschaft', Deutsches Institut fur Normung e.V., Berlin.

FACTA UNIVERSITATIS
Series: **Working and Living Environmental Protection** Vol. 21, Nº 4, Special Issue, 2024, pp. 255 - 260
https://doi.org/10.22190/FUWLEP240911024Z

Original scientific paper

POLYESTER APPAREL CUTTING WASTE AS SOUND INSULATION MATERIAL

UDC 628.4.08:677.494.674.021.12:534

Koleta Zafirova, Elena Tomovska

University "Ss Cyril and Methodius", Faculty of Technology& Metallurgy, Skopje, N. Macedonia

ORCID iDs: Koleta Zafirova https://orcid.org/0000-0002-0429-3977
Elena Tomovska https://orcid.org/0000-0001-5714-2155

Abstract. *This study developed an insulation structure using waste from apparel cutting and examined its sound insulation capabilities. Shredded polyester apparel cuttings served as the primary material for this structure. Results indicate that the insulation made from apparel waste exhibits superior sound absorption properties compared to conventional sound and thermal insulators. The average sound absorption ranged from 54.7% to 74.7% across frequencies from 250 to 2000 Hz. This research proposes a method to reduce environmental pollution by repurposing polyester apparel waste for insulation in roofs and internal walls.*

Key words: *apparel cutting waste, sound insulation*

1. INTRODUCTION

Traditionally, textiles in buildings primarily serve aesthetic purposes but also offer various functional advantages. Decorative textile materials such as carpets, curtains, upholstery, and textile wall coverings play a significant role in the acoustic conditioning of spaces. Additionally, textile materials, being porous, are commonly utilized as sound insulators and absorbers in building construction, with non-woven textiles being the preferred structure for this purpose. Numerous studies by researchers including Shoshani and Yakubov [1, 2, 6], Shoshani and Wilding [3], Shoshani and Rosenhouse [4], and Lou et al. [5], have investigated the acoustic properties of non-woven fabrics. Similarly, research on woven [7, 8, 9] and knitted fabrics [10, 11] has also been conducted. Garai and Pompoli [12], as well as Narang [13], focused on studying the sound absorption coefficient of polyester fiber materials concerning mass density and sample thickness values.

Received September 11 / Accepted October 7, 2024
Corresponding author: Koleta Zafirova
University "Ss Cyril and Methodius", Faculty of Technology& Metallurgy, Ruger Boskovic 161000 Skopje, North Macedonia
E-mail: koleta@tmf.ukim.edu.mk

However, few studies have explored the use of textile waste for insulation purposes. While research has examined the thermal insulation properties of textiles [14, 15] and their potential as sound-absorbing materials [5], there is a notable gap in addressing textile waste specifically for insulation applications. Generally, textiles with a loose structure, such as knits, are preferred for recycling due to lower energy consumption and the effort required to return them to fibrous form compared to woven fabrics. Whether virgin or recycled, the effectiveness of sound absorption materials depends on their porous structure and thickness.

Today, pressing environmental concerns stem from the escalating global production and consumption of textiles, generating significant volumes of textile waste worldwide. Therefore, finding innovative ways to reuse textile waste not only offers environmental benefits but also promotes sustainability and economic efficiency. This research endeavors to develop a novel insulation structure using waste from woven polyester apparel cuttings and assess its sound insulation properties.

2. EXPERIMENTAL

2.1. Materials

Polyester fabric cuttings were used as raw material for designing a new insulation structure. The characteristics of fabrics used for the preparation of samples A, C, and D are shown in Table 1. Differences among the three fabrics arise from mass, structural characteristics and fibre content. Sample B obtained from knitted polyester fabric in a partly fibrous form was used for comparison.

Table 1 Polyester fabric characteristics

Fabric	A	C	D
Thickness (mm)	0.16	1.2	1.6
Cv (%)	2.17	1.80	1.38
Mass per unit area (g/m^2)	92	245	272
Cv (%)	3.13	1.16	1.38
Warp density (cm^{-1})	74	37	44
Weft density (cm^{-1})	45	25	28
Warp count (tex)	7.4	36	36
Weft count (tex)	7.4	36	36
Fiber content (%)	100 PES	100 PES	95/5 PES/Lycra

To prepare the fabric cuttings for the insulation structure they were additionally shredded in different sizes using a cutting machine with rotational knives, as given in Table 2. Subsequently, the shreddings were used as filler in casings made of 100% polypropylene non-woven fabric. To be comparable to commercially available insulation materials the designed sample thickness was 100mm. The insolation structure was secured by stitching with 4 seams along its length and width distanced by 15 cm. A total of ten samples, of which nine samples with different degrees of shredded fabric and one sample with a partially fibrous structure were prepared.

Table 2 Sample characteristics and preparation

Sample	Type of material	Fabric form	ρ (g/m^3)
A_1	cutting waste	partially cut, pieces with different size	215.6
A_2	cutting waste	cut into small pieces with different size	209.1
A_3	cutting waste	in original form without preparation	226.4
A_4	cutting waste	in original form without preparation	249.4
B	knitted fabric partially fibrous	mechanical recycling	127.0
C_1	cutting waste	cut, pieces' average dimensions 6x4cm	249.4
C_2	cutting waste	cut, pieces' average dimensions 8x4cm	265.4
D	cutting waste	cut, pieces' average dimensions 8x4cm	173.9
ABC	cutting waste -fabric A	A- cut, pieces with different size	164.3
	knitted fabric partially fibrous -fabric B	B- knitted fabric partially fibrous	
	cutting waste -fabric C	C-cut, pieces' average dimensions 6x4cm	
ABD	cutting waste -fabric A	A- cut, pieces with different size	163.0
	knitted fabric partially fibrous -fabric B	B- knitted fabric partially fibrous	
	cutting waste -fabric D	D- cut, pieces' average dimensions 8x4cm	

2.2. Methods

As the obtained sample dimensions were not suitable for standard sound absorption tests, a modified testing procedure based on the impendence tube technique was used. The procedure used a sound generator (KYE Systems Corp Multimedia hi-fi speaker system sp-diameter), microphone (A4 mi-10), GoldWave computer software for transmitted sound recording and filtering, and OriginPro 8.5.1 software for analyzing the recorded sound. The sound signals were generated for 30s on frequencies of 125, 250, 500, 1000, 2000, and 4000Hz, i.e. 5s on each frequency. Three tests for each of the samples were conducted. The recorded sound was filtered using Gold Wave software on each of the 6 frequencies, with a cutoff frequency of ±5%. The same procedure was conducted for a referent sample, using air as a sound transmission medium. The amplitudes of the sound signal on each frequency for each sample were recorded.

3. Results and Discussion

To calculate the sound absorption coefficient (α) the difference in amplitude of the sample sound absorption and the referent sound absorption was used:

$$\alpha = 100 - \frac{b}{c} \cdot 100(\%) \tag{1}$$

where:

b – amplitude of the output sound waves of the insulation structure

c – referent amplitude of the output sound waves

The results for the sound absorption coefficients of the samples are given in Table 3, whereas the resulting sound absorption curves in Figure 1.

In order to obtain a single figure rating the noise reduction coefficient (NRC) defined as the arithmetic average of sound absorption coefficients at 250, 500, 1000, and 2000Hz was calculated for the samples, Table 3.

Table 3 Sound absorption characteristics of samples

Sample	α (%)						NRC (%)
	125 Hz	250 Hz	500 Hz	1000 Hz	2000 Hz	4000 Hz	
A_1	22.52	41.36	68.94	85.56	80.99	70.33	69.21
A_2	11.89	23.69	69.45	81.45	95.43	73.99	67.51
A_3	29.37	44.62	67.57	77.83	68.27	56.07	64.57
A_4	34.95	55.01	84.16	84.78	67.78	56.07	72.93
B	30.09	41.53	63.00	91.50	85.05	62.81	70.27
C_1	14.05	41.28	70.40	77.97	70.99	71.68	65.16
C_2	32.07	57.72	71.36	75.70	72.59	53.76	69.34
D	13.33	42.20	46.74	78.89	50.99	88.25	54.71
ABC	16.22	50.60	64.25	69.90	91.98	86.71	69.18
ABD	36.76	50.02	76.93	82.75	89.38	61.27	74.77

All samples show increasing sound absorption with the increase in frequency. For the lowest measured frequency of 125Hz, the sound absorption is minor, ranging from 11.89% to 34.95%. At mid frequencies (500, 1000 Hz) an increase of sound absorption can be seen, achieving the maximum values at 1000Hz for most of the samples, ranging from 69,9% to 91.5%. The high frequencies show a trend of decreasing sound absorption.

The obtained insulation structures exhibit sound absorption properties typical of fibrous materials. The sound absorption curves of all samples show the same trend with maximum absorption achieved at the interval of 1000Hz to 2000Hz. Improved absorption at higher frequencies is typical of porous structures, as they function through the mechanism of dissipative absorption which is particularly efficient at high frequencies.

Sound insulators function by blocking the transmission of airborne sound, thus any gaps in the structure allow sound to “leak”, in just the same ways that water can pass through seemingly insignificant holes. Therefore, the more homogenous the textile structures the better their sound insulation properties should be. As homogeneity is easily achieved in structures containing materials in partially fibrous form, such as sample B, in comparison to those made of fabric cuttings, structure B should theoretically have better sound absorption properties. However, the variation coefficient of NRC for the tested samples is 7,3% indicating that all obtained structures, regardless of the preparation method, have comparatively similar sound absorption properties. In other words, when taking into account the human perception of sounds the difference in sound insulation provided by the various samples is negligible. The achieved sound absorption with NRC ranging from 54,71% to 74,77% is comparable to commercially used insulators, such as glass wool (NRC=66,3% for thickness of 50mm and density of 50g/m3), stone wool (NRC=63,8% for thickness of 50mm and density of 80g/m3) or polystyrene (NRC=51,8% for thickness of 50mm and density of 28g/m3) [16].

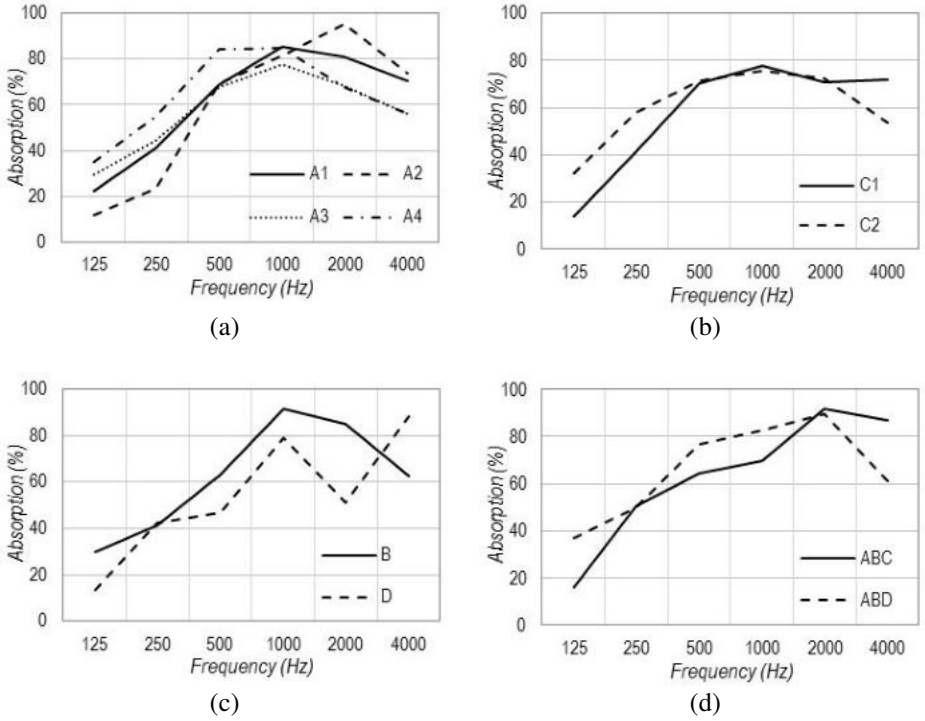

Fig. 1 Absorption curves for samples (a)A, (b) C, (c) B and D, (d) ABC and ABD

4. Conclusion

Sustainability in textiles continues to drive innovative research and development. The research presented in this paper focuses on analyzing the sound insulation properties of a new insulation structure made from polyester apparel cutting waste. The noise reduction coefficient of this structure is comparable to commercially used building insulators for both thermal and sound insulation purposes. Utilizing textile waste as insulation offers environmental, sustainable, and economic benefits due to its ready availability and cost-effective production process. However, its application is currently limited to internal walls and roofing constructions.

References

1. Shoshani,Y., and Yakubov, Y. A model for calculating the noise absorption capacity of nonwoven fiber webs. Textile Research Journal, 1999, 69, p.519.
2. Shoshani,Y., and Yakubov, Y. Numerical assessment of maximal absorption coefficients for nonwoven fiberwebs. Applied Acoustics, 2000, 59, p.77.
3. Shoshani, Y., and Wilding, M.A. Effect of pile parameters on the noise absorption capacity of tufted carpets. Textile Research Journal, 1991, 736, p.736.

4. Shoshani, Y., and Rosenhouse, G. Noise-insulating blankets made of textile. Applied Acoustics 1992, 35, p.129.
5. Lou, C.W., Lin, J.H., and Su, K.H. Recycling polyester and polypropylene nonwoven selvages to produce functional sound absorption composites. Textile Research Journal, 2005, 75, p.390.
6. Shoshani,Y., and Yakubov, Y. Use of Nonwovens of variable porosity as noise control elements. International Nonwovens Journal, 2001, 10, p.23.
7. Shoshani,Y., and Rosenhouse, G. Noise absorption by woven fabrics. Applied Acoustics, 1990, 30, p.321
8. Shoshani,Y.K. Noise absorption by a combination of woven and nonwoven fabrics. Journal of Textile Institute, 1991, 82, p.500.
9. Zafirova, K.,Uzunovich,R. Some Investigations of Sound Absorption Properties of Upholstery Textile Materials, Tekstilna Industrija, 1998, 1-2, p.19.
10. Dias, T., and Monaragala, R. Sound absorbtion in knitted structures for interior noise reduction in automobiles. Measurment Science and Technology, 2006, 17, p.2499.
11. Dias, T., Monaragala, R., and Lay, E. Analysis of thick spacer fabrics to reduce automobile interior noise. Measurment Science and Technology, 2007, 18, p.1979.
12. Garai, M., and Pompoli, F. A simple empirical model of polyester fibre materials for acoustical applications. Applied Acoustics, 2005; 66, p.1383.
13. Narang, P.P. Material parameter selection in polyester fibre insulation for sound transmission and absorption. Applied Acoustics,1995, 45, p.335.
14. Briga-Sa, A. at all., Textile Waste as an alternative thermal insulation building material solution. Construction and Building Material, 2013, 38, p.155.
15. Jordeva S., Tomovska, E., Trajkovic, D., Zafirova, K. (2014) Textile waste as a thermal insulation material, Tekstil 63 (5-6)174-178.
16. Valverde, I. C., Castilla, L. H., Nuñez, D. F., Rodriguez-Senín, E., & de la Mano Ferreire, R. (2013). Development of new insulation panels based on textiles recycled fabrics. *Waste and Biomass Valorization, 4*, 139–146

FACTA UNIVERSITATIS
Series: **Working and Living Environmental Protection** Vol. 21, Nº 4, Special Issue, 2024, pp. 261 - 269
https://doi.org/10.22190/FUWLEP240918025R

Original scientific paper

APPLICATION OF CONTEMPORARY MATERIALIZATION OF INTERIOR PARTITION IN INDUSTRIAL BUILDINGS AS AN ACOUSTIC CHALLENGE

UDC 674.21:725.4:534

Đurđina Rančić, Miomir Vasov

Faculty of Civil Engineering and Architecture, University of Niš, Serbia

ORCID iDs: Đurđina Rančić N/A
Miomir Vasov https://orcid.org/0000-0002-4525-9644

Abstract. *In recent years, the construction of industrial buildings in local areas has been dynamically increasing. In the context of modern architecture and construction, besides functionality in terms of meeting basic structural requirements, technological processes, and building design, achieving acoustic comfort within the workspace has become one of the primary design challenges. Analyzing contemporary design trends in the field of industrial building architecture reveals an increasing prevalence of using "flexible" interior partitions, both in their materialization and in architectural-functional organization. The tendency to use "light materialization," which aims to provide visual interaction as well, represents a unique engineering-architectural challenge. This paper investigates the impact of applying modern materialization of interior partitions, through a case study of an industrial building in Niš, on the potential to achieve adequate acoustic comfort. The aim of the study is to explore to what extent and in what way the application of different types of materialization, determined by the functional requirements of the space, influences the creation of an appropriate acoustic environment. The paper will analyze the possibilities of optimizing the materialization of interior partitions to achieve adequate acoustic ambiance while respecting architectural- design requirements. By simulating the acoustic performance of several models of modern materializations of interior partitions, an analysis of their acoustic characteristics (insulation power) will be conducted. The simulation of the models was carried out using the INSUL program, specialized for calculating sound insulation through various elements and construction assemblies. The obtained results will provide a preliminary "path to follow" in the architectural search for adequate acoustic comfort in the interior spaces of industrial buildings.*

Key words: *industrial architecture, interior wall partitions, contemporary materials, acoustic insulation*

Received September 18, 2024 / Accepted October 21, 2024
Corresponding author: Miomir Vasov
University of Niš, Faculty of Civil Engineering and Architecture, Aleksandra Medvedeva 14, 18000 Niš, Serbia
E-mail: m.vasov@me.com

1. INTRODUCTION

Thanks to the industry's dynamic development in recent decades, industrial architecture has become an increasingly essential branch. Due to the significant size of these objects, intensive development has led to the need for the construction of assembly and "lightweight" structures, as well as flexible internal partitions that must meet basic functional and technological requirements. The use of "light" materialization, in combination with glass segments, allows for interaction among employees and their engagement in the production process. It also allows for quick partition rearrangement, enabling the production process to be reorganized in a concise time frame in case of a need for change. In light of these facts, the disruption of acoustic comfort within the workspace represents a significant design challenge that should be considered.

As manufacturing halls often represent sources of noise that can harm users' health, acoustic comfort is an important aspect when designing modern industrial architecture. The development of innovative materials and construction techniques increasingly enables the creation of internal partitions with insulating properties that achieve high-quality spatial response and sound aesthetics, thus contributing to smooth operation and health preservation.

Partitions' physical properties always limit the effects of sound insulation on reducing noise in industrial buildings. The paper investigates the influence of the application of various modern materials for internal partitions on the transmission of sound between the manufacturing hall and the administrative part of the building. An industrial building in Niš was selected for the case study to determine the most favorable materials for internal partitions with the fulfillment of minimum acoustic comfort requirements through software calculation, comparative analysis, and optimization. Methodologically, the paper uses the case study method and experimental modeling as the primary research approaches. In addition, unique scientific methods such as quantitative analysis, comparative analysis, and induction and deduction are applied.

The paper is divided into five chapters. After the introduction chapter gives an overview of the research problem, the second chapter focuses on the importance of modern industrial buildings, the principles of their design, and the application of modern materials in their construction. The third chapter explains in detail the applied methodology, including the definition of the internal partition model and the input data necessary for the simulation using Insul's specialized software. The fourth chapter provides an analysis of the generated results and their discussion, while the last chapter contains a synthesis of the research conclusions. At the very end, there is a list of used literature.

2. ON THE SIGNIFICANCE OF INDUSTRY AND THE IMPLEMENTATION OF CONTEMPORARY MATERIALS

Modern industrial buildings are designed to meet the complex requirements of technological processes, providing optimal conditions for work and integrating advanced technologies. In the design process, it is essential to consider the rational use of resources, material recycling, reduction of negative environmental impacts, and improvement of energy efficiency. This approach includes the application of sustainable materials, energy-efficient systems, and technologies to minimize the ecological footprint, and the creation of flexible spaces that can be adapted to market changes and technological trends [1]. This is reflected in simple architectural solutions that enable efficient space organization. As a result, manufacturing spaces

feature unique structural assemblies of supporting structures, which differ from architectural solutions in other types of buildings [2]. Industrial buildings can be classified based on their shape or the technological process. Based on their shape, they are divided into low halls, high halls, and multi-story buildings. In terms of the technological process, buildings are classified based on horizontal or vertical organization [3].

In industrial facilities, width often presents a challenge due to the dimensions of machinery, traffic aisles, and working space. It can vary from a few meters to several tens of meters, which can result in the presence of internal columns[3]. On the other hand, the placement and dimensions of machinery require a considerable amount of free space. In light of these considerations, many modern industrial production halls are designed as single-story structures with large spans, as this approach allows for optimal integration of functionality and construction efficiency [4].

In modern design, which is based on the appropriate selection of location, definition of spatial solutions, and the shapes of industrial buildings, the careful choice of natural and recycled materials plays a crucial role, not only in terms of ecological sustainability but also in achieving optimal working conditions. When selecting materials, it is essential to consider their ability to contribute to acoustic comfort within the space, as noise can significantly impact productivity and worker well-being. Sound-absorbing materials and adequate insulation can reduce noise levels and create a more pleasant working environment, enhancing both the psychological and physical comfort of space users. Achieving the right acoustic balance allows for uninterrupted task performance, reduces stress, and contributes to the overall satisfaction of employees in industrial buildings [5].

Internal partitions, such as walls and intermediate floor structures, must be designed to reduce sound transmission to achieve an optimal level of sound insulation. According to their structure, partitions can be classified as single-layer (composed of one material), double-layer (composed of two materials), or multi-layer (composed of multiple different materials) [6]. Multi-layer partitions significantly reduce sound transmission, especially when heavier and more rigid layers are combined with lighter and more flexible ones. Additionally, multi-layer partitions filled with low-rigidity insulating materials often provide higher sound insulation than single-layer partitions of the same surface mass. Regardless of the partition type, their purpose is to isolate rooms from potential noise sources. The level of this insulation is measured as sound insulation (R), expressed in decibels (dB) [6]. Appropriate calculations can provide approximate values of sound insulation, which, while involving some degree of approximation, are sufficiently accurate to serve as a basis for partition design. Additionally, proper joint sealing and avoidance of sound bridges further reduce sound transmission through partition walls [7].

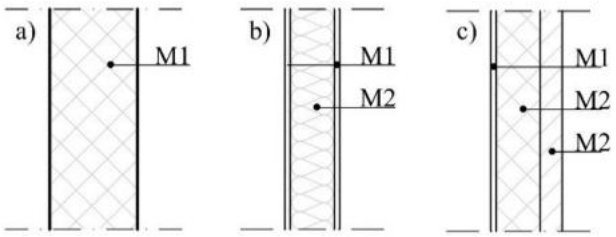

Fig. 1 Type of partition: a) Single-layer, b) Double-layer, c) Multi-layer [5]

3. MODELING THE CHARACTERISTIC INTERNAL PARTITION AND SIMULATION OF ITS ACOUSTIC PERFORMANCE

3.1. INSUL – predicting sound insulation software

INSUL is a program for predicting the sound insulation of walls, floors, roofs, ceilings and windows and impact sound and rain noise of floors and roofs. It has been available for over 20 years, and evolved over many releases into a very easy-to-use tool which has been refined by continued comparison with laboratory tests to provide acceptable accuracy for a wide range of constructions. The programme can make good estimates of the Transmission Loss (TL) or Impact Sound (Ln) in 1/3 octave bands and Weighted Sound Reduction Index (Rw) or Impact Rating (LnTw) for use in noise transfer calculations or acoustical design or specification. Also, it takes account of finite size effects and can be used to quickly evaluate new materials and systems, or to investigate the effects of changes to existing designs. Like any prediction tool, INSUL is not a substitute for measurement. However, comparisons with test data indicate that programme reliably predicts Rw values to within 3 dB for most constructions.

Since the INSUL is adapted to most regions in the world, it will greatly enhance the ability of acoustic consultants and product manufacturers to quickly and confidently specify constructions in order to achieve the desired airborne sound insulation [8].

3.2. Analysis of the characteristic internal partition and simulation of the optimization of its acoustic performance

In modern industrial architecture, the demand for flexible spaces and employee interaction makes acoustic comfort a key challenge for designers. This study will focus on optimizing the characteristic internal partition (Fig. 2) using the example of the ”Integrated Micro Electronics - IMI” industrial facility in Niš. Analyzing the performance of partitions through various modern material variations aims to achieve optimal acoustic comfort in the early stages of design, thus preventing discomfort in the working environment. The analysis also underscores the necessity of a thorough design approach to ensure that the minimum sound insulation values of partitions meet the requirements of the standard JUS U.J6.201:1989 (Acoustics in Building Construction - Technical Requirements for the Design and Construction of Buildings), which specifies a minimum sound insulation of 57 dB between operational and office spaces [9].

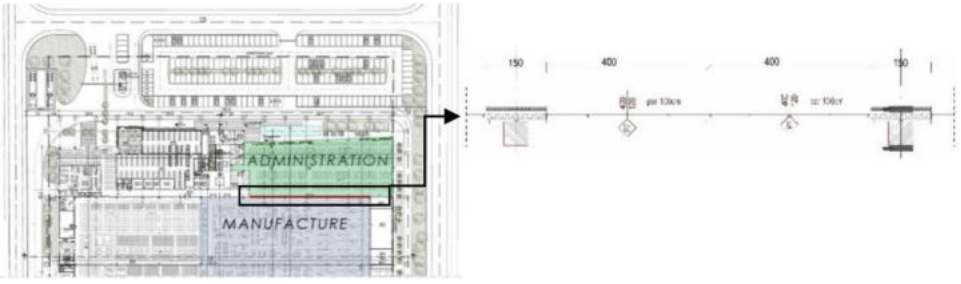

Fig. 2 Detail of the analyzed wall between administration and manufacture

Table 1 provides an overview of the analyzed models and types of partitions, with a detailed depiction of the wall structure and glass surfaces.

Table 1 Overview of the characteristics of the models used for analysis

	Type of partition	Structure of partition	Window/Glazing	Total thickness
MODEL 0	Triple	▪ Gypsum plasterboard 2x1,25 cm ▪ Mineral wool insulation 5 cm ▪ Air space 10cm ▪ Panel with mineral insulation 15 cm	Window: 2 x 400/120 cm	31,75 cm
MODEL 1	Triple	▪ Gypsum plasterboard 2x1,25 cm ▪ Mineral wool insulation 5 cm ▪ Air space 10 cm ▪ Panel with mineral insulation 15 cm	Window: 2 x 200/120 cm	31,75 cm
MODEL 2	Triple	▪ Gypsum plasterboard 2x1,25 cm ▪ Mineral wool insulation 5 cm ▪ Air space 10 cm ▪ Panel with mineral insulation 15 cm	Window: 0	31,75 cm
MODEL 2’	Triple	▪ Gypsum plasterboard 2x1,25 cm ▪ Mineral wool insulation 15 cm ▪ Panel with mineral insulation 15 cm	Window: 0	31,75 cm
MODEL 3	Triple	▪ Glass 6 mm ▪ Air space with argon gas 15 cm ▪ Glass 4 mm ▪ Air space with argon gas 15 cm ▪ Glass 6 mm	Glazing: 100%	31,60 cm
MODEL 3’	Triple	▪ Laminated Glass 6 mm ▪ Air space with argon gas 15 cm ▪ Laminated Glass 4 mm ▪ Air space with argon gas 15 cm ▪ Laminated Glass 6 mm	Glazing: 100%	31,60 cm

The width of the analyzed partition segment is 950 cm, while its height is 500 cm. The partition wall, whose characteristics are taken from the design documentation of the industrial facility, represents MODEL 0. It is a triple-layer wall consisting of a self-supporting wall cladding with a steel substructure and a double-layer of gypsum plasterboard (d=2x1.25 cm), filled with mineral wool insulation (d=5 cm), and an air space (d=10 cm) between the facade panel and the facade panel (steel coated sheet - mineral wool - steel coated sheet) with mineral wool insulation (d=15 cm), resulting in a total thickness of 31.75 cm. The construction is designed to position the wall panel closer to the production area for greater impact resistance and easier maintenance. At the same time, the gypsum plasterboard is closer to the administrative area. The triple-glazed window, measuring 2×400/120 cm, which allows visual communication between the administrative and production areas, consists of 6 mm thick glass, an air-filled with argon gas of 150 mm thickness, 4 mm thick glass, another air-filled with argon gas of 150 mm thickness, and 6 mm thick glass.

Partitions MODEL 1, MODEL 2, and MODEL 3 represent modifications of the designed partition MODEL 0, with variations in their characteristics, while the length and height of the partitions remain unchanged across all models. Partition MODEL 1 has the same structural characteristics as the designed MODEL 0, with the only difference being that the window area in MODEL 1 is reduced by 50%, measuring 2x 200/120 cm. The glass structure is the same as in the designed MODEL 0. The subsequent partition, MODEL 2, also has the same structural characteristics as the previous two models. However, it does not include a window for visual communication between the administrative and production areas.

Unlike the models mentioned above, MODEL 3 represents an entire glass partition, also classified as a ”light” modern construction commonly used for partitioning office spaces. This glass partition provides complete visual interaction among employees, offering a view of the production process at all times and from any angle. MODEL 3 is a triple-glazed glass partition consisting of 6 mm thick glass, an air-filled with argon gas of 150 mm thickness, 4 mm thick glass, another air-filled with argon gas of 150 mm thickness, and 6 mm thick glass.

To achieve the minimum sound insulation value of 57 dB specified by the standard JUS U.J6.201:1989, optimization of partitions MODEL 2 and MODEL 3 has been carried out. The newly designed partition MODEL 2' retains the same width and similar characteristics as MODEL 2, with the difference being in the thickness of the insulating layer between the gypsum plasterboard and the facade panel, which is now 15 cm. The newly designed partition MODEL 3' also maintains the same width as MODEL 3. However, the difference lies in the type of glass, where regular glass has been replaced with Laminated Glass (1 mm Acoustic Resin).

4. Results and Discussion

The Insul program [8] is a significant tool in the initial design phase - conceptual design, whose analyses are sufficiently accurate to enable effective material and construction choices, ensure acoustic comfort, and provide a pleasant environment, which is particularly important for facilities such as industrial buildings.

Figures 3 to 8 show the reference values of insulation performance obtained through software calculations. International standards that describe methods for quantifying sound insulation arose from the need to compare the obtained values, which are inherently frequency-dependent, uniformly and to compare them with established criteria that need to be met [8]. The curves of the insulation performance for the analyzed models, which depend on the frequency and are calculated and measured in 1/3 octave frequency bands, are displayed in Figures 3 to 8 [6].

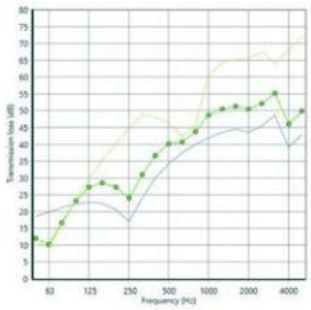

Fig. 3 Model 0

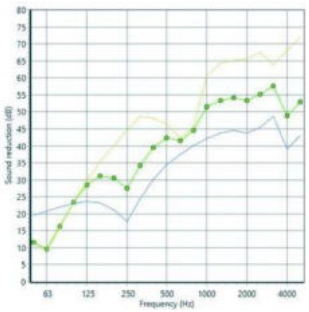

Fig. 4 Model 1

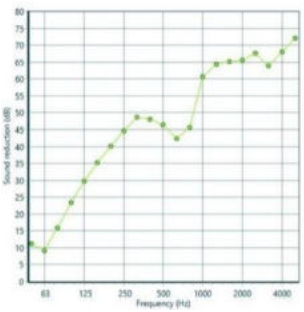

Fig. 5 Model 2

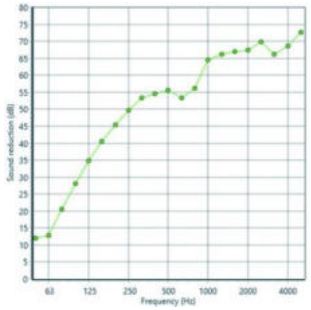

Fig. 6 Model 2’

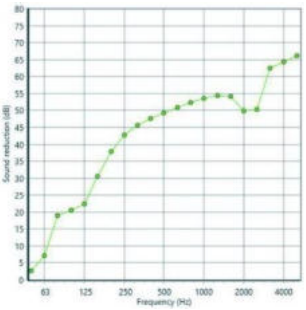

Fig. 7 Model 3

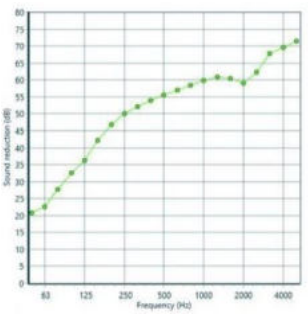

Fig. 8 Model 3’

Reference values in third-octave frequency bands from 63 Hz to 4000 Hz, which need to be compared with each other, are numerically provided in Table 2.

Table 2 Values of the reference curves for the analyzed partitions

	Frequency (Hz)							IzolacionamoćRw
	63	125	250	500	1000	2000	4000	(dB)
MODEL 0	10	27	24	40	49	50	46	**39**
MODEL 1	10	29	28	42	52	53	49	**44**
MODEL 2	9	30	45	46	61	66	68	**49**
MODEL 2’	13	35	50	56	65	67	69	**57**
MODEL 3	7	22	43	49	54	50	64	**48**
MODEL 3’	23	36	50	56	60	59	70	**57**

Frequency analysis results show that the designed partition MODEL 1 has the lowest insulation performance (39 dB), which is 10 dB lower compared to partition MODEL 2 (49 dB), which has the same characteristics as MODEL 1 but without glass partitions, i.e., without windows. This indicates that the presence of windows leads to a significant deterioration in acoustic comfort. The insulation performance of the glass partition MODEL 3 (48 dB) is nearly identical to MODEL 2 (49 dB).

The optimized partition MODEL 2, MODEL 2', increases the insulation layer without changing the width of the partition, leading to a significant improvement in acoustic performance, meeting the minimum requirement of the standard (57 dB). Similarly, for partition MODEL 3' (57 dB), changing the type of glass compared to MODEL 3 (48 dB) also significantly increases insulation performance, ensuring better acoustic comfort and meeting the standard's minimum requirement of 57 dB.

When calculating the insulation performance of partitions using software, it is essential to remember that the obtained results often cannot be fully realized under actual conditions. Therefore, these values should be cautiously approached, as achieving the planned sound insulation in constructed partitions can be challenging. M. Mijić recommends selecting partitions with a calculated insulation performance of several decibels (dB) higher for specific lightweight partitions to mitigate such issues [10].

5. CONCLUSION

This study used experimental modeling to analyze and optimize the interior partition of the industrial facility ”IMI” for acoustic comfort. Six partitions were examined, showing that MODEL 0 (a base wall with many windows) had the lowest sound insulation (39 dB). Reducing the glass area improved insulation, with MODEL 2 (a windowless wall) achieving the highest level (49 dB). MODEL 2 was then optimized to meet sound insulation standards. The research also explored glass partitions, often used in modern buildings, for visual interaction between production and administrative areas. Analysis of a glass partition of the exact dimensions as the designed one revealed that not all glass types provide adequate acoustic performance. MODEL 3, with ordinary glass, had nearly 10 dB less insulation than required, underscoring the need for optimization to meet acoustic standards.

Increasing the thickness of partitions is not an optimal solution for improving sound insulation; understanding material properties and their proper use is essential. Sound insulation depends on the partition and surrounding constructions, including vertical and horizontal elements that can affect overall acoustic performance [11]. Future research will focus on sound insulation field measurements to validate the accuracy of software calculations and refine the methods for achieving effective acoustic solutions.

Acknowledgment: *The paper was funded by the Ministry of Science, Technological Development, and Innovation of the Republic of Serbia, under the contract for the implementation and financing of scientific research at the Faculty of Civil Engineering and Architecture of the University of Niš for the year 2024, reference number: 451-03-65/2024-03/200095. The results of the paper are part of a broader scientific research project by Đurđina Rančić, a third-year doctoral student in the Architecture department and a scholarship recipient of the Ministry of Science, Technological Development, and Innovation.*

REFERENCES

1. Stanojević, A., Jevremović, Lj., Turnšek, B., Rančić, Đ., *Sustainable industrial architecture: ecological design of contemporary wineries*, Proceedings of 2nd International Conference of Sustainable Environment and Technologies, University „UNION- Nikola Tesla“, Belgrade, Serbia, September - 24, 2022, pp. 119-126
2. Rančić Đ., Stanojević A., Jevremović Lj.: *Uticaj forme krova i karakteristike otvora na optimizaciju energetske potrošnje industrijskih šed hala,* IX Conference Industrial Energy and Environmental Protection in South Eastern Europe – IEEP 2024*,* Belgrade
3. Damjanović, V., *Industrijske zgrade i kompleksi (IV izd.)*, Građevinska knjiga, Beograd, 1990.
4. Reisinger J., Hollinsky P., Kovacic I., *Design Guideline for Flexible Industrial Buildings Integrating Industry 4.0 Parameters,* Sustainability, Technical University of Vienna-TU Wien, Austria 2021.
5. Vasiliev V.V., Morozov, E. V., *Advanced Mechanics of Composite Materials and Structures*, 4th ed.; Elsevier: Amsterdam, The Netherlands, 2018; p. 882
6. Vasov M., *Građevinska fizika - zvučna zaštita zgrada,* Građevinsko-arhitektonski fakultet u Nišu, 2o22.
7. Praščević M., Mihajlov D., Buka i vibracije – priručnik za laboratorijske vežbe. Univerzitet u Nišu, Niš 2022.
8. https://www.insul.co.nz/ (01.09.2024.)
9. https://iss.rs/en/project/show/iss:proj:11963 (01.09.2024.)
10. Mijić M., ETF Beograd, *Akustički komfor*, Predavanje po pozivu: Knauf akademija, 2012.
11. Kalić D., *Kvalitet zvučne zaštite zgrada,* Beograd, 2004.

FACTA UNIVERSITATIS
Series: **Working and Living Environmental Protection** Vol. 21, Nº 4, Special Issue, 2024, pp. 271 - 282
https://doi.org/10.22190/FUWLEP241003026J

Original scientific paper

MULTI-SLOPE ENERGY DECAY CURVES GENERATED BY MOVING AVERAGE APPROACH

UDC 543.843.7

Marko Janković[1], Dejan Ćirić[1], Maro Puljizević[2], Aleksandar Pantić[3]

[1]University of Niš, Faculty of Electronic Engineering in Niš, Serbia
[2]Knauf Insulation d.o.o., Škofja Loka, Slovenia
[3]Knauf Insulation d.o.o., Surdulica, Serbia

ORCID iDs: Marko Janković https://orcid.org/0009-0002-1109-3241
Dejan Ćirić https://orcid.org/0000-0003-4974-3131
Maro Puljizević N/A
Aleksandar Pantić https://orcid.org/0000-0003-2351-498X

Abstract. *Sound energy decay is typically represented by an energy decay curve (EDC), which depicts the decrease in sound energy over time after the sound source in a room is turned off. In spaces with single-slope decay, the EDC appears as a straight line. Such curves can be analyzed using linear regression to calculate parameters such as reverberation time. However, due to factors like room geometry, absorption, and other effects of sound transmission in enclosed spaces, an EDC may exhibit multi-slope decay. When linear regression is applied to such a curve, the results depend heavily on the range over which the curve is approximated by a straight line.*
This paper analyzes EDCs generated using the moving average approach, based on impulse responses measured in two rooms: a reverberation chamber and a classroom. The focus is on multi-slope EDCs and a comparison between moving average EDCs and those generated using the Schroeder backward integration method. The moving average EDCs exhibit a greater dynamic range than the Schroeder-integrated EDCs, revealing the final part of the reverberation decay, which is obscured in the latter due to the cumulative summation of background noise.

Key words: *sound energy decay, energy decay curve, moving average, multi-slope decay*

1. INTRODUCTION

Sound energy decay is a very important characteristic in room acoustics, particularly in performance spaces like auditoria [1,2]. The concept of energy decay refers to the gradual reduction in sound as it dissipates over time after the sound source has stopped due to

Received October 3, 2024 / Accepted November 21, 2024
Corresponding author: Dejan Ćirić
University of Niš, Faculty of Electronic Engineering in Niš, Aleksandra Medvedeva 4, 18000 Niš, Serbia
E-mail: dejan.ciric@elfak.ni.ac.rs

factors such as absorption, reflection, diffusion and other acoustic interactions [2-5]. This phenomenon is crucial in the study of room reverberation. Reverberation time (RT), a key parameter for room acoustics, describes the time required for the sound pressure level in a room to decrease by 60 dB once the sound source is turned off [2-4].

The sound decay is typically represented by energy decay curves (EDCs) or functions, which are important for understanding how sound behaves in rooms. In the sound decay process, acoustic conditions can be assumed to be static, but also dynamic where factors like room geometry or the position of sound sources vary [3]. Numerous studies address the challenge of estimating sound decay, particularly RT calculated from the EDC. Understanding the decay of sound energy is essential for assessing the acoustical properties of spaces, like clarity of sound in rooms such as classrooms or concert halls [4].

EDCs can be generated in different ways. One of the traditional methods includes the measurement of a room impulse response (RIR) and backward integration of this RIR, introduced by Schroeder [6,7]. Here, the squared RIR is integrated over reverse time to produce the EDC. The generated EDC shows a continuous decline as energy is absorbed by the room's materials and dissipated into the air. By plotting the EDC on a logarithmic scale, the sound decay becomes evident, where an exponential decay typically appears as a straight line. The Schroeder integration allows for detailed EDC analysis. It represents an important instrumental in identifying how sound diminishes over time in a given environment, especially in spaces with complex acoustical properties [1,8], such as capturing the multiple sloped decays [9]. One of the main benefits of the Schroeder integration is its ability to smooth out fluctuations in the decay, providing a clearer view of the reverberation process. However, the method has some drawbacks, particularly its sensitivity to background noise. The cumulative summing of noise in real-world RIRs can distort the EDC, causing the late decay part of the curve to bend upwards, which compromises the accuracy of the RT measurements [10]. In this way, a useful dynamic range of such an EDC is reduced.

From the implementation point of view, linear fitting of the reverberation decay of Schroeder decay curves is often applied, which might lead to inaccurate results in practice [1]. This is why a number of references deal with proposals on how to overcome this situation, e.g., improve the procedures of calculating the quantities from the EDCs as RT and absorption coefficient [11]. Going in that direction, some proper parametric models are proposed in the literature, as done in [1], allowing for a better understanding of energy decay, thereby enabling more effective acoustic design and analysis of rooms like auditoria.

In contrast to ideal conditions where the reverberation decay of an EDC should form a straight line on a logarithmic plot, in real-world settings, deviations are common, leading to multi-slope or concave shapes [12]. In rooms with uneven absorption, the EDC can display complex behaviors, especially at low frequencies, such as double-slope decay, where the initial decay is faster than the subsequent decay. When analyzing these deviations**,** the use of linear regression to estimate the slope (calculate RT) requires careful selection of the dynamic range – range where this regression is applied. The wider the dynamic range, the more likely it is that deviations from the ideal linear decay will affect the estimated slope. Therefore, the focus of this study is on multi-slope EDCs measured in a reverberation chamber.

This paper presents an alternative method for generating EDCs by applying a moving average to the logarithm of squared RIRs. The proposed approach is compared with the traditional method, which is based on Schroeder's backward integration of squared RIRs.

The focus is on multi-slope EDCS and their analysis for the purpose of calculating relevant quantities from EDCs, such as reverberation time. The potential of the proposed moving average approach is demonstrated through characteristic examples of EDCs from different environments. For this purpose, both synthesized and measured RIRs are used.

2. Multi-slope Decays and Linear Regression

2.1. Single-Slope versus Multi-Slope Decays

Multi-slope energy decays are common in various environments, such as coupled spaces, rooms with non-uniform distributions of absorbing materials and reverberation chambers [7,11]. In these cases, the energy decay exhibits multiple slopes, indicating different decay rates at various stages of the sound's dissipation [8]. Multi-exponential decays are influenced by factors such as room shape, scattering objects, and absorber positioning. For example, in rectangular rooms, non-grazing modes decay faster, contributing to the curvature of the energy decay [9]. The literature highlights that a uniform distribution of absorptive materials leads to more consistent and reliable EDCs [13]. Additionally, seating positions in a room can affect the sound energy decay pattern, too [6]. In seats near lateral walls, energy decay plateaus are observed due to early reflections, while seats in the middle display a more stable, exponential decay.

EDCs in non-diffuse environments also deviate from the standard exponential decay typically seen in diffuse sound fields [14]. In such environments, non-diffuse fields can accelerate energy decay due to the formation of the anisotropic sound field. When analyzing the EDC and calculating RT, non-diffuse sound decay is critical, as the non-linearity of the EDC can result in inconsistent RT values across different measurement intervals [14,15]. The presence of multi-exponential decay (i.e., decay curve non-linearity) complicates RT calculation in EDC analysis.

In spaces with multi-slope EDCs, the sound decay cannot be modeled by a single exponential function. Instead, an approach is to use multi-exponential decay functions, which incorporate multiple exponential terms to represent the different rates at which sound decays [7,16]. Research of EDC in reverberation chamber utilizes the exponential fits rather than traditional linear regression methods, highlighting that multi-exponential decays more accurately reflect the complex acoustic conditions present [9]. While this approach is useful, it can become overly complex, especially when applied to environments with spatially varying source-receiver configurations or non-uniform absorption properties [16]. A contrasting approach would be to use a "common-slope model," which simplifies the analysis of reverberation by describing sound energy decay with a set of common decay rates or slopes, regardless of spatial and directional variations [16].

2.2. Approaches to Solve Linear Regression Problem

The decay functions generated by the Schroeder backward integration are a valuable tool for distinguishing between single-slope and multiple-slope decay characteristics. However, challenges arise when utilizing these functions. One challenge relates to deviations from expected exponential decay patterns caused by noise, as highlighted in [1]. Another issue, mentioned in a number of references, is the use of linear regression (or the single-exponential decay model) to calculate the slope of the Schroeder EDC, specifically

the reverberation decay [17]. This approach is often insufficient for environments with complex acoustic properties. As a result, it is suggested that a more accurate framework beyond traditional linear regression is required [11]. In other words, more advanced modeling techniques are needed to better capture the complexity of the decay process.

As a result, advanced methods such as nonlinear regressions, Bayesian analysis, and artificial neural networks (NNs) have been developed to improve the accuracy of sound decay analyses [1]. For instance, nonlinear regression is applied in [6] to determine the early time limit in EDCs. Identifying this early time limit, which separates direct sound from lateral reverberation, enhances the accuracy of distinguishing early reflections from late reverberation. Additionally, a nonlinear decay model, incorporating a double-slope decay term and noise, is also applied to detect the truncation time of an RIR used in EDC generation through Schroeder integration [15].

A Bayesian decay time estimation framework is introduced in [11] as an alternative to traditional methods. This framework allows for more accurate modeling of the initial energy decay, which is often discarded in linear regression approaches. By focusing on this initial portion, the framework provides more reliable estimates of decay times, even in cases of multi-exponential decays. Three methodologies — the variable projection algorithm (VARPRO), regularized inverse Laplace transform (RILT), and maximum entropy decay-time distribution (MEDD) — are introduced in [17] to achieve more robust, accurate, and time-efficient analysis, particularly when multiple decay slopes are present. Each of these methodologies is designed to handle complex EDCs.

Another approach involves the use of deep NN for estimating the decay slope, or more specifically, the RT under both static or dynamic conditions [3]. In a recent study, NNs are used to estimate the parameters of multi-slope EDCs, including the decay rates and amplitude of each exponential component [7]. Another NN-based method models multi-slope decays, where the network estimates key parameters such as decay times and amplitudes for different slopes [18].

3. METHODOLOGY

3.1. EDC Generated by Moving Average

To address the limitations of Schroeder integration, an alternative approach based on averaging the logarithmic squared RIR (applying the moving average) has been explored in [10]. In this approach, a decay curve is first generated by taking the logarithm of the squared RIR, resulting in a curve with strong fluctuations. Then, each point on this curve is replaced by the average value of the data points within a window of a certain length, with the point to be replaced positioned at the center of the window. This process is repeated along the entire logarithmic squared RIR curve, from beginning to end. This is why the described procedure is referred to as the moving average.

The moving average method reduces fluctuations and provides a smoother EDC. It is particularly advantageous in noisy environments where traditional methods might be skewed. Unlike the Schroeder method, this approach does not involve cumulative summing, thus eliminating noise-related distortion. As a result, a greater dynamic range of the EDC is obtained compared to the Schroeder method. However, it also presents challenges, particularly in selecting the appropriate averaging interval (the size of the averaging window) that must be carefully chosen. A window that is too short may not

sufficiently smooth the fluctuations, while a larger window can introduce distortions, especially at the beginning of the curve or near the "knee" – the intersection between reverberation decay and noise floor [10].

It is shown in [10] that the best results are typically obtained when the averaging window contains around 5000 data points (with a sampling frequency of 44.1 kHz). This provides a balance between reducing fluctuations and maintaining accuracy. The optimal window size varies depending on the frequency band, with higher frequencies requiring shorter windows. Additionally, the exact window length depends on the specific characteristics of the RIR. While averaging helps mitigate noise effects, it is not without drawbacks. For example, the averaging process can distort the initial part of the EDC, especially when the window is too large.

In this study, both the Schroeder integration and moving average method are used to generate the EDCs, see Fig. 1. These curves are compared in terms of their shape and dynamic range, which represents the range of decay from the beginning of the curve up to a certain point, such as the knee of the curve.

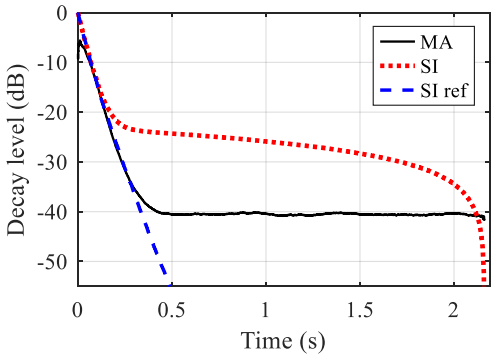

Fig. 1 EDCs generated from noisy synthesized RIR by moving average (MA) and Schroeder integration (SI) together with EDC generated by Schroeder integration from noiseless synthesized RIR (SI ref)

3.2. RIRs used for generating EDCs

Two types of RIRs are used for this study: synthesized and measured. The synthesized RIRs are generated using the image source model, as described in [19], resulting in noiseless RIRs. Depending on the model parameters, these RIRs can exhibit varying degrees of irregularities, such as curvatures in the reverberation decay. In order to have noisy RIRs, white or pink noise of a particular amplitude (level) is added. The sampling frequency for these RIRs is set to 44.1 kHz.

The measured RIRs were obtained from two different rooms: a reverberation room and a classroom, having RT from 6 s to 11 s and from 1.6 s to 1.9 s at mid frequencies, respectively. Both rooms are located at the Faculty of Electronic Engineering in Niš. The construction elements of the reverberation room are typical for such spaces, as shown in Fig. 2.a), featuring an irregular shape and ceiling-mounted diffusers. A unique feature of this room is its small volume, only 65.05 m^3, which is below the volume specified in the ISO 354 standard for sound absorption measurement. Generally, it is assumed that a diffuse

sound field is generated in a reverberation room, where sound decay should be truly exponential, represented by a single slope. However, numerous studies have shown that this assumption does not always hold in practice, especially when absorption materials are unevenly distributed within the room [20]. The second room used for measurements is a typical classroom, with unique ceiling geometry, as shown in Fig. 2.b). The floor area of this room is approximately 117 m^2, with a ceiling height of about 2.8 m at the lower section and around 4 m at the higher section. As with the synthesized RIRs, the sampling frequency for the RIRs measured in both rooms was 44.1 kHz.

Fig. 2 Rooms where RIRs were measured: a) reverberation room, and b) classroom

4. Analysis of Generated EDCs

One of the major challenges in generating EDCs using the moving average approach is selecting the appropriate window size for averaging the data points (averaging interval). The window size must be chosen as a compromise to produce a sufficiently smooth EDC without losing important details from short decays. The effects of varying the window size in generating broadband EDC are presented in Fig. 3.

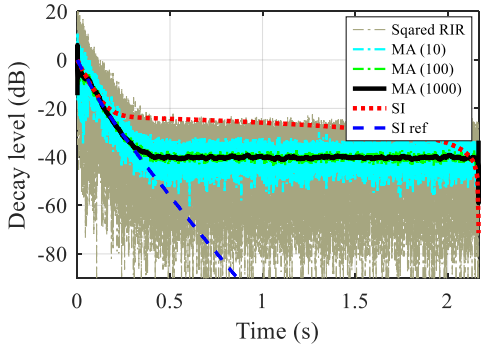

Fig. 3 EDCs generated from noisy synthesized RIR by moving average (MA) and Schroeder integration (SI) using different averaging intervals (given in number of samples in legend) together with EDC generated by Schroeder integration from noiseless synthesized RIR (SI ref)

Since the moving average approach does not involve the cumulative summing of noise, it results in a greater dynamic range of the EDC compared to Schroeder backward integration, as shown in Fig. 4. A longer averaging window smooths out fluctuations caused by both noise and the reverberation process, At the same time, the slope of the EDC remains largely unchanged (close to that of the reference EDC – noiseless Schroeder EDC), except when the averaging window is too long, as seen in Fig. 4.

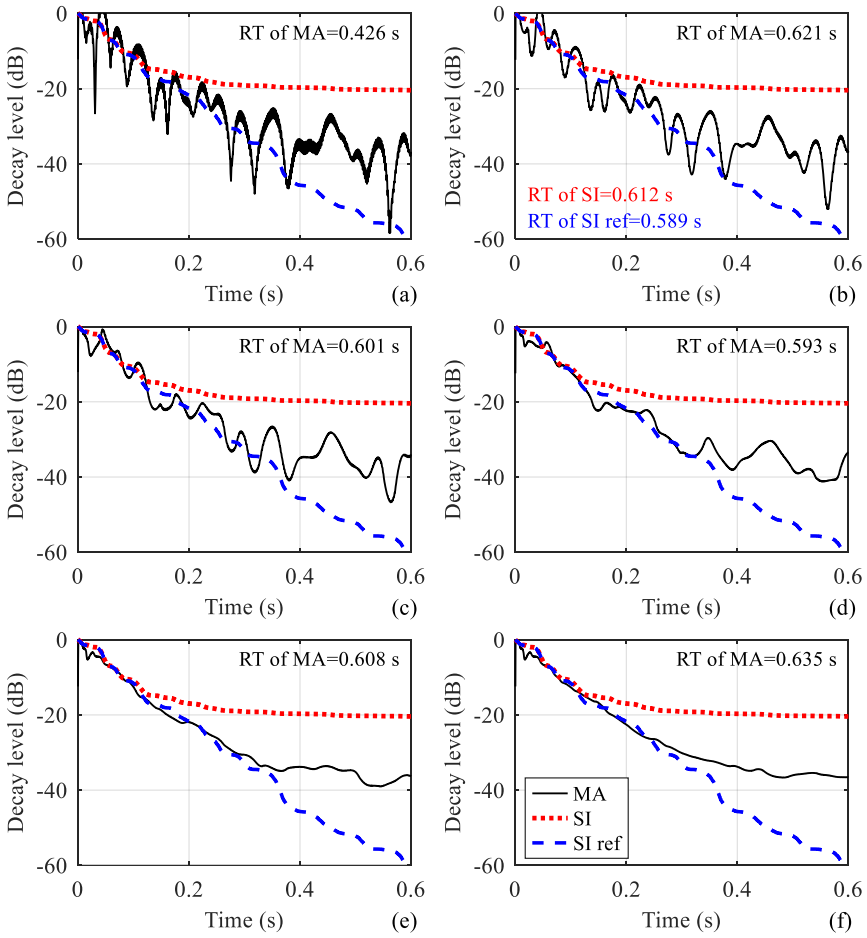

Fig. 4 EDCs generated from noisy synthesized RIR by moving average (MA) using different averaging window sizes: a) 100, b) 500, c) 1000, d) 2000, e) 5000 and f) 10000 samples, together with EDCs generated by Schroeder integration (SI) from both noisy and noiseless synthesized RIR (SI ref)

To illustrate the use of these curves, the RT is calculated by applying linear regression within the same range (the decay range between -5 dB and -30 dB) from both the moving average EDCs and reference (noiseless Schroeder) EDC. The RT is also calculated in the same manner from the noisy Schroeder EDC, but using the decay range from -5 dB to -

15 dB, since the available dynamic range of this curve is too small. From the calculated RTs, shown in Fig. 4, it is evident that a short averaging interval in the moving average method may lead to a significant deviation of the obtained RT from the reference one of the noiseless EDC. This deviation decreases as the averaging interval increases, and for a window size of 200 samples already, the relative error of RT in comparison to the reference RT is reduced to about 5%, see Fig. 4.b). Further increasing the averaging interval results in a smoother EDC, but the calculated RT remains almost unchanged, see Fig. 4.c) to 4. e). However, an overly long averaging interval can alter the global shape of EDC, including its slope, and the calculated RT, see Fig. 4.f).

The dynamic range of the noisy Schroeder EDC used for RT calculation is significantly smaller than that of the moving average EDC (in this case, too small), and the calculated RT differs from the reference RT for a certain amount. This difference strongly depends on the EDC shape and the dynamic range used for regression. The effect of the applied dynamic range is less significant or even negligible in single-slope, flat EDCs, but this is not the case in Fig. 4.

Analyzing an EDC and calculating parameters such as RT becomes more complex when the EDC exhibits multi-slope decay. Such EDCs used for calculating absorption coefficient are investigated in [12]. When generating multi-slope EDCs using the moving average approach, the choice of averaging window size becomes even more critical. The reverberation decay of a multi-slope EDC can be divided into multiple segments, each with its own slope. In this case, the averaging interval for points near the boundary between segments will include data from both segments, each with different slopes. As a result, the EDC shape may change, especially near these segment boundaries, and this effect is more pronounced with longer averaging intervals.

At the same time, if an appropriate averaging window size is used to generate the EDC, the curve will exhibit a larger dynamic range, as mentioned earlier, and it will reveal parts of the sound decay that are not visible in the Schroeder EDC. This is illustrated in Fig. 5, which presents multi-slope and concave-shaped EDCs generated from the RIRs measured in the reverberation room. While the multi-slope nature is less visible in some of the curves, such as in Fig. 5.b) and d), which show a concave reverberation decay, the double-slope decay becomes more prominent in the moving average EDCs.

The effects of changing the averaging interval when generating a multi-slope EDC from the RIR measured in the reverberation room are shown in Fig. 6, presenting the curves generated from the same RIR as in Fig. 5.c). The general characteristics of the moving average EDC are visible in all curves, regardless of the averaging interval, including the greater dynamic range compared to the Schroeder EDC and the double-slope decay. As the averaging interval increases, the distant features of the reverberation decay become more prominent. EDC irregularities, such as fluctuations and curvatures, are typically more pronounced in the third-octave bands at lower frequencies, as shown in Figs. 5 and 6.

When comparing the moving average and Schroeder EDCs for RT calculation, the most significant difference lies in the dynamic range available for this calculation. This is especially important for methods like linear regression. The mentioned difference is illustrated in Fig. 7, which shows double-slope EDCs in the third-octave band at 200 Hz generated from the RIR measured in the reverberation room. Linear regression is applied to two different regression ranges corresponding to two different slopes. While the range is the same for the first slope, it is considerably larger for the moving average approach in the case of the second slope.

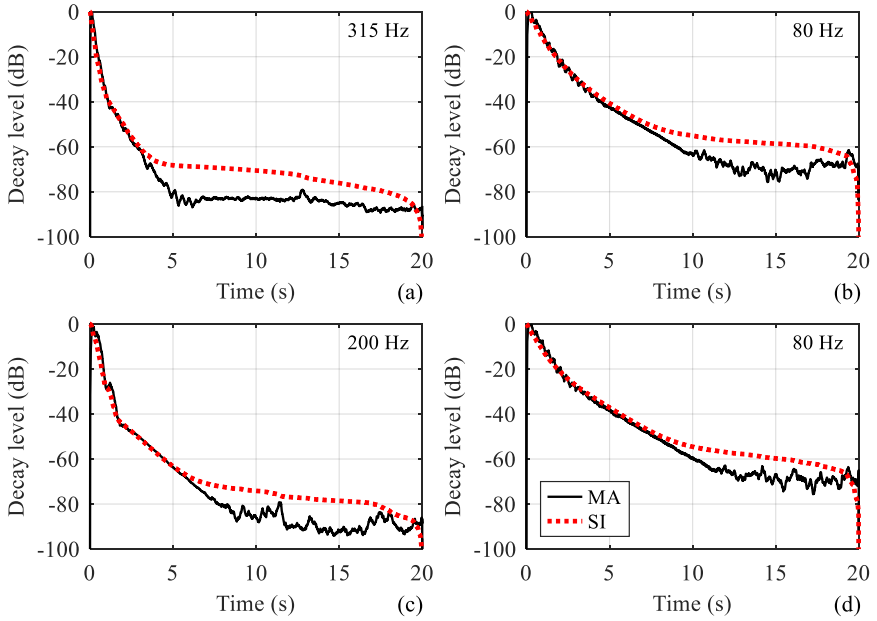

Fig. 5 EDCs in third-octave bands generated from RIRs measured in reverberation room by moving average (MA) (averaging in 10000 samples) and Schroeder integration (SI)

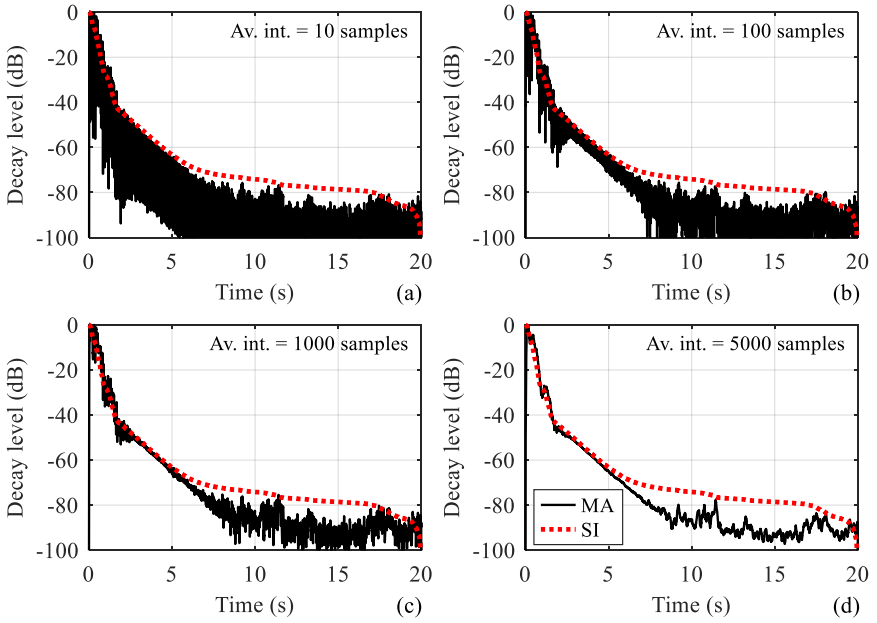

Fig. 6 EDCs in third-octave band at 200 Hz generated from RIR measured in reverberation room by moving average (MA) (different averaging intervals) and Schroeder integration (SI)

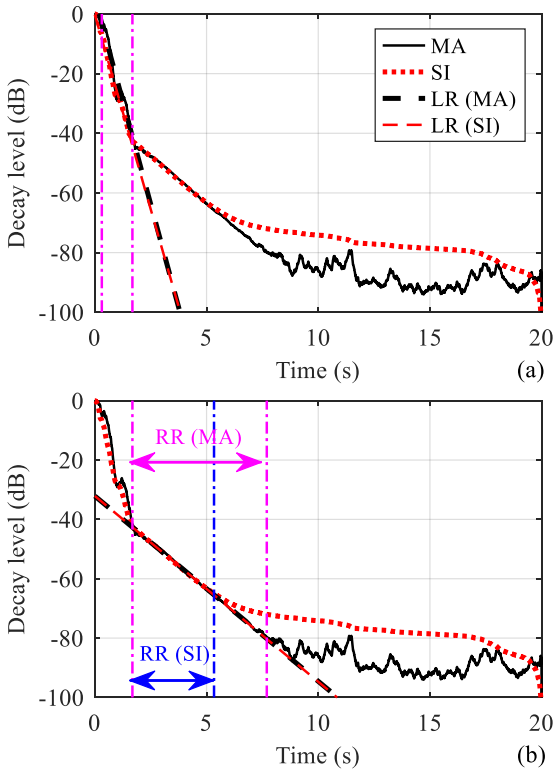

Fig. 7 EDCs in the third-octave band at 200 Hz generated from RIR measured in reverberation room by moving average (MA) (averaging in 10000 samples) and Schroeder integration (SI), as well as linear regression (LR) lines for both methods (MA and SI) and a) the first slope, and b) the second slope (RR = regression range)

The RIRs measured in the second room (the classroom) are mainly regular, and this is also reflected in the EDCs generated from these RIRs, as shown in Fig. 8. Although a slightly concave shape is observed in the EDC in the third-octave band at 100 Hz, the EDCs are primarily single-slope decay curves. Some fluctuations in the reverberation decay can be seen, particularly at low frequencies, as shown in Fig. 8.b). The EDCs obtained by the moving average and Schroeder integration methods coincide well up to the point near the knee of the Schroeder EDCs. Beyond that point, the moving average EDCs typically continue to descend by about 15 dB or more dB, depending on the characteristics of the RIRs.

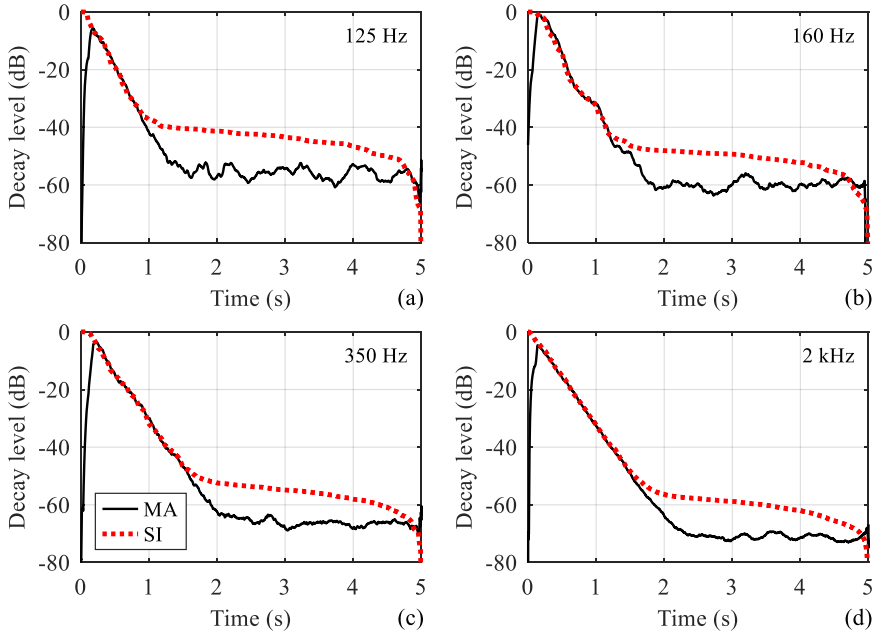

Fig. 8 EDCs in third-octave bands generated from RIRs measured in the classroom by moving average (MA) (averaging in 10000 samples) and Schroeder integration (SI)

5. Conclusions

The study presents a comprehensive comparison between the moving average approach and Schroeder integration for generating EDCs, emphasizing the benefits and limitations of each method. The moving average method offers significant advantages, particularly in environments with noise, as it avoids the cumulative summing process used in Schroeder integration, which can distort the later parts of the decay curve. By averaging the logarithmic squared RIRs, the moving average method produces smoother curves, reducing fluctuations and improving the dynamic range of the EDC. This extended dynamic range allows for better detection of the final stages of reverberation decay, which are often obscured in traditional methods due to noise interference.

However, in the moving average method, if the averaging window is too short, it may fail to sufficiently smooth fluctuations, while a window that is too long can introduce distortions, especially at critical points like the start of the curve or near the "knee," where the reverberation decay transitions into the noise floor. Despite this challenge, when the window size is carefully chosen, the method not only provides a clearer representation of sound decay but also allows for more accurate RT calculations, particularly in complex acoustic environments where multi-slope decays are present. The study demonstrates that the moving average method is a robust alternative, offering improved accuracy for analyzing acoustic spaces with complex or multi-slope energy decay patterns.

Acknowledgement: *This work was supported by the Ministry of Science, Technological Development and Innovation of the Republic of Serbia [grant number 451-03-65/2024-03/200102].*

REFERENCES

1. Xiang N., Gul Z. Su, (2023), Efficiency of sound energy decay analysis in auditoria, *Auditorium Acoustics 2023*, Athens, Greece, September 28-30, 2023, DOI:10.25144/16006.
2. Muhammad N. I., Abdullahi M. Y., Aliyu A. B., (2023), Comparison of blind reverberation time estimation in an enclosed space by analysing energy decay curve, *Fudma Journal of Sciences*, Vol. 7, No. 3, 2023, pp. 194-200, DOI:10.33003/fjs-2023-0703-1762.
3. Götz P., Tuna C., Walther A., Habets E. A. P., (2022), Blind reverberation time estimation in dynamic acoustic conditions, *ICASSP 2022 - 2022 IEEE International Conference on Acoustics, Speech and Signal Processing (ICASSP)*, Singapore, Singapore, May 22-27, 2022, pp. 581-585, DOI:10.1109/ICASSP43922.2022.9746457.
4. Nowoświat A., (2023), Determination of the reverberation time using the measurement of sound decay curves, *Applied Science*, Vol. 13, 2023 p. 8607, DOI:10.3390/app1315860.
5. Kanev N., (2011), Sound decay in a rectangular room with specular and diffuse reflecting surfaces, *Forum Acusticum 2011*, Aalborg, Denmark, June 27-July 1, 2011, pp. 1935-1940.
6. Xia C. Q., Tang S. K. (2023), Finding early time limits t_e with nonlinear regression on energy decay curves, *Auditorium Acoustics 2023*, Athens, Greece, September 28-30, 2023.
7. Götz, G., Hold, C., McKenzie, T., Schlecht, S., Pulkki, V., (2022), Analysis of multi-exponential and anisotropic sound energy decay, *Jahrestagung für Akustik – DAGA 2022*, Stuttgart, Germany, March 21-24, 2022.
8. Edwards N., Kemp J. A., Gül Z. S., (2022), Measurement and subjective responses to the sound decay from coupled volumes in the McPherson Room, St Andrews University, *24th International Conference on Acoustics*, Gyeongju, Korea, October 24-28, 2022.
9. Balint J., Muralter F., Nolan M., Jeong C.-Ho, (2018), Energy decay curves in reverberation chambers and the influence of scattering objects on the absorption coefficient of a sample, *Euronoise 2018*, Crete, Greece, May 27-31, 2018, pp. 2025-2030.
10. Miletić M., Ćirić D., Janković M., (2019), Usage of averaging in generation of room energy decay curve, *International Conference on Electrical, Electronic, and Computing Engineering (IcETRAN)*, Srebrno Jezero, Serbia, June 3-6, 2019, pp. 29-34.
11. Balint J., (2020), *Evaluating the Decay of Sound*, Ph.D. Thesis, Graz University of Technology, Austria, 2020.
12. Ćirić D., Puljizević M., Pantić A., Janković M., (2024), Effects of energy decay curve deviation on absorption coefficient calculation, *59th International Scientific Conference on Information, Communication and Energy Systems and Technologies (ICEST)*, Sozopol, Bulgaria, July 1-3, 2024.
13. Wogu G. C., (2017), *Reverberation Time Analysis Averaged by Energy Decay Curve*, M.Sc. Thesis, Thesis, London South Bank University, UK, 2017.
14. Novoselova A., Kanev N., (2020), Decay of non-diffuse sound fields in a room, *MATEC Web of Conferences*, September 24, 2020, Article number 00006.
15. Chen M., Lee C.-M., (2022), The optimal determination of the truncation time of non-exponential sound decays. *Buildings*, Vol. 12, 2022, p. 697, DOI:10.3390/buildings12050697.
16. Götz G., Schlecht S. J., Pulkki V., (2023), Common-slope modeling of late reverberation, *IEEE/ACM Transactions on Audio, Speech, and Language Processing*, Vol. 31, 2023, pp. 3945-3957, DOI:10.1109/TASLP.2023.3317572.
17. Muralter F., Balint J., (2019), Analysis tools for multiexponential energy decay curves in room acoustics, *Jahrestagung für Akustik – DAGA 2019*, Rostock, Germany, March 18-21, 2019, pp. 1302-1305.
18. Götz G., Falcon Perez R., Schlecht S., Pulkki, V., (2022), Neural network for multi-exponential sound energy decay analysis, *Journal of the Acoustical Society of America*, Vol. 152, No. 7, 2022, pp. 942-953, DOI:10.1121/10.0013416.
19. Lehmann E. A., Johansson A. M., (2008), Prediction of energy decay in room impulse responses simulated with an image-source model, *Journal of the Acoustical Society of America*, Vol. 124, No. 1, 2008, pp. 269-277, DOI:10.1121/1.2936367.
20. Balint J., Berzborn M., Nolan M., Vorländer M., (2023), Measuring sound absorption: The hundred-year debate on the reverberation chamber method, *Acoustics Today*, Vol. 19, No. 3, 2023, pp. 13-21, DOI:10.1121/AT.2023.19.3.13.

FACTA UNIVERSITATIS
Series: **Working and Living Environmental Protection** Vol. 21, Nº 4, Special Issue, 2024, pp. 283 - 291
https://doi.org/10.22190/FUWLEP241009027S

Original scientific paper

EFFECTIVENESS OF THE CONSTRUCTION OF SOUND BARRIERS ON TWO HIGHLY BUSY ROADS IN BELGRADE

UDC 534.2:625.02(497.1BEOGRAD)

Damir Savković, Aleksandar Milenković, Danica Boljević, Stevka Baralić

IMS Institute, Belgrade, Serbia

ORCID iDs: Damir Savković N/A
Aleksandar Milenković https://orcid.org/0000-0002-2381-0095
Danica Boljević https://orcid.org/0000-0002-8702-2434
Stevka Baralić N/A

Abstract. *The application of sound barriers is considered to be one of the important environmental and occupational noise protection measures, especially when it comes from noise sources such as road traffic. It represents a secondary measure of noise protection, because it is applied on the path of propagation of sound waves from the sound source to the place of immission, while the primary measure is applied at the source itself or its immediate surroundings. In this case, the place of immission is the place where a person resides as the main subject of noise protection. In this paper, the efficiency of this application of protection is discussed on the example of two sections of extremely busy traffic roads in Belgrade: a) Arsenija Čarnojevića Boulevard along UHMC Bežanijska kosa (former section of highway E-70 Belgrade-Zagreb) and b) Franše d'Eperea Boulevard along the building of the City Institute for Medical Emergency (former section of the E-75 Belgrade-Niš highway).*

Key words: *sound barrier, noise, sound, sound insulation, noise level, sound attenuation, efficiency.*

1. INTRODUCTION

Protection of the population from environmental and occupational noise that originates from sources of noise such as traffic, whether it is road, rail, air or river traffic, is certainly one of the significant needs in modern living conditions, especially since there is a constant tendency to increase both the number of inhabitants and the number of vehicles used in traffic.

The application of sound barriers, especially when it comes from noise sources such as road traffic, is a secondary measure of protection against noise because it is applied on the path of

Received October 9, 2024 / Accepted October 31, 2024
Corresponding author: Damir Savković
IMS Institute, Vojvode Mišića Boulevard 43, 11040 Belgrade, Serbia
E-mail: damir.savkovic@institutims.rs

propagation of sound waves from the sound source to the place of immission, which in this case is the place where the human lives and works as the main protection subject. At the same time, as a primary noise protection measure, it is carried out at the source itself or its immediate surroundings, which in the case of road traffic, at least in our area, is carried out by moving traffic or making roundabouts instead of classic intersections with traffic lights.

This paper presents the effectiveness of sound barriers installing as one of the ways to protect against road traffic noise, on two sections of the busiest and noisiest traffic roads in Belgrade: a) Arsenija Čarnojevića Boulevard (former section of the E-70 Belgrade-Zagreb highway) and b) Franše d'Eperea Boulevard (former section of highway E-75 Belgrade-Niš). These are the sections of the traffic road that stretch along the UHMC Bežanijska kosa and next to the building of the City Institute for Medical Emergency near Mostar Interchange. At the selected measurement points near the facades of the selected buildings along these sections, noise level measurements were made before and after the construction of sound barriers. The estimated height of the sound barriers along both sections is 5 m, while the length of the barrier on the section along UHMC Bežanijska kosa is about 650 m and on the section next to the building of the City Institute for Medical Emergency is about 350 m.

2. DESCRIPTION OF THE MEASUREMENT PROCEDURE

As an immission place on the section along UHMC Bežanijska kosa, the Pulmonology building was chosen, that is, the principal's room on the high ground floor, which is directly oriented towards the road that is, the subject of the investigation. This measuring point is marked with MM1.

As an immission place on the section along City Institute for Medical Emergency, Hall A on the 1st floor was chosen, which is directly oriented towards the road that is, the subject of investigation. This measuring point is marked with MM2.

The measuring points MM1 and MM2 are shown with black dots in Fig. 1 where estimates are given at what distances these measuring points are located in relation to the

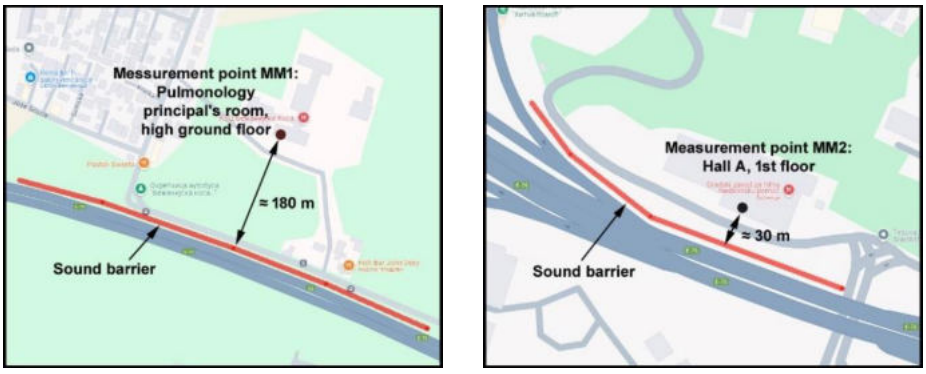

a) b)

Fig. 1 Measurement points and their distances from sound barriers: a) the section along UHMC Bežanijska kosa and b) the section next to the building of the City Institute for Medical Emergency

constructed sound barrier. These measuring points are at different distances from the noise source, that is, roads with mixed road traffic that takes place in four traffic lanes in both directions.

3. Measurement Results

The paper presents noise level measurements at selected measuring points before and after the construction of sound barriers along traffic roads, which were carried out by the Laboratory for Acoustics and Vibrations of the IMS Institute in Belgrade.

The measurement of the noise level at the selected measuring points MM1 and MM2 was carried out according to accredited methods [1,2], which were valid at the time of measurement, in the outdoor environment. The measuring point MM1 was chosen to be located in front of the window of the principal's room of Pulmonology of UHMC Bežanijska kosa on the high ground floor at a height of about 3 m from the ground, and it is about 187 m away from the center axis of the road [3,4], while the measuring point MM2 was chosen that it is located in front of the window of Hall A of the City Institute for Medical Emergency on the first floor at a height of about 6 m from the ground, that is, about 3 m from the level of the road, and it is about 40 m from the center line of the road [5,6].

Noise level measurements were made using a windscreen. Meteorological conditions did not affect the measurement results, except on the third day of measurement at measuring point MM1 after the construction of the sound barrier, when the wind speed exceeded the value of 5 m/s. Those results were not considered in further analysis.

The dominant noise source on the subject sections is road traffic originating from traffic from the roads Arsenija Čarnojevića Boulevard and Franše d'Epere Boulevard. Also, the impact of other activities is evident at the measurement points, and given that the measurement points are defined within the hospital or medical emergency, including local parking lots and access roads in the further vicinity.

During all the measurements, the traffic was counted against the measuring point for 15 minutes, for each direction of the road separately, according to the classification of traffic into light vehicles, heavy vehicles and motorcycles. The traffic count will not be shown separately in the paper, but it was estimated that on average around 1800 vehicles pass by the measuring point MM1 in the daily measurement period in an interval of 15 minutes, and around 2100 vehicles pass by the measuring point MM2, while it was stated that the traffic flow during practically unchanged by all measurements.

Noise level measurements covered a continuous period of time within five days including weekend days on MM1 and within three working days on MM2 and included monitoring of statistical parameters: A-weighted equivalent continuous sound pressure level $L_{Aeq,15min}$ and percentage levels $L_{AF5,15min}$, $L_{AF10,15min}$, $L_{AF50,15min}$, $L_{AF90,15min}$ and $L_{AF95,15min}$. determined in successive 15-minute intervals during a period of 93 h at measuring point MM1, that is, 47 h at measuring point MM2. The paper will show only the A-weighted equivalent continuous sound pressure levels $L_{Aeq,15min}$ as a representative parameter that will be used on both sections when comparing the results obtained before and after the construction of sound barriers.

Calculated A-weighted equivalent continuous sound pressure levels values L_{day} for the daily measurement period, $L_{evening}$ for the evening measurement period and L_{night} for the night measurement period, as well as the value of the noise level for day-evening-night L_{den} were done with a software SLC ver 4.1 (2008).

The measurement results are tabulated with the calculated A-weighted equivalent continuous sound pressure levels for the day L_{day}, evening $L_{evening}$ and night L_{night} during the measurement period of 24 h, their average values during the entire measurement period as well as the average noise level for day-evening-night L_{den} during the same measurement period.

At the measuring point MM1, these values are given in Tab. 1 before the construction of the sound barrier and in Tab. 2 after its construction, while at the measuring point MM2 they are given in Tab. 3 before the construction of the sound barrier and in Tab. 4 after its construction.

Table 1 Calculated values L_{day}, $L_{evening}$, L_{night} and L_{den} at the measuring point MM1 before the construction of the sound barrier

No.	Day L_{day} (dB (A))	Evening $L_{evening}$ (dB (A))	Night L_{night} (dB (A))	Day rec.no.	Evening rec.no.	Night rec.no.
1	55.1	58.8	55.2	25	16	32
2	55.3	57.2	54.0	48	16	32
3	54.3	55.8	51.0	48	16	32
4	57.3	55.9	52.7	48	16	32
5	58.1	–	–	14	–	–
Average	56.0	57.1	53.5	183	64	128
L_{den} = 61 dB(A)						

Table 2 Calculated values L_{day}, $L_{evening}$, L_{night} and L_{den} at the measuring point MM1 after the construction of the sound barrier

No.	Day L_{day} (dB (A))	Evening $L_{evening}$ (dB (A))	Night L_{night} (dB (A))	Day rec.no.	Evening rec.no.	Night rec.no.
1	53.5	52.2	50.7	25	16	32
2	53.0	51.0	48.1	48	16	32
3	–	–	–	–	–	–
4	54.5	51.7	47.8	48	16	32
5	56.7	–	–	13	–	–
Average	54.1	51.7	49.1	134	48	96
L_{den} = 57 dB(A)						

Table 3 Calculated values L_{day}, $L_{evening}$, L_{night} and L_{den} at the measuring point MM2 before the construction of the sound barrier

No.	Day L_{day} (dB (A))	Evening $L_{evening}$ (dB (A))	Night L_{night} (dB (A))	Day rec.no.	Evening rec.no.	Night rec.no.
1	67.3	66.8	62.6	19	16	32
2	67.1	66.8	62.5	48	16	32
3	65.4	–	–	29	–	–
Average	67.3	66.8	62.6	96	32	64
L_{den} = 70 dB(A)						

Table 4 Calculated values L_{day}, $L_{evening}$, L_{night} and L_{den} at the measuring point MM1 after the construction of the sound barrier

No.	Day L_{day} (dB (A))	Evening $L_{evening}$ (dB (A))	Night L_{night} (dB (A))	Day rec.no.	Evening rec.no.	Night rec.no.
1	57.3	57.5	53.6	19	16	32
2	57.6	57.5	54.6	48	16	32
3	58.6	–	–	29	–	–
Average	57.9	57.5	54.1	96	32	64
L_{den} = 62 dB(A)						

Measurements both before and after the construction of sound barriers at the measuring point MM1 began on Friday at 12.00, and the value L_{day} for the first daily period was calculated from 23 data for A-weighted equivalent continuous sound pressure levels measured in 15-minute intervals. Value L_{day} for the last daily period was calculated from 13 data for A-weighted equivalent continuous sound pressure levels measured in 15-minute intervals, considering that measurement ended on Tuesday at 9.00.

Measurements both before and after the construction of sound barriers at the measurement point MM2 began on Wednesday at 1:30 p.m, and the value L_{day} for the first daily period was calculated from 19 data for A-weighted equivalent continuous sound pressure levels measured in 15-minute intervals. Value L_{day} for the last daily period was calculated from 29 data for A-weighted equivalent continuous sound pressure levels measured at 15-minute intervals, because the measurement ended on Friday at 1:15 p.m.

In both cases, the average values for L_{day}, $L_{evening}$ and L_{night} as well as the average value L_{den} for the entire measuring period of 93 h at the measuring point MM1, that is, 47 h at the measuring point MM2.

The calculated values of A-weighted equivalent continuous sound pressure levels were made for the correct belonging of the measurement interval to the day, evening, or night time measurement period. During all calculations, local effects were taken into account as they appeared in the record and were not specially corrected. However, due to unfavorable weather conditions on the third day of measurement at measuring point MM1 after the construction of the sound barrier, the results are not relevant, so they were not taken into account during the calculation L_{day}, $L_{evening}$, L_{night} and L_{den}, and in the corresponding diagram below they will be blurred.

2.1. Comparative results

The measurement results are shown in diagrams as comparative results of A-weighted equivalent continuous sound pressure levels $L_{Aeq,15min}$ at 15-minute intervals before and after the construction of sound barriers at each of the measuring points. In the tables, the average values for L_{day}, $L_{evening}$ and L_{night} as well as the average value for L_{den} before and after the construction of sound barriers and according to the measurement point.

At the measuring point MM1, the comparative results are shown in the diagram in Fig. 4 and in Tab. 5, and at measuring point MM2 in the diagram in Fig. 5 and Tab. 6.

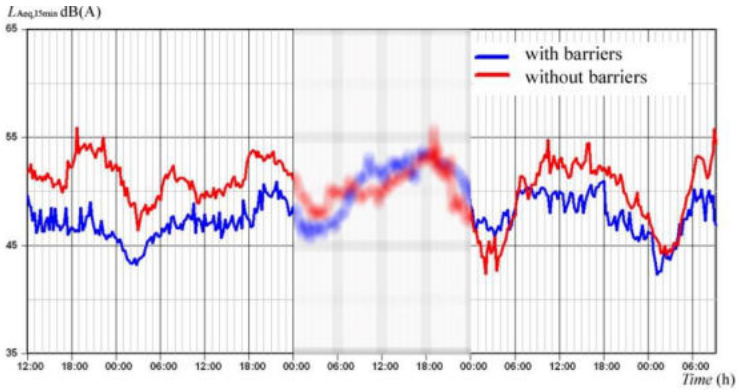

Fig. 4 Comparison chart of A-weighted equivalent continuous sound pressure levels $L_{Aeq,15min}$ before and after the construction of sound barriers at the measurement point MM1

Table 5 Calculated values L_{day}, $L_{evening}$, L_{night} and L_{den} at the measuring point MM1 after the construction of the sound barrier

MM1	L_{day} (dB (A))	$L_{evening}$ (dB (A))	L_{night} (dB (A))	L_{den} (dB (A))
Before	56.0	57.1	53.5	61
After	54.1	51.7	49.1	57
Difference	1.9	5.4	4.4	4

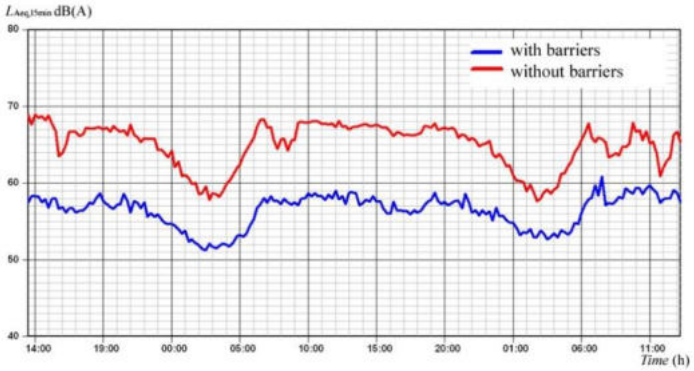

Fig. 5 Comparison chart of A-weighted equivalent continous sound pressure levels $L_{Aeq,15min}$ before and after the construction of sound barriers at the measurement point MM2

Table 6 Calculated values L_{day}, $L_{evening}$, L_{night} and L_{den} at the measuring point MM2 after the construction of the sound barrier

MM1	L_{day} (dB (A))	$L_{evening}$ (dB (A))	L_{night} (dB (A))	L_{den} (dB (A))
Before	67.3	66.8	62.6	70
After	57.9	57.5	54.1	62
Difference	9.4	9.3	8.5	8

3. The Obtained Results Comment

From the presented comparative diagrams of A-weighted equivalent continuous sound pressure levels $L_{Aeq,15min}$ along two busy roads in Belgrade: a) on the section along UHMC Bežanijska kosa and b) on the section next to the building of the City Institute for Medical Emergency, and from the tables of calculated values L_{day}, $L_{evening}$, L_{night} and L_{den} it can be stated that the existing noise levels caused by road traffic decreased after the construction of the sound barriers, and that their construction is justified.

On the section along UHMC Bežanijska Kosa, which is far from the sound barrier, a trend of decreasing noise level values can be seen on average for L_{day} 1.9 dB (A), for $L_{evening}$ 5.4 dB (A), for L_{night} 4.4 dB (A), and for the overall level for day-evening-night L_{den} 4 dB (A).

On the section next to the building of the City Institute for Medical Emergency near Mostar Interchange, which is located near the sound barrier, a trend of decreasing noise level values can be seen on average for L_{day} 9.4 dB (A), for $L_{evening}$ 9.3 dB (A), for L_{night} 8.5 dB (A), and for the overall level for day-evening-night L_{den} 8 dB (A).

A rough sketch of the measuring points showing the measuring points in relation to the road is given in Fig. 6 for both sections in question. In the sketch, it can be clearly seen that both measuring points MM1 and MM2 are largely protected from the direct propagation of sound (road traffic noise) by a sound barrier as a physical barrier, where the acoustic properties of the selected barriers play an important role, in the first place the single-number rating of airborne sound insulation DL_R and single-number rating of sound absorption DL_α [7,8]. The same sketch also shows that the sound can reach the imission point via a detour, due to the diffraction phenomenon, but the measuring point MM2 on the section next to the building of the City Institute for Medical Emergency is largely in the sound shadow created by the constructed barrier because it is located directly behind it and that this is one of the main reasons why the noise level reduction values at that measuring point are much higher than in the case of the section along UHMC Bežanijska kosa where measuring point MM1 is significantly far from the road and is not in the sound shadow created by the barrier [9].

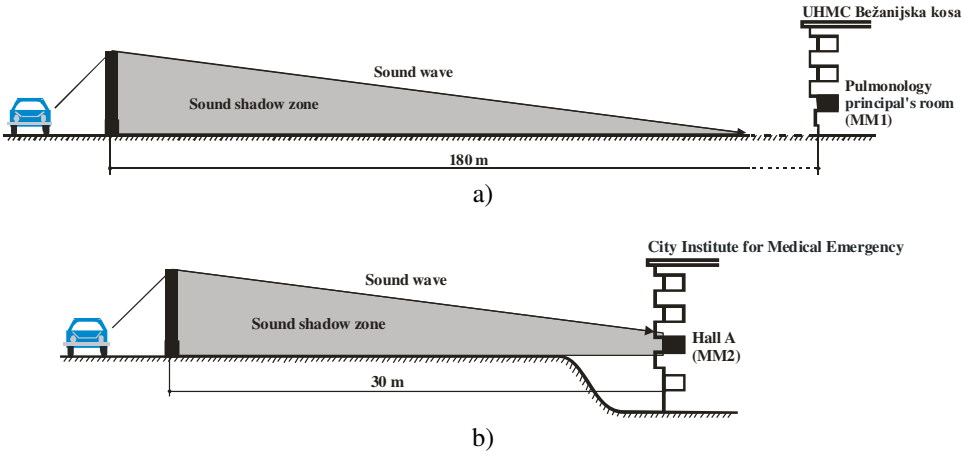

Fig. 6 A rough sketch of measuring points and their positions in relation to the sound shadow zone: a) at measuring point MM1 and b) at measuring point MM2

However, the reduction of the noise level by the construction of a barrier on the section along UHMC Bežanijska kosa is not negligible, because the facilities and population (citizens and staff) in the vicinity of the hospital, which are located at a high distance from the road, are still protected from the direct spread of the noise of the busy road, primarily bearing in mind that the traffic road belongs to acoustic zone 5, and the clinic-hospital center to acoustic zone 1 [10,11] where the required noise levels are far lower than the level near the road.

A similar situation is with the section next to the building of the City Institute for Medical Emergency, which is located right next to a busy traffic road, belongs to acoustic zone 5, and the City Institute for Medical Emergency to acoustic zone 1, where the required noise levels are far lower than the levels near the road. and citizens and staff staying in this building are particularly exposed to this type of noise.

4. CONCLUSION

Based on the presented measurement results, it is concluded that the effectiveness of the construction of sound barriers on the sections along traffic roads is sometimes less and sometimes more significant. Their construction is certainly justified at whatever distance the immission point is located, because based on the results obtained, no matter how much the noise reduction is (perhaps it seems that 4 dB or 8 dB is a small reduction in the noise level), it is very significant for the population which should be protected from excessive noise that harmful effects on human health first and then all aspects of human live and work, because these are not insignificant values.

From the technical point of view, the efficiency of the construction of sound barriers depends on the distance of the barrier from the point of immission. When the noise source is directly behind the barrier (case of road traffic noise) the following rule applies - the more distant the barrier is from the point of immission, the smaller the sound shadow is, and the diffraction occurrence and larger sound waves result in less protection efficiency, regardless of the barrier's acoustic properties.

Acknowledgement: *The work was created during the duration of the contract between the IMS Institute and the Ministry of Science, Technological Development and Innovation (registration number of the contract: IMS No. 30-1331d 08.02.2024). The paper used measurement of noise levels before and after the construction of sound barriers on sections of traffic roads in Belgrade: Arsenija Čarnojevića Boulevard (former section of highway E-70 Belgrade-Zagreb) and Franše d'Eperea Boulevard (former section of highway E- 75 Belgrade-Niš) during 2016 and 2017. The authors would like to thank the client of the study, CPG d.d, Radnička SStreet 5g, Belgrade-Čukarica.*

REFERENCES

1. SRPS ISO 1996-1: 2010 Acoustics — Description, measurement and assessment of environmental noise – Part 1: Basic quantities and assessment procedures.
2. SRPS ISO 1996-1: 2010 Akustika – Acoustics — Description, measurement and assessment of environmental noise – Part 2: Determination of sound pressure levels.
3. IMS Institute Belgrade, Laboratory for Acoustics and Vibrations, (2016), Test report No. LAV 5077/16.
4. IMS Institute Belgrade, Laboratory for Acoustics and Vibrations, (2017), Test report No. LAV 5124/17.
5. IMS Institute Belgrade, Laboratory for Acoustics and Vibrations, (2017), Test report No. LAV 5153/17.

6. IMS Institute Belgrade, Laboratory for Acoustics and Vibrations, (2017), Test report No. LAV 5220/17.
7. SRPS EN 1793-2:2018 – Road traffic noise reducing devices – Test method for determining the acoustic performance – Part 2: Intrinsic characteristics of airborne sound insulation under diffuse sound field conditions.
8. SRPS EN 1793-1:2017 – Road traffic noise reducing devices – Test method for determining the acoustic performance – Part 1: Intrinsic characteristics of sound absorption under diffuse sound field conditions.
9. Maekawa, Z., (1968), Noise reduction by screens. *Applied AcousticsAcoustics*, *1*(3), 157-173.
10. Pravilnik o metodologiji za određivanje akustičkih zona, *Službeni glasnik RS br. 72/10.*
11. Uredba o indikatorima buke, graničnim vrednostima, metodama za ocenjivanje indikatora buke, uznemiravanja i štetnih efekata buke u životnoj sredini, *Službeni glasnik RS br. 75/10.*

FACTA UNIVERSITATIS
Series: **Working and Living Environmental Protection** Vol. 21, Nº 4, Special Issue, 2024, pp. 293 - 303
https://doi.org/10.22190/FUWLEP241003028S

Original scientific paper

THE POLAR CHARACTERISTIC OF AN ACOUSTIC PARABOLIC REFLECTOR

UDC 534

Violeta Stojanović[1], Zoran Milivojević[2]

[1]Academy of Applied Technical and Preschool Studies, Niš Department, Niš, Serbia
[2]MB University Belgrade, Serbia

ORCID iDs: Violeta Stojanović https://orcid.org/0009-0009-4877-6696
Zoran Milivojević https://orcid.org/0000-0002-2240-3420

Abstract. *The first part of the paper presents the geometry of the acoustic parabolic reflector. After that, analytical formulas for calculating the amplification and polar characteristics of the reflector are shown. The second part of the paper describes the experiment in which measurements were made and the acoustic characteristics of the parabolic reflector located in the yard of the Academy of Applied Technical and Preschool Studies, Department of Niš, in Niš were calculated. First, acoustic impulse responses for acoustic excitation at angles from -90° to 90° were measured. After that, the polar characteristic of the radiation was calculated. Finally, the beamwidth of the radiation, beam solid angle of the radiation, and directivity of the acoustic parabolic reflector were determined. The results of the experiment are presented numerically and graphically.*

Key words: *impulse response, polar characteristic, directivity.*

1. INTRODUCTION

The concentration and behavior of waves on curved surfaces have been studied since ancient times. The Greek mathematician Diocles, somewhere between 190 and 180 BC, wrote about the "surface of a mirror which, when positioned towards the Sun, reflects the sun's rays that converge to a single point, thus causing ignition" [1]. This concept was applied in 1896 during the lighting of the first Olympic torch relay using sunlight, concentrated by a parabolic mirror. A. W. Love noted in his articles published before 1978 that as early as 1888, Heinrich Hertz, who experimentally proved the existence of electromagnetic waves, constructed the first antenna from a metal plate that was a curved,

Received October 3, 2024 / Accepted October 10, 2024
Corresponding author: Violeta Stojanović
Academy of Applied Technical and Preschool Studies, Niš Department, Aleksandra Medvedeva 20, 18000 Niš, Serbia
E-mail: violeta.stojanovic@akademijanis.edu.rs

cylindrical parabolic surface ensuring that the focal area was a line, not a point. J. W. S. Rayleigh's first insights into the reflection of sound waves on curved surfaces are associated with the cave of Dionysius' Ear in Syracuse, Sicily (Dionysius ruled Syracuse between 432 and 376 BC). He also highlights St. Paul's Cathedral in London and its Whispering Gallery inside the dome, built in 1710, for its unique acoustic effects.

Kremer and Miller, referencing the impressions of Reverend John Blackburn in 1828, state that the first use of acoustic parabolic reflectors occurred in churches in the 19th century [2]. They emphasize the necessity of an adequately sized acoustic parabolic reflector and note that the priest should not be positioned at the reflector's focus during the liturgy, as the noise from the congregation would significantly disturb him. V. C. Sabine, who studied room reverberation time, also provided theoretical assumptions and explanations related to this issue [3].

Acoustic parabolic reflectors were used before the development of radar, between the First and Second World Wars, for detecting airplanes [4]. There were: a) small reflectors mounted on the listener's head, b) large ones transported by trucks, and c) gigantic stationary concrete structures, some of which still exist near the coast of Great Britain, aimed at the English Channel. In 1930, Olson and Wolff published two papers proposing the use of parabolic constructions that function as a horn at low frequencies and as a reflector at higher frequencies [5]. In 1932, Kellogg constructed a parabolic reflector for recording wildlife sounds, publishing his research in 1938.

Today, acoustic parabolic reflectors are used in various applications: a) in engineering research for the detection of acoustic signals in non-contact testing methods, b) with parabolic microphones for sound recording in nature (such as bird recording, locating and rescuing lost people and animals), field sound for sports broadcasting and eavesdropping on conversations. They are also used in education and entertainment, such as telescopes in astronomy and sound reflectors in auditoriums and amphitheaters.

This paper presents the polar characteristic of an acoustic parabolic reflector located in the yard of the Academy of Applied Technical and Preschool Studies, Department of Niš, in Niš. After discussing the geometry and analytical formulas for calculating the amplification and polar characteristics of the acoustic reflector, the experiment is explained. The basis of the experiment consists of impulse responses h_θ for acoustic excitation at angles $\theta = -90^o: 15^o: 90^o$. Based on the impulse responses, the amplitude characteristics of sound waves as a function of angle θ are presented. The following were calculated: a) the amplification of the reflector, b) the polar radiation characteristic, c) beamwidth and the beam solid angle of radiation, and d) directivity. The results of the experiment are presented both numerically and graphically.

The organization of the paper is as follows: Section 2 presents the geometry and characteristics of the acoustic parabolic reflector, Section 3 explains the experiment, presents and analyzes the results of the experiment, and Section 4 presents the conclusion.

2. ACOUSTIC PARABOLIC REFLECTOR

2.1. Geometry and characteristics of the reflector

A parabolic surface or paraboloid is formed by rotating a parabolic curve around its axis of symmetry [6]. The main characteristic of a paraboloid is that all incident rays parallel to the axis of rotation correspond to reflected rays that pass through and intersect at a single common point, the focus. When a section is cut from the surface of the paraboloid (which is mathematically

infinite), a parabolic reflector is obtained. If the plane cutting the paraboloid is perpendicular to the axis of symmetry, a circular section of the paraboloid is formed, with its focus at the center – on the axis of symmetry at a certain distance from the geometric center of the surface. In most parabolas, the focus is located outside the parabola's aperture because the cutting plane is usually closer than the focal distance. The section obtained in this manner is a classic parabolic reflector.

In Fig. 1, a model of a parabolic reflector is given where: h – the depth of the reflector, R – the aperture radii, h_v – the distance from the vertex O of the parabola and the wavefront, z_s – the distance of a point located on the surface of the reflector (P_1) from the line passing through the vertex O, z_F – the distance from the focus F to the vertex (FO) [7]. The movement of the acoustic wavefront is represented by rays (1) and (2). The path that a wave takes from any position in the plane of the parabola's aperture (P_0, P_2) to the focus F is constant, i.e., the equation holds: $P_0F = P_2F$. This means that the energy of the wavefront from the plane of the aperture will be concentrated at the focus F. The equation of the parabolic reflector is:

$$r^2 = 4 \cdot z_F \cdot z \,. \tag{1}$$

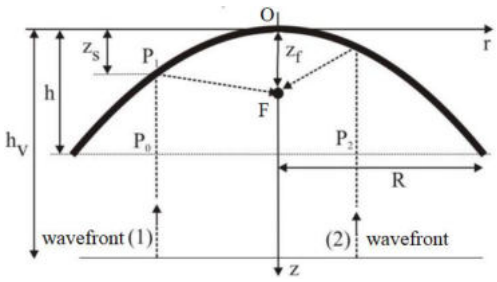

Fig. 1 Model of an acoustic parabolic reflector

The ratio of sizes z_F/h determines the angle at which the edges of the parabola are seen from the focus. The smaller the ratio z_F/h, the deeper the reflector, and the larger this angle. Conversely, if the ratio z_F/h is larger, the reflector is shallower, and the angle is smaller. Fig. 2 shows the geometry of parabolic reflectors with equal radii R but different z_F/h ratios.

2.2. Amplification and polar characteristic of the reflector

In the plane of the reflector's aperture, acoustic waves have an acoustic pressure, P_i. After reflection, the waves are concentrated at the focus of the reflector, where they generate a pressure P_z [8]. The amplification of the reflector is defined as $F_z = P_z / P_i$. The formula for calculating the theoretical amplification of the reflector is:

$$F_z = \left(\begin{array}{l} 1 + \left[4\pi \dfrac{z_F}{\lambda} \ln\left(1 + \dfrac{h}{z_F} \right) \right] + \\ 8\pi \dfrac{z_F}{\lambda} \ln\left(1 + \dfrac{h}{z_F} \right) \sin\left(4\pi \dfrac{z_F}{\lambda} \right) \end{array} \right)^{\frac{1}{2}}, \tag{2}$$

where λ is the wavelength of the incident acoustic wave. When sin $(4\pi z_F/\lambda) = \pm 1$, the following equation is obtained:

$$F_z = 4\pi \frac{z_F}{\lambda} \ln\left(1+\frac{h}{\lambda}\right) \pm 1 . \tag{3}$$

For high amplification, Eq. (3) becomes:

$$F_z = 4\pi \frac{z_F}{\lambda} \ln\left(1+\frac{R^2}{4{z_F}^2}\right). \tag{4}$$

The amplification of an acoustic parabolic reflector depends on its dimensions h, R and z_F as well as the wavelength λ (or frequency) of the acoustic wave. The amplification of an acoustic parabolic reflector, expressed in dB, can be represented as follows:

$$G = 20\log_{10}\left(F_z\right). \tag{5}$$

The increase in amplification per octave can be analyzed as a function of the z_F/λ: a) the amplification increases by 6 dB/octave in the frequency range where $z_F/\lambda \geq 1$ (Figs. 2a and 2b), b) the amplification is equal to 0 in the low-frequency region where $z_F/\lambda < 1/64$ and c) the amplification is variable for $1/64 < z_F/\lambda < 1$, which is a result of the sine term in Eq. (2). The last enhancement in strength is more pronounced in flat reflectors where $h/z_F < 1$ (Fig. 2c). Specifically, when the direct and reflected sound waves are approximately equal in strength, the reflected sound wave initiates the formation of a standing wave.

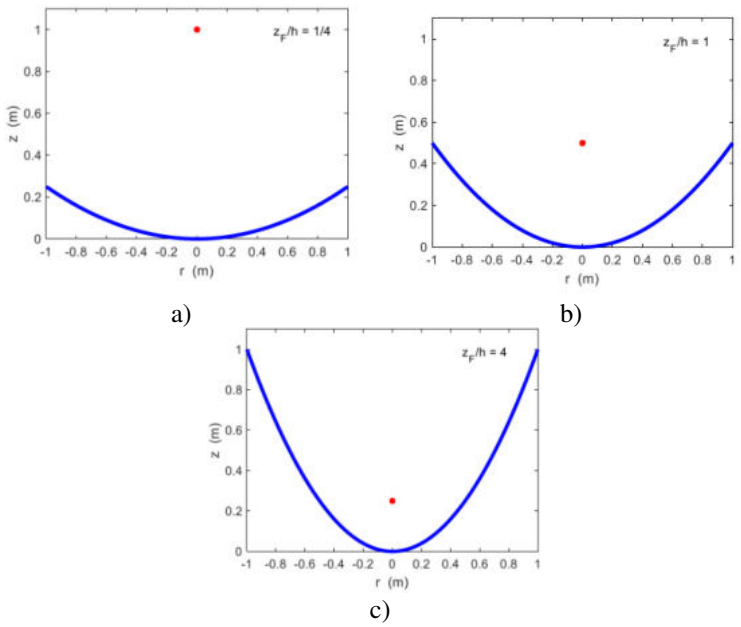

Fig. 2 Geometry of parabolic reflectors with equal radii R and: a) z_F/h = ¼; b) z_F/h = 1; c) z_F/h =4

The polar characteristic of an acoustic parabolic reflector represents a graphical representation of the distribution of acoustic amplification of sound waves in different directions (after their reflection and directing) in a polar diagram [9].

Normalized amplification of the acoustic parabolic reflector represents the ratio of the reflector's gain G (dB) (given Eqs. (2) and (5)), and the maximum gain G_{max} (dB) (given by Eqs. (4) and (5)) [8]. The beamwidth of the reflector, $\Delta\theta_B$, represents a parameter measured at half of the radiation power [9]. It is defined as the angle between two points on the main radiation beam of the reflector that is 3 dB lower in value than the level of maximum emission. The beam solid angle can be calculated as a function of the beamwidth as follows:

$$\Delta\Omega = \frac{\pi}{4}\left(\Delta\theta_B\right)^2 . \tag{6}$$

Directivity represents a measure of the directionality of the radiation pattern of the reflector. Since the acoustic parabolic reflector has a highly directional radiation diagram, directivity can be expressed by the following formula:

$$D_{\max} = \frac{16}{\Delta\theta_B{}^2} . \tag{7}$$

Directivity in dB is:

$$D = 10\log_{10} D_{\max} . \tag{8}$$

The beam width and the beam solid angle of the radiation are illustrated in Fig. 3.

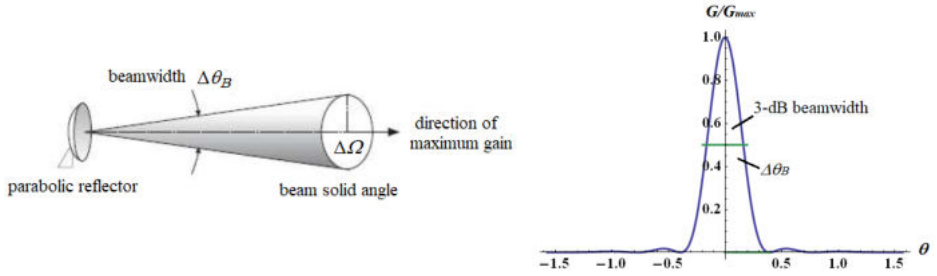

Fig. 3 Beamwidth and beam solid angle of the radiation

3. Experimental Results and Analysis

3.1. Experiment

For the purpose of determining the polar characteristics of the radiation and the characteristics of the acoustic parabolic reflector, an experiment was conducted. The experiment included: a) measurement of acoustic impulse responses for acoustic excitation as a function of the angular displacement of the sound source relative to the axis of the reflector $\theta = (-90^o \div 90^o)$ with a step of $\Delta\theta = 15^o$, b) calculation of the reflector's amplification (G (dB) and G_{max} (dB)) at the focus as a function of angle θ, c) calculation of the polar characteristic of the reflector ($G/G_{max} = f(\theta)$), d) amplitude characteristics of sound waves

for different angles θ and f) calculation of reflector parameters: beamwidth $\Delta\theta_B$, beam solid angle $\Delta\Omega$ and maximum directivity, D_{max}.

For the experiment, the measurement was conducted on the acoustic parabolic reflector located in the courtyard of the Academy of Applied Technical and Preschool Studies, Department of Niš, in Niš (Fig. 4a). The geometry of the reflector is shown in Fig. 2a. The dimensions of the reflector are a) depth h = 0,3571 m, b) aperture radii R = 1 m, c) focal length z_F = 0,7 m. The reflector is made of concrete. The surface of the reflector opening was considered ideally smooth (the reflection coefficient is equal to 1).

The measurement procedure consists of the following: the excitation signal was emitted by a sound source whose position was changed along a semicircle (with the center in the vertex of the reflector) with a radius r = 5 m for angles θ with a step of $\Delta\theta$. The receiver was positioned at the focus of the reflector (Fig. 4b). The ambient temperature was t = 32° and the speed of sound was c=350.39 m/s. The results of the experiment are presented graphically and numerically. The software support used was EASERA and Matlab.

The equipment used for the experiment as follows: a) an omnidirectional microphone (PCB 130D20), having a diaphragm diameter of 7 mm; b) B&K omnidirectional sound source type 4295 (dodecahedron loudspeaker); c) B&K audio power amplifier, rated at 100W RMS, stereo, type 2716-C; d) a laptop, incorporating a Soundmax Integrated Digital Audio sound card from Analog Devices.

a) b)

Fig. 4 a) The acoustic parabolic reflector in the yard of the Academy of Applied Technical and Preschool Studies, Department of Niš, in Niš and b) the position of the receiver during the experiment

3.2. The Base

The basis of the experiment consists of impulse responses. In order to determine the impulse responses h_θ from the transmitting side, a sweep signal was emitted with the following parameters: $f_d = 20$ Hz, $f_g = 20$ kHz, (that is $\lambda_g = 17.52$ m, $\lambda_d = 0.018$ m), $t = 5$ s, sampling frequency $f_S = 44.1$ kHz and 16 bps. Impulse responses were recorded in 13 measuring points for $\theta = -90^o : 15^o : 90^o$.

3.3. The Results

Table 1 presents the calculated values for the considered parameters of the acoustic parabolic reflector: a) amplification G for sound waves of frequencies: $f = \{20, 100, 1000, 10000, 20000\}$ Hz, b) beamwidth of the radiation $\Delta\theta_B$, c) beam solid angle of the radiation $\Delta\Omega$ and d) maximum directivity of the reflector D_{max}.

Table 1 The calculated values of the parameters of the acoustic parabolic reflectors

f (Hz)	20	100	1000	10000	20000
G (dB)	-13.681	0.298	20.298	40.298	46.319
$\Delta\theta_B$ (°)			17.46		
$\Delta\theta_B$ (rad)			0.305		
$\Delta\Omega$ (sr)			0.073		
D_{max}			172.336		
D_{max} (dB)			22.363		

Figure 5 shows: a) the theoretical amplification of the analyzed reflector at the focus as a function of the ratio z_F/λ and b) the theoretical amplification of the reflector at the focus as a function of the ratio z_F/λ calculated without the sine term in Eq. (2) [8].

The acoustic impulse responses h are shown in: a) Fig. 6a ($\theta = 0^0$), b) Fig. 7a ($\theta = 45^o$) and c) Fig. 8a ($\theta = 90^o$). The amplitude characteristics $20\cdot\log_{10}(H)$ are shown in: a) Fig. 6b ($\theta = 0^o$), b) Fig. 7b ($\theta = 45^o$) and c) Fig. 8b ($\theta = 90^o$). The normalized acoustic amplification $|G/G_{max}|$ as a function of the angle θ is shown in Fig. 9a. The polar characteristic is presented in Fig. 9b.

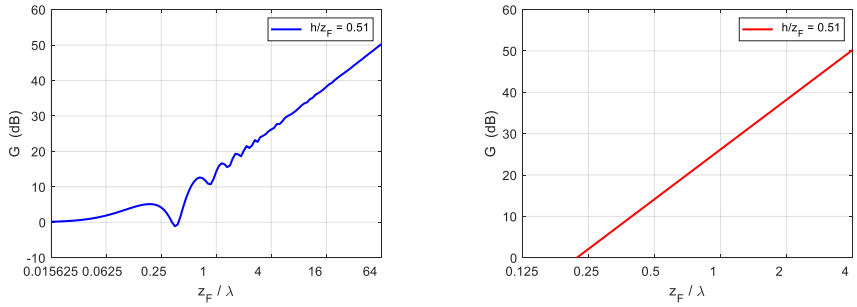

a) b)

Fig. 5 a) The theoretical amplification of the analyzed reflector at the focus as a function of the ratio z_F/λ and b) the theoretical amplification of the reflector at the focus as a function of the ratio z_F/λ calculated without the sine term in Eq. (2)

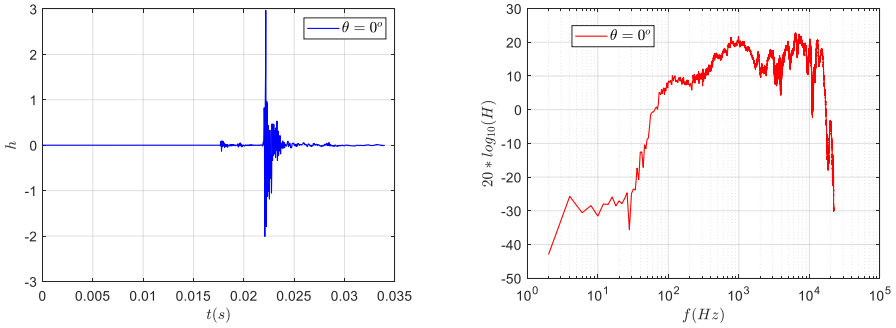

a) b)

Fig. 6 Acoustic impulse response for $\theta = 0^o$: a) time domain and b) amplitude characteristic

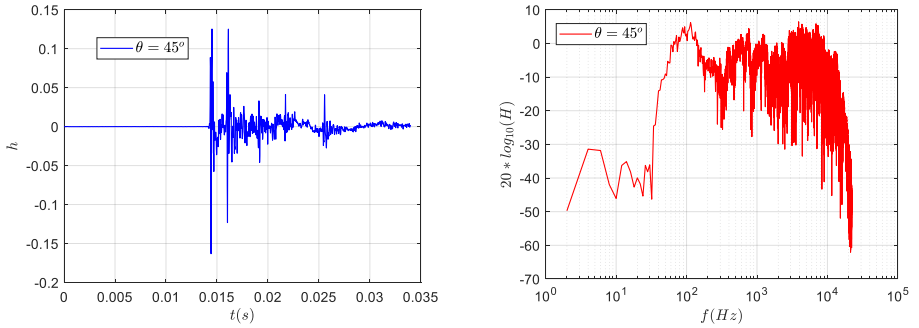

a) b)

Fig. 7 Acoustic impulse response for $\theta = 45^o$: a) time domain and b) amplitude characteristic

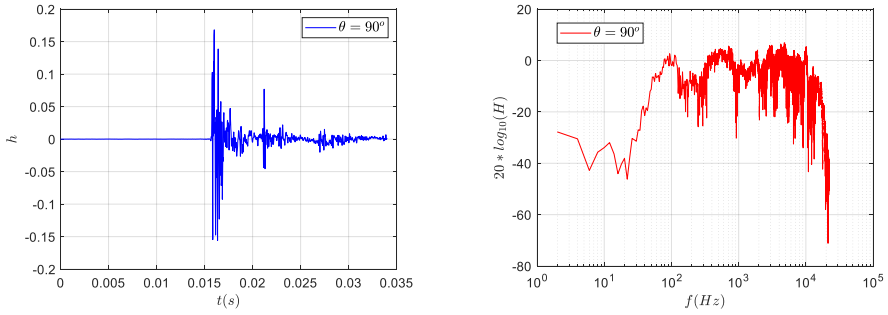

a) b)

Fig. 8 Acoustic impulse response for $\theta = 90^o$: a) time domain and b) amplitude characteristic

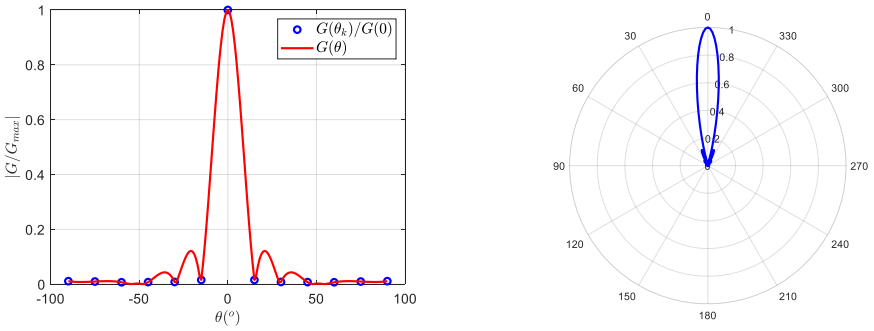

a) b)

Fig. 9 a) The normalized acoustic amplification as a function of the angle θ, b) polar characteristic of the acoustic parabolic reflector

3.4. The Results Analysis

Based on the results presented in Tab. 1 and in Figs. 5÷9, the following conclusions can be drawn:

1) Regarding the amplification of the acoustic parabolic reflector:
   a) based on the theoretical assumptions, the amplification at the focal point of the reflector was calculated as a function of the ratio z_F/λ [8]. For sound waves with frequencies f = 20 Hz ÷ 20 kHz the amplification values are: G = -13.681 ÷ 46.319 dB. For f = {20, 100} Hz, there is no amplification, as this reflector has limited efficiency at lower frequencies. With increasing frequency, the amplification value also rises. Amplification depends on the dimensions of the reflector,
   b) this reflector demonstrates high amplification for waves with frequencies f = {1000, 10000} Hz and a ratio z_F/λ = 1.998 ÷ 19.978: G = 20.298 ÷ 40.298 dB. For waves with frequencies f = {10, 20} kHz and for z_F/λ = 19.978 ÷ 39.956 the amplification is G = 40.298 ÷ 46.319 dB.
   These values indicate that the reflector has extreme amplification, and exceptional efficiency, meaning that it enables high directionality of sound waves with minimal losses [10].
2) Regarding the parameters of the acoustic parabolic reflector:
   a) the values for the beamwidth, $\Delta\theta_B$ = 17.46° and the solid angle $\Delta\Omega$ = 0.073 sr indicate that the reflector focuses the reflected sound waves into a relatively narrow beam and that there is greater efficiency in transmitting sound energy to a specific point or in a particular direction [11]. This allows for better sound clarity, but it also means that the coverage of the sound space is limited and
   b) the maximum directivity of the reflector has a value of D_{max} = 172.336, or, D_{max} = 22.363 dB. This value categorizes the analyzed acoustic reflector among those with excellent directivity and confirms the reflector's efficiency in focusing the sound signal.
3) Regarding the amplitude characteristics of the acoustic parabolic reflector:
   a) the acoustic reflector, with the sound source positioned on its axis, θ = 0°, is most efficient for transmitting sound signals with frequencies f = 10^3 Hz and $f \approx$

10^4 Hz and sound level values of 21 dB and 23 dB, respectively. The peaks in Fig. 6b, with steep drops on both sides, indicate that the reflector is very precise in its directionality within this narrow range of frequencies [11]. This is also a result of the high amplitude being maintained within the narrow bands of the mentioned frequencies,

b) when changing the position of the sound source in relation to the axis of the reflector, for positions $\theta = 45^o$ and $\theta = 90^o$, the maximum amplitudes of the sound signals significantly decrease. Their levels are 5 dB and from 1 ÷ 3 dB, respectively, in the frequency range $f = 10^2 \div 5 \cdot 10^3$ Hz. In Figs. 7b and 8b, broader maxima can be observed with a slight drop on both sides. This indicates that as the source moves away from the axis, the directivity of the reflector decreases, and the reflector does not efficiently focus the sound, resulting in scattering and a loss of sound quality,

c) the maximum amplitudes for the position of the sound source: a) $\theta = 0^o$ are found in a higher frequency range, and b) $\theta = 45^o$ and $\theta = 90^o$ focus on lower frequencies. This indicates that the reflector performs better at higher frequencies when the source is directed straight toward it.

4) Regarding the polar characteristics of the acoustic parabolic reflector:

a) the normalized acoustic amplifications $|G/G_{max}|$ as a function of the sound source position, with respect to the angle θ, confirm the maximum directionality of the reflector along its axis and the maximum sound intensity at the focus. This enhances sound quality and reduces noise from other directions [10]. The smaller peaks in Fig. 9a for $|G/G_{max}| = \{0.01, 0.05\}$ indicate that the reflector slightly directs sound in the directions $\theta = \{20^o, 35^o\}$, but this is much weaker than the main beam. This is due to the reflection of the waves [10],

b) Figure 9 a is presented in a polar coordinate system (Fig. 9b). The normalized power is depicted as the radius r relative to the center. The main peak (leaf-shaped) indicating the maximum power of the reflector for the sound source position $\theta = 0^o$ has the largest radius, $r = 1$. The other peaks, which are symmetric with respect to the main peak (corresponding to the sound source positions $\theta = \{20^o, 35^o\}$), have much smaller radii. The uniform symmetry around the main axis indicates that the reflector evenly directs sound on both sides of the reflector's axis. This means that the reflector's performance remains consistent whether sound waves spread to the left or right of the main axis.

4. CONCLUSION

This paper analyzes the polar characteristics of the acoustic parabolic reflector located in the courtyard of the Academy of Applied Technical and Preschool Studies, Department of Niš, in Niš.

Based on the experiment, which involved recording acoustic impulse responses for acoustic excitation at angles $\theta = -90^o: 15^o: 90^o$, the following results were obtained:

1) the amplification of the reflector is:

a) $G = 20.298 \div 40.298$ dB for waves whose frequencies are $f = \{1000, 10000\}$ Hz and for $z_F/\lambda = 1.998 \div 19.978$ and

b) $G = 40.298 \div 46.319$ dB for waves whose frequencies are $f = \{10, 20\}$ kHz and for $z_F/\lambda = 19.978 \div 39.956$,

2) the beamwidth of the radiation, $\Delta\theta_B = 17.46^o$ and the solid angle of the radiation $\Delta\Omega = 0.073$ sr,
3) the maximum directivity of the reflector $D_{max} = 22.363$ dB,
4) the maximum amplitudes for the position of the sound source:
   a) $\theta = 0^o$ are found in a higher frequency range where the sound signal levels are $21 \div 23$ dB, and
   b) $\theta = 45^o$ and $\theta = 90^o$ focus on lower frequencies where the sound signal levels are $1 \div 5$ dB,
5) the normalized acoustic amplification: a) $|G/G_{max}| = 1$ for the position of the sound source along its axis and b) $|G/G_{max}| = \{0.01, 0.05\}$ for the positions of the sound source $\theta = \{20^o, 35^o\}$ and
6) the polar characteristic shows the maximum power of the reflector for the position of the sound source $\theta = 0^o$.

Based on the obtained results, it can be concluded that the analyzed acoustic parabolic reflector shows reduced efficiency at lower frequencies, indicating limitations in sound transmission in that range. However, in the direction of the main axis, it exhibits extreme amplification at higher frequencies, exceptional efficiency, excellent directivity, and maximum normalized acoustic amplification, which is also confirmed by the polar characteristics of the reflector.

Thanks to these characteristics, the analyzed acoustic parabolic reflector is very suitable not only for further scientific research but also for the educational activities of students.

REFERENCES

1. Cormack J. M, Hamilton M. F. (2019), *Transient Solution for the Directional Response at the Focus of a Paraboloidal Reflector*, Acoustical Society America, Proceedings of Meetings on Acoustics, Vol. 35, 045002, pp. 1 – 10.
2. Cremer L., Muller H. A. (1978), *Principles and Applications of Room Acoustics*, Vol. 1, Applied Science, New York, pp. 92 – 96.
3. Sabine W. C. (1927), *Collected Papers on Acoustics,* Harvard.
4. Heifer M. (2009), *Sound Source Localisation with Acoustic Mirrors*, NAG/DAGA, Rotterdam.
5. Wahlstrom S. (1985), *The Parabolic Reflector as an Acoustical Amplifier*, J. Audio Eng. Soc., Vol 33, No. 6, pp. 418 – 429.
6. Dobričić D. (2007), *Efficient feed for offset parabolic antennas for 2.4 GHz*, AntenneX, pp. 1 - 20.
7. Y. T. Tsai, J. Zhua, (2013), *Transient Axial Solution for Plane and Axisymmetric Waves Focused by a Paraboloidal Reflector*, The Journal of the Acoustical Society America, Vol. 133 (4), pp. 2025-2035.
8. Milivojević Z. (2018), *Parabolični reflektor kao akustički pojačavač*, Zbornik radova VTŠSS Niš, pp. 36 – 39.
9. Balanis C. A. (2005), *Antenna Theory and Design – 3rd Edition*, John Wiley &Sons, Inc., Hoboken, New Jersey.
10. Pierce A. D. (2019), *Acoustics: An Introduction to ITS Phynciples and Applications*, Springer.
11. Kraus J. D., Marhefka R. J. (2017), *Antennas for All Applications – 2rd Edition*, Internet Archive HTML5 Uploader 1.6.3.

FACTA UNIVERSITATIS
Series: **Working and Living Environmental Protection** Vol. 21, Nº 4, Special Issue, 2024, pp. 305 - 315
https://doi.org/10.22190/FUWLEP241023029D

Original scientific paper

OPTIMIZATION OF NON-ACOUSTIC PARAMETERS OF FIBROUS MATERIALS USING BIOLOGICALLY INSPIRED ALGORITHMS

UDC 534:699.812.3

Tanja Dulović, Branko Radičević, Mišo Bjelić, Marina Ivanović

University of Kragujevac, Faculty of Mechanical and Civil Engineering in Kraljevo, Serbia

ORCID iDs:	Tanja Dulović	https://orcid.org/0000-0003-3265-5661
	Branko Radičević	https://orcid.org/0000-0002-4182-4095
	Mišo Bjelić	https://orcid.org/0000-0002-6148-1982
	Marina Ivanović	https://orcid.org/0000-0002-1576-7613

Abstract. *This paper deals with the optimization of the acoustic properties of samples made of fibrous materials, using biologically inspired algorithms. Samples with a thickness of 10 mm were tested, and the results showed that cotton fibers bonded with polyurethane resin have excellent absorption properties in a wide frequency range. GWO, BW and Puma were used for optimization. The optimization results showed significant improvements in the acoustic properties of the material, opening up possibilities for further application in sound insulation and other relevant areas.*

Key words: *non-acoustic parameters, porous materials, biologically inspired algorithms*

1. INTRODUCTION

Acoustic materials play a key role in the design of sound insulation systems, noise reduction and sound comfort enhancement in many branches. Noise control is relevant more than ever in cities, where high noise exposure has proven to have a number of negative consequences for health, namely, stress, sleep disturbance, work performance etc. [1]. One of the common solutions to improve noise performance is the introduction of high sound-absorbing materials, such as fibrous materials [2]. Sound absorption is viewed in terms of the sound absorbing coefficient, which quantifies the energy loss of the sound wave when it strikes a given surface.

However, one of the most important problems in the design of acoustic systems is the choice and optimization of properties of appropriate materials to obtain the best possible

Received October 23, 2024 / Accepted November 1, 2024
Corresponding author: Branko Radičević
University of Kragujevac, Faculty of Mechanical and Civil Engineering in Kraljevo, Dositejeva 19, 36000 Kraljevo, Serbia
E-mail: radicevic.b@mfkv.kg.ac.rs

results for different ranges of frequency. It was established that fibrous materials, like cotton fibres, are good sound absorbents because of their porous structure that promotes the scattering and absorption of waves. Their applications are particularly great in construction, the automotive sector, and the furniture industry, whereby noise reduction requirements are of primary importance.

The sound absorption performance normally is described by the sound absorption coefficient, experimentally measurable using an impedance tube [3] or predictable using acoustic transmission analysis methods in tandem with experimental measurements [4]. Various models have been developed to accurately determine the sound absorption coefficient of porous materials. The JCA model (Johnson-Champoux-Allard) is one of the most famous in this field, because it allows a detailed analysis by taking into account parameters such as air-flow resistance, porosity, and thermal conductivity of the material [5]. Despite the fact that the JCA model finds extensive application, the determination of its non-acoustic parameters is difficult to obtain. Normally, such parameters relate to a class that is difficult to quantify because of the variation of either structure or geometry from one fibrous material to another, which makes their analysis precise. Biologically inspired optimization algorithms find an increasing application in the effort to avoid these problems.

For a long period of time, the geometrical complexity involved with the material structure or the associated nonlinearity with the problem restricted the traditional methods of optimization. Biologically inspired algorithms like Gray Wolf Optimizer (GWO), Beluga Whale Algorithm (BW), and Puma algorithm (PO) provide novel solutions to these challenges [6,7,8]. These algorithms, inspired by nature make them incredibly much more efficient in searching for an optimum solution in complex multidimensional space. Kolarević et al. [9] showed that the application of the GWO algorithm to porous materials significantly improves the sound absorption coefficient in high-frequency ranges, while the application of hybrid algorithms further increases the efficiency in the middle-frequency range [10]. In addition, in the work of Miodragović et al. [11], different metaheuristic methods were compared in the optimization of sound absorption, where biologically inspired algorithms showed superior results compared to classical optimization methods.

The aim of this work is to optimize the acoustic properties of fiber materials, especially cotton fibers bonded with polyurethane resin, using GWO, BW and PO. The optimization is aimed at increasing the sound absorption coefficient in a wide frequency range, which is of key importance for applications in areas such as construction and the automotive industry. The application of biologically inspired algorithms allows solving problems related to the determination of non-acoustic parameters and opens new opportunities for more efficient use of fibrous materials in acoustic applications.

2. METHODOLOGY

In this work for the analysis of the sound absorption in porous materials, the JCA model was applied. The JCA model is widely used for describing the acoustic properties of materials because it gives the possibility to make detailed modeling of a coefficient of sound absorption, taking into account non-acoustic parameters: air-flow resistance, the porosity of the material, and thermal conductivity [5]. These parameters are very important in predicting the behavior of materials for running various frequency ranges. However,

determining the exact value of these parameters is quite demanding due to such diversified and complex structure of fibrous materials. In this paper, optimization is performed using biologically inspired algorithms to provide closer-to-real values of the model parameters and hence increase the coefficient of sound absorption.

As the basic material for testing, cotton fibers were used, which are known for their good absorption properties due to their porous structure, which enables efficient absorption and dispersion of sound waves. These fibers are bonded with polyurethane resin to increase mechanical stability and durability. Cotton fibers were chosen due to their environmental benefits, ease of processing and already proven effectiveness in sound applications, especially in the construction and automotive industries [12].

2.1. Biologically inspired algorithms

Biologically inspired algorithms were used to optimize model parameters and improve the acoustic properties of the material. These algorithms have become popular due to their ability to solve complex optimization problems in multidimensional spaces, where classical methods often fail. Three algorithms were used in this work: Gray Wolf Optimizer (GVO), Beluga Whale Algorithm (BW) and Puma algorithm, due to their proven effectiveness in optimizing acoustic parameters. Below is given a brief overview of each algorithm.

The Gray Wolf algorithm, also known as the Gray Wolf Optimizer (GWO), was proposed by Seyedali Mirjalili, Seyed Mohammad Mirjalil, and Andrew Lewis [6], and is based on the behavior of gray wolves during the search, pursuit, and hunt for prey. Gray wolves are social animals that live in packs, adhering to a strict social hierarchy. The pack is led by the dominant male or female, collectively known as alpha (α), who makes the most important decisions. The second rank is beta (β), who assists the alpha in organizing the pack and can be a potential successor. The lowest rank is omega (Ω), subordinate to all. Additionally, deltas (δ) execute the orders of alpha and beta, and this group includes sentinels, hunters, and caretakers. Gray wolves also exhibit highly organized hunting behavior, which involves three main phases: tracking and approaching, pursuing and encircling the prey, and attacking. These social and hunting behaviors have been mathematically modeled to design the GWO algorithm [6]. In the hierarchy, the best solution is represented by alpha (α), followed by beta (β) and delta (δ), with omega (Ω) representing other potential solutions.

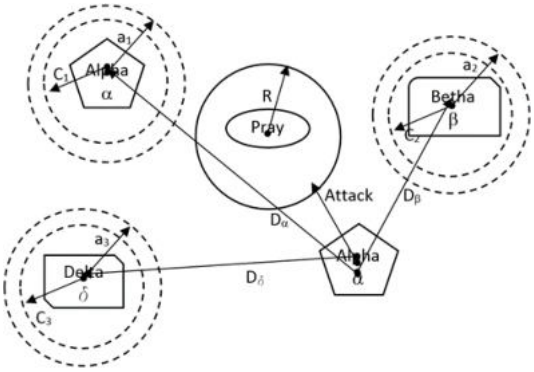

Fig. 1 Illustration of updating search agent positions in the GWO algorithm [6]

Inspired by the swim behaviors while hunting and “falling” of the beluga whale, Changting Zhong, Gang Li, and Zeng Meng proposed the Beluga Whale Algorithm (Beluga whale optimization - BWO) [5]. Belugas are social animals that live in groups ranging from 2 to 25 members. It has been observed that a pair of belugas often swim in sync or in a 'mirror' mode. Belugas typically feed together in groups, directing fish into shallow water and sharing information about the position of the best candidate. During migrations and hunting, belugas face threats from humans, killer whales, and polar bears, and some do not survive, ending up on the seabed – a phenomenon known as “whale fall”. These three key behaviors of beluga whales have been mathematically formulated into an optimization algorithm.

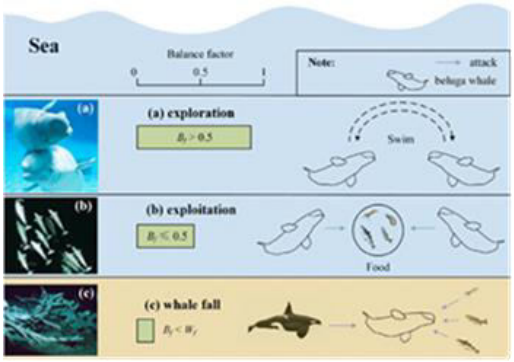

Fig. 2 Behaviors of beluga whales, (a) swim-exploration phase; (b) foraging – exploitation phase, (c) whale fall-whale fall phase [5]

PO is a newly developed metaheuristic algorithm inspired by solving optimization problems with extended search spaces [8]. Like many metaheuristic algorithms, it draws from natural phenomena, mimicking puma behavior for guiding searches. PO separates exploration and exploitation phases, each with distinct mechanisms to balance the search, allowing it to explore new areas while efficiently exploiting known solutions. A key feature is its intelligent phase-switching mechanism, automatically balancing exploration and exploitation based on the problem’s nature, improving adaptability and performance. Despite its complexity, PO maintains computational efficiency, applying the cost function only once per agent per iteration, making it robust in optimizing non-acoustic parameters and navigating complex search spaces.

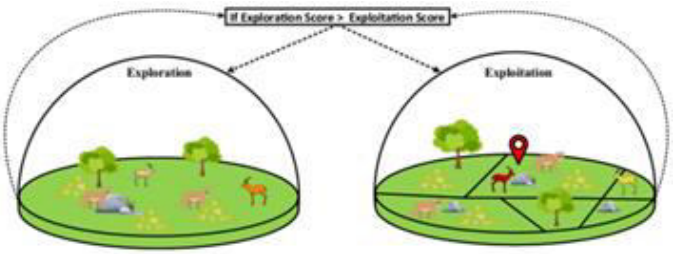

Fig. 3 PO optimization procedure [8]

3. Result and Discussion

In the present study, three nature-inspired algorithms, BW, PO, and GW, were applied for the acoustic optimization of cotton fibers bonded with polyurethane resin. The objective of the optimization was the maximization of the sound absorption coefficient. The main parameters to be optimized were: the air-flow resistance σ, tortuosity α_∞, and the parameters c and c′ describing the shape factor and scale factor of the pore cross-section. Every algorithm tried to find these parameters as precisely as possible, based on experimental data and model assumptions. The solution space consisted of four parameters, and the number of agents was set at 50 with a maximum of 1000 iterations. Convergence analysis and the search process were conducted along with the accuracy of the results obtained for each algorithm and compared to the values obtained experimentally. While the convergence of the algorithms is presented diagrammatically, the results from both experimental and algorithmic modeling are presented in a comparative graphical form.

The BW algorithm demonstrated extremely fast convergence, as shown in Fig. 4. The trend of decreasing or maintaining the best-obtained value persists throughout the entire search process, as illustrated in Fig. 5. In some cases, this would be a good characteristic of the algorithm, but on the other hand, it indicates the risk of falling into a local minimum and being unable to escape that zone. This is demonstrated in Fig. 5, where the algorithm does not attempt to leave the local minimum zone. The results of the algorithm are presented in Tab. 1 and the algorithm's execution time was 458.950541 seconds. Figure 6 provides a comparative presentation of sound absorption coefficients obtained experimentally and those obtained through the BELUGA algorithm. The error obtained (using the least squares method) is 4.80676633 %, which is quite a significant deviation, as shown in Fig. 6.

Table 1 BW algorithm results

σ	α_∞	c	c'	The best solution	Algorithm duration time [sec]
1120.71900	4.00000	2.60275	2.16378	**0.0480676633**	458.9505410000

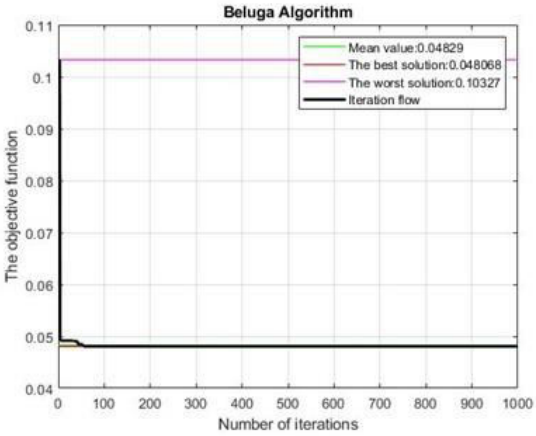

Fig. 4 Convergence diagram of the BW algorithm

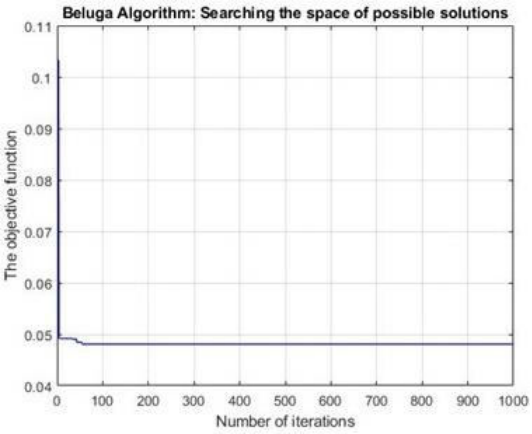

Fig. 5 BW algorithm search process

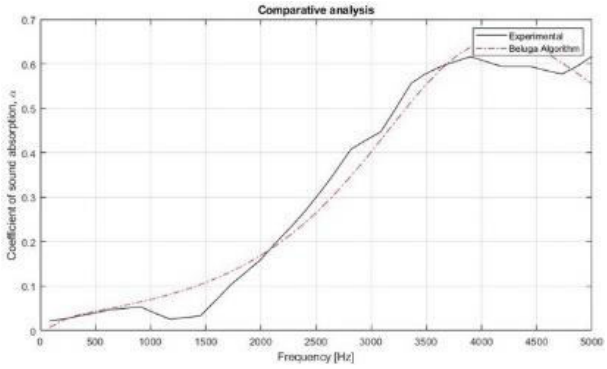

Fig. 6 Comparative presentation of experimental results and results obtained by BW algorithm

The main characteristic of the PO algorithm, also evident in this case, is its extremely fast convergence. After about 10 iterations, Fig. 7, convergence occurs, and the algorithm enters a local minimum. However, the algorithm does not show the ability to escape the local minimum, as demonstrated in Fig. 8, which shows the search process through the possible solution space. As can be seen from Fig. 8, the algorithm attempted to exit the local minimum zone – there are peaks between the 20^{th} and 30^{th} iterations – but quickly returned to the local minimum and did not leave it for the remainder of the iterative process. The results of the algorithm are presented in Tab. 2 and the execution time of the algorithm was 416.9659089 seconds. Figure 9 shows a comparative presentation of sound absorption coefficients obtained experimentally and those obtained through the PO algorithm. The error obtained (using the least squares method) is 4.80406358 %, which is still considered a significant deviation, as shown in Fig. 9. The convergence of the PO algorithm is similar to that of the BW algorithm – extremely fast. Both the PO and BW algorithms showed no inclination to exit the local minimum zone, although the PO algorithm attempted to do so in the first 20 iterations by exploring another part of the solution space.

The result obtained by the PO algorithm is slightly better than that of the BW algorithm (4.80406358 % < 4.80676633 %), and the execution time is shorter (416.9659089 < 458.950541 seconds), but the result is still unsatisfactory.

Table 2 PO algorithm results

σ	α_∞	c	c'	The best solution	Algorithm duration time [sec]
1000.0000	4.00000	2.75627	2.27319	**0.0480406358**	416.9659089000

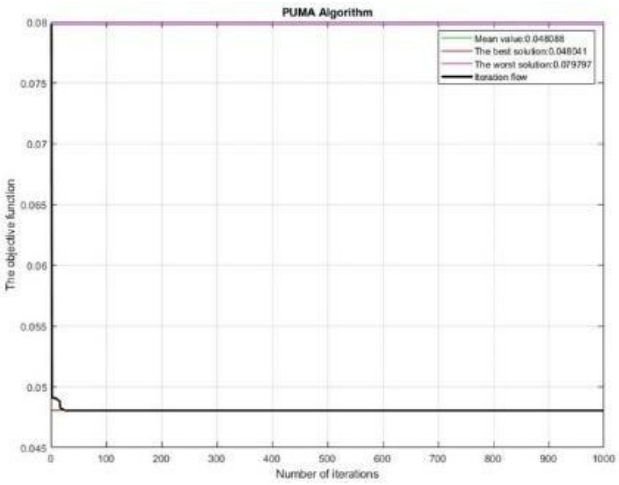

Fig. 7 Convergence diagram of the PO algorithm

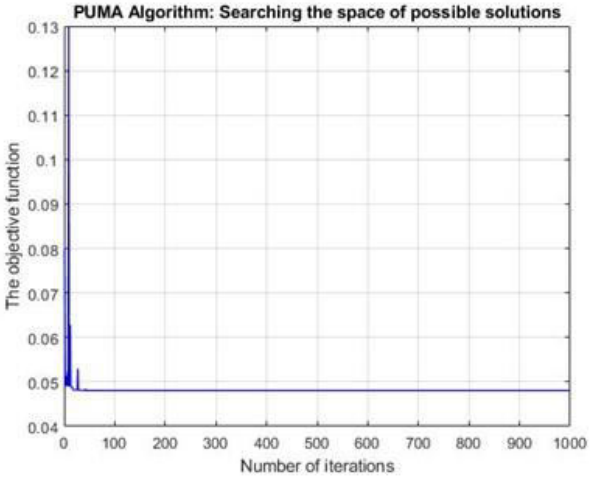

Fig. 8 PO algorithm search process

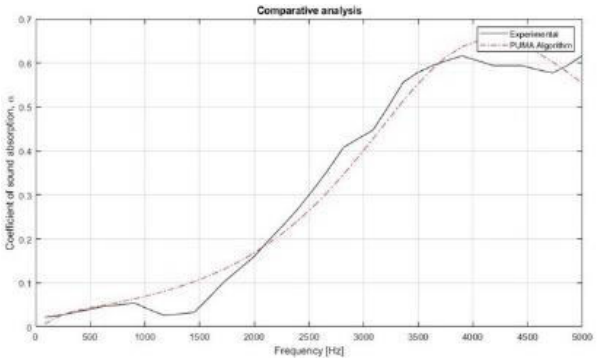

Fig. 9 Comparative presentation of experimental results and results obtained by PO algorithm

The Grey Wolf algorithm produced worse results compared to the PO and BW algorithms. The error obtained was 4.93304091 %. Unlike the PO and BW algorithms, the Grey Wolf algorithm has somewhat slower convergence, as shown in Fig. 10, but its execution time is shorter (223.2760058 seconds). While the PUMA and BELUGA algorithms did not search the entire possible solution space during the iterative process, the Grey Wolf algorithm explored the entire solution space throughout the entire iterative process, as shown in Fig. 11. Figure 12 provides a comparative presentation of sound absorption coefficients obtained experimentally (by measurement) and those obtained through the Grey Wolf algorithm.

Table 3 GWO algorithm results

σ	α_∞	c	c'	The best solution	Algorithm duration time [sec]
1583.79635	3.97780	2.13780	1.90663	**0.0493304091**	223.2760058000

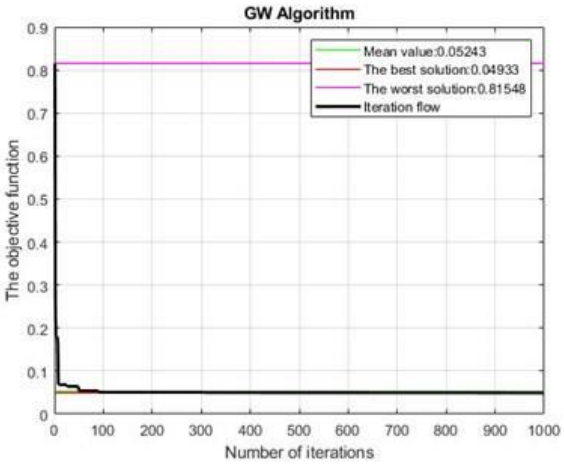

Fig. 10 Convergence diagram of the GW algorithm

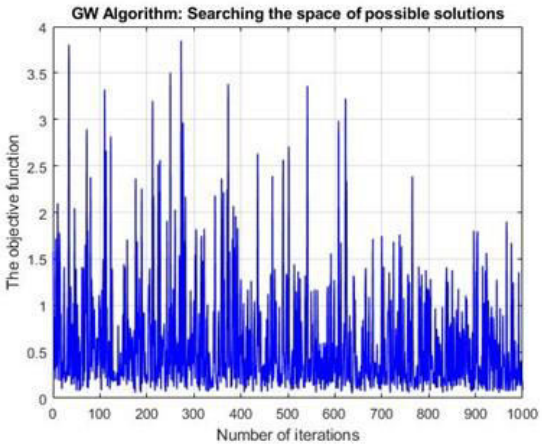

Fig. 11 GW algorithm search process

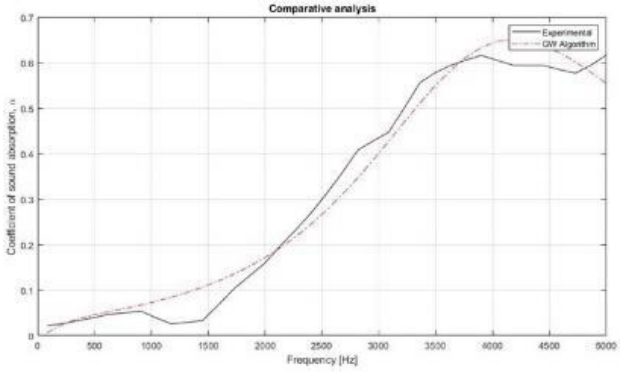

Fig. 12 Comparative presentation of experimental results and results obtained by GW algorithm

A comparative analysis of all algorithms Tab. 4 shows that the PUMA algorithm achieved the best results in terms of the smallest error (4.80 %) and execution time (416.97 seconds), but it still has the problem of escaping local minima. The BELUGA algorithm was slightly less accurate but significantly faster. The Grey Wolf algorithm, although slower in convergence, offers better coverage of the solution space but with a higher error rate.

Table 4 Comparative result analysis

Algorithm	σ	α_∞	c	c'	The best solution	Algorithm duration time [sec]
Beluga	1120.71900	4.00000	2.60275	2.16378	0.0480676633	458.9505410000
Puma	1000.0000	4.00000	2.75627	2.27319	**0.0480406358**	416.9659089000
GW	1583.79635	3.97780	2.13780	1.90663	0.0493304091	**223.2760058000**

4. CONCLUSION

This study demonstrated that biologically inspired algorithms are powerful tools in the search for optimal acoustic properties of fibrous materials. Each of them has some specific strengths and weaknesses. Among the tested algorithms, PUMA showed the best overall efficiency with the smallest error and relatively short execution time. On the other hand, this algorithm also demonstrated its limitations concerning getting stuck in local minima. The BELUGA algorithm was faster, but with ultra-fast convergence, it tended to skip the deeper investigation of possible solutions; hence, it gave a higher error. The GW algorithm, on the other hand, converged the slowest but succeeded in searching a broader solution space; however, it was less precise compared to the other two algorithms.

Future research should be directed at hybrid algorithms that will be capable of both fast convergence and escaping from the local minima. Another probable research direction might be the combination of strengths from the PUMA and GW algorithms, exploiting the ability of the GW algorithm for more thorough explorations of the solution space with faster convergence of the PUMA algorithm. This can result in drastic improvement in accuracy for the prediction of acoustic properties in materials. This research thus shows the opening of a very interesting perspective toward new applications in industrial sound insulation systems and the relevance of continuous acoustic materials optimization as a key factor for the development of really effective noise control in several applications.

Acknowledgement: *This work is co-financed by the Ministry of Science, Technological Development and Innovation of the Republic of Serbia on the basis of contract no 451-03-66/2024- 03/200108. The authors thank the Ministry of Science, Technological Development and Innovation of the Republic of Serbia for supporting this research.*

REFERENCES

1. Marquis-Favre C., Premat C., Aubrée D, Noise and Its Effects—A Review on Qualitative Aspects of Sound. Part II: Noise and Annoyance, *Acta Acustica United with Acustica*, Vol.91, No. 4, 2005., pp. 626-642.
2. Cao L., Fu Q., Si Y., Ding B., Yu J., Porous materials for sound absorption, *Composites Communications*, Vol.10, 2018, pp. 25-35. DOI 10.1016/ j.coco.2018.05.001
3. Berardi U., Iannace G., Acoustic characterization of natural fibers for sound absorption applications, *Building and Environment*, Vol.94, No.2, 2015, pp. 840-852. DOI 10.1016/ j.buildenv.2015.05.029
4. Fouladi M. H., Nor M. J. M., Ayub M., Leman Z. A., Utilization of coir fiber in multilayer acoustic absorption panel, *Applied Acoustics*, Vol.71, No.3, 2010, pp. 241-249. DOI 10.1016/j.apacoust.2009.09.003
5. Allard J. F., Champoux Y., New empirical equations for sound propagation in rigid frame fibrous materials, *Journal of the Acoustical Society of America*, Vol.91, No.6, 1992, pp. 3346-3353.
6. Mirjalili S., Mirjalili S. M., Lewis A., Grey Wolf Optimizer, *Advances in Engineering Software*, Vol.69, No. 22, 2014, pp. 46-61. DOI 10.1016/j.advengsoft.2013.12.007
7. Zhong C., Li G., Meng Z., Beluga whale optimization: A novel nature-inspired metaheuristic algorithm, *Knowledge-Based Systems*, Vol. 251. DOI 10.1016/j.knosys.2022.109215
8. Abdollahzadeh B., Khodadadi N., Barshandeh S. *et al*, Puma optimizer (PO): a novel metaheuristic optimization algorithm and its application in machine learning, *Cluster Comput* , Vol. 27, 2024, pp. 5235-5283, DOI 10.1007/s10586-023-04221-5
9. Kolarević M., Radičević B., Bjelić M., Miodragović T., Miodragović G., Application of Biologically Inspired Algorithms for Determining the Coefficients of Empirical Models for Determining Sound Absorption, *Proceedings of the X International Conference "Heavy Machinery-HM 2021"*, Vrnjačka Banja, June 23-25, 2021 pp. F.13 – F.19.
10. Miodragović T., Radičević B., Miodragović G., Ivanović M., Hybrid optimization algorithm for determining sound absorption, *Proceedings of the 27th International Conference Noise and Vibration*, Niš, 2022.

11. Miodragović T., Radičević B., Miodragović G., Bjelić M., Comparative analysis of the application of different metaheuristic methods for determining the coefficients of empirical models for determining sound absorption, *Proceedings of the 17th International Conference Acoustics and Vibration of Mechanical Structures - AVMS 2023*, Timisoara, Romania, May 26-27, 2023, e-ISBN 978-3- 031-48087-4.
12. Yang T., Hu L., Xiong X., Petrů M., Noman M.T., Mishra R., Militký J., Sound Absorption Properties of Natural Fibers: A Review, *Sustainability*, Vol.12, No.20, 2020. DOI 10.3390/su12208477

FACTA UNIVERSITATIS
Series: **Working and Living Environmental Protection** Vol. 21, N° 4, Special Issue, 2024, pp. 317 - 328
https://doi.org/10.22190/FUWLEP240912030B

Original scientific paper

CASE STUDY: PREDICTION OF THE EFFECT OF PERFORMED ACOUSTIC INSULATION ON MACHINE PARTS ON REDUCING OCCUPATIONAL NOISE EXPOSURE

UDC 534:331.4

Biljana Beljić Durković[1], Jovan Miočinović[2]

[1]Zmaj Jova Jovanović Primary School, Belgrade, Serbia
[2]TEHPRO d.o.o., Belgrade, Serbia

ORCID iDs: Biljana Beljić Durković N/A
Jovan Miočinović N/A

Abstract. *In the plastic injection moulding plant, at the operator's position at the machine, the noise was measured in situ before and after the acoustic insulation lining of the parts of the machine to determine whether the intervention has an impact on reducing occupational noise exposure. As the work environment is variable (different modes of operation of the machine and other machines in the plant), a model of the contribution of the noise sources to the measured noise was made, and based on the model, the effect of the intervention was predicted.*

Key words: *occupational noise, indoor noise reduction, indoor noise model*

1. INTRODUCTION

In one plastic injection moulding plant, there was a desire to reduce the noise emitted by the machines and equipment through subsequent interventions on the machines.

When considering industrial noise reduction, before implementing engineering or administrative measures to control noise, it is necessary to define the problem regarding the persons affected by the exposure, the type and location of noise sources, and the appropriate criteria for assessing the severity of the situation [1]. Although every noise control problem must be examined individually, there are three separate components which should always be considered, namely the source, the propagation path, and the receiver (worker) [2]. Acoustical treatment may be applied to any or all of these components [3] with the general order of precedence being as listed, i.e., the most satisfactory solution usually results from noise reduction at or near the source [1,3,4]. That hierarchy of control

Received September 12, 2024 / Accepted November 21, 2024
Corresponding author: Jovan Miočinović
TEHPRO d.o.o., Lole Ribara 120, 11250 Belgrade, Serbia
E-mail: jovan.miocinovic@tehpro.rs

measures also corresponds to the representation of applied noise control techniques in case studies presented in the literature [5,6,7].

In this case, the noise source has been pointed out before any noise survey prior to the selection of control measures, and technique to reduce the noise – acoustic lining of the machine parts was selected as the most practical solution. As one of the techniques to reduce the generation of airborne and structure borne noise in machines, acoustical lining [8] in enclosures requires a carefully balanced combination of absorbing, damping, and insulating materials incorporated to prevent high reverberant sound levels within the enclosure from degrading the overall insulating properties [1].

The idea was to measure the noise before the intervention on one such machine and after and compare the measured noise levels in order to see if it makes sense to carry out such interventions on other machines as well. Such a comparison would make sense for ideally the same test conditions before and after, e.g. the same mode of operation of all machines. It would be best if all the machines were running at full capacity.

The measurements were carried out as part of the testing of the working environment [9]. However, the test conditions in working environment testing in practice are usually such that there is limited test time and little or no possibility of influencing the operating mode. While the impact on plant operation by the examiner's influence would result in production downtime, scrap production, and additional time to restart and full production, the test is usually carried out under the conditions of the current operation of the production plant found at the time of the test.

Here it was the case, as will be shown in detail, that the machines in the first trial were operating in one mode, in the post-intervention trial in another, with little to no possibility of influence on the operation of the machines by the examiner.

In the first test, the machines in the hall worked each in its own mode with the possibility of turning off the tested machine, when two measurements were performed. In the second, the machines worked in a different mode from the first without the possibility of influence, when the third measurement was performed.

Since, due to the impossibility of controlling the parameters, it is not a standard experimental design, in order to draw conclusions, the starting point is the model of the contribution to noise in the working environment from individual sources and the mode of operation of the sources. It will also be necessary to analyse the contributions and introduce additional assumptions about the impact of individual contributions. A model is only as good as the assumptions on which it is based, and the conclusions and applicability of the model are limited by the validity of the assumptions.

2. Test Conditions and Results

There are 24 injection moulding machines in the facility. The situation plan is given in Fig. 1.

The machine on which the intervention was performed is the M-6 machine. In the first test (before intervention), neighbouring machine M-5 was operating, neighbouring machine M-4 was not operating, and machine M-6 was operating idle (first measurement). A measurement was also performed after turning off the M-6 machine (second measurement).

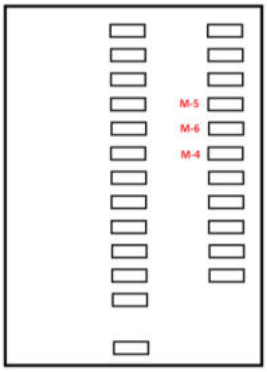

Fig. 1 Situational plan of a plant.

In the second test (after intervention), neighbouring machine M-4 was operating, neighbouring machine M-5 was not operating, and machine M-6 was operating at full capacity (third measurement).

Measurements were made according to ISO 9612 [10] with the microphone positioned at the locations of the worker's head during normal performance of the job or task for standing worker: 1.55 m ± 0.075 m above the ground on which the worker is standing.

Fig. 2 shows a sketch of the position of the measuring point in relation to the M-6 machine and neighboring machines, and Fig. 3 shows a photograph of the position of the measuring point.

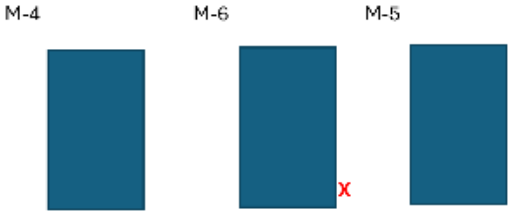

Fig. 2 Sketch of the position of the measuring point

Fig. 3 A photograph of the position of the measuring point

In the first test (before intervention), the measured noise level was 80.6 dB (first measurement). In the second measurement, the measured level was 78.7 dB. In the second test (after intervention), the measured level was 84.8 dB (third measurement). It is noticeable that the noise level measured after the intervention is significantly higher than the level measured before the intervention.

As mentioned above, it would be ideal if the tests were carried out in the same operating conditions of the technological capacities, in the full capacity of the machine on which the intervention was carried out, with the same mode of operation of the other machines in the hall. Since the working conditions during the tests before and after differ greatly, in order to be able to draw relevant conclusions from the test results about the possible effect of the intervention on the machine on noise reduction, it is necessary to start from the contribution model of noise sources in the workspace.

3. A Model of the Contribution of Noise Sources to the Measured Noise in the Workspace

In making the model, we start from several observations and initial assumptions.

Since the measuring point is between machines M-5 and M-6 and machine M-4 is much further away from the measuring point than machine M-5 (see Fig. 2), the noise contribution from machine M-5 at the measuring point is greater than the contribution from machine M-4.

Starting from the model of the sum of noise contributions at the measuring point, the noise can be expressed as the sum of the contributions from machine M-6, denoted here as $L_{\text{(M-6)pAeq}}$, machine M-5, denoted $L_{\text{(M-5)pAeq}}$ and, since M-4 is further from the measuring point, the sum of contributions from machine M-4 and the other machines in the hall, denoted $L_{\text{(E)pAeq}}$.

$$L_i = {L_{(M-6)pAeq}}_i^j (+) {L_{(M-5)pAeq}}_i^j (+) {L_{(E)pAeq}}_i^j \tag{1}$$

Here i stands for i-th measurement (i = 1, 2, 3, for the first, second and third measurement), j stands for test (j = B for the test before intervention and j = A for the test after the intervention). The addition sign in bracket stays not for arithmetic addition but for the logarithmic addition of sound pressure levels from multiple noise sources [11].

Thus, for all three measurements, we can express the measured equivalent levels via components.

$$L_1 = {L_{(M-6)pAeq}}_1^B (+) {L_{(M-5)pAeq}}_1^B (+) {L_{(E)pAeq}}_1^B \tag{2}$$

$$L_2 = {L_{(M-5)pAeq}}_2^B (+) {L_{(E)pAeq}}_2^B \tag{3}$$

$$L_3 = {L_{(M-6)pAeq}}_3^A (+) {L_{(E)pAeq}}_3^A \tag{4}$$

The components $L_{\text{(M-6)}}$ from Eq. (3) and $L_{\text{(M-5)}}$ from Eq. (4) are missing because M-6 and M-5 do not operate during the corresponding measurements (see 2. above).

The Eqs. (2), (3) and (4) can be reformulated as follows.

$$L_1 = {L_{(M-6)}}_I^B (+) L_{(M-5)} (+) L_{(E)} \tag{5}$$

$$L_2 = L_{(M-5)}(+)L_{(E)} \tag{6}$$

$$L_3 = L_{(M-6)}{}_F^A(+)L_{(M-4+E)} \tag{7}$$

From the Eqs. (5) and (6) indexes are omitted because $L_{(M-5)}$ and $L_{(E)}$ are the same while the operating conditions of contributing equipment are the same. In Eq. (5) with index *I* the idle operating mode of M-6 is marked, and in Eq. (7) with index *F* the full capacity operating mode of M-6 is marked. With M-4+E in $L_{(E)}$ component in Eq. (7) the contribution of M-4 is pointed out while it does not contribute to the noise in Eqs. (5) and (6).

Graphic printout for the measurements is given in Fig. 4 (first measurement), Fig. 5 (second measurement), and Fig. 6 (third measurement). The parameters shown in the graphic are A-weighted equivalent continuous sound pressure level L_{AFeq}, C-weighted peak sound pressure level L_{Cpeak}, A-weighted impulse equivalent continuous sound pressure level L_{AIeq}, and A-weighted minimum sound pressure level L_{AFmin} [12].

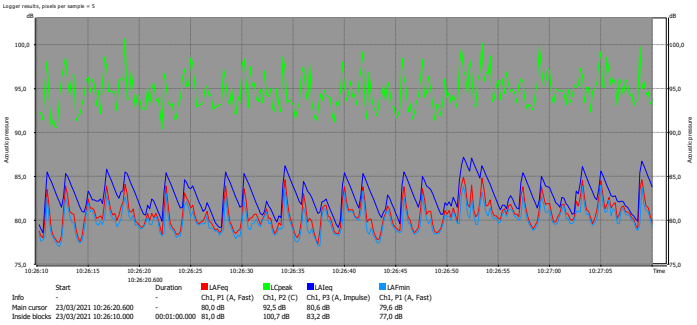

Fig. 4 Graphic printout of the noise level during the first measurement (The calibration factor is −0.4 dB)

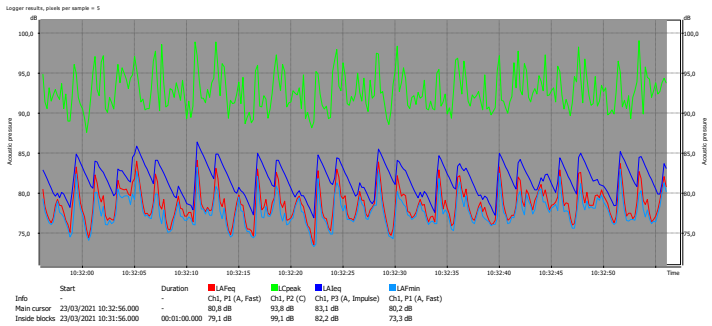

Fig. 5 Graphic printout of the noise level during the second measurement (The calibration factor is −0.4 dB)

$L_{(E)}$ can be estimated from the second measurement as the minimum sound level measured during the measurement period, L_{AFmin}. The assumption is that now when the

neighbouring machine M-5 is the quietest, the noise contribution from the other machines comes to the fore. It is 72.9 dB (the L_{AFmin} value from Fig. 5, minus the calibration factor).

From Eq. (6) noise contribution from M-5, $L_{(\mathrm{M\text{-}5})}$ can be determined as the difference of the measured noise in the second measurement, L_2 (78.7 dB, the L_{AFeq} value from Fig. 5, minus the calibration factor), and $L_{(\mathrm{E})}$ as in the previous step determined.

$$L_{(M-5)} = L_2(-)L_{(E)} \tag{8}$$

Again, the difference is the value that, when added to the known value of $L_{(\mathrm{E})}$ using the logarithmic addition of sound pressure levels, equals the known value of L_2. Thus, for the noise contribution from M-5, $L_{(\mathrm{M\text{-}5})}$ we get 77.4 dB.

From Eq. (5) noise contribution from M-6 (when idle, before the intervention), $L_{(\mathrm{M\text{-}6})}{}^{\mathrm{B}}{}_{\mathrm{I}}$, can be determined as the difference of the measured noise in the first measurement, L_1 (80.6 dB, the L_{AFeq} value from Fig. 4, minus the calibration factor), and the sum of noise contributions from M-5, $L_{(\mathrm{M\text{-}5})}$ and the rest of the machines and equipment, $L_{(\mathrm{E})}$ as in the previous steps determined.

$$L_{(M-6)}{}_{I}^{B} = L_1(-)\{L_{(M-5)}(+)L_{(E)}\} \tag{9}$$

Once again, the difference is the value that, when added by means of logarithmic addition of sound pressure levels to the known values of $L_{(\mathrm{E})}$ and $L_{(\mathrm{M\text{-}5})}$, equals the known value of L_1. Thus for the noise contribution from M-6 (when idle), $L_{(\mathrm{M\text{-}6})}{}^{\mathrm{B}}{}_{\mathrm{I}}$, we get 76.1 dB.

Now we will introduce an additional assumption, which is that the noise of the machine operating at full capacity consists of the superimposed operating noise and the idle noise, so that the idle noise can be found in the minimum measured in the measurement interval (see Fig. 7).

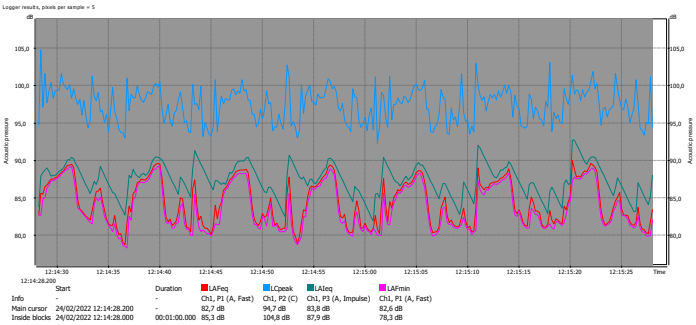

Fig. 6 Graphic printout of the noise level during the third measurement (The calibration factor is −0.5 dB)

Thus the noise contribution from M-6 (when idle, after the intervention), $L_{(\mathrm{M\text{-}6})}{}^{\mathrm{A}}{}_{\mathrm{I}}$, equals the difference of the minimum sound level measured during the measurement period (77.8 dB, the L_{AFmin} value from Fig. 6, minus the calibration factor) and the contribution from M-4 and the rest of the machines and equipment, $L_{(\mathrm{M\text{-}4+E})}$.

$$L_{(M-6)}{}_{I}^{A} = L_{3AFmin}(-)L_{(M-4+E)} \tag{10}$$

Here again, the difference implies logarithmic subtraction [11].

Now we need to evaluate the contribution of M-4 to the contribution of the rest of the machines and equipment, $L_{(M\text{-}4+E)}$. If neglected and taken $L_{(E)}$ for $L_{(M\text{-}4+E)}$:

$$L_{(M-4+E)} = L_{(E)} \tag{11}$$

From Eq. (10) we get for the contribution of M-6 (when idle) 76.1 dB.

However, considering that it is the closest neighbour and the biggest source of noise in the environment when M-5 not operating, if we assume its contribution is at least equal to the contribution of other machines and equipment

$$L_{(M-4+E)} = L_{(E)}(+)L_{(E)} \tag{12}$$

From Eq. (10) we get for the contribution of M-6 (when idle) 73.3 dB.

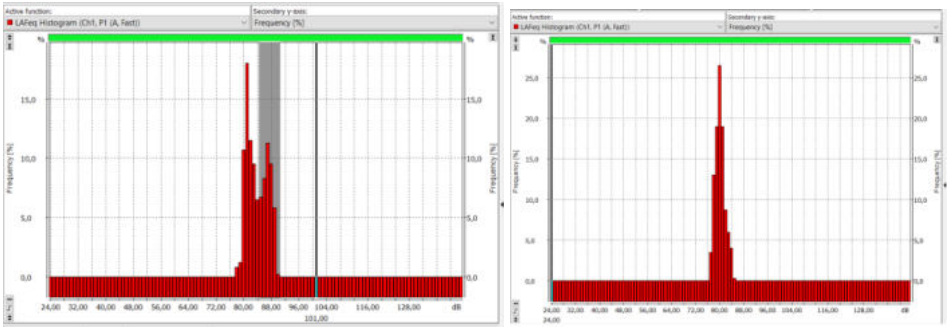

Fig. 7 Statistical distribution of the noise level for the third and first measurements. A machine operating at full capacity can be viewed as consisting of superimposed operating noise (shaded part) and idle noise

4. Evaluation of the Effectiveness of the Intervention on the Machine to Reduce Occupational Noise Exposure

4.1. Assessment of noise level reduction of the equivalent noise level

Based on the model, the noise contribution of M-6 (when operating idle), $L_{(M\text{-}6)}{}^{B}{}_{I}$, of 76.1 dB was estimated from the measured noise value at the measuring point before the intervention of the acoustic insulation of the machine.

From the calculated value of the noise at the measuring point after the intervention of the acoustic insulation of the machine, based on the model, the noise contribution of M-6 (when operating idle) $L_{(M\text{-}6)}{}^{B}{}_{I}$, was estimated between 73.3 and 76.1 dB.

It was established that the noise level originating from the machine (when operating idle) will be reduced from the initial 76 dB by an amount of 0 – 2.5 dB after the intervention of acoustic insulation of the machine.

4.2. Assessment of noise level reduction in a specific frequency domain

Let's try to establish from the frequency analysis of the measurement results at which of single octave bands, assuming that it works, the acoustic insulation intervention works.

To compare noise levels by octave bands coming from the M-6 machine before and after intervention on the machine we use the model of components contribution (Eqs. (5), (6), and (7)).

From Eqs. (5) and (6), for the noise component coming from M-6 before the intervention, may be seen to be obtained by subtracting the Eq. (6) from Eq. (5)

$$L_1(-)L_2 = L_{(M-6)_I}^{\ B} \tag{13}$$

While considering the octave bands, Eq. (13) may be rewritten as

$$\{L_1(-)L_2\}^i = \left\{L_{(M-6)_I}^{\ B}\right\}^i \tag{14}$$

where i = 1, …, 9 stays for octave bands 31.5; 63; … 8000 Hz.

That is, Eq. (14) represents 9 equations for corresponding single octave bands.

To find the contribution of M-6 (operating idle) after intervention, we rely on the machine idling model (that is, Eq. (10)) and Eq. (7). Considering contribution of the rest of the machines and equipment by Eq. (11) and $L_{(E)}$ estimated from the second measurement as the minimum sound level measured during the measurement period, L_{AFmin} as considered above, we find that wanted contribution is subtraction of the minimum sound level measured during the second measurement period, L_{2AFmin}, from the minimum sound level measured during the third measurement period, L_{3AFmin} (see Eqs. (6) and (7)):

$$L_{3AFmin}(-)L_{2AFmin} = L_{(M-6)_I}^{\ A} \tag{15}$$

While considering the octave bands, Eq. (15) may be rewritten as

$$\{L_{3AFmin}(-)L_{2AFmin}\}^i = \left\{L_{(M-6)_I}^{\ A}\right\}^i, \tag{16}$$

where i =1, …, 9 stays for octave bands 31,5; 63; … 8000 Hz.

That is. Eq. (16) represents 9 equations for corresponding single octave bands.

Noise levels by octave bands coming from the M-6 machine before the intervention calculated by Eq. (14) (when adding by means of logarithmic addition of sound pressure levels) are given in Tab. 1.

Table 1 Noise levels by octave bands coming from the M-6 machine before the intervention

Octave band [Hz]	31.5	63	125	250	500	1000	2000	4000	8000
Noise level [dB]	17.8	32	44.3	61.1	74.3	70.2	67.2	62.6	59

Noise levels by octave bands coming from the M-6 machine (operating idle) after the intervention are given in Tab. 2. The values for the octaves are obtained as the equivalent levels for the seven minimum values during the measurement period. This is done in order to preserve the minimum equivalent value calculated from the octaves. Namely the minimum octave values are expected to be reached at different moments of time, so the equivalent value calculated from the octave minimums would be below the true equivalent minimum value. Values thus obtained calculated by Eq. (16) (when adding by means of logarithmic addition of sound pressure levels) are given in Tab. 2.

Table 2 Noise levels by octave bands coming from the M-6 modelled idle operating machine after the intervention

Octave band [Hz]	31.5	63	125	250	500	1000	2000	4000	8000
Noise level [dB]	38.7	45.8	58.3	65.1	72.1	74.0	72.6	70.9	65.7

By comparing the octave band values from Tabs. 1 and 2, it may be seen that at the 500 Hz octave, the level decreased by 2.2 dB.

If we calculate the equivalent levels for situations before and after the intervention from the octave band sound levels modelled in this way [13], we see that the total level of noise coming from the machine when operating idle is 76.7 dB before the intervention and 79 dB after the intervention, which would mean that the machine is noisier than before, which was shown not to be the case. That is, in the model, we overestimated the contribution of the M-5 operation compared to the noise coming from the other machines.

If we do not compensate for the noise of M-5 but assume instead that the contribution of all machines in the environment is the same for the measurement as well before and after the intervention

$$L_{(M-4+E)} = L_{(M-5)}(+)L_{(E)} \tag{17}$$

contribution of M-6 (operating idle) after the intervention is

$$L_{3AFmin}(-)L_2 = L_{(M-6)_I^A} \tag{18}$$

While considering the octave bands, Eq. (18) may be rewritten as

$$\{L_{3AFmin}(-)L_2\}^i = \left\{L_{(M-6)_I^A}\right\}^i \tag{19}$$

where i =1, …, 9 stays for octave bands 31.5; 63; … 8000 Hz.

Thus obtained noise levels by octave bands coming from the M-6 machine (operating idle) after the intervention are given in Tab. 3.

Table 3 Noise levels by octave bands coming from the M-6 modelled idle operating machine after the intervention when the contributions of noise from other machines in the hall were taken as equal in the situations before and after the intervention

Octave band [Hz]	31.5	63	125	250	500	1000	2000	4000	8000
Noise level [dB]	38.4	39.2	57.7	57.5	68.1	69.2	63.8	58.2	59

By comparing the octave band levels from Tabs. 1 and 3, it may be seen that at the 500 Hz octave, the level has decreased by 6.2 dB. If we calculate the equivalent level from octave band sound levels [13], 73.0 dB is obtained, which corresponds to the calculated maximum expected reduction of the noise contribution of M-6 (see 4.1.). Figure 8 shows a graphic representation of the data from Tabs. 1 – 3.

If we now look at the octave spectrum before the intervention (Tab. 1), we see that the machine is the noisiest at the level of 500 Hz, where the acoustic insulation according to the model proves to be the most effective (values in column 500 in Tabs. 2 and 3). If we calculate the equivalent level from the octave band sound levels from Tab. 1 with the determined reduction of 2.2 - 6.2 dB for the octave level of 500 Hz, we get the equivalent

level of 75.5 - 74.2 dB, which corresponds to a total reduction of noise from the machine by 1.1 - 2.5 dB.

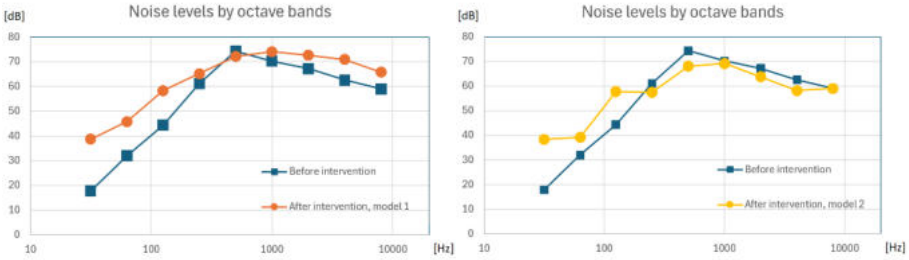

Fig. 8 Models of octave band levels of noise from the M-6 operating idle modelled before and after the intervention. In the first one (on the left), the contribution of M-5 is considered separately from background noise, and in the other as a part of it.

The trend of reduction at higher frequencies (Tabs. 1 and 3 and Fig. 8 on the right) corresponds to the predicted selection of technique to reduce the noise. Namely, since the absorption coefficient of absorbent lining is generally highest at high frequencies, the high-frequency components of any noise will suffer the highest attenuation [4]. The obtained increase at low frequencies may be a reflection of the inadequacy of the approximations for that range or an unaccounted external source, but due to the A-weighting of the equivalent level, it does not significantly affect the overall results. If we compare the noise level reduction obtained in this way with typical values for insulating wrapping [3], we see that it is at best twice less than expected (5 - 10 dB according to ISO 11690-2). The reasons can be found in the noise reduction technique itself (see considerations in 1.), as well as in possible defects in the insulating layer, e.g. for enclosures with leak ratios of 10 %, the expected reduction of A-weighted emission sound pressure levels is limited to 10 dB [4] and, accordingly, for larger leaks, lower limitations are to be expected.

4.3. Consideration of the impact of the intervention on the machine on noise reduction at full capacity operation mode and of the subsequent interventions on all machines in the workplace

When considering full capacity operation mode, there are two issues. First, there is no data on the noise of the machine in full operating mode before the intervention, and second, as already discussed in 3. (see Fig. 7) machine noise is modelled as consisting of superimposed operating noise and idle noise. Looking at its construction, the machine consists of a physically separated drive part and a working part, while the acoustic insulation was performed on its drive part. With this in mind, the noise from the machine at full capacity before the intervention can be modelled as the sum of the idle noise before the intervention and the working part component after the intervention, assuming that the intervention does not affect the noise from the working part. When calculated like this, a 2.5 dB idle noise reduction yields a corresponding noise reduction at a full capacity of 0.3 dB. The reasons for such a result can be found in the following. First, in the very construction of the machine, i.e. separation of the working part from the driving part, whereby intervention is performed only on the working part. Secondly, due to the fact that

the procedure was not followed during the selection of control measures (see considerations in 1.), and third, in the model limitation, a model developed on the basis of a very limited set of tests and assumptions that gives good predictions in one domain (predictions of insulating acoustic properties at idle) is extended in application (to predictions of properties at full operation).

This poor result of the impact of the intervention on the machine on noise reduction at full capacity operation mode, even if it turns out to be a good prediction, is not necessarily bad for the overall result of noise reduction in the workplace. Namely, the accumulative impact of performing such an intervention on other machines in the workspace could contribute to a cumulative reduction of background noise (in the model marked with L_E). Then, any intervention of this type on the working part of the machine without prior proper evaluation would be inappropriate [4,5,6]. Measures taken in practice on working parts of injection moulding machines are measures of specific interventions on the design (source control by design [4]). If additional appropriate measures were taken on the working parts to the extent that they would be effective, in conjunction with the performed measures of the acoustical lining of drive parts, they could contribute to a significant reduction of noise in the working environment.

5. Conclusion

Based on the results of measuring occupational noise in the production plant of plastic injection moulding and the model developed for this purpose, it has been shown that the contribution of noise from the machine operating idle to the noise in the work environment had been reduced by 0 to 2.5 dB by the intervention of performing acoustic insulation - the lining of the machine parts. Also, the effect of noise reduction in the frequency domain in which the machine is the noisiest (in the 500 Hz octave band) was determined, in amounts of 2.2 to 6.2 dB, which corresponds to a total reduction in the noise level of the machine by 1.1 to 2.5 dB. When considering the impact of the intervention on noise reduction at full capacity operation mode and the reduction of noise at the workplace in general, under the condition of carrying out such interventions on other machines in the workplace as well as additional adequate noise control measures on the working parts of the machines, all the measures taken in conjunction could lead to to a significant reduction of noise in the working environment.

References

1. Orr, W. G. Handbook for Industrial Noise Control NASA SP-5108, NASA, Washington D.C. 1981
2. SRPS EN ISO 11690-1:2021, ISO 11690-1:2020 Acoustics - Recommended practice for the design of low-noise workplaces containing machinery - Part 1: Noise control strategies
3. SRPS EN ISO 11690-2:2021, ISO 11690-2:2020 Acoustics - Recommended practice for the design of low-noise workplaces containing machinery - Part 2: Noise control measures
4. Hansen, C. H. and Goelzer B. I. F. Engineering noise control, in: *Occupational exposure to noise evaluation, prevention and control*, pp.245-296, Office of Occupational Health, World Health Organization, Geneva, 1995
5. Sound Solutions: Techniques to Reduce Noise at Work (Guidance Booklets) HSG138, HSE Books, Norwich, 1995
6. Sound Solutions Case Studies, published by the Health and Safety Executive and licensed under the Open Government Licence https://www.hse.gov.uk/noise/casestudies/soundsolutions/index.htm

7. Industrial Noise Reduction, Advanced Noise Solutions Ltd., Colney Heath Ln, St Albans AL4 0UP https://www.advanced-noise-solutions.co.uk/industrial-noise-reduction/
8. Berendt, R. D. and Corliss, E. L. R. Quieting: a Practical Guide to Noise Control, NBS Handbook 119, US National Bureau of Standards, 1976
9. Rulebook on the procedure for inspecting and checking equipment for work and inspecting and testing electrical and lightning protection installations and testing working environment conditions, *"Official Gazette of RS"*, number 76 of September 13, 2024
10. ISO 9612:2009, SRPS EN ISO 9612:2016 Acoustics — Determination of occupational noise exposure — Engineering method
11. Logarithmic Addition of Sound Levels, WKC Group https://www.wkcgroup.com/tools-room/logarithmic-addition-sound-pressure-levels/
12. Acoustic Glossary, Gracey & Associates, W T Gracey Ltd., Upper Dean, PE28 0NQ https://www.acoustic-glossary.co.uk/definitions-l.htm
13. Calculating dB(A) from Octave Band Sound Levels, Cirrus Research plc, North Yorkshire, YO14 0PH https://cirrusresearch.com/calculation-of-dba-from-octave-band-sound-pressure-levels/

FACTA UNIVERSITATIS
Series: **Working and Living Environmental Protection** Vol. 21, Nº 4, Special Issue, 2024, pp. 329 - 340
https://doi.org/10.22190/FUWLEP241010031G

Original scientific paper

STRATEGIC NOISE MAP FOR BELGRADE NIKOLA TESLA AIRPORT

UDC534.831:656.71(497.11BEOGRAD)

Emir Ganić[1], Aleksandar Gajicki[2], Bojana Mirković[1], Matija Sindik[1]

[1]University of Belgrade, Faculty of Transport and Traffic Engineering, Belgrade, Serbia
[2]Saobraćajni Institut CIP d.o.o., Belgrade, Serbia

ORCID iDs:	Emir Ganić	https://orcid.org/0000-0002-7036-9538
	Aleksandar Gajicki	N/A
	Bojana Mirković	https://orcid.org/0000-0003-2284-4100
	Matija Sindik	https://orcid.org/0009-0009-9538-6148

Abstract. *Environmental noise management is a critical aspect of public health policy, particularly within the European Union, which established Directive 2002/49/EC to standardize noise assessment and mitigation efforts across member states. Serbia has integrated the Directive's provisions through its Law on Environmental Noise Protection and accompanying by-laws. This paper presents the strategic noise mapping process for Belgrade Nikola Tesla Airport, Serbia's largest international airport, marking a significant milestone as it is the first time a strategic noise map is being developed for a major airport in Serbia. The legal framework, methodology, and results of this mapping process are discussed in detail. Utilizing the CNOSSOS-EU:2015 method and the Aviation Environmental Design Tool (AEDT) for acoustic calculations, the study defines the affected areas, noise indicators, and population exposure based on 2023 air traffic data. The results indicate that the L_{den} noise levels exceeding 55 dB impacted 24223 residents, while the L_{night} noise levels exceeding 50 dB affected 7493 residents. The analysis also includes the estimated number of dwellings, schools, hospitals, and people affected by different noise levels, providing necessary data for developing action plans aimed at mitigating noise pollution. Additionally, the study examines the potential health impacts, including population annoyance and sleep disturbance, using dose-effect relationships as defined by the European Commission. The results underline the importance of ongoing noise monitoring and the need for timely revisions of strategic noise maps and action plans to ensure compliance with both national and EU regulations. This research contributes to the broader effort of environmental noise management, offering insights into the methodologies and challenges of strategic noise mapping for airports in Serbia.*

Key words: *environmental noise, noise mapping, airport, noise indicators, aircraft noise, population exposure*

Received October 10, 2024 / Accepted November 29, 2024
Corresponding author: Emir Ganić
University of Belgrade, Faculty of Transport and Traffic Engineering, Vojvode Stepe 305, Belgrade, Serbia
E-mail: e.ganic@sf.bg.ac.rs

1. INTRODUCTION

The European Parliament, as a basis for assessing and managing environmental noise, adopted Directive 2002/49/EC (hereinafter referred to as: the Directive) in 2002 [1]. The primary aim of the Directive is to define a common approach intended primarily to avoid, prevent, or reduce harmful effects due to exposure to environmental noise, including disturbances caused by noise. Serbia has implemented the provisions of the Directive through the Law on Environmental Noise Protection from 2021 [2] and the by-laws from 2010 [3,4] and 2023 [5].

Strategic noise mapping has become an essential tool for managing environmental noise across Europe, particularly in urban areas and around major transportation hubs such as airports. These maps provide a visual representation of noise exposure, allowing policymakers, urban planners, and environmental agencies to assess the extent of noise pollution and its impact on public health. In the context of airports, strategic noise maps are crucial for identifying areas where noise levels exceed acceptable limits, informing the development of mitigation strategies, and ensuring compliance with both national and European regulations. Across Europe, numerous airports have developed and regularly updated their strategic noise maps as part of broader environmental noise management plans. These efforts are essential for balancing the growth of air traffic with the need to protect communities from the adverse effects of noise.

In Serbia, the development of strategic noise maps is still in its early stages. Until now, the only strategic noise map for an airport in Serbia was developed for Niš Constantine the Great Airport, as part of the strategic noise map for the agglomeration of the City of Niš. However, this paper represents a significant milestone as it marks the first time a strategic noise map is being developed for a major airport in Serbia—Belgrade Nikola Tesla Airport. This effort reflects Serbia's commitment to aligning with European standards in environmental noise management and addressing the growing concerns related to airport noise in the country's largest urban area.

The aim of this research is to provide a comprehensive analysis of the strategic noise mapping process for Belgrade Nikola Tesla Airport, utilizing the latest methodologies and data. The study examines the legal framework governing noise management in Serbia, the specific methodologies employed in the mapping process, and the results of the noise analysis. The research is structured into several key chapters: the legal framework overview, the methodology of noise mapping, the specific case study of Belgrade Nikola Tesla Airport, and the results of the strategic noise mapping. Each chapter provides insights into the challenges and outcomes of the mapping process, contributing to the broader understanding of environmental noise management in Serbia.

2. LEGAL FRAMEWORK

The legal regulations of the Republic of Serbia, used in the preparation and analysis of strategic noise maps, included:

- Law on Environmental Noise Protection ("Official Gazette of the RS", No. 96/21) [2],
- Regulation on Noise Indicators, Limit Values, Noise Indicators Assessment Methods, Disturbance and Harmful Effects of Environmental Noise ("Official Gazette of the RS", No. 75/10) [3],

- Rulebook on the Methodology for Determining Acoustic Zones (”Official Gazette of the RS”, No. 72/10) [4], and
- The Rulebook on the Content and Methods of Developing Strategic Noise Map and Action Plan, the Manner of Their Development and Presentation to the Public, as well as Their Forms ("Official Gazette of the RS", No. 90/23) [5].

The obligation to report on the state and impact of noise on the population through the development of strategic noise maps is prescribed by the Directive and the legal regulations of the Republic of Serbia. This ensures the provision of information on noise exposure at local, national, and international levels and the development of action plans aimed at managing and reducing the negative impacts of noise. All information from the strategic noise maps shall be communicated to the public in a clear and accessible manner, using the most suitable information technologies.

Strategic noise maps represent data on existing and estimated noise levels, which are shown using noise indicators. A strategic noise map contains data on noise levels in a specific area for the calendar year preceding the year of the strategic noise mapping, specifically including data on: the existing, previous, or predicted state of environmental noise expressed by noise indicator values; exceedance of noise indicator limit values; the estimated number of residences, schools, and hospitals exposed to certain noise indicator values; and the estimated number of people exposed to noise in a given area.

The Republic of Serbia has mandated that strategic noise maps for agglomerations, main roads, main railways, and main airports be prepared and adopted by June 30, 2024, and revised by June 30, 2027, at the latest [2]. Environmental noise protection action plans shall be adopted no later than one year after the adoption of the strategic noise maps [2].

Strategic noise maps are used as a basis for the development of action plans and as a means of informing the public about environmental noise levels and their harmful effects.

The City of Belgrade, in accordance with legal obligations, has designated acoustic zones by Decision on the establishment of acoustic zones in the territory of the city of Belgrade ("Official Gazette of the City of Belgrade", no. 2/22). In accordance with Article 17 of the Law on Environmental Noise Protection ("Official Gazette of the RS", no. 96/21), in areas where it has not yet been implemented, the values prescribed for Acoustic Zone 5 are applied as limit values.

3. Overview of the Belgrade Nikola Tesla Airport

Belgrade Nikola Tesla Airport (IATA: BEG, ICAO: LYBE) is the largest international airport in Serbia, serving nearly 8 million passengers and handling 83,311 commercial take-off and landing operations in 2023.

It is located 19 km west of downtown Belgrade, near the settlement of Surčin. The airport covers an area of approximately 3 850 000 m². Currently, runway 12L-30R, which is 3,400 m long, is undergoing reconstruction, and these works could only commence after the construction of the new (inserted) runway 12R-30L, which is 3500 m long. After the completion of the reconstruction, the inserted runway will serve as a parallel taxiway and as a reserve runway only in case the main runway (12L-30R) is closed. Belgrade Nikola Tesla Airport currently has 18 taxiways, the airport's category is 4E, and its fire category is 8.

4. METHODOLOGY

The process of strategic noise mapping consists of seven phases, with each phase defined by the previous ones [6]. This ensures that all requirements and specifications are addressed before the development of data sets and noise models.

4.1. Phase 1 – Defining the Area for Which the Strategic Noise Map Should Be Created

The starting point for defining the area for which the noise mapping needs to be carried out for 2023 are the noise contours previously developed for Belgrade Nikola Tesla Airport. To define the area for the strategic noise mapping, the noise contours developed based on 2019 traffic data were used. By comparing the areas of these noise contours with the boundaries of the municipalities surrounding the airport, it was determined that air traffic noise above 55 dB L_{den} and/or 40 dB L_{night} affects eight municipalities: Stara Pazova, Zemun, Surčin, Novi Beograd, Savski venac, Rakovica, Voždovac, and Čukarica.

4.2. Phase 2 – Defining the Calculation Methods

For the development of noise maps for Belgrade Nikola Tesla Airport, the CNOSSOS-EU:2015 (Directive 2002/49/EC, Directive 2015/996) method was used for assessing air traffic noise [7]. The calculation program used for the computations complies with the 4th edition of ECAC.CEAC Doc 29 [8], which is required by the CNOSSOS-EU:2015 method for assessing air traffic noise.

4.3. Phase 3 – Defining the Input Data Specifications

The definition of data required for the calculations is based on the specifications of the chosen method for estimating the size of noise indicators, the process of preparing noise maps, and the area where strategic noise mapping is conducted. The data needed for the strategic noise mapping for air traffic include digital model of the observed area, air traffic data, meteorological and demographic data.

4.4. Phase 4 – Collecting and Creating Data Sets

4.4.1. Digital Terrain Model

The data for creating the three-dimensional digital terrain model in the area for which the strategic noise map is being developed were obtained from the Republic Geodetic Authority (RGA). The data were collected from the Basic Topographic Model (BTM), which was established in accordance with the Law on State Survey and Cadastre and the by-law governing topographic survey and development of topographic-cartographic products – the Regulation on Topographic Survey and Topographic-Cartographic Products.

4.4.2. Buildings

The data on facilities (buildings) in the area of strategic noise mapping were obtained from the RGA. Two sets of data were obtained. The first data set provided information on the layout position of facilities (digital cadastre). The second set, which included data on the purposes and heights of the facilities, was also obtained through the RGA, but using

the alphanumeric service of eKatastar (KnWEB - web service intended for accessing real estate cadastre data). The data for 129 616 facilities were used for further work and detailed consideration.

4.4.3. Air Traffic Data

Belgrade Airport d.o.o. provided data on aircraft movements for each individual take-off and landing operation during 2023, and data from the continuous noise monitoring system for aircraft taking off and/or landing at Belgrade Nikola Tesla Airport (NTK system).

The implemented flight schedule provided by BA included 84 871 operations (commercial and non-commercial), of which 340 operations were cargo truck transport operations (not aircraft) that were not considered. Furthermore, according to the CNOSSOS-EU method [7], noise generating activities associated with airport operations that do not contribute materially to the overall population exposure to aircraft noise and associated noise contours (such as helicopters, taxiing, engine testing and use of auxiliary power-units), may be excluded. Therefore, we excluded 194 helicopter operations and 172 ultralight aircraft operations which do not significantly impact noise contours, along with the 54 military operations that are excluded by the regulation [2,7]. Finally, 84,111 were used for strategic noise mapping. For each individual take-off and landing operation in 2023, BA provided data on the aircraft type, date and time of take-off and landing, departure and arrival airport, approach and departure paths (radar data), and the runway in use. The annual average distribution of departures and arrivals during the day, evening, and night periods on the runways in use is given in the table below. For most operations, runways 12R and 12L were in use, with 64 % for take-offs and 61 % for landings.

Table 1 Number of Take-off and Landing Operations During the Day, Evening, and Night Periods on the Runways in Use

L_{den} time	Landings				Takeoffs			
periods	12L	30R	12R	30L	12L	30R	12R	30L
Day	4774	4545	10371	5990	6228	4347	12386	6299
Evening	1199	898	2193	1516	1744	1313	3250	2359
Night	2423	1188	4866	2095	1174	230	2327	396
Total	8396	6631	17430	9601	9146	5890	17963	9054

In terms of the number of takeoff and landing operations by aircraft type, the A319, AT72, and A320 collectively account for over 50% of all operations. Furthermore, the aircraft types A319, AT72, A320, A321, E195, B738, A21N, C56X, E190, C525, B38M, E170, BCS3, A332, and C550 together represent 90 % of total operations, which consisted of around 180 different aircraft types.

4.4.4. Meteorological Parameters

The meteorological parameters are obtained from the publication “Belgrade Nikola Tesla Airport Climatography” issued by the Republic Hydrometeorological Service of Serbia in 2018, covering the period from 2005 to 2017, and which was downloaded from

the official RHMZ website[1]. For the period from 2018 to 2023, the meteorological parameters are based on meteorological data contained in METAR reports provided by the Serbia and Montenegro Air Traffic Services SMATSA llc (SMATSA).

4.4.5. Population

The population data for the area covered by the strategic noise map were obtained from the Statistical Office of the Republic of Serbia. The data include information about residents and dwellings, by statistical and enumeration areas based on the 2022 Census. The core area, which includes four urban municipalities (Surčin, Zemun, Novi Beograd, and Čukarica), which was the subject of further detailed analysis, comprises 2,500 enumeration areas (the smallest spatial unit for which data are recorded in the Register of Spatial Units and formed for census purposes) with a population of 610 867 and 284 911 dwellings.

4.5. Phase 5 – Development of the Acoustic Model

All collected data were processed and adapted in accordance with the requirements for their use in the computational program *Aviation Environmental Design Tool (AEDT)*, version 3f, by the American *Federal Aviation Administration (FAA)*, which was used for acoustic calculations and analysis of population exposure to noise. For the 2023 strategic noise map, all operations were modeled as if they occurred solely on the main runway at Belgrade Nikola Tesla Airport, reflecting the planned return to its exclusive use after the completion of runway reconstruction in 2024.

4.5.1. Routes and Dispersion

Analysis of radar trajectories revealed significant dispersion in arrival and departure paths. Due to considerable deviation of implemented trajectories in relation to the standard procedures for approach and departure published in the Aeronautical Information Publication, it was decided that a series of backbone tracks for arrivals and departures should be established for each runway in use, along with an assessment of the dispersion around these backbone tracks in order to examine how the aircraft deviates from the average value with the increase in distance from the airport. In total, 31 backbone tracks were defined, i.e. 175 including the dispersed sub-tracks (see Figs. 1 and 2).

4.5.2. Aircraft substitutions

In the development of the acoustic model, the predominant aircraft types operating at the airport were accurately identified using available databases. For certain aircraft types, particularly those associated with general aviation and accounting for a very small number of operations, substitutions were made. In these cases, the most similar aircraft from the same manufacturer were selected as substitutes. This approach was based on similarities in performance characteristics, size, and operational profiles, ensuring minimal impact on the accuracy of the resulting noise contours. Given the low frequency and limited contribution of these substituted aircraft to overall noise levels, their impact on the final contours is negligible.

[1] https://www.hidmet.gov.rs/data/aerodromi/Klimatografija%20aerodroma%20-%20BEOGRAD%20-%20SURCIN.pdf - accessed on 20.02.2024

4.6. Phase 6 – Calculating Noise Levels

The basic settings in the software package during the calculation of noise indicators, in accordance with the requirements of the Directive 2002/49/EC and the legislation of the Republic of Serbia in the field of noise protection, included the following: the calculation was performed on a grid resolution 10 × 10 meters; the calculation of noise indicators was performed at a height of 4 meters above the ground; and a long-term time correction for the given meteorological data was used during the calculation with different conditions for each period of the day (L_{day}, $L_{evening}$ and L_{night}).

4.7. Phase 7 – Post-Processing and Analysis

After completing the noise level calculations, an analysis of the results was conducted to obtain summary statistics that can be reported to the Serbian and European Environment Agency. The results of the analysis are presented in the following text.

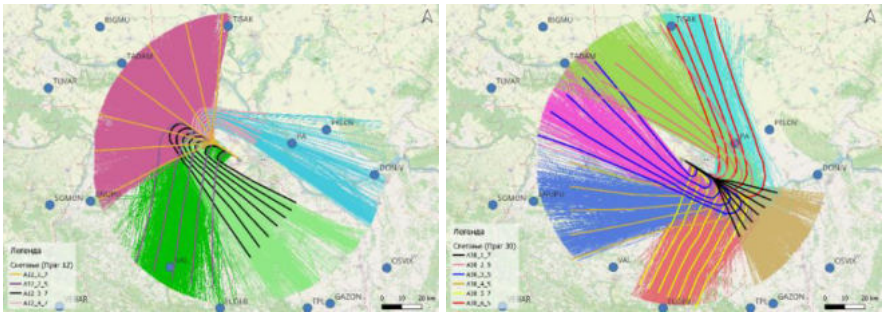

Fig. 1 Trajectory Clusters for Landings on RWY 12 (Left) and RWY 30 (Right)

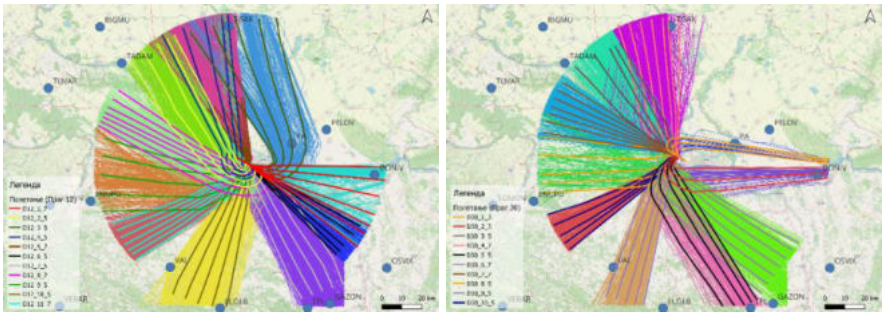

Fig. 2 Trajectory Clusters for Take-Offs on RWY 12 (Left) and RWY 30 (Right)

5. Results of Strategic Noise Mapping

The final phase in the process of strategic noise mapping involves developing maps of equal noise levels, estimating the areas, residential units, and people exposed to noise; assessing population disturbance due to noise, and determining the exceedance of noise limit values in certain areas. The graphical part of the strategic noise map for the night

period (noise indicator L_{night}) is shown in Fig. 3, while the graphical part of the strategic noise map for the day-evening-night period (noise indicator L_{den}) is shown in Fig. 4.

Fig. 3 Strategic noise map for noise indicator L_{night}

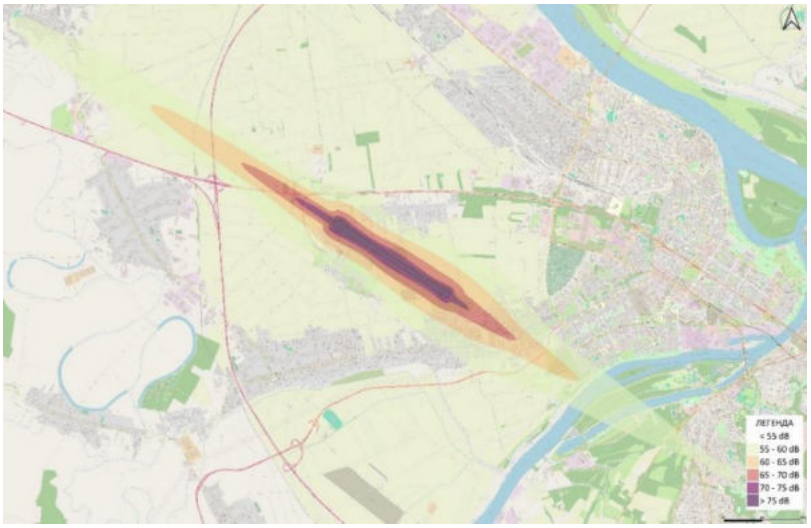

Fig. 4 Strategic noise map for noise indicator L_{den}

The results of the analysis of the area and residential units, including the estimated number of inhabitants for the strategic noise mapping for Belgrade Nikola Tesla Airport, are presented in Table 2. The results of the analysis of school buildings (preschool institutions, primary education, secondary education, and higher education) and hospital buildings

(healthcare institutions providing long-term patient care) of the strategic noise mapping for Belgrade Nikola Tesla Airport are presented in Table 3.

Table 2 Analysis of Exposure of Areas, Dwellings, and People (Including Agglomerations)

Noise indicator range L_{den},dB	Exposed area in km²	Estimated number of dwellings (in hundreds)	Estimated number of inhabitants (in hundreds)
> 55	30.1	149	314
> 65	4.5	7	17
> 75	0.7	0	0

Table 3 Analysis of the Exposure of Schools and Hospitals

Noise indicator range, dB	L_{night}		L_{den}	
	Number of school buildings	Number of hospital buildings	Number of school buildings	Number of hospital buildings
< 50	422	13	416	13
50 - 54	1	0		
55 - 59	2	0	7	0
60 - 64	0	0	2	0
65 - 69	0	0	0	0
70 - 74	0	0	0	0
> 75	0	0	0	0

The data on the estimated number of people (in hundreds) living in non-agglomerated residential areas, exposed to L_{den} and L_{night} noise indicators calculated at 4 m above ground on the most exposed facade are presented in Table 4.

Table 4 Analysis of the Population Exposure Outside the Agglomerations*

Noise indicator range, dB	Population exposed to the noise ranges of indicator	
	L_{night}	L_{den}
< 50	599 760	579 511
50 - 54	7493	
55 - 59	3246	24223
60 - 64	368	5482
65 - 69	0	1651
70 - 74	0	0
> 75	0	0

* data refer to the entire area under the influence of aircraft noise

The number of people living in residential units with quiet facades, where the L_{den} value on the quiet facade is more than 20 dB lower than the facade with the highest L_{den} value, is not available due to the nature of air traffic noise. Due to the unavailability of information, it was not possible to estimate the number of people living in residential units with special sound insulation measures.

To assess the harmful effects of noise on the population during strategic noise mapping, the dose-effect relationship is used. The regulation defines the dose-effect relationship for the percentage of the affected and highly affected population based on exposure to L_{den}, as

well as the percentage of the population whose sleep is disturbed and those whose sleep is highly disturbed based on exposure to L_{night}. The European Commission Directive 2020/367 dated March 4, 2020, established a new method for assessing the harmful impacts of environmental noise, which has been used for evaluating population disturbance due to environmental noise.

The number of people who may be highly affected by air traffic noise during the day-evening-night period has been estimated and is presented in Table 5. The number of people at high risk of sleep disturbance due to air traffic noise during the night period has been estimated and is presented in Table 6.

Table 5 Analysis of Population Disturbance

Noise indicator range L_{den}, dB	Population exposed to the noise ranges of indicator L_{den}	Mean value of the noise range L_{den}, dB	The percentage of the population that may be highly affected by air traffic noise	Estimated number of people who may be disturbed by air traffic noise
55 - 59	24 223	57.5	31.3 %	7584
60 - 64	5482	62.5	40.7 %	2232
65 - 69	1651	67.5	50.5 %	833
70 - 74	0	72.5	60.6 %	0
75 - 80	0	77.5	71.1 %	0
80 - 85	0	82.5	81.9 %	0
Total	31 356	--	--	10 649

Table 6 Analysis of Sleep Disturbances in the Population

Noise indicator range L_{night}, dB	Population exposed to the noise ranges of indicator L_{night}	Mean value of the noise range L_{night}, dB	The percentage of the population at high risk of sleep disturbance due to air traffic noise	The estimated number of people at high risk of sleep disturbance due to air traffic noise
50 - 54	7493	52.5	22.6%	1691
55 - 59	3246	57.5	28.8%	935
60 - 64	368	62.5	36.1%	133
65 - 69	0	67.5	44.3%	0
70 - 75	0	72.5	53.5%	0

For public information and the action plan development purposes, the strategic noise map shall include maps showing areas where noise indicator limit values are exceeded, known as conflict maps.

A conflict noise map is a noise map developed based on the strategic noise map and shows the difference between the current and/or predicted noise level expressed through the noise indicator and the limit values established by acoustic zones. It was not possible to assess the exceeding of noise limit values for L_{den} noise levels because the legal framework of the Republic of Serbia does not have defined limit values for the L_{den} noise indicator. The conflict map for the night period is presented in Fig. 5.

Fig. 5 Map disclosing the exceeding of a limit value for the night period

6. CONCLUSION

This research provides a comprehensive analysis of the strategic noise mapping process for Belgrade Nikola Tesla Airport, contributing to the broader understanding of environmental noise management in Serbia. The study utilized the CNOSSOS-EU method and the Aviation Environmental Design Tool (AEDT) to assess noise exposure based on 2023 air traffic data. The results highlighted the significant impact of aircraft noise on the surrounding municipalities, particularly in areas where noise levels exceeded 55 dB L_{den} and 40 dB L_{night}. The analysis identified the number of residential units, schools, hospitals, and people affected by different noise levels, providing a crucial foundation for future action plans aimed at mitigating the effects of noise pollution.

The findings from this research underscore the critical role that strategic noise maps play in environmental noise management. By providing detailed insights into the areas most affected by aircraft noise, this study lays the groundwork for the development of effective noise mitigation strategies. The strategic noise maps produced from this analysis will serve not only as a vital tool for policymakers in crafting action plans aimed at reducing noise pollution but also as an essential resource for informing the public about the levels of environmental noise and the associated risks. As required by national legislation, environmental noise protection action plans must be adopted within one year following the completion of these maps. Ensuring that these plans are timely and well-informed by accurate data is crucial for mitigating the harmful effects of noise on the community and for aligning Serbia's environmental policies with broader European standards.

Acknowledgement: *The paper is a part of the work done within the project "Development of strategic noise map with action plan" (UN-38/2023). The authors would like to express their gratitude to the Belgrade Airport d.o.o. Beograd, especially to colleagues from the Sustainability department for their valuable input and assistance throughout this study.*

REFERENCES

1. European Commission. (2002). Directive 2002/49/EC of the European Parliament and of the Council of 25 June 2002 relating to the assessment and management of environmental noise. Official Journal of the European Communities, 189, 12-25.
2. Law on environmental noise protection ("Official Gazette of RS",no. 96/2021)
3. Regulation on Noise Indicators, Limit Values, Noise Indicators Assessment Methods, Disturbance and Harmful Effects of Environmental Noise ("Official Gazette of the RS", No. 75/10),
4. Rulebook on the Methodology for Determining Acoustic Zones ("Official Gazette of the RS", No. 72/10)
5. Rulebook on the Content and Methods of Developing Strategic Noise Map and Action Plan, the Manner of Their Development and Presentation to the Public, as well as Their Forms ("Official Gazette of the RS", No. 90/23)
6. The Republic of Serbia, Ministry of Environmental Protection, Ministry of Finance, AECOM International Development Europe SL, Guidelines for the development of strategic noise maps in Serbia, 12 August 2019
7. European Commission. (2015). COMMISSION DIRECTIVE (EU) 2015/996 of 19 May 2015 establishing common noise assessment methods according to Directive 2002/49/EC of the European Parliament and of the Council
8. European Civil Aviation Conference. (2016). Report on Standard Method of Computing Noise Contours around Civil Airports (ECAC.CEAC Doc 29, 4th ed.). European Civil Aviation Conference.

FACTA UNIVERSITATIS
Series: **Working and Living Environmental Protection** Vol. 21, Nº 4, Special Issue, 2024, pp. 341 - 349
https://doi.org/10.22190/FUWLEP241021032J

Original scientific paper

RECONNAISSANCE DRONE NOISE REVIEW

UDC 534:623.746-519

Snežana Jovanović[1], Martin Jovanović[2], Aleksandar Đurić[3], Dragan Stojadinović[1], Milica Ivić Nikolić[1]

[1]Technical Test Center, Serbian Army, Ministry of Defense, Belgrade, Serbia
[2]Clarivate, Belgrade, Serbia
[3]Military Academy, University of Defence, Belgrade, Serbia

ORCID iDs: Snežana Jovanović https://orcid.org/0009-0004-6468-7726
Martin Jovanović https://orcid.org/0009-0000-8638-9392
Aleksandar Đurić https://orcid.org/0000-0002-2165-528X
Dragan Stojadinović https://orcid.org/0009-0004-6534-8443
Milica Ivić Nikolić https://orcid.org/0009-0007-6217-4929

Abstract. *The paper analyzes the sound of drones, both as environmental noise and as a parameter for their detection. The reasons for the psychoacoustic character of the noise and the conditions for effective acoustic detection are examined. Comparative results of sound measurements are provided for three types of reconnaissance drones individually, while hovering at different altitudes.*

Key words: *drone, anti-drone, reconnaissance drone, noise, psychoacoustic, detection*

1. INTRODUCTION

Although drones are a symbol of innovative freedom and technical power in the airspace, in terms of noiselessness, they have not surpassed birds, as their operation is always accompanied by sound. In the world of drones, acoustics is found in two areas: the noise of drones in the environment and the sound detection of drones.

Unmanned aerial vehicles (UAVs – Unmanned Aerial Vehicles), or drones, are a synthesis of aerodynamics, electrical engineering, computing, and new materials. Thanks to their unmanned operation, whether remotely controlled or autonomously programmed, and their three-axis movement, drones enable wide, cost-effective, and easy applications, dependent only on creativity and needs.

Drones are easily accessible in their basic design and, with optimal performance, are increasingly integrated into our daily lives (for: filming, entertainment, journalism, delivery,

Received October 21, 2024 / Accepted November 29, 2024
Corresponding author: Snežana Jovanović
Technical Test Center, Serbian Army, Vojvode Stepe 445, 11000 Belgrade, Serbia
E-mail: sneza.jovanovic.toc@gmail.com

research, surveillance and security, agriculture, real estate, construction, logistics, etc.). They are classified by weight, operational range, and risk (open-category drones can fly within visual range), and can also be divided into: fast (racing) drones and slow (hovering cameras or cargo drones).

Civil aviation authorities in some technologically advanced countries have allowed the production of drones for transporting people, passenger UAVs (unmanned aerial vehicle-UAV) or some eVTOL (electric vertical take-off and landing-eVTOL). Technological platforms for urban air mobility involve vertical takeoff and landing, three-axis operationality controlled from the ground or autonomously via routing protocols. Certainly, safety requirements are the most important for this air mobility sector. Due to traffic in populated areas, environmental pollution and noise emission requirements are also important.

Electronic commerce is rapidly growing and engaging consumer drones that fly at low altitudes to deliver packages to customers, which can significantly increase the noise in populated areas (above the thresholds of 45 dBA at night and 55 dBA during the day, according to Regulation about noise in the Republic of Serbia (Official Gazette of RS 75/2010, Directive EC 49/2002 and ISO 1996).

Mostly used unmanned aerial vehicles are based on electric motors (with or without brushes, which are quieter but shorter-lived), batteries (lithium-ion 3.7 V or lithium-polymer 3.6 V), composite materials, and other sophisticated components (GPS systems, controllers, voltage regulators, cameras, sensors (accelerometers, gyroscopes, magnetometers, barometers, etc.)), which make them intelligent and powerful.

Hardware-wise, drones are multirotors, whose movement in all directions is achieved by changing the speed of the propellers (the kinetic energy of rotation generates thrust). On the commercial market, quadcopters are the most common, with four rotors, that is, four motors connected to two pairs of propellers that rotate in opposite directions to achieve movement (as rotating in the same direction would cause them to spin around their axis). Propellers, through fast rotation, generate force that lifts, lowers, and moves the drone through the air, causing vibrations and sound.

Drone noise mostly depends on the propellers (shape, number, size, and material), followed by: the propulsion system (motor power and type – brushless motors are quieter), aerodynamics, volume, and payload, as well as environmental noise and wind speed.

The type of drone can be recognized by its sound: higher-speed drones usually have smaller propellers with a higher pitch and are noisier, while slower drones (mostly used for cargo, filming, etc.) have larger propellers with a lower pitch.

Lower noise is achieved through design and an optimal relationship between the diameter of the blades and the rotor. To achieve good aerodynamics characteristics, and reduce energy consumption and noise, the propeller blades are individually balanced with precision. Larger diameter, smooth, and light propellers will overcome air resistance with fewer revolutions and produce less noise.

There is also an attempt to manufacture an ultra-quiet drone without propellers, for cargo transport and delivery, based on space technology and ion propulsion (the generated ion cloud creates thrust).

Drone noise is irritating, with psychoacoustic impact, resembling the fluctuating buzz of a large insect or a swarm of insects. Compared to other sources, drone noise is equally unpleasant as that of vehicles (though drone noise levels are about 6 dBA lower) and traditional aircraft (at 100m distance a helicopter noise is about 95 dBA and a large quadcopter about 55 dBA), due to prominent tones in the spectrum (motor hum and whistling during rotor

rotation). The irritability of the noise depends on the axial distance between the rotors and can be reduced through optimal design, and spacing between opposing rotating propeller pairs. Although propellers should rotate at the same speed, sometimes a prominent tone is heard because two close frequencies (from the two pairs of opposing rotors) create a third virtual frequency (from their difference), producing a periodic loud sound.

Considering the environment noise criteria, the question arises as to what altitude a drone should fly to be discreet. The greatest challenge and coverage is a silent and unobtrusive drone in rural areas, where ambient noise is minimal.

The application of drones for surveillance and security is a priority, as they quickly provide precise data and images from large areas that the human eye cannot detect. In order to have good-resolution data while remaining unnoticed, drones must be silent and fly at optimal heights, which should be predicted considering that ambient noise varies by area and time of day. Noise levels decrease by 6 dB at double the distance, so its spreading can be roughly predicted.

The flight control system sends commands to the motors via radio transceiver signals and transmits data that microcontrollers process and execute algorithms for stabilization and navigation. Most drones use radio frequencies of 2.4 GHz or 5.8 GHz, with a range from several hundred meters to several tens of kilometers. With higher frequency, the transmission of radio data increases but the signal range decreases. Data from the camera is compressed and sent via the radio transmitter to the receiver, which decompresses it and displays it on the screen.

In a short time, the „celebratory" use of drones has evolved into military applications. Unmanned aerial vehicles (UAVs) with integrated weapons, such as suicide drones, are becoming a significant part of warfare, supported by intelligence gathered through reconnaissance. Military drones conduct delivery, observation, and reconnaissance of enemy positions, and "guided munitions" attacks, reducing human losses.

Prototypes are tested in real combat conditions, so development is rapid, and the market is quickly supplied not only with cheap, mass-produced but also expensive, precise flying weapons.

The military drone industry is simultaneously developing and producing anti-drone systems, which involve tracking drones.

Active tracking for counter-drone operations includes the processes of detection, classification with identification, and localization with countermeasures, integrating sensors: radar, radio frequency analyzers, cameras, and microphones.

Individually, these systems are not always successful:

- Radar ignores small flying objects such as small drones and birds.
- Radio frequency analyzers have a relatively short range, lower effectiveness in areas with multiple radio signal sources, and cannot detect autonomous drones that do not maintain contact with a controller.
- Optical and infrared (IR) cameras do not work well in fog and darkness and, when operating alone, can mistakenly identify birds as drones.
- Acoustic detectors (systems of microphones) have a short range, up to 500 m due to noise and environmental interference, and may be useless if the aircraft shuts down its engines in the final phase when dropping payload or performing a kamikaze mission.

An audio detector system on an active drone records the sound of the motor and propellers of the drone it tracks and compares it with an acoustic profile from the database. Through triangulation, it accurately locates the object and distinguishes between: aircraft

sizes, drones from birds, and fixed-wing aircraft from multirotor ones. It does not depend on radio signals, so it can detect: autonomous drones, those in areas with multiple signals, those changing radio frequencies, and so on. It also detects small drones (small for radar) and those that do not emit heat (without infrared, made of composite materials).

2. METHODOLOGY

Small commercial drones are often modified for reconnaissance and target location, and it is desirable for them to be quiet and barely noticeable (with high-resolution cameras in three axes to transmit live footage and thermal cameras for nighttime conditions). They usually fly above 50 meters to remain visually inconspicuous when combined with the terrain.

Laboratory-controlled measurements (in an anechoic chamber) ensure repeatability of results, unaffected by the environment, which is why the drone's acoustic model is recorded under these conditions depending on motor power and propeller rotation speed. Wind tunnel testing allows for a more realistic (and expensive) two-dimensional assessment of noise emissions.

Field-based, realistic measurements include environmental influences (ambient noise, ground absorption, reflection from obstacles, wind, humidity, temperature, etc.). Under these conditions, the drone's acoustic model is treated as a point source of sound, where noise emission must be synchronized with the geometry and coordinates of the position.

The drone's acoustic model has four operational states: hovering, horizontal forward/backward flight, climbing, and descending.

In horizontal flight (moving forward/backward with different rotor speeds), noise emission is similar to that of hovering (with a difference of $0 \div 3$ dB), as long as the number of revolutions remains constant.

In the vertical direction, as altitude is gained and the air becomes thinner, the noise becomes more pronounced. During descent, due to airflow and maneuvers with changing rotor speeds, the sound pressure and noise level increase. Descent is slower with more time spent at lower altitudes, thus amplifying the environmental impact of the noise.

According to the test plan for the demonstration of three types of smaller reconnaissance unmanned aerial vehicles (UAVs) at the test site, in a free sound field, in the vertical plane, individual noise measurements of drones, and quadcopters, were conducted while hovering at different altitudes.

The microphone measurement point was located at a height of 1.2 meters from the ground and in the vertical plane beneath the drone (while hovering) at altitudes of 50 m, 100 m, 200 m, or 300 m.

The measurement (at a sampling rate of 51.2 kHz) was performed with a G.R.A.S Pressure Microphone 40AD and a noise and vibration measurement amplifier system NetDB.

3. RESULTS

The measurement results are presented in Tab. 1 and in the time signal graphs (equivalent level L_{eq} expressed in dB(A)fast) and their 1/3 octave spectra.

The fundamental harmonic at 125 Hz is from electric motors, while the next ones are from rotating propellers.

Table 1 Results of noise measurement in the vertical plane, under the drone, quadcopter

Hover height drone (m)	Drone noise level, L_{eq}, (dB(A)fast)			Ambient noise, L_{eq} (dB(A))
	MATRICE 300 (higher, 9 kg)	MATRICE 30 T (medium, 4 kg)	MAVIC 3E (small, 1 kg)	
50	56.3	57.4	49.7	42.8
100	53.1	50.8	53.2	
200	54.6	49.3	55.5	
300	48.3	50.2	54.0	

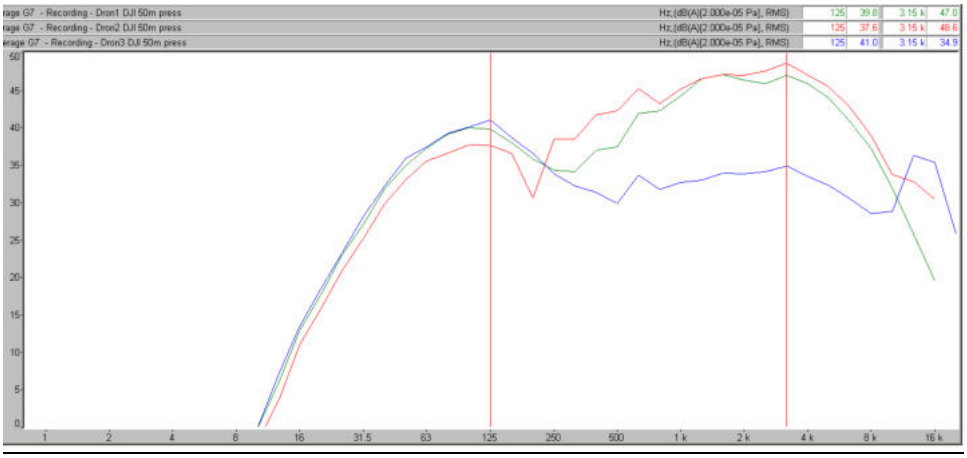

Fig. 1 The 1/3 noise spectrum of a large, medium and small drone in the vertical plane, at a height of 50 m

Figure 1 shows noise spectrum from the engine of large (Matrice 300), medium (Matrice 30T) and small (Mavic 3E) drones measured at a height of 50 m at a frequency of 125 Hz. The propeller frequency is around 3.15 KHz. The data are given in different colors for Figs. 1 and 2:

- Green color – large drone data (Matrice 300).
- Red color – medium drone data (Matrice 30T).
- Blue color – small drone data (Mavic 3E).

The smallest noise level is from a small drone, which is also visible in the data given in Tab. 1. The data in Tab. 1 also shows that small drone noise is higher at higher heights, because of the need to compensate for thin air and increase in height. That is why it is prescribed for small drones to fly at heights lower than 100 m.

Figure 2 shows, similar to Fig. 1, the noise spectrum from engines of large (Matrice 300), medium (Matrice 30T) and small (Mavic 3) drones measured at a height of 100 m at a frequency of 125 Hz. The propeller frequency is around 125 KHz. The similar conclusions we can make here like given in Fig. 1, for a height of 50 m.

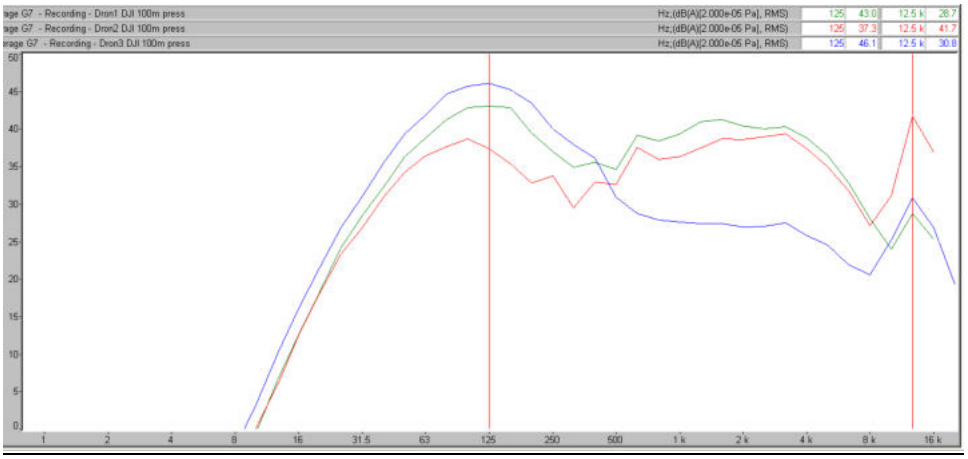

Fig. 2 The noise spectrum of a large, medium and small drone in the vertical plane, at a height of 100 m

Figure 3 gives the data for a small drone at heights of 50 m (green color), 100 m (red color), 200 m (blue color) and 300 m (purple color), where it can be seen that the small drone noise amplitude is getting lower with increase of height.

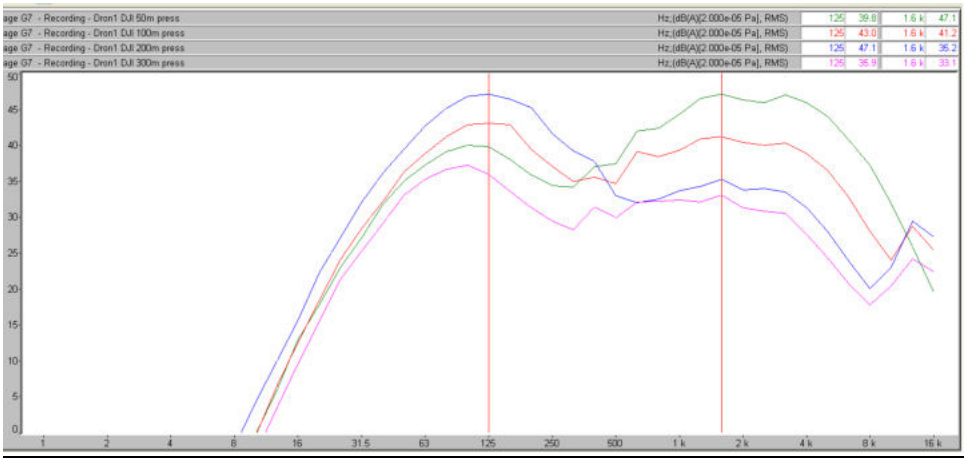

Fig. 3 The noise spectrum of a small drone in the vertical plane, at heights of 50 m, 100 m, 200 m and 300 m

Figure 4 gives the data for a medium drone at heights of 50 m (green color), 100 m (red color), 200 m (blue color) and 300 m (purple color), where it can be seen that a medium drone noise amplitude is getting lower with increase of height.

Figure 5 gives the data for a large drone at heights of 50 m (green color), 100 m (red color), 200 m (blue color) and 300 m (purple color), where it can be seen that the noise

from engine of a drone is higher than the noise from propellers, because it is much easier for him to stay in the air.

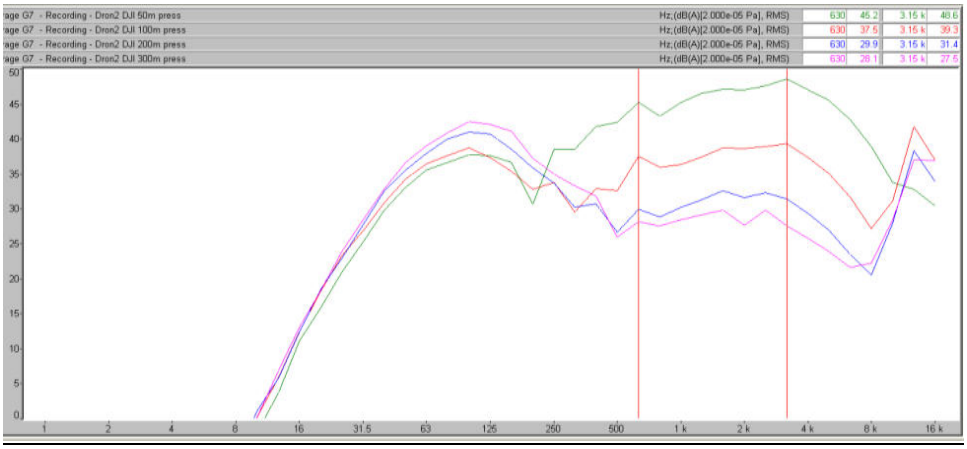

Fig. 4 The noise spectrum of a medium drone in the vertical plane, at heights of 50 m, 100 m, 200 m and 300 m

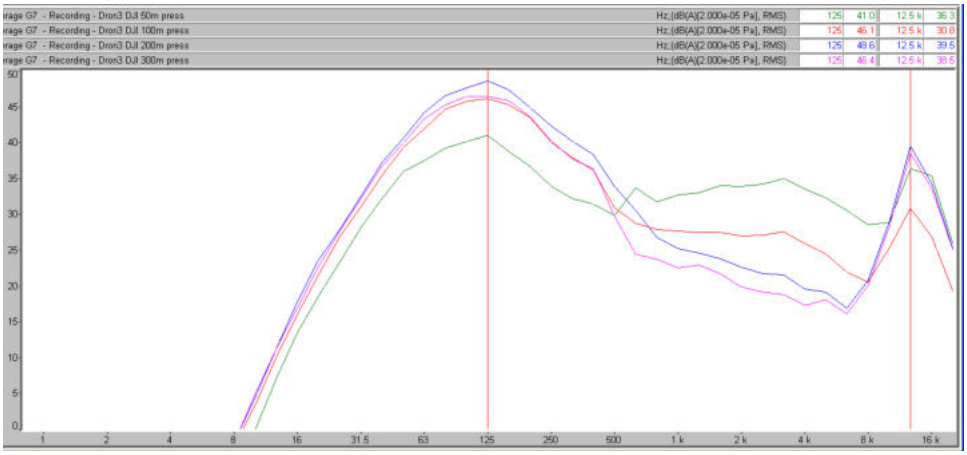

Fig. 5 The noise spectrum of a larger drone in the vertical plane, at heights of 50 m, 100 m, 200 m and 300 m

4. Conclusions

The application of drones in all areas of life is for the benefit of humans (for an easier, (un)healthier life), but it is accompanied by noise emissions as a new, additional environmental pollutant.

Depending on the hardware design, payload, and operational function, drones emit irritating noise that is more unpleasant in terms of their character and spectral content than

their level. Measuring noise levels quantifies the sound, while psychoacoustics analyzes the tonality and other characteristics to which people strongly react (loudness, sharpness, roughness, fluctuation, etc.). Theoretically, noise decreases with altitude, but the allowable flying height is legally limited depending on the drone's designated category.

The results of measurements on reconnaissance drones show that the smallest drone with a pair of ”quiet” propellers (made of carbon fibers, which have high aerodynamic efficiency, lower noise, and reduced energy consumption) above (50 / 100) meters is no longer quiet, as it struggles in the increasingly thin air by increasing the propeller speed. At the same time, in order to be a reconnaissance drone and remain visually inconspicuous, it is desirable for it to fly above 50 m.

A drone's flight is always accompanied by sound, and thus each drone has its own audio profile, which serves as a reliable parameter for detecting them.

To determine the sound profile of an aerial vehicle, both laboratory and field testing should be applied.

Acoustic detectors, made up of a series of microphones, record the sound of the drone they are tracking and compare it with the audio profile stored in the server database.

Detecting small reconnaissance drones is complex because they do not emit heat (no infrared signature, due to the plastic body and electric motors), and intentionally change radio frequencies, which is why acoustic detection is significant. For nighttime conditions, combined audio-IR visual detection is preferable.

REFERENCES

1. ISO 5305:2024, Noise measurements for UAS (unmanned aircraft systems)
2. Schaffer B., Pieren R., Heutschi K., Wunderli J., Becker S., Drone noise emission characteristics and noise effects on humans—A systematic review," International Journal of Environmental Research and Public Health, vol. 18, no. 11, pp. 1-27, 2021
3. Torija A., Clark C., A psychoacoustic approach to building knowledge about human response to noise of unmanned aerial vehicles," International Journal of Environmental Research and Public Health, vol. 18, no. 2, p. 682, 2021
4. EU, 2019/945, *Commission delegated regulation on unmanned aircraft systems and on third-country operators of unmanned aircraft systems*
5. ISO 3744, *Acoustics — Determination of sound power levels and sound energy levels of noise sources using sound pressure — Engineering methods for an essentially free field over a reflecting plane*
6. EU, 2020/1058, *Commission delegated regulation on amending Delegated Regulation (EU) 2019/945 as regards the introduction of two new unmanned aircraft systems classes*
7. European Union Aviation Safety Agency, *Guidelines on noise measurement of unmanned aircraft systems lighter than 600 kg operating in the specific category (low and medium risk)*
8. Landstrom U., Akerlund E., Kjellberg A., Tesarz M., Exposure levels, tonal components, and noise annoyance in working environment," Environment International, vol. 21, no. 3, pp. 265-275, 1995
9. Burkard R., Hecox K., The effect of broadband noise on the human brainstem auditory evoked respose. I. Rate and intensity effects," The Acoustical Society of America, vol. 74, pp. 1204-1213, 1983
10. ISO 21895, *Categorization and classification of civil unmanned aircraft systems*
11. ISO 3745:2012, *Acoustics — Determination of sound power levels and sound energy levels of noise sources using sound pressure — Precision methods for anechoic rooms and hemi-anechoic rooms*
12. ISO/TR 25417, *Acoustics — Definitions of basic quantities and terms.*
13. Betz A., The ground effect on lifting propellers," NACA Technical Memorandum No. 836, 1937
14. Anderson M., Stephenson J., Zawodny N., Gee K., Characterizing the effects of two ground-based outdoor microphone configurations," Proceedings of Meetings on Acoustics, vol. 39, p. 055011, 2021
15. ISO 1996-2, *Acoustics — Description, measurement and assessment of environmental noise — Part 2: Determination of sound pressure levels*

16. ISO 9613-2, *Acoustics — Attenuation of sound during propagation outdoors — Part 2: General method of calculation*
17. AnnexICAO, 16 Volume 1, Aircraft noise.
18. Stephenson J. H., Weitsman D., Zawodny N. S., Effects of flow recirculation on unmanned aircraft system (UAS) acoustic measurements in closed anechoic chambers," The Journal of Acoustical Society of America, pp. 1153-1155, 2019
19. Welch P. D., The use of fast Fourier transform for the estimation of power spectra: a method based on time averaging over short, modified periodograms," IEEE Transactions on Audio and Electroacoustics, vol. 15, no. 2, pp. 70-73, 1967
20. Ma Z., Wu H., Jiang H., Zhong S., Zhang X., Acoustic measurement of multi-rotor drones in anechoic and hemi-anechoic chambers," in *Quiet Drones Second International e-Symposium on UAV/UAS noise*, Paris, 2022
21. Uredba o indikatorima buke, graničnim vrednostima, metodama za ocenjivanje indikatora buke, uynemiravanja i štetnih efekata buke u životnoj sredini, „Sl. glasnik RS" 75/2010

FACTA UNIVERSITATIS
Series: **Working and Living Environmental Protection** Vol. 21, Nº 4, Special Issue, 2024, pp. 351 - 360
https://doi.org/10.22190/FUWLEP240819033P

Original scientific paper

METHODOLOGY FOR UNCERTAINTY ESTIMATION OF SHORT-TERM TOTAL ENVIRONMENTAL NOISE MEASUREMENTS

UDC 534.83.083

Momir Praščević, Darko Mihajlov, Petar Jovanović

University of Niš, Faculty of Occupational Safety, Niš, Serbia

ORCID iDs: Momir Praščević https://orcid.org/0000-0002-7017-1038
Darko Mihajlov https://orcid.org/0000-0003-4528-170X
Petar Jovanović https://orcid.org/0009-0007-1706-4456

Abstract. *The third edition of the ISO 1996 series describes the methods for measuring and assessing environmental noise from different noise source types (road, rail and air traffic, and industrial plants). Additionally, these standards provide guidelines for assessing the uncertainty of short-term and long-term environmental noise measurements, considering the impact of various sources of uncertainty. The procedure described for assessing measurement uncertainty refers to the specific noise of individual noise sources (road, rail and air traffic, and industrial plants) and cannot be directly applied when considering the total noise contributed by multiple, diverse, near and far sources in each situation at a specific time, along with the corresponding measurement uncertainty. The limit values of the noise indicators specified by the Serbian regulations refer to the total noise, so it is necessary to determine the noise indicators for the total noise to assess environmental noise in each situation and at a given time. Although Serbian legislation does not require the use of measurement uncertainty in environmental noise assessments, the uncertainty must be determined and reported in the measurement report according to the requirements of the third edition of the ISO 1996 series. This paper aims to provide a detailed procedure for assessing the uncertainty of total environmental noise measurements for individual noise in the context of Serbian legislation and the third edition of the ISO 1996 series. The presented procedure can also be applied in other countries where noise limit values refer to total noise.*

Key words: *environmental noise measurement, short-term measurement, measurement uncertainty*

Received August 19, 2024 / Accepted October 16, 2024
Corresponding author: Momir Praščević
University of Niš, Faculty of Occupational Safety, Čarnojevića 10A, 18000 Niš, Serbia
E-mail: momir.prascevic@znrfak.ni.ac.rs

1. INTRODUCTION

The law on environmental noise protection [1] establishes the obligation to monitor environmental noise (long-term measurements) and periodically measure individual noise sources (short-term measurements). According to the by-law [2], long-term and short-term noise measurements must be conducted in accordance with the requirements of ISO 1996 [3, 4]. Environmental noise is assessed using noise indicators for long-term measurements (L_{day}, L_{evening}, and L_{night}), and the rating level for short-term measurements (L_{Req}). All assessment values must be determined for total noise, as the regulation specifies [5] the limit values that refer to total noise. Total noise is illustrated in Fig. 1, including specific and residual noise.

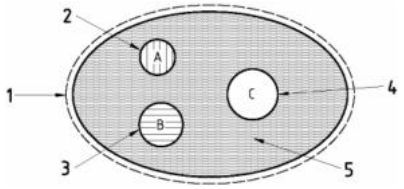

Fig. 1 Total (1), specific (2, 3, 4), and residual noise (5) [3]

Generally, measurement uncertainty is a quantitative indicator of the reliability of any measurement results. Determining the measurement uncertainty is particularly important in environmental noise measurement because environmental noise can fluctuate significantly due to variations in the operation of noise sources and changes that occur during noise propagation.

In recent years, there has been considerable interest in investigating the uncertainty of environmental noise measurements. Many papers [6-15] address environmental noise measurement uncertainty, possible sources of uncertainty, and approaches for determining environmental noise measurement uncertainty, which comply with ISO/IEC Guide 98-3 (GUM) [16]. Most of these studies focus on the uncertainty of short-term measurements, with some papers [13-15] addressing the uncertainty of long-term measurements, but not according to the ISO 1996-2 guidelines [4].

Although Serbian legislation does not require the use of measurement uncertainty in environmental noise assessments, accredited laboratories must determine and report measurement uncertainty in their measurement reports. In practice, accredited laboratories apply different approaches for determining measurement uncertainty.

Therefore, the measurement uncertainty of short-term environmental noise measurements according to the ISO 1996-2 guidelines is considered to specify a unique methodology for estimating the uncertainty of short-term environmental noise measurements.

2. DETERMINATION OF THE RATING TOTAL NOISE LEVEL DETERMINED BY SHORT-TERM MEASUREMENTS

Short-term measurements are conducted during a measurement time interval with well-defined sound emission and meteorological conditions. The measurement time interval must cover all relevant variations in noise emission and typically ranges between 10

minutes and a few hours. For periodic noise, the measurement time interval should cover an integer number of several periods or cycles. If continuous measurements during the selected period are not possible, the measurement time intervals should be chosen so that each represents a part of the cycle, and all intervals collectively represent the complete cycle. For single-event noise, the measurement time intervals should be chosen so that the sound exposure level of the single event can be determined.

Short-term measurements are usually attended and conducted with instrumentation that includes a sound level meter, filters and a sound calibrator, all of which must meet the requirements for a class 1 instrument according to the appropriate standards. The sound level meter, filters and sound calibrator should be verified according to the relevant test methods at intervals not exceeding two years. Additionally, the entire measuring system should be checked by the sound calibrator at the start and end of every measurement series. A windscreen should always be used during outdoor measurements.

Short-term measurements should be conducted during favorable ($3 \le v \le 6$ m/s) and very favorable conditions ($v > 6$ m/s (day), $v \ge -1$ m/s (night), , where v is the wind speed (with a negative sign indicating wind direction from receiver to source), "day" refers to the time between sunrise and sunset and "night" refers to the time between sunset and sunrise or when Eq. (1) is applied [4]:

$$\frac{h_s + h_r}{D} \ge 0.1\,, \tag{1}$$

where h_s and h_r are the source and the receiver heights and D is the horizontal distance between the source and receiver.

If the ground is hard, larger distances may be acceptable, although no studies have specifically addressed this topic. In practice, the authors of this paper apply distances three times larger for hard ground.

A minimum time of 10 minutes is usually sufficient to average meteorological variations under favorable and very favorable conditions, or when eq. (1) is applied. For short-term measurements under unfavorable ($v < 1$ m/s (day), $v < -1$ m/s (night)) and neutral ($1 \le v \le 3$ m/s) conditions, measurements should be taken for at least 30 minutes [4]. These minimum times should be increased to achieve sufficient averaging of source conditions. The increase in the measurement time interval depends on the type of noise source.

The ISO 1996 [4] guidelines can be applied to road and rail traffic, aircraft noise and industrial noise. For road and rail traffic and aircraft noise, increasing the measurement time interval reduces measurement uncertainty, and the selection of the measurement time interval depends on the required measurement uncertainty. For industrial noise, the selection of the measurement time interval depends on the source operating conditions.

The source operating conditions should be divided into classes where variations in sound emission are stationary and less significant than the variation in transmission path attenuation due to meteorological conditions. The operating conditions should be defined by the activity as well as its location. To categorize the operating conditions, the equivalent continuous sound pressure level should be measured over 5 to 10 minutes at a distance long enough to include noise contributions from all major sources, yet short enough to minimize meteorological effects. If the equivalent-continuous sound pressure levels vary considerably, a new categorization of the operating conditions should be made. Guidelines for selecting the measurement time interval for industrial noise can be found in ISO 9612, clause 9.2

[17]. These guidelines are illustrated in Fig. 2, which presents noise situations with three different source operating conditions (classes), where t is the selected measurement time interval and T is the duration of the classes.

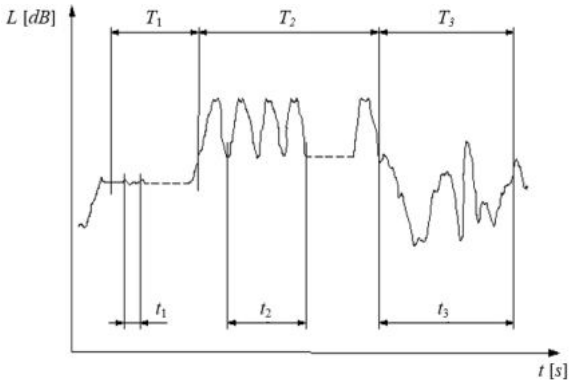

Fig. 2 An example of three cycles with different noise situations (adopted from [17])

To assess the total environmental noise at the assessment point, one or more short-term measurements of the total noise level (at least 3, preferably 5) should be conducted, each lasting at least 10 minutes. These measurements should be taken for each operating condition of the observed source(s) within each reference time interval (day, evening and night), under favorable or very favorable conditions, or when applicable, using a formula for moderate changes in sound pressure due to meteorological conditions (1).

Afterward, the average value of the measured levels is determined for each reference time interval, adding adjustments for noise source rating levels made for the noise character during periods when the noise is tonal and/or impulsive. Additionally, the duration of each class of operating conditions is taken into account. The determined value represents the rating equivalent-continuous level for total noise (abbreviated rating total noise level):

$$L_{\mathrm{Req},T} = 10 \log \frac{1}{M} \sum_{j=1}^{M} 10^{L_{\mathrm{Req},j}/10}, \tag{2}$$

where

M is the number of the classes of operating conditions,

T_0 is the duration of the reference time interval (12 h for day, 4 h for evening and 8 h for night),

$L_{\mathrm{Req},j}$ is the rating level for the class of operating conditions j,

$$L_{\mathrm{Req},j} = 10 \log \frac{1}{n_j} \sum_{i=1}^{n_j} 10^{L_{\mathrm{eq},i}/10} + K_j + 10 \log \frac{T_j}{T_0}, \tag{3}$$

n_j is the number of the measurements for the class of operating conditions j,

$L_{\mathrm{eq},i}$ is the equivalent-continuous sound pressure level for measurement i, at the assessment point for the class of operating conditions j,

T_j is the duration of the class of operating conditions j,

K_j is the adjustment for noise character for the class of operating conditions j.

Adjustments for tonal or impulsive character of noise are suggested in Table A.1 of ISO 1996 [3]. These adjustments are added only to levels of total noise, not to levels of residual sound. Adjustments are made only to specific sound sources, not to residual sound levels.

If the duration of specific noise source(s) activities T_{ss} is not equal to the duration of the reference time interval T_0, the residual noise is considered as one of the classes of source operating conditions within the reference time interval. The rating total noise level is then determined by combining the total noise level calculated according to (2) and the residual noise level determined by averaging the short-term measurements conducted when the observed specific sound source(s) is (are) off (at least 3 measurements):

$$L_{\mathrm{Req},T} = 10 \log \left(\frac{T_{ss}}{T_0} 10^{L_{\mathrm{Req},T_{ss}}/10} + \frac{T_0 - T_{ss}}{T_0} 10^{L_{\mathrm{res}}/10} \right). \tag{4}$$

3. Determination of Measurement Uncertainty

When determining the measurement uncertainty of the rating total noise level from short-term measurements, two scenarios must be considered. The first scenario is when the duration of the operating conditions of the observed noise source(s) is equal to the reference time interval. The second scenario occurs when the duration is not equal, and the residual noise is considered as one of the classes of operating conditions within the reference time interval.

The measurement uncertainty should be determined in compliance with the ISO Guide to Uncertainty in Measurements (GUM) [16].

According to GUM, each significant source of error must be identified and corrected. If the quantity to be measured is L', which is a function of quantities x_j the equation becomes:

$$L' = f(x_j) . \tag{5}$$

If each quantity has a standard uncertainty u_j, the combined uncertainty u is given by:

$$u(L_{Aeq,m}) = \sqrt{\sum_{j=1}^{n} (c_j u_j)^2} , \tag{6}$$

where the sensitivity coefficients c_j are given by:

$$c_j = \frac{\partial f}{\partial x_j} . \tag{7}$$

The estimated (true) value of the rating total noise level at the assessment point is defined as follows:

$$L = L' + \delta_{\mathrm{slm}} + \delta_{\mathrm{sou}} + \delta_{\mathrm{met}} + \delta_{\mathrm{loc1}} + \delta_{\mathrm{loc2}} , \tag{8}$$

where

L' is the calculated value of the rating total noise level according to Eq. (2) or (4),

δ_{slm} is an error due to the selection of the measurement chain (sound level meter) [4],

δ_{sou} is an error due to the deviations from the expected operating conditions of the source [4],

δ_{met} is an error due to meteorological conditions deviating from the assumed conditions [4],

δ_{loc1} is an error due to the selection of receiver location relative to reflective surfaces [4],

δ_{loc2} is an error due to the selection of microphone location representative of the assessment point (choice of microphone position, height above ground level, orientation) [17,18].

An error due to the selection of microphone location, δ_{loc2}, is added to the uncertainty budget recommended by ISO 1996-2 [4] according to the guidelines in [17,18].

The combined standard measurement uncertainty of the estimated value of rating total noise level is given by:

$$u_L^2 = c_{L'}^2 u_{L'}^2 + c_{slm}^2 u_{slm}^2 + c_{sou}^2 u_{sou}^2 + c_{met}^2 u_{met}^2 + c_{loc1}^2 u_{loc1}^2 + c_{loc2}^2 u_{loc2}^2 , \quad (9)$$

where

$c(L')$ is the sensitivity coefficient for L',

c_{slm} is the sensitivity coefficient for the sound level meter,

c_{sou} is the sensitivity coefficient for the source operating conditions,

c_{met} is the sensitivity coefficient for the meteorological conditions,

c_{loc1} is the sensitivity coefficient for selecting the receiver location relative to the reflective surfaces,

c_{loc2} is the sensitivity coefficient for selecting the receiver location relative to the assessment point,

$u(L')$ is the standard uncertainty for L' in dB,

u_{slm} is the standard uncertainty for the sound level meter in dB (u_{slm} = 0,5 dB for a class 1 sound level meter and u_{slm} = 1,5 dB for a class 2 sound level meter [4]),

u_{sou} is the standard uncertainty for the source operating conditions,

u_{met} is the standard uncertainty for the meteorological conditions,

u_{loc1} is the standard uncertainty due to selection of the receiver location relative to reflective surfaces in dB (estimated according to Annex B of ISO 1996-2 [4]),

u_{loc2} is the standard uncertainty due to selection of the receiver location relative to the assessment point in dB (u_{loc2} = 1 dB [17] or can be determined as the standard deviation of the measurement repeatability).

All the sensitive coefficients in (9) have been estimated as 1.

The standard uncertainty for the source operating conditions is considered only for single measurements of the equivalent-continuous sound pressure level at the assessment point. In this case, the standard uncertainty for L' is equal to 0.

The standard uncertainty for the source operating conditions is determined from at least 3, and preferably 5 measurements under repeatability conditions (the same measurement procedure, the same instruments, the same operator and the same place) at a position where variations in meteorological conditions have little influence on the results, using the following equation:

$$u_{sou} = \sqrt{\sum_{i=1}^{n} \frac{(L_i' - \overline{L'})^2}{n-1}} , \quad (10)$$

where

L_i' is the measured value for measurement *i,*

$\overline{L'}$ is the arithmetic average of all measurements,

n is the total number of all measurements.

Additionally, the standard uncertainty for the source operating conditions for the road, rail, and air traffic can be determined based on the number of vehicle pass-by (for road and rail traffic) and the number of sound events during the measurement time interval, using Eqs. 7-9 in ISO 1996-2 [17].

If short-term measurements are conducted under favorable and very favorable conditions or when eq. (1) is applied, then the standard uncertainty for meteorological conditions is 2 dB for distances $D \leq 400$ m. For longer distances:

$$u_{met} = 1 + \frac{D}{400}, \tag{11}$$

The standard uncertainty for meteorological conditions can be neglected when the sound source and the assessment point are in the same building.

The standard uncertainty for meteorological and the source operating conditions cannot be calculated as the combined uncertainty directly from the short-term measurements because these measurements cannot be concerned as independent measurements (see Table 4 in ISO 1996-2 [4] for the minimum time between two measurements to be independent).

If the reference time interval consists of a mixture of source operating conditions, including the residual noise, repeated measurements of the equivalent-continuous sound pressure level at the assessment point are recommended (at least 3, and preferably 5). Then, the total noise level can be calculated as [4]:

$$L' = 10 \cdot \log\left(p_1 10^{\overline{L'}_1/10} + p_2 10^{\overline{L'}_2/10} + ... + p_M 10^{\overline{L'}_M/10} \right), \tag{12}$$

where

$\overline{L_j'}$ is the energy averaged equivalent-continuous sound pressure level for repeated measurements for the class of source operating conditions *j,*

p_j is the duration of the class of source operating conditions j relative to the duration of the reference time interval, T_0,

$$p_i = \frac{T_i}{T_0}, \quad \sum_i p_i = 1, \tag{13}$$

where

T_j is the duration of the class of source operating conditions *j,*

M is the number of classes of operating conditions.

The combined standard uncertainty for L' is then [4]:

$$u_{L'} = \sqrt{\sum_{j=1}^{M} c_{L_j'}^2 u_{L_j'}^2 + \sum_{j=1}^{M-1} c_{p_j}^2 u_{p_j}^2}. \tag{14}$$

To avoid underestimating the error, p_M is the period with the highest average sound level and this period has been omitted in (14).

The sensitivity coefficients in (12) can be calculated as [4]:

$$c_{L'_j} = \frac{\partial L'}{\partial \overline{L'}_j} = \frac{p_j 10^{\overline{L'}_j/10}}{\sum_{j=1}^{M} p_j \cdot 10^{\overline{L'}_j/10}}, \tag{15}$$

$$c_{p_j} = \frac{\partial L'}{\partial p_j} = 10 \cdot \log(e) \frac{10^{\overline{L'}_j/10} - 10^{\overline{L'}_M/10}}{\sum_{j=1}^{M} p_j 10^{\overline{L'}_j/10}} . \tag{16}$$

For n repeated measurements, the standard uncertainty is the standard deviation of the mean value; otherwise, it is equal to 0:

$$u_{L_j} = \sqrt{\sum_{i=1}^{n_j} \frac{(L'_i - \overline{L'})^2}{n_j (n_j - 1)}} \text{ dB} = \frac{\sigma_{L'}}{\sqrt{n_j}} . \tag{17}$$

Repeated measurements carried out using the same equipment are not independent with respect to the uncertainty due to sound level meter.

The standard uncertainty of observations of the duration of the class of source operating conditions is determined as the standard deviation of observations (estimation and/or measurement):

$$u_{p_j} = \sqrt{\sum_{k=1}^{m_j} \frac{(p_{jk} - \overline{p_j})^2}{(m_j - 1)}} . \tag{18}$$

Finally, the expanded measurement uncertainty with a coverage probability of 95% and an associated coverage factor of 2 is:

$$U = \pm 2 u_L . \tag{18}$$

The estimated (true) value of the rating total noise level at the assessment point then becomes:

$$L = L' \pm 2U . \tag{19}$$

4. CONCLUSION

Serbian regulations in the field of environmental noise require the measurement and assessment of total environmental noise at the assessment point. Although these regulations do not mandate the use of measurement uncertainty in the assessment of environmental noise at the assessment point, accredited laboratories must determine and report measurement uncertainty in accordance with the requirements of ISO 1996-1 and ISO 1996-2.

In practice, accredited laboratories interpret and apply the guidelines for determining measurement uncertainty provided in ISO 1996-2 in various ways. To unify procedures, this paper describes in detail the methodology for determining the rating total noise level based on short-term measurements and corresponding measurement uncertainty. Although the methodology is consistent with the guidelines provided in the ISO 1996 series, there are some differences:

- the methodology in the ISO 1996 series refers to determining the rating noise level and corresponding measurement for specific noise;
- the guidelines for determining the measurement time interval depending on the operating conditions of the noise source are presented as described in ISO 9612;
- the acceptable distances for hard surfaces in (1) are recommended;
- the number of short-term measurements of the total noise level for repeated measurements is recommended;
- it is recommended that if the duration of specific noise source(s) activities is not equal to the duration of the reference time interval, the residual noise should be considered as one of the classes of source operating conditions within the reference time interval;
- a new contribution to measurement uncertainty related to the selection of microphone location representative of the assessment point (choice of microphone position, microphone height above ground level, microphone orientation) is also added according to the guidelines in ISO 9612;
- it is recommended that the standard uncertainty for meteorological conditions and the source operating conditions is not calculated as the combined uncertainty directly from the short-term measurements;
- special attention is given to the case of a mixture of source operating conditions and repeated short-term measurements are recommended in order to determine the combined standard uncertainty of the calculated value of the rating total noise level according to Eq. (2) or Eq. (4).

Acknowledgement: *This research was sponsored by the NATO Science for Peace and Security Programme under grant SPS MYP G6006 "Acoustic Multi-Functional Composites for Environmental Risks and Health Hazards Reduction" and by the Ministry of Science, Technological Development and Innovation of the Republic of Serbia under the contract no. 451-03-66/2024-03/200148.*

REFERENCES

1. Law, RS. (2021). Law on environmental noise protection, "Official Gazette of Republic of Serbia" No. 96/2021" (in Serbian).
2. Rulebook, RS (2022). Rulebook on noise measurement methods, contents and scope of environmental noise measurement reports, "Official Gazette of Republic of Serbia" No. 139/2022"
3. International Organization for Standardization. (2016). Acoustics – Description, measurement and assessment of environmental noise – Part 1: Basic quantities and assessment procedures (ISO Standard No. 1996-1:2016).
4. International Organization for Standardization. (2017). Acoustics – Description, measurement and assessment of environmental noise – Part 2: Determination of sound pressure levels (ISO Standard No. 1996-2:2017).
5. Regulation, RS (2010). Regulation on noise indicators, limit values, assessment methods for noise indicators, disturbance and harmful effects of environment noise, "Official Gazette of Republic of Serbia" No. 75/2010"
6. Ruggiero, A, Russo, D. & Sommella, P. (2016). Determining environmental noise measurement uncertainty in the context of the Italian legislative framework. Measurement, 93, 74-79.

7. Petošić, A., Franček, P., Štrbac, M., Zatko, P., Urban, D. & Szabo, D. (2018). Measurement uncertainty in the field of environmental noise and building acoustic measurements: experience from interlaboratory comparisons. In Proceedings of 8th Congress of the Alps Adria Acoustics Association.
8. Cvetković, D., Praščević, M. & Mihajlov, D. (2011). Estimation of uncertainty in environmental noise measurement. In Proceedings of the VII Triennial International Conference "Heavy Machinery HM 2011", 7(6), 39-44.
9. Praščević, M., Cvetković, D. & Mihajlov, D. (2011). The uncertainty sources in environmental noise measurements and the uncertainty estimation, Facta Universitatis Series "Mechanical Engineering", 9(2), 183-192.
10. Badida, M., Lumnitzer, E., Fil`o, M. & Bil`ova, M. (2008). Determination of the uncertainties of noise measurements, Annals of the Oradea university, Fascicle of Management and Technological Engineering, VII(XVII), 65-72.
11. Manvell, D., & Aflalo, E. (2005). Uncertainties in Environmental Noise Assessments – ISO 1996, Effects of Instrument Class and Residual Sound. In In Proceedings of Forum Acusticum 2005.
12. Wsyolek, T. & Klacyznski, M. (2006). Effect of traffic noise statistical distribution on LAeq,T measurement uncertainty, Archives of acoustics, 31(4), 311-318.
13. Kuehner, D. (2005). Long-term Leq Errors Expected and how long to Measure (Uncertainty and Noise Monitoring). In Proceedings of Forum Acusticum 2005.
14. Pryzsucha, B. (2013). Uncertainty Analysis in Acoustic Investigations. In Proceedings of "Computer science & engineering 2013". 124-129
15. Maijala, P. (2013). A measurement-based statistical model to evaluate uncertainty in long-range noise assessments, Thesis for the degree of Doctor of Technology. 178.
16. International Organization for Standardization. (2008). Uncertainty of Measurement Part 3: Guide to the Expression of Uncertainty in Measurement (GUM:1995) (ISO/IEC Guide 98-3:2008).
17. International Organization for Standardization. (2009). Determination of occupational noise exposure — Engineering method (ISO Standard No. 9612:2009).
18. Craven, N. J., & Kerry, G. (2007). A good practice guide on the sources and magnitude of uncertainty arising in the practical measurement of environmental noise.

FACTA UNIVERSITATIS
Series: **Working and Living Environmental Protection** Vol. 21, Nº 4, Special Issue, 2024, pp. 361 - 370
https://doi.org/10.22190/FUWLEP240902034M

Original scientific paper

APPLICATION OF INDICATORS IN NOISE CONTROL

UDC 534.831

Jelena Malenović-Nikolić, Bojana Zlatković, Uglješa Jovanović

University of Niš, Faculty of Occupational Safety, Niš, Serbia

ORCID iDs: Jelena Malenović-Nikolić https://orcid.org/0000-0002-1965-080X
Bojana Zlatković https://orcid.org/0000-0001-8051-1510
Uglješa Jovanović https://orcid.org/0000-0003-3204-6276

Abstract. *Indicators provide a foundational basis for offering essential data and describing changes in the environment at national, regional, or local levels. An indicator created to highlight the cause of change, the consequences of changes, the state of the environment, or the significance of implementing protective measures may be considered relevant for research. An adopted indicator, as part of the National List of Indicators, forms the basis for developing strategies, creating national policies, and establishing legal norms. Serbia's National List of Environmental Indicators includes two noise indicators, which belong to the sixth thematic section and are classified as indicators of state. The overall noise indicator, designated as 6.40 and part of the sixth thematic section entitled "State", describes noise disturbance over a 24-hour period, including the day-evening-night segments. According to the regulation, the day period lasts from 6 AM to 6 PM, the evening period from 6 PM to 10 PM, and the night period from 10 PM to 6 AM. The night noise indicator, also under the "State" category, with the designation 6.41, specifically describes noise disturbance during the night period (10 PM to 6 AM). This paper analyzes the use of indicators in noise control at both local and national levels. The use of indicators in noise control is a significant prerequisite for systematically and internationally accepted determination of the state of the environment, and for creating conditions to compare noise level values on an international level. Indicators are based on highly reliable data, which must be monitored in accordance with statistical correctness and internationally recognized methodology. The value of these indicators, published in the Report on the State of the Environment, becomes publicly available and is subject to comparative analysis.*

Key words: *indicators, control, measurement range, the environment*

Received September 2, 2024 / Accepted October 16, 2024
Corresponding author: Jelena Malenović-Nikolić
University of Niš, Faculty of Occupational Safety, Čarnojevića 10A, 18000 Niš, Serbia
E-mail: jelena.malenovic@znrfak.ni.ac.rs

1. INTRODUCTION

Noise indicator values signal improvements or deteriorations of the state of the environment and are considered as either ecological or professional indicators, depending on research needs. Noise monitoring should be conducted with the proper selection of measurement locations while considering existing data and information about identified problems.

The Regulation on the National List of Environmental Indicators of the Republic of Serbia [1] stipulates that noise control is conducted based on two indicators. These indicators are expressed in decibels (dB) and are used to determine the state of the environment, develop strategic noise maps, and plan preventive and corrective protection measures.

2. NOISE INDICATORS WITHIN THE NATIONAL LIST OF ENVIRONMENTAL INDICATORS

According to the Law on Environmental Noise Protection [2], local self-government units are responsible for financing and conducting noise monitoring within their territories.

Figures 1 and 2 show the territories (local self-governments and agglomerations) for which noise monitoring data are reported.

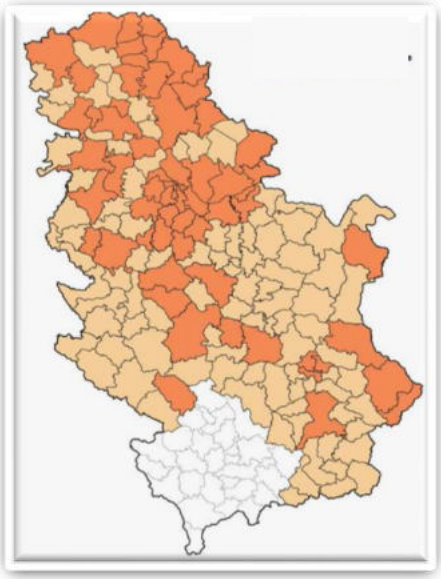

Fig. 1 Reporting of noise monitoring by the local self-governments in 2021 [3]

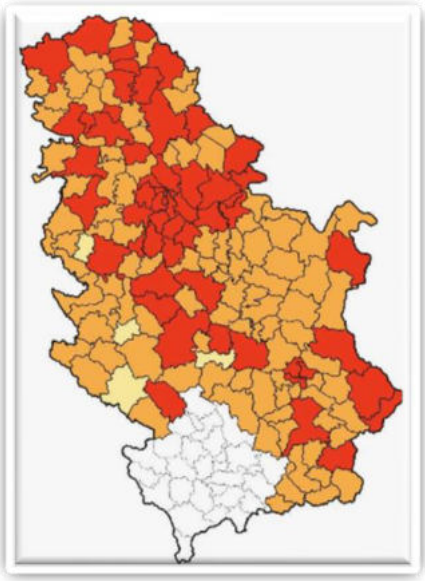

Fig. 2 Reporting of noise monitoring by the local self-governments in 2022 [4]

Based on Figs. 1 and 2, it is evident to what extent the local self-governments of Serbia fulfill their legally required obligations regarding noise monitoring. The darker-shaded areas represent local government units that have submitted data to the Environmental Protection

Agency. In contrast, the lighter-shaded areas represent local self-government units that have submitted declarations stating that no noise measurements were conducted within their territories. The primary reason cited for not adhering to the legal requirements is the lack of financial resources in their budgets. The state of the environment reports from 2015 to 2022 include only two maps marking the territories where monitoring was conducted. Therefore, from 2015 to 2020, only the number of local self-governments and agglomerations that provided data is known. These data are presented in Tab. 1. Additionally, the number of measurement points in agglomerations is graphically represented in Fig. 3.

Table 1 Number of measurement points in agglomerations [3-10]

Year	2015	2016	2017	2018	2019	2020	2021	2022
Agglomerations	86	/	68	36	69	50	56	63
Local self-governments	242	195	181	131	269	156	393	457

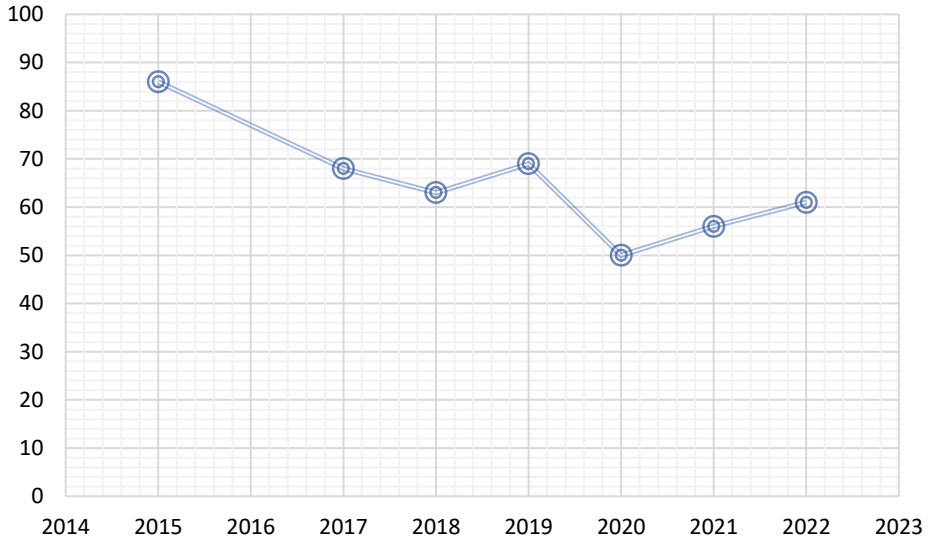

Fig. 3 Number of noise level measurement points in agglomerations [3-10]

Agglomerations, as parts of a territory with over 100,000 inhabitants and a population density that classifies them as urbanized areas, include Belgrade, Niš, Novi Sad, Kragujevac, and Subotica. According to the 2020 Report on the State of the Environment, only four agglomerations submitted reports on noise measurement, but it is not specified which agglomeration failed to fulfill its legal obligation under Article 9, Paragraph 4 [2], regarding financing and implementing environmental noise monitoring within its territory.

The tabular data indicate that the highest number of measurements in agglomerations were conducted in 2015. For 2016, aggregated data for the number of local self-governments and agglomerations were published. The trend of the number of noise level measurements in local self-governments is shown in Fig. 4.

Table 2 Number of submitted reports by local self-governments [3-10]

Year	2015	2016	2017	2018	2019	2020	2021	2022
Number	20	14	14	12	24	16	42	46

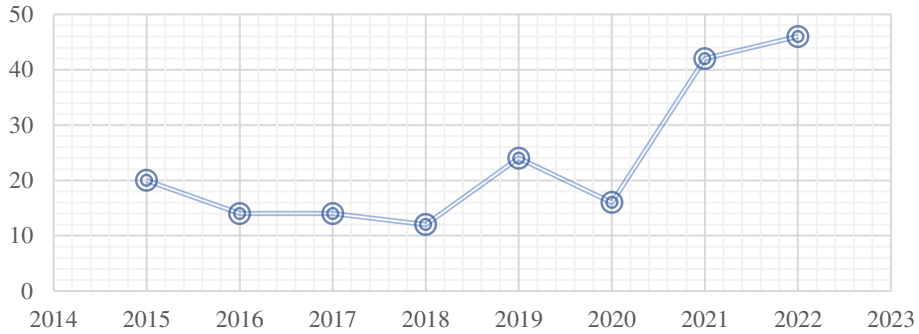

Fig. 4 Number of local self-governments that conducted noise monitoring [3-8]

Figure 5 presents data on the number of measurement points in local self-government units. Figure 6 shows a comparative overview of the number of local self-governments that conducted noise monitoring and the number of measurement points within the implemented monitoring system.

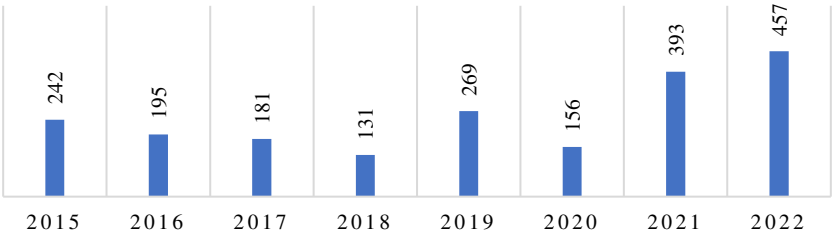

Fig. 5 Number of noise monitoring measurement points in local self-governments [3-10]

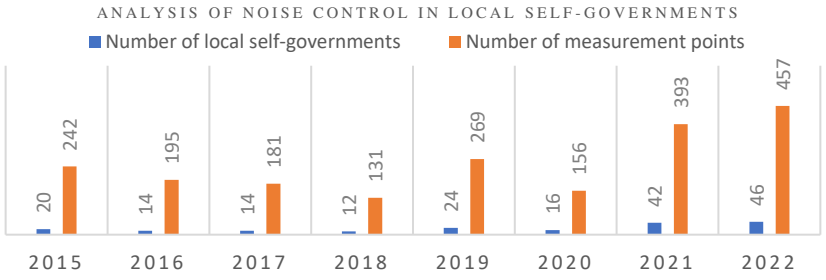

Fig. 6 Comparative overview of the number of local self-governments and the number of noise monitoring measurement points [3-10]

Based on the data from Tab. 2, it is evident that the highest number of noise level measurement data from local self-governments were submitted in 2022.

Figures 3 and 4 indicate a decreasing trend in the number of noise monitoring points in agglomerations and an increasing trend in the number of local self-governments conducting noise monitoring. Approximately 100 local governments [3, 4] are unable to implement noise monitoring.

The graph in Fig. 5 clearly indicates an upward trend in the number of measurement points in local self-governments. It is also noticeable that the fewest measurements were conducted in 2018 (131), with only 12 local self-governments submitting measurement data.

The graph in Figure 6 clearly shows an increase in the number of measurements in 2021 and 2022. Compared to the period from 2016 to 2018, the number of measurement points and local self-governments has increased by approximately threefold.

2. Analysis of Noise Indicator Values

A systematic approach to analyzing the number of measurement points and the number of local self-governments submitting noise monitoring data requires that the analysis be conducted under approximately the same conditions for the examined period.

Creating an indicator of the number of local self-governments per one hundred measurement points is considered a reliable solution. The proposed indicator is the ratio of the number of local self-governments submitting data to the number of measurement points, multiplied by a correction factor of 100. This method allows for the establishment of a foundation for evaluating the noise level monitoring process for the period from 2015 to 2022 or any other specified period. The indicator values are presented in Tab. 3.

Table 3 Number of noise monitoring measurement points per 100 local self-governments [3-10]

Year	Number of local self-governments	Number of measurements	Number of measurement points per 100 local self-governments
2015	20	242	8.26
2016	14	195	7.18
2017	14	181	7.73
2018	12	131	9.16
2019	24	269	8.92
2020	16	156	10.26
2021	42	393	10.69
2022	46	457	10.07

The analysis of the indicator values for the number of measurement points per 100 local self-governments reveals a slight upward trend in the number of measurement points. This trend is particularly noticeable during the period from 2020 to 2022, where, on average, ten measurements were conducted per local self-government. Figure 7 provides clearer calculation results.

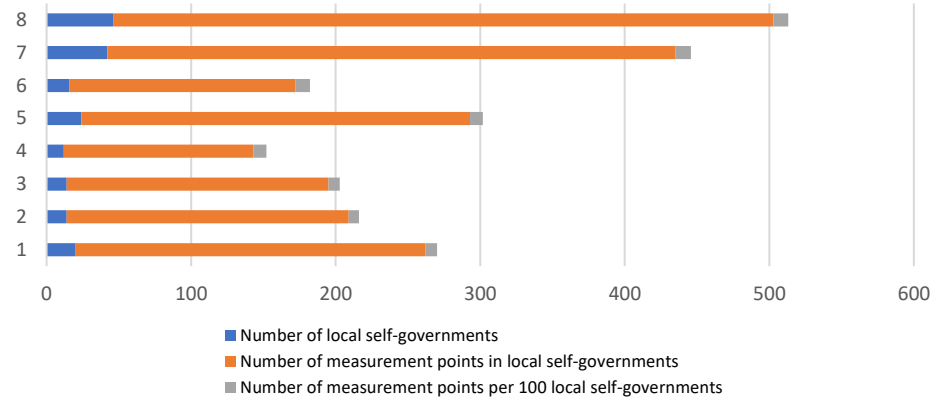

Fig. 7 Analysis of noise control indicators in local self-governments [3-10]

The analysis of the graph shown in Fig. 7 reveals significant progress at the end of the eight-year period, as the results of noise level monitoring in local self-governments are continuously published in the reports on the state of the environment.

The National List of Environmental Indicators defines the description and methodology for calculating the overall noise indicator and the night noise indicator, as well as the method and deadlines for submitting the necessary data.

The reports on the state of the environment present the noise indicators for overall disturbance (L_{den}) and the sleep disturbance indicator during the night (L_{night}) from 10 PM to 6 AM for local self-governments and agglomerations (Tabs. 4-7).

Table 4 Percentage of overall noise level measurement (L_{den}) results for local self-governments, by ranges [3-10]

Year	40-45	46-50	51-55	56-60	61-65	66-70	70-74	> 75
2015	1	10	10	13	30	54	8	1
2016	/	7	7	9	26	39	12	/
2017	/	/	11	13	23	29	14	6
2018	1	6	17	12	33	23	9	/
2019	4	8	15	40	33	27	6	/
2020	3	10	10	14	30	29	4	/

Table 5 Percentage of overall noise level measurement (L_{den}) results for agglomerations, by ranges [3-10]

Year	46-50	51-55	56-60	61-65	66-70	70-74	> 75
2015	/	6	10	14	42	21	7
2016	/	4	10	21	34	18	7
2017	/	4	10	21	34	18	7
2018	5	8	11	27	32	17	/
2019	/	9	19	33	30	9	/
2020	/	8	11	27	32	17	/

Table 6 Percentage of night noise level measurement (L_{night}) results for local self-governments, by ranges [3-10]

Year	<40	40-45	46-50	51-55	56-60	61-65	66-70	70-74
2015	4	11	17	25	26	14	2	/
2016	2	10	12	24	37	13	2	/
2017	3	16	12	19	31	16	2	/
2018	2	18	10	27	28	15		/
2019	4	13	13	25	26	17	2	/
2020	9	12	16	22	23	18	1	/

Table 7 Percentage of night noise level measurement (L_{night}) results for agglomerations, by ranges [3-10]

Year	<40	40-45	46-50	51-55	56-60	61-65	66-70	70-74
2015	2	7	11	14	36	24	5	/
2016	2	10	12	24	37	13	2	/
2017	7	7	9	16	38	19	3	/
2018		16	8	30	24	21		/
2019	1	14	13	21	21	27	3	/
2020	4	10	18	22	24	20	2	/

The analysis of the measurement results presented in Tabs. 5-8 shows that the highest percentage of measurements falls within the range of 66 - 70 dB for the overall noise level and 56 - 60 dB for night noise levels except for 2015 (66 - 70 dB). Figure 8 shows the results for overall noise measurements.

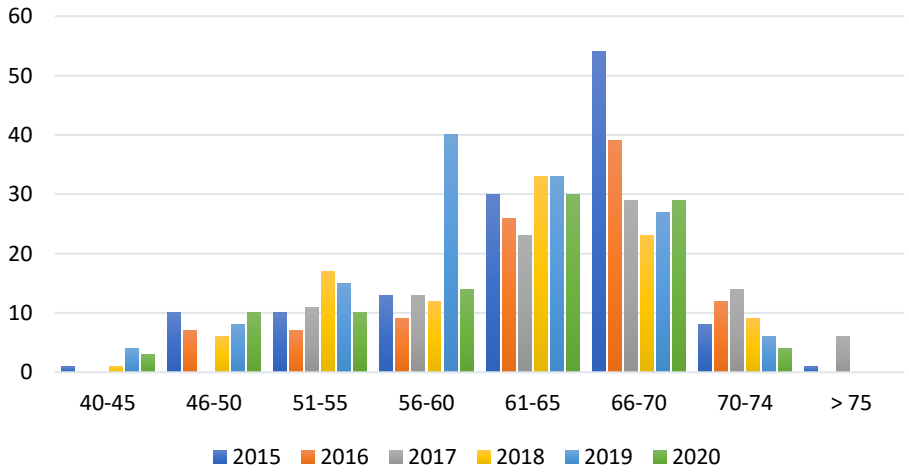

Fig. 8 Comparison of percentages of overall noise level measurement results for local self-governments, by ranges [3-10]

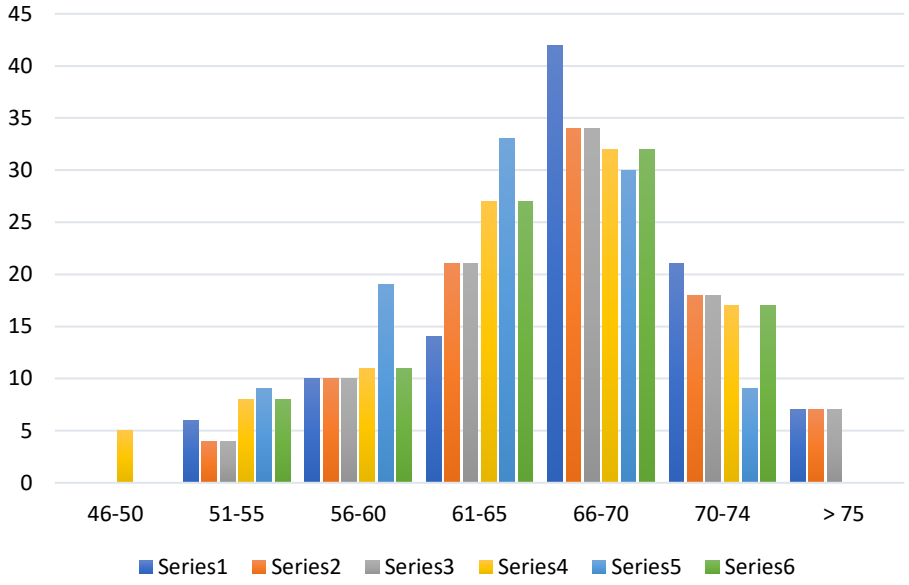

Fig. 9 Comparison of percentages of overall noise level measurement results for agglomerations, by ranges [3-10]

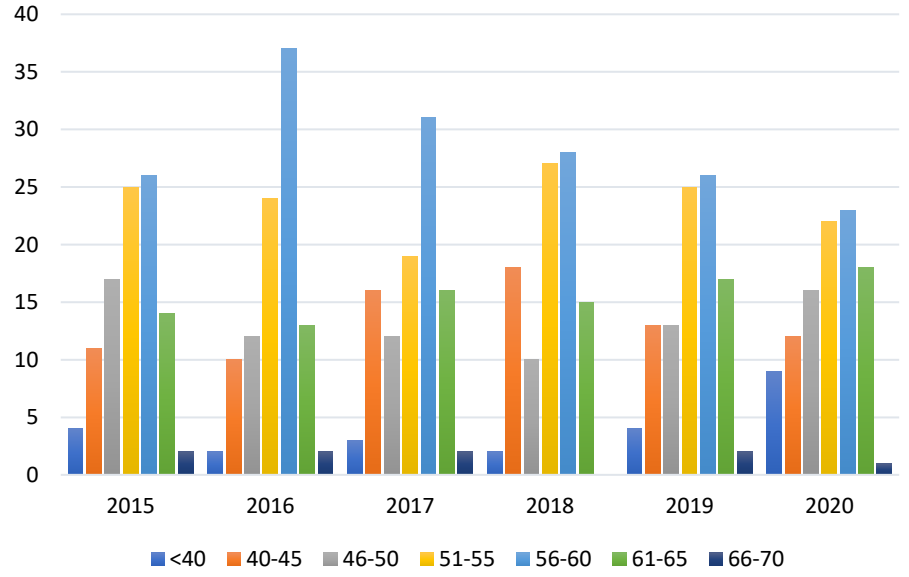

Fig. 10 Comparison of percentages of night noise level measurement results for local self-governments, by ranges [3-10]

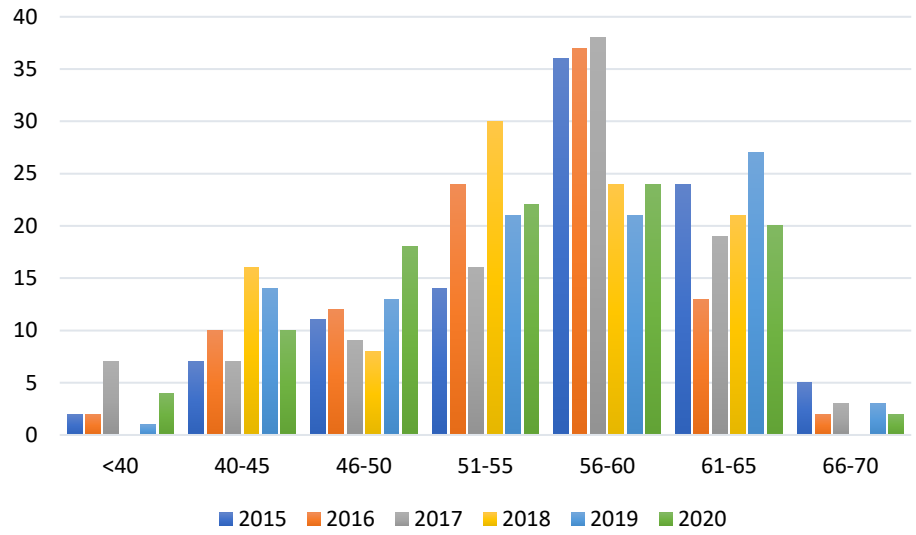

Fig. 11 Comparison of percentages of night noise level measurement results for agglomerations, by ranges [3-10]

From the graphs shown in Figs. 8 and 9, it is evident that the highest percentage of overall noise level values falls within the 66 - 70 dB range. The issue of exceeding limit values is more pronounced in agglomerations, where a significant percentage of results also fall within the 70 - 74 dB range, with some values exceeding 75 dB. The most severe issue was recorded in 2015, both for the overall noise indicator in local self-governments and agglomerations. The reports on the state of the environment for 2021 and 2022 indicate that the highest percentage of total noise indicators for local self-governments and agglomerations is within the 60 - 64 dB range, although the reports do not provide a detailed breakdown of noise level results by ranges.

Similarly, the graphs in Figs. 10 and 11 show that the highest percentage of night noise level indicator values falls within the 56 - 60 dB range, with this trend continuing in the 2021 and 2022 reports. Again, the issue of exceeding limit values is more pronounced in agglomerations, with a significant percentage of results falling within the 61 - 65 dB range, and some values even exceeding 70 dB.

3. Conclusion

The analysis of the state of the environment, particularly concerning noise level as an indicator of state, leads to a conclusion that a systematic approach to addressing noise control issues is needed. A prominent issue is the non-compliance with legal procedures in local self-government units, which lack sufficient financial resources to implement effective noise monitoring. In such cases, it is necessary to reevaluate the number of measurement points, as the analysis showed that the average number of measurements conducted is similar across local self-governments and agglomerations.

To ensure the accessibility of measurement results to the broader public, there is a need to continue presenting data in the same detailed manner as was done until 2020. Reports from 2021 and 2022 provide a more favorable view of the environmental situation but do so by offering only final conclusions without the specific data that would reveal the percentage of results in the 70 - 74 dB and over 75 dB ranges for overall noise indicators, as well as results in the 66 - 70 dB range for night noise indicators. Since noise level limits depend on the intended use of a specific space, it is crucial to include the locations of measurement points to realistically assess excessive noise levels in rest and recreation areas, hospital zones, rehabilitation centers, school zones, or residential areas.

Acknowledgement: *The presented research has been funded by the Ministry of Education, Science and Technological Development of the Republic of Serbia, Agreement on implementation and financing of scientific research work: 451-03-66/2024-03/ 200148.*

REFERENCES

1. Regulation on the National List of Environmental Indicators of the Republic of Serbia, Official Gazette of the Republic of Serbia, No. 37/2011.
2. Law on Environmental Noise Protection, Official Gazette of the Republic of Serbia, No. 96/2021.
3. Report on the State of the Environment in the Republic of Serbia for 2021, Ministry of Environmental Protection, Environmental Protection Agency, Belgrade, 2022.
4. Report on the State of the Environment in the Republic of Serbia for 2022, Ministry of Environmental Protection, Environmental Protection Agency, Belgrade, 2023.
5. Report on the State of the Environment in the Republic of Serbia for 2015, Ministry of Agriculture and Environmental Protection, Environmental Protection Agency, Belgrade, 2016.
6. Report on the State of the Environment in the Republic of Serbia for 2016, Ministry of Environmental Protection, Environmental Protection Agency, Belgrade, 2017.
7. Report on the State of the Environment in the Republic of Serbia for 2017, Ministry of Environmental Protection, Environmental Protection Agency, Belgrade, 2018.
8. Report on the State of the Environment in the Republic of Serbia for 2018, Ministry of Environmental Protection, Environmental Protection Agency, Belgrade, 2019.
9. Report on the State of the Environment in the Republic of Serbia for 2019, Ministry of Environmental Protection, Environmental Protection Agency, Belgrade, 2020.
10. Report on the State of the Environment in the Republic of Serbia for 2020, Ministry of Environmental Protection, Environmental Protection Agency, Belgrade, 2021.

FACTA UNIVERSITATIS
Series: **Working and Living Environmental Protection** Vol. 21, Nº 4, Special Issue, 2024, pp. 371 - 381
https://doi.org/10.22190/FUWLEP240819035M

Original scientific paper

ENVIRONMENTAL NOISE IN THE VICINITY OF THE BREWERY - A CASE STUDY

UDC 613.644:663.4

Darko Mihajlov, Momir Praščević, Petar Jovanović

University of Niš, Faculty of Occupational Safety, Niš, Serbia

ORCID iDs: Darko Mihajlov https://orcid.org/0000-0003-4528-170X
Momir Praščević https://orcid.org/0000-0002-7017-1038
Petar Jovanović https://orcid.org/0009-0007-1706-4456

Abstract. *Industrial plants can noticeably affect environmental noise pollution. In addition to the noise generated by industrial processes, vehicles used for transporting raw materials and finished products represent a significant noise source. As production capacity increases, particularly in the case of modern factories that evolved from traditional family manufactories, the problem becomes more pronounced within the existing infrastructure. This paper specifically analyzes environmental noise in the immediate vicinity of a brewery, located in the central part of one city in Serbia. Through analysis of noise monitoring results, certain machines and processes within the brewery that significantly impact environmental noise indicator values were identified. Accordingly, recommendations were provided for implementing appropriate measures within the brewery aimed at enhancing acoustic comfort in the surrounding environment near the brewery. Environmental noise measurements were repeated after the acoustic treatment of the dominant noise source in the brewery, after which the effect of the measures taken in terms of reducing the noise levels in the immediate vicinity of the source was examined.*

Key words: *industrial noise, environmental noise monitoring, environmental noise indicators, environmental noise limit values*

1. INTRODUCTION

Life in cities often takes place under conditions of compromised environmental quality, primarily characterized by polluted air and noise [1,2]. The consequence of living in noisy environments can be impaired health in multiple segments, considering the confirmed

Received August 19, 2024 / Accepted October 7, 2024
Corresponding author: Darko Mihajlov
University of Niš, Faculty of Occupational Safety, Čarnojevića 10A, 18000 Niš, Serbia
E-mail: darko.mihajlov@znrfak.ni.ac.rs

physiological and psychological impact of noise [3]. Noise may lead to sleep disturbance, annoyance, anxiety, hearing damage, and stress-related cardiovascular problems [4].

The primary source of noise in cities is certainly noise traffic [5]. However, due to poor urban planning, it sometimes happens that residential buildings are located in close proximity to industrial facilities (factories, heating plants, etc.), making industry the primary source of noise in such situations [6]. The overall noise levels in such environments are further exacerbated by the transport of raw materials and products, which involves the use of large trucks or trains.

European Noise Directive (END) [7] serves as the basis for noise management in the environment within EU member states. To describe environmental noise, in accordance with the END, noise indicators are used that are associated with its harmful effects on public health.

The assessment of environmental noise from individual sources or any combination of sources is performed based on the guidelines provided in the ISO 1996-1 standard [8]. In situations where specific noise is present, the primary metric used to describe the noise is the rating equivalent continuous sound pressure level, $L_{\mathrm{Req},T}$, in dB (hereinafter referred to as the rating noise level) [8]. The limit values for noise levels are set by the competent authorities based on knowledge of the impact of noise on human health [9]. These limits are influenced by the time of the day (day, evening, or night), the type of living space (open or closed space), the type of human activities carried out within the given space, the type of noise source, as well as the potential for new situations within existing circumstances. Procedures for verifying compliance with regulations can be based either on calculations from sound prediction models or on measurements.

Standard ISO 1996-2 [10] contains guidelines for determining sound pressure levels that are intended as a basis for assessing environmental noise. The standard can be applied to all types of environmental noise sources, such as road and rail traffic noise, aircraft noise and industrial noise.

Addressing the problem of noise in residential areas caused by nearby industrial facilities, without the presence of a buffer zone between areas with significantly different noise indicator limit values, often represents a serious engineering challenge. The generally accepted approach to solving this type of problem is based on taking measures primarily at the noise source itself (enclosing the source, replacing the existing source, or changing the operating mode of the source if possible), taking measures on the noise transmission paths from the source to the receiver (installing noise barriers), or taking measures at the receiver location itself (improving the acoustic characteristics of the façade and windows of the affected building) [11-15].

The paper presents the results of research on the impact of industrial noise from a brewery in Serbia on the surrounding environment. The reason for the research is the complaints from residents about the increasing noise from the brewery, which is a result of the continuous increase in production capacities, as well as the introduction of new products according to market demands, which requires the installation of new technologies and machines that further burden the environment with noise. The objectives of the research are: 1) to identify the noise sources in the brewery that affect the noise levels in the environment, 2) to examine the compliance of the existing noise levels with the environmental noise limit values, and 3) to verify the effectiveness of the technical measures taken to reduce noise in the brewery by examining the compliance of noise levels after the measures were implemented with the environmental noise limit values.

2. METHODOLOGY

2.1. Location and description of noise sources

The brewery is located in the central area of the city and borders a residential area on one side (Fig. 1).

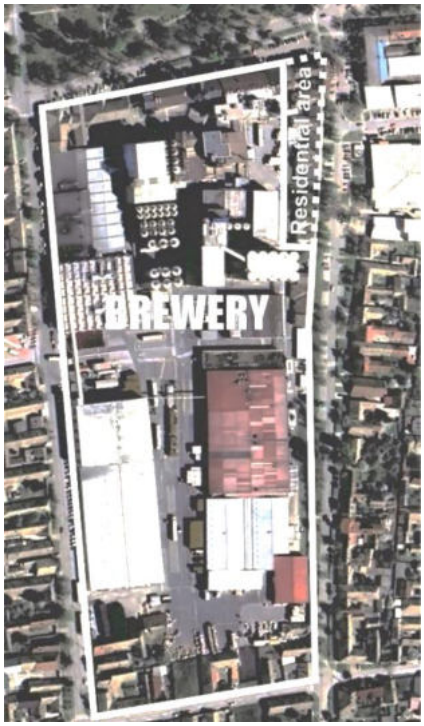

Fig. 1 Locations of the brewery and residential area in the immediate vicinity of the brewery (Source: Google Earth)

In the immediate vicinity of the residential buildings marked in Fig. 1, noise sources have been identified within the brewery that significantly impact the noise levels in the residential area (Tab. 1).

Table 1 Noise sources in the brewery that affect the environmental noise levels

No.	Brewery noise source
1.	Cogenerator
2.	Compressor station
3.	Old system for pneumatic malt transport
4.	New system for pneumatic malt transport
5.	Spent hops transport system
6.	Fermentation plant
7.	Tankers for corn grits unloading

The locations of the mentioned noise sources in the brewery (Tab. 1) are shown in Fig. 2.

Fig. 2 Locations of noise sources in the brewery (positions 1 ÷ 7); Locations of areas in the environment affected by noise from the brewery (A and B); Locations of measurement points MP1 ÷ MP4 (Source: Google Earth)

2.2. Noise measurement conditions

Noise measurements were conducted for two situations with characteristics described below. The reason for applying different noise measurement techniques in situations 1 and 2 lies in the fact that the measurement results in the first case (situation 1) showed exceedances of noise indicator limit values during the night period, but without the possibility of precise identification of the noise sources and processes causing it.

Situation 1:

- Normal daily execution of all work activities in the brewery (technological and transport) continuously for 24 hours, in operating modes of the plants (Tab. 1) dictated by the production process;
- No restriction on the operating time (stopping) of certain processes and plants in the brewery during noise-sensitive periods of the day;
- No measures taken to reduce the noise produced by the brewery's processes and plants in the environment;
- At measurement points MP1 and MP2 (Fig. 2), due to the mutual positioning of buildings, roads and the measurement points themselves, no audible noise sources unrelated to the brewery (road traffic and other communal activities) are registered;
- Simultaneous 24-hour continuous automated unattended noise measurement at two locations in the open space within the brewery (measurement points MP1 and MP2 – Fig. 2), in the immediate vicinity of the areas potentially affected by noise from the brewery (locations A and B in Fig. 2).

Situation 2:

- Scheduled execution of certain technological activities in the brewery over 24 hours, in operating modes dictated by the production process;
- No operation of the cogenerator during the reference night time interval, 22:00 ÷ 06:00 (Tab. 3);
- A sound barrier installed in front of the brewery's cogenerator;

- At measurement points MP3 and MP4 (Fig. 2), due to the mutual positioning of buildings, roads and the measurement points themselves, no audible noise sources unrelated to the brewery (road traffic and other communal activities) are registered;
- Series of short-term environmental noise measurements in the open space (measurement points MP3 and MP4 – Fig. 2), for different combinations of simultaneous operation of certain plants and processes listed in Tab. 1, during the reference time intervals.

Based on the defined operational times of individual noise sources and the specific technological production process in the brewery, possible operating modes of plant equipment (noise sources) during a four-hour brewing cycle for day and evening (Tab. 2) and for night (Tab. 3) have been defined for situation 2. Each mode includes four different combinations of active noise sources.

Table 2 Operating modes of noise sources in the brewery during one production cycle for day and evening

Mode	Combination of active sources	Mark of active noise sources (Tab. 1)						
		1	2	3	4	5	6	7
Normal day-evening mode	DE/C1	✓	✓				✓	
	DE/C2	✓	✓	✓			✓	
	DE/C3	✓	✓			✓	✓	
	DE/C4	✓	✓	✓		✓	✓	
Reserve day-evening mode	DE/C1	✓	✓				✓	
	DE/C2.1	✓	✓		✓		✓	
	DE/C3	✓	✓			✓	✓	
	DE/C4.1	✓	✓		✓	✓	✓	
Normal day-evening mode + Tankers for corn grits unloading	DE/C1	✓	✓				✓	
	DE/C2.2	✓	✓	✓			✓	✓
	DE/C3	✓	✓			✓	✓	
	DE/C4	✓	✓	✓		✓	✓	

Table 3 Operating modes of noise sources in the brewery during one production cycle for night

Mode	Combination of active sources	Mark of active noise sources (Tab. 1)						
		1	2	3	4	5	6	7
Normal night mode	N/C1		✓				✓	
	N/C2		✓	✓			✓	
	N/C3		✓			✓	✓	
	N/C4		✓	✓		✓	✓	
Reserve night mode	N/C1		✓				✓	
	N/C2.1		✓		✓		✓	
	N/C3		✓			✓	✓	
	N/C4.1		✓		✓	✓	✓	

The choice of short-term measurement strategy is motivated by the need to determine the noise levels generated in the environment during various operating modes of noise sources in the brewery and to identify the loudest events. This information is essential for implementing technical and organizational measures aimed at reducing environmental noise pollution from the brewery. The main difference between the day-evening modes and night modes (Tab. 2 and 3) is that the cogenerator is only used during the day and evening.

This operational schedule of the cogenerator results from decisions made by the brewery authorities after analyzing the measurement results for situation 1.

The normal mode and reserve mode (Tab. 2 and 3) differ in their use of different systems for pneumatic malt transport. In situations where there is an issue with the operation of the old system for pneumatic malt transport in the normal mode, typically due to pipe blockages, the brewery switches to the reserve mode and utilizes the new system for pneumatic malt transport. The new system is used until the old system is restored to normal functioning.

2.3. Noise measurements results

For noise measurements, Brüel&Kjær Hand-held Analyzer Type 2250D and Brüel&Kjær Hand-held Analyzer Type 2250-S-G4 were used. Utility Software for Hand-held Analyzers BZ 5503 was used for processing and managing the measurement results.

Situation 1:

Figure 3 shows the noise measurement results at measurement points MP1 and MP2 for situation 1, represented as 15-minute values of equivalent continuous sound pressure levels (hereinafter referred to as equivalent noise levels). The noise measurements included records of active noise sources, which are also depicted in Fig. 3.

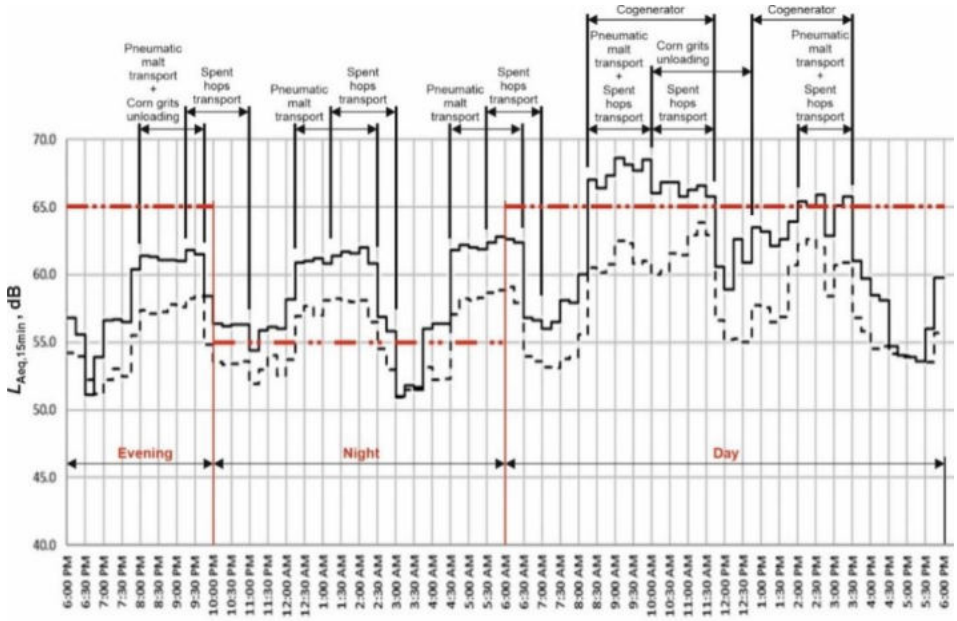

Fig. 3 15-minute values of equivalent noise levels, $L_{Aeq,15min.}$ in dB, at MP1 (solid line) and MP2 (dashed line), noise indicator limit values for day, evening and night (dash-dot line), along with records of the operation of different noise sources during measurements

The measurement results at measurement points MP1 and MP2 were considered as if these points belonged to the environment, because noise at the boundary of any zone must not exceed the noise indicator limit values for the zone it borders.

Situation 2:

The results of noise level measurements at measuring points MP3 and MP4 during the reference time intervals of day, evening and night are shown in Tab. 4.

Table 4 The average values of equivalent noise levels, $L_{Aeq,5min.}$ in dB, at MP3 and MP4 for different combinations of active noise sources in the brewery

Reference time interval	Combination of active noise sources (Tabs. 2 and 3)	$L_{Aeq,5min.}$	
		MP3	MP4
Day / Evening	DE/C1	55.1 dB	58.1 dB
	DE/C2	60.2 dB	60.7 dB
	DE/C2.1	58.2 dB	56.9 dB
	DE/C2.2	60.2 dB	60.7 dB
	DE/C3	58.7 dB	59.2 dB
	DE/C4	60.1 dB	60.2 dB
	DE/C4.1	60.1 dB	60.2 dB
Night	N/C1	49.8 dB	49.3 dB
	N/C2	50.9 dB	54.4 dB
	N/C2.1	53.6 dB	56.7 dB
	N/C3	57.8 dB	58.0 dB
	N/C4	58.6 dB	57.1 dB
	N/C4.1	59.2 dB	60.4 dB

The results represent the energy average values of equivalent noise levels, $L_{Aeq,5min.}$ in dB, obtained based on multiple noise measurements for one combination of active noise sources.

Considering that in the case of all combinations of active noise sources (Tabs. 2 and 3), it is steady noise (noise level changes over time less than 5 dB), a measurement time interval of 5 minutes was used.

2.4. Results of the rating noise levels calculation and noise rating

The purpose of environmental noise measurement is its rating. The rating of environmental noise at the positions of measuring points MP1 ÷ MP4 was performed by comparing the values of rating noise levels with the limit values of environmental noise indicators for the corresponding reference time intervals for the observed acoustic zone [9]. Measurement uncertainty is not taken into account during noise rating.

Situation 1:

According to the measurement technique, the values of rating noise level during the reference time intervals correspond to the rounded values for the day sound level ($L_{day,12h}$), evening sound level ($L_{evening,4h}$), and night sound level ($L_{night,8h}$), which are calculated as energy average values of 15-minute equivalent noise levels during specific reference time intervals (Fig. 3). The calculation results are given in Tabs. 5 and 6.

Table 5 Results of the calculation of rating noise levels and noise rating for MP1

Measurement point:	MP1		
Reference time interval, duration	Day	Evening	Night
T in h:	06:00 ÷ 18:00	18:00 ÷ 22:00	22:00 ÷ 06:00
	T_d = 12 h	T_e = 4 h	T_n = 8 h
Equivalent noise level:	$L_{day,12h}$ = 64.0 dB	$L_{evening,4h}$ = 59.3 dB	$L_{night,8h}$ = 59.5 dB
Rating noise level:	$L_{Req,12h}$ = 64 dB	$L_{Req,4h}$ = 59 dB	$L_{Req,8h}$ = 60 dB
Noise indicator limit value [9]:	65 dB	65 dB	55 dB
Exceeding the limit value:	-	-	5 dB
Noise rating:	Not exceed	Not exceed	Exceed

Table 6 Results of the calculation of rating noise levels and noise rating for MP2

Measurement point:	MP2		
Reference time interval, duration	Day	Evening	Night
T in h:	06:00 ÷ 18:00	18:00 ÷ 22:00	22:00 ÷ 06:00
	T = 12 h	T = 4 h	T = 8 h
Equivalent noise level:	$L_{day,12h}$ = 59.2 dB	$L_{evening,4h}$ = 55.8 dB	$L_{night,8h}$ = 56.0 dB
Rating noise level:	$L_{Req,12h}$ = 59 dB	$L_{Req,4h}$ = 56 dB	$L_{Req,8h}$ = 56 dB
Noise indicator limit value [9]:	65 dB	65 dB	55 dB
Exceeding the limit value:	-	-	1 dB
Noise rating:	Not exceed	Not exceed	Exceed

Situation 2:

The values of rating noise levels at the measurement points were calculated based on the duration of the noise of defined combinations of active noise sources (Tabs. 2 and 3) during the reference time intervals, and on the values of equivalent noise levels produced by the combinations of active specific noise sources at the measurement points during the reference time intervals.

As each cycle/mode consists of four combinations of active noise sources, the rating noise level for one cycle is determined based on the duration and measured values of the noise levels of individual combinations using the equation:

$$L_{\mathrm{Req},T} = 10\log\sum_{i=1}^{4}\frac{t_i}{T}10^{0.1L_{\mathrm{Aeq,5min},i}} \text{ dB}, \tag{1}$$

where: t_i – duration of the i-th combination of operating modes in minutes, $L_{\mathrm{Aeq,5min},i}$ – averaged noise level in dB for the i-th combination of operating modes (Tabs. 7 ÷ 10), and T – duration of the beer production technological cycle in minutes (T = 4 h = 240 min).

The results of the calculation of rating noise levels for each cycle/mode (Tabs. 2 and 3) at measurement points MP3 and MP4, as well as the noise rating, are presented in Tabs. 7 ÷ 10. During all measurements, the noise had a wide frequency range, was steady, and did not contain impulses. In the time intervals when the noise was tonal, a correction of 5 dB was added to the measured/averaged values. Tonal noise occurs during the operation of the new system for pneumatic malt transport as a result of adjusting transport parameters (speed and material flow through the pipeline), as well as the fact that the pipeline of the new system, unlike the old one, is not soundproofed.

Table 7 Rating noise levels and noise rating at MP3 for day and evening

Measurement point:	MP3							
Reference time interval:	Day / Evening							
Mode:	Reserve mode				Normal mode + Tankers for corn grits unloading			
Combination of active noise sources:	DE/ C1	DE/ C2.1	DE/ C3	DE/ C4.1	DE/ C1	DE/ C2.2	DE/ C3	DE/ C4.1
i:	1	2	3	4	1	2	3	4
Duration t_i, min:	60	90	60	30	60	90	60	30
Noise level $L_{Aeq,5min,i}$, dB:	55.1	58.2	58.7	60.1	55.1	60.2	58.7	60.1
Rating noise level $L_{Req,4h}$, dB:	58				59			
Noise indicator limit value [9], dB:	65				65			
Exceeding the limit value Δ, dB:	-				-			
Noise rating:	Not exceed				Not exceed			

Table 8 Rating noise levels and noise rating at MP4 for day and evening

Measurement point:	MP4							
Reference time interval:	Day / Evening							
Mode:	Reserve mode				Normal mode + Tankers for corn grits unloading			
Combination of active noise sources:	DE/ C1	DE/ C2.1	DE/ C3	DE/ C4.1	DE/ C1	DE/ C2.1	DE/ C3	DE/ C4.1
i:	1	2	3	4	1	2	3	4
Duration t_i, min:	60	90	60	30	60	90	60	30
Noise level $L_{Aeq,5min,i}$, dB:	58.1	61.9*	59.2	60.2	58.1	65.7*	59.2	60.2
Rating noise level $L_{Req,4h}$, dB:	60				63			
Noise indicator limit value [9], dB:	65				65			
Exceeding the limit value Δ, dB:	-				-			
Noise rating:	Not exceed				Not exceed			

* An additional correction of 5 dB due to the tonal noise.

Table 9 Rating noise levels and noise rating at MP3 for night

Measurement point:	MP3							
Reference time interval:	Night							
Mode:	Normal mode				Reserve mode			
Combination of active noise sources:	N/ C1	N/ C2	N/ C3	N/ C4	N/ C1	N/ C2.1	N/ C3	N/ C4.1
i:	1	2	3	4	1	2	3	4
Duration t_i, min:	60	90	60	30	60	90	60	30
Noise level $L_{Aeq,5min,i}$, dB:	49.8	50.9	57.8	58.6	49.8	53.6	57.8	59.2
Rating noise level $L_{Req,4h}$, dB:	55				56			
Noise indicator limit value [9], dB:	55				55			
Exceeding the limit value Δ, dB:	-				1			
Noise rating:	Not exceed				Exceed			

Table 10 Rating noise levels and noise rating at MP4 for night

Measurement point:	MP4							
Reference time interval:	Night							
Mode:	Normal mode				Reserve mode			
Combination of active noise sources:	N/ C1	N/ C2	N/ C3	N/ C4	N/ C1	N/ C2.1	N/ C3	N/ C4.1
i:	1	2	3	4	1	2	3	4
Duration t_i, min:	60	90	60	30	60	90	60	30
Noise level $L_{Aeq,5min,i}$, dB:	49.3	54.4	58.0	57.1	49.3	56.7	58.0	60.4
Rating noise level $L_{Req,4h}$, dB:	55				57			
Noise indicator limit value [9], dB:	55				55			
Exceeding the limit value Δ, dB:	-				2			
Noise rating:	Not exceed				Exceed			

3. CONCLUSION

The existence and operation of industrial plants in an urban environment potentially threaten the quality of the environment, with noise pollution in most cases representing a serious problem. Solving such problems requires a detailed analysis of the existing noise conditions, which involves identifying all noise sources (machines, plants, processes) that contribute to this state and assessing the contribution of each to the overall noise level. The contribution of individual noise sources to the tonal noise depends on the noise level generated by the source and the duration of the noise from each source. This approach enables noise control through recommendations on the duration of operation of individual sources, their use during noise-sensitive periods, and technical measures that may be taken to remediate the current situation.

In the case analyzed in the study, after the first noise measurement in the environment, in the immediate vicinity of the brewery, it was determined that operation of the cogenerator had the dominant influence on the noise level at both measurement points. Additionally, there were exceedances of the noise indicator limit values during the night. To reduce the noise originating from the brewery's noise sources in those locations, a sound-absorbing barrier was placed in front of the cogenerator, and the operation of the cogenerator was stopped during the night. Subsequent noise measurements at the same measurement points were repeated in a series of short-term measurements in all reference time intervals. Based on the noise measurement results and the calculation of rating noise levels, it was found that exceedances of the noise indicator limit values for the night occur during the technological process of beer production in reserve night mode. Since normal night mode and reserve night mode differ in the use of different systems for pneumatic malt transport, it was concluded that the use of the new system for pneumatic malt transport is the primary cause of the exceedance of the noise indicator limit values for the night. The use of the new system for pneumatic malt transport contributes to an increase in noise levels at the given measurement points during the day and evening, but there are no exceedances due to the higher limit values of the noise indicators for those reference time intervals.

The conducted research indicates the importance of the proper selection of machines and technological processes in terms of noise emission, as well as planning their location within the production conditions, especially in situations where industrial activity can threaten the quality of the environment.

Acknowledgement: *The authors acknowledge the support of the Ministry of Science, Technological Development and Innovation of the Republic of Serbia to its institution through the grant No. 451-03-66/2024-03/200148.*

REFERENCES

1. Peeters, I. B., & Nusselder, R. (2019). Overview of critical noise values in the European Region. *EPA Network Interest Group on Noise Abatement (IGNA): Vught, The Netherland*, 182.
2. Istrate, I. A., Oprea, T., Rada, E. C., & Torretta, V. (2014). Noise and air pollution from urban traffic. *WIT Transactions on Ecology and the Environment*, *191*, 1381-1389.
3. Smith, R. B., Fecht, D., Gulliver, J., Beevers, S. D., Dajnak, D., Blangiardo, M., ... & Toledano, M. B. (2017). Impact of London's road traffic air and noise pollution on birth weight: retrospective population-based cohort study. *bmj*, *359*.
4. World Health Organization. (2011). *Burden of disease from environmental noise: Quantification of healthy life years lost in Europe*. World Health Organization. Regional Office for Europe.
5. Grubesa, S., & Suhanek, M. (2020). Traffic noise. In *Noise and Environment*. IntechOpen.
6. Morillas, J. M. B., Gozalo, G. R., González, D. M., Moraga, P. A., & Vílchez-Gómez, R. (2018). Noise pollution and urban planning. *Current Pollution Reports*, *4*(3), 208-219.
7. European Commission. (2002). Directive 2002/49/EC of the European Parliament and of the Council of 25 June 2002 relating to the assessment and management of environmental noise. *Official Journal of the European Communities*, *189*, 12-25.
8. International Organization for Standardization. (2016). ISO 1996–1: 2016 Acoustics – Description, Measurement and Assessment of Environmental Noise – Part 1: Basic quantities and assessment procedures.
9. Law, RS. (2010). Regulation on noise indicators, limit values, methods for assessing noise indicators, disturbance and harmful effects of environmental noise. *Official Gazette of Republic of Serbia, No. 75/10* (in Serbian), 2010.
10. International Organization for Standardization. (2017). ISO 1996–2: 2017 Acoustics—Description, Measurement and Assessment of Environmental Noise – Part 2: Determination of Sound Pressure Levels.
11. González, A. E. (2022). Overview of noise control techniques and methods. In *Noise Control*. IntechOpen.
12. Fan, X., Li, L., Zhao, L., He, H., Zhang, D., Ren, Z., & Zhang, Y. (2020). Environmental noise pollution control of substation by passive vibration and acoustic reduction strategies. *Applied Acoustics*, *165*, 107305.
13. Casas, W. J. P., Cordeiro, E. P., Mello, T. C., & Zannin, P. H. T. (2014). Noise mapping as a tool for controlling industrial noise pollution.
14. Mihajlov, D., Praščević, M., Ličanin, M., & Gajicki, A. (2021). Acoustic Treatment Solution of the Technical Room in Water Pumping Station – Case Study. In *Acoustics and Vibration of Mechanical Structures—AVMS 2019: Proceedings of the 15th AVMS, Timisoara, Romania, May 30–31, 2019* (pp. 131-143). Springer International Publishing.
15. Ličanin, M., Mihajlov, D., Praščević, M., Đorđević, A., Raos, M., & Živković, N. (2021). Solution of the Environmental Noise Problem Generated by HVAC Systems – Case Study. In *Acoustics and Vibration of Mechanical Structures – AVMS 2019: Proceedings of the 15th AVMS, Timisoara, Romania, May 30–31, 2019* (pp. 145-154). Springer International Publishing.

FACTA UNIVERSITATIS
Series: **Working and Living Environmental Protection** Vol. 21, Nº 4, Special Issue, 2024, pp. 383 - 391
https://doi.org/10.22190/FUWLEP241003036B

Original scientific paper

NOISE LEVEL MEASUREMENTS OF ROAD TRAFFIC AT DIFFERENT HEIGHTS IN RELATION TO THE NOISE SOURCE

UDC 534.83.083:656.1.08

Danica Boljević, Aleksandar Milenković, Damir Savković

IMS Institute, Belgrade, Serbia

ORCID iDs: Danica Boljević https://orcid.org/0000-0002-8702-2434
Aleksandar Milenković https://orcid.org/0000-0002-2381-0095
Damir Savković N/A

Abstract. *The paper provides an analysis of the results of noise levels originating from road traffic measured at different heights on the example of an eighteen-story solitaire in the Dušanovac, which is located along the traffic road Bulevar Franše d'Eperea in Belgrade (the former section of the E-75 Belgrade-Niš highway). Measurements were made simultaneously at three measuring points, on the second, tenth and eighteenth (last floor) of the solitaire.*

Key words: *noise, road traffic, heights, levels.*

1. INTRODUCTION

The paper presents an experimental approach to noise level measurements at different heights in relation to road traffic as a source of noise. The measurements included a statistical analysis of the noise levels during the 24-hour measurement period for consecutive 15-minute intervals in the zone of one of the noisiest and busiest traffic roads through Belgrade - Franše d'Eperea Boulevard (former section of the E-75 Belgrade-Niš highway). For this experiment, the highest solitaire was chosen along the mentioned road, in the Dušanovac, and the goal was to confirm or deny the fact that the highest noise levels are obtained in the places closest to the road. Based on these measurements, a comparative analysis of the results was given, which showed that high levels are also obtained at high altitudes that are quite far from the road.

Received October 3, 2024 / Accepted October 10, 2024
Corresponding author: Danica Boljević
IMS Institute, Vojvode Mišića Boulevard 43, Belgrade, Serbia
E-mail: danica.boljevic@institutims.rs

2. DESCRIPTION OF THE MEASUREMENT PROCEDURE

A statistical analysis of the noise levels during the 24-hour measurement period, which originates from road traffic in the zone of the traffic road through Belgrade - Franše d'Eperea Bulevar, on which traffic takes place in two directions (towards the Mostar Interchange and towards Niš), was carried out in the outdoor environment at the measuring points MM1, MM2 and MM3 selected at different heights of the eighteen-floor high-rise building at the address 12 Ljermontova street in Belgrade.

The measuring points MM1, MM2, and MM3 are located on the terraces of the high-rise building on the second, tenth, and eighteenth floors [1], and a detailed description with the dimensions relevant to the measurements in question is given in the sketch in Fig. 1. Measuring point MM1 was chosen at a height of 6.4 m from the ground (second floor), measuring point MM2 at a height of 28.8 m from the ground (tenth floor) and measuring point MM3 at a height of 51.2 m from the ground (eighteenth floor), while their direct distances from the central axis of the road are 65.1 m, 71.8 m, and 84.2 m, respectively. The distance of the solitaire itself from the nearest edge of the road is about 51 m.

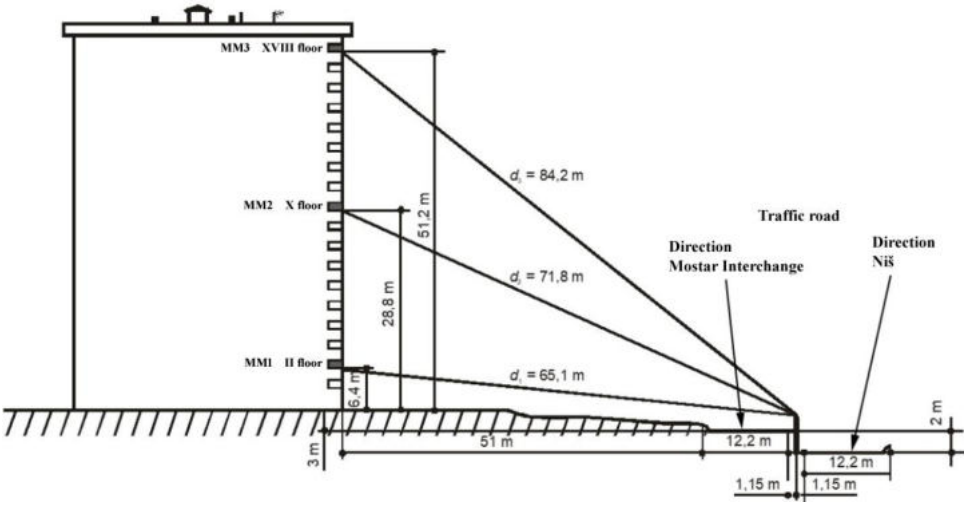

Fig. 1 Sketch of measuring points MM1, MM2, and MM3 and their position in relation to the noise source

3. MEASUREMENT RESULTS

Noise level measurements at selected measuring points MM1, MM2, and MM3 were performed according to accredited methods [2,3].

Measurements were made during two working days in a period of 24 hours. Statistical analysis was performed for successive 15-minute intervals with frequency weighting A and time weighting Fast, while the following noise levels were monitored: $L_{\mathrm{Aeq,15min}}$, $L_{\mathrm{AF5,15min}}$, $L_{\mathrm{AF10,15min}}$, $L_{\mathrm{AF50,15min}}$, $L_{\mathrm{AF90,15min}}$ and $L_{\mathrm{AF95,15min}}$.

All measurements were performed in automatic mode with sound level meters manufactured by Rion, Japan, models NL-18, NL-32, and NA-28, and the processing of the obtained results was done in the software SLC ver 2.1.

All measurements were taken with a windscreen. The windscreen did not affect the noise level measurement results.

Measurements were made during the daytime (day) and nightime (night) reference time intervals. The day includes the time period from 06.00 to 22.00, and the night from 22.00 to 06.00. The measurements were started on Wednesday, October 21, 2009, at around 11.30 am and ended on Thursday, October 22, 2009, at about the same time. In this way, the day is divided into two intervals: from the beginning of the measurement until 22.00 and from 06.00 of the next date until the end of the measurement period. The night has one interval: from 22.00 to 06.00 of the next starting date.

During the period in which the measurement was performed, there was a lot of traffic in the area of the measuring points in both directions of the traffic road - towards the Mostar Interchange and towards Niš, in two-day and one-night intervals lasting 1 hour (4×15 minutes). Vehicles are grouped as light (car, van, pickup), heavy (truck, small truck, and bus), and motorcycles, and the number of vehicles is presented in Tab. 1.

Table 1 The total number of vehicles in both directions that passed the traffic road on October 21, 2009, in front of the measuring points at the specified intervals

Vehicles type	Day interval 11:30-12:30			
	11:30-11:45	11:45-12:00	12:00-12:15	12:15-12:30
Light	1212	1069	1043	1234
Heavy	150	97	130	126
Motocycles	4	4	4	4
	Day interval 16:30-17:30			
	16:30-16:45	16:45-17:00	17:00-17:15	17:15-17:30
Light	1433	1260	1238	1425
Heavy	64	74	95	89
Motocycles	6	5	4	10
	Night interval 22:30-23:30			
	22:30-22:45	22:45-23:00	23:00-23:15	23:15-23:30
Light	585	607	497	466
Heavy	35	43	35	32
Motocycles	1	0	4	2
	Total in all intervals			
Light	12069			
Heavy	970			
Motocycles	48			

All the results of the statistical analysis are presented in diagrams and tables as follows. For each measuring point, the measurement diagram is presented in the corresponding figure (Fig. 2 for MM1, Fig. 3 for MM2, and Fig. 4 for MM3) showing the measured equivalent continuous sound pressure levels values $L_{\mathrm{Aeq,15min}}$ and statistical parameters $L_{\mathrm{AF5,15min}}$, $L_{\mathrm{AF10,15min}}$, $L_{\mathrm{AF50,15min}}$, $L_{\mathrm{AF90,15min}}$ and $L_{\mathrm{AF95,15min}}$ during the period of 24 h.

Under each diagram, there are three tables with a unique label for the measuring point (Tab. 2 for MM1, Tab. 3 for MM2, and Tab. 4 for MM3). For each measuring point individually, the tables on the left show the equivalent continuous sound pressure levels for the day or night during the 24-hour measurement period, total calculated values L_{day} and L_{night}, as well as the total number of measurements in the given measurement period. In the tables on the right below the same diagrams, the highest values of the parameters are shown $L_{AF5,15min(max)}$ and $L_{AF10,15min(max)}$, as well as the smallest values $L_{AF90,15min(min)}$ and $L_{AF95,15min(min)}$ during the same measurement period. The tables below show the rounded total calculated values from the left table for the day L_{day} and for the night L_{night}.

On the diagrams with the measurement results of statistical noise analysis, the day and night intervals are marked with circles. The calculation of the equivalent level was made for the exact belonging of the measurement interval to the day or night measurement period, so that the interval (less than 5 min) that started before 22.00 is fully included in the daytime, and the measurement interval started before 06.00 in the night.

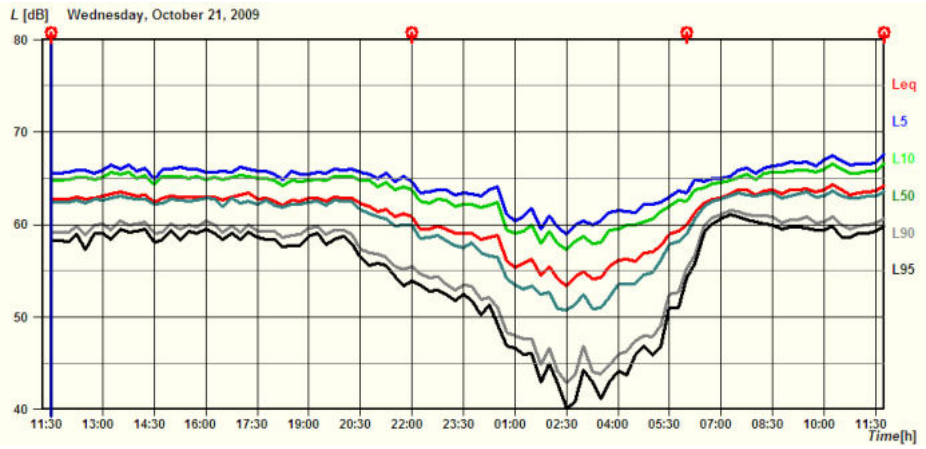

Fig. 2 Statistical noise levels analysis at the measurement point MM1

Table 2 Calculated values at the measuring point MM1 L_{day} and L_{night} and measured statistical levels $L_{AF5(max)}$, $L_{AF10(max)}$, $L_{AF90(min)}$ and $L_{AF95(min)}$

No.	Day L_{day}	Night L_{night}	Day No. rec.	Night No. rec.
	dB (A)			
1	62.7	57.6	42	32
2	63.3	–	23	–
Total	63.0	57.6	–	–

No.	Period	L_{5max}	L_{10max}	L_{90min}	L_{95min}
		dB (A)			
1	Day	66.4	65.6	55.1	53.3
2	Night	64.6	63.7	42.8	40.1
3	Day	67.6	66.6	55.2	54.2

L_{day} = 63 dB (A)
L_{night} = 58 dB (A)

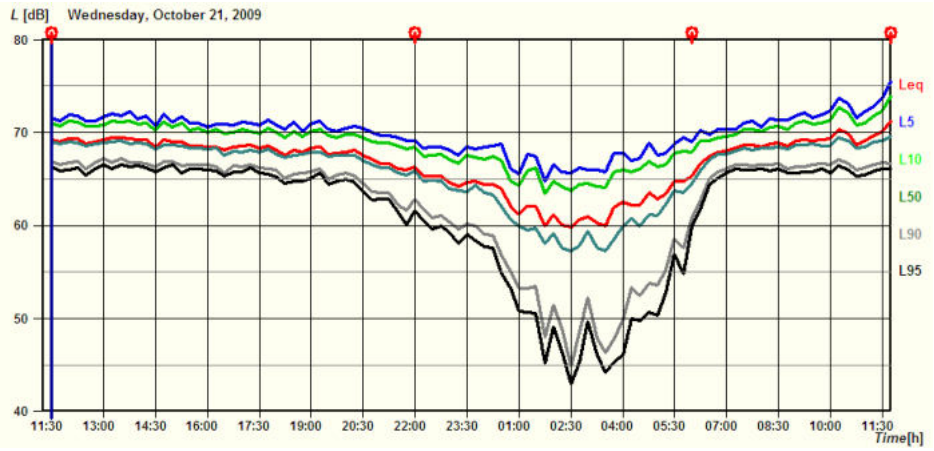

Fig. 3 Statistical noise levels analysis at the measurement point MM2

Table 3 Calculated values at the measuring point MM2 L_{day} and L_{night} and measured statistical levels $L_{AF5(max)}$, $L_{AF10(max)}$, $L_{AF90(min)}$ and $L_{AF95(min)}$

No.	Day L_{day} dB (A)	Night L_{night} dB (A)	Day No. rec.	Night No. rec.
1	68.4	63.3	42	32
2	68.9	–	23	–
Total	68.7	63.3	–	–

No.	Period	L_{5max} dB (A)	L_{10max}	L_{90min}	L_{95min}
1	Day	72.2	71.3	61.6	60.1
2	Night	69.4	68.4	44.8	42.9
3	Day	75.5	73.9	60.8	59.9

L_{day} = 69 dB (A)
L_{night} = 63 dB (A)

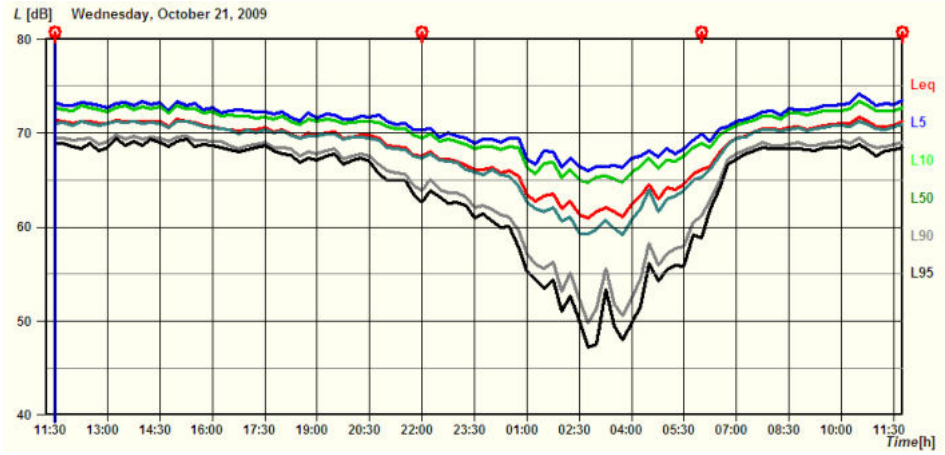

Fig. 4 Statistical noise levels analysis at the measurement point MM3

October levels $L_{AF5(max)}$, $L_{AF10(max)}$, $L_{AF90(min)}$ and $L_{AF95(min)}$

No.	Day L_{day}	Night L_{night}	Day No. rec.	Night No. rec.
	dB (A)			
1	70.4	64.8	42	32
2	70.3	–	23	–
Total	70.4	64.8	–	–

No.	Period	L_{5max}	L_{10max}	L_{90min}	L_{95min}
		dB (A)			
1	Day	73.4	72.9	63.9	62.6
2	Night	70.5	69.9	49.8	47.2
3	Day	74.2	73.4	61.2	58.8

L_{day} = 70 dB (A)
L_{night} = 65 dB (A)

3.1. Comparative analysis of noise levels by measurement points

In Fig. 5, a comparative diagram of measured values $L_{Aeq,15min}$ at different heights at measuring points MM1, MM2, and MM3 during a period of 24 h is presented, while in Tab. 5 a comparative table of total calculated values at the same measuring points and for the same time period was presented.

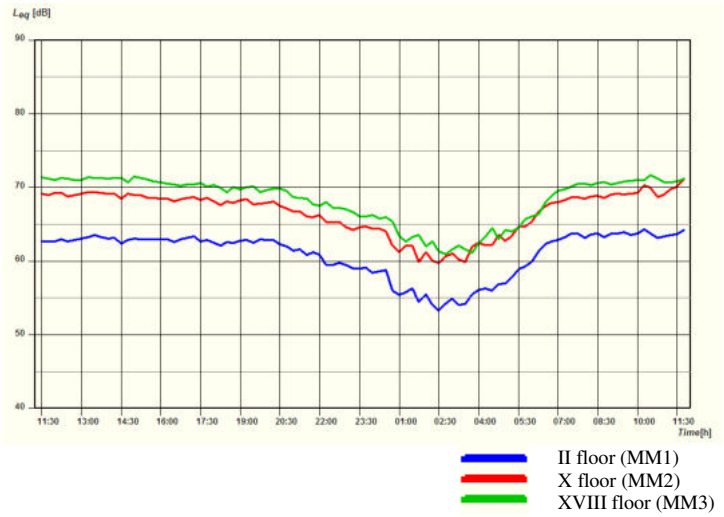

Fig. 5 Diagram of the comparative analysis of the noise level at different heights by measurement points MM1, MM2 and MM3

Table 5 Comparative results of calculated values L_{day} and L_{night} by measuring points

Measuring point mark	Measuring point height (m)	L_{day} (dB (A))	L_{night} (dB (A))
MM1	6.4	63	58
MM2	28.8	69	63
MM3	51.2	70	65
The total number of counted vehicles of all categories		10780	2307

4. The Obtained Results Comment

As for the purposes of this experiment, the measuring points were carefully selected so that they were evenly spaced from each other every 22.4 m in height and the same vertical plane and axis in relation to the noise source, that is, the traffic road in question, and that the measurements on them were carried out at the same time, there are provided the same conditions for the noise source at all measurement points and the results are completely comparable.

From the comparison diagram of the equivalent continuous sound pressure levels $L_{Aeq,15min}$ measured at different heights (MM1, MM2 and MM3) given in Fig. 5 as well as from the table of calculated values for the day L_{day} and night L_{night} given in Tab. 5, it can be seen that the level of noise originating from road traffic on the observed section of the traffic road increases with the increase in height.

Also, it is noticeable that a greater noise level jump with the increase in height was recorded on the lower floors, namely 3 dB (A) during the day and 5 dB (A) during the night between the second and tenth floors, while on the higher floors a noise levels jump of 1 dB (A) for the day and 2 dB (A) for the night between the tenth and eighteenth floor.

The reason why the level of noise originating from road traffic in this case and on this terrain of the selected section increases with the increase in height can be found in the topographic influence of the terrain itself, but also in the direction of the propagation of the acoustic energy radiation of vehicles. Although the emission of acoustic energy from vehicles depends on several superimposed sources, the dominant influence is caused by motor sources that arise during the mechanical excitation of the engine itself as well as the combustion process, and the radiation of which spreads upward in most vehicles, due to the position of the engine itself.

The reason why the increase in road traffic noise level is higher at lower heights can be found in models and analyzes where such a source is considered as point or linear, as is the case with the calculation model shown in Fig. 6 [4], where it can be seen that the sound decreases slowly with increasing height at lower distances from the source, and then due to the square of the distance it already loses a lot of sound power at higher/longer distances from the source.

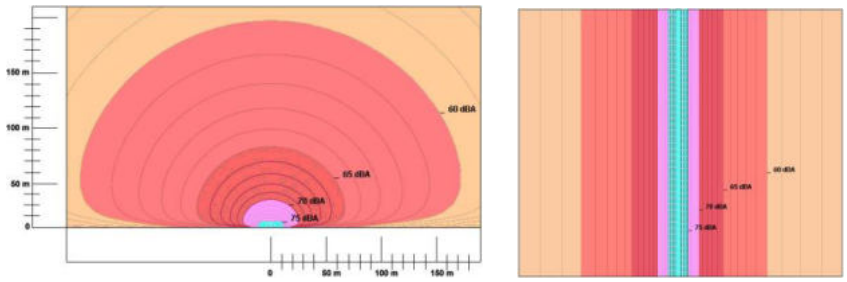

a) point source noise model b) line noise source model

Fig. 6 A model of the distribution of noise levels originating from road traffic for height h = 3 m according to [4]

5. CONCLUSION

Based on the presented measurement results, it is concluded that the direction of propagation of sound energy of road traffic is more dominant towards higher heights, that is, floors.

Also, due to the slow decrease of the noise level with close distance from the sound source (up to about 50 m, which is the height of the eighteenth floor in our case), that is, the road where there is heavy traffic, the constant level of which is about 75 dB according to existing research and models (for $h = 3$ m), the proposal is to find a solution for noise protection on higher floors in solitaires located next to the big traffic roads through further research.

During that, it should be borne in mind that the construction of common sound barriers (4 to 5) m high, and even broken (5 to 7) m high, would not be of importance, because the protection of the higher floors would require a much higher construction (at least 20 m of height) which is impractical for static reasons.

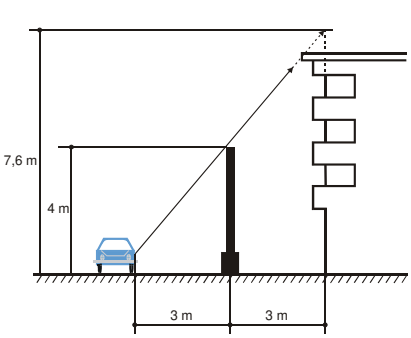

a) An example of a common sound barrier

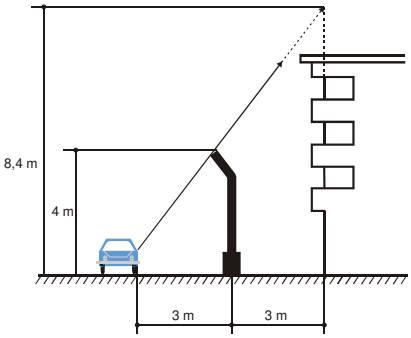

b) An example of a broken sound barrier

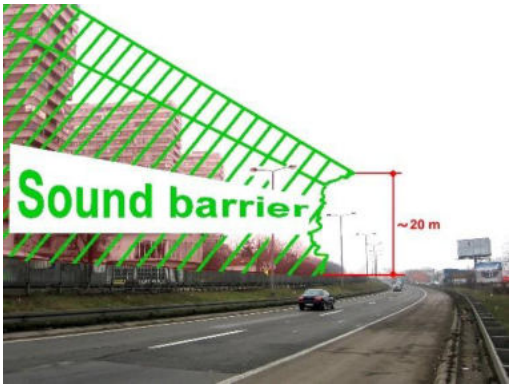

c) An example of a high sound barrier to protect higher floors

Fig. 7 Sketches of some examples of sound barriers

In the picture Fig. 7 illustratively, under a) and b) are presented barrier constructions that contribute to noise protection only on the lower floors, while under c) the possible

appearance and height of the sound barrier so that the higher floors are also protected from noise is presented.

An eventual possible solution for protecting the higher floors from noise coming directly from the busy traffic road would be the construction of a tunnel, which increases the protection of the target objects, but then it should be borne in mind that in that case the acoustic energy would be amplified at the exit opening of the tunnel, which would certainly require carefully selected position of the same.

Acknowledgement: *The work was created during the duration of the contract between the IMS Institute and the Ministry of Science, Technological Development and Innovation (registration number of the contract: IMS No. 30-1331d 08.02.2024). The paper uses experimental noise level measurements of the Laboratory for Acoustics and Vibrations of the IMS Institute in Belgrade during October 2009.*

REFERENCES

1. Test Report No. LAV 4709/09, IMS Institute, Laboratory for Acoustics and Vibrations, 2009.
2. SRPS ISO 1996-1: 2010 Acoustics — Description, measurement and assessment of environmental noise – Part 1: Basic quantities and assessment procedures
3. SRPS ISO 1996-1: 2010 Akustika – Acoustics — Description, measurement and assessment of environmental noise – Part 2: Determination of sound pressure levels
4. DIRECTIVE 2002/49/EC OF THE EУROPEAN PARLIAMENT AND OF THE COУNCIL of 25 June 2002 relating to the assessment and management of environmental noise, *Official Journal of the European Communities L* 189, 2002

FACTA UNIVERSITATIS
Series: **Working and Living Environmental Protection** Vol. 21, N° 4, Special Issue, 2024, pp. 393 - 399
https://doi.org/10.22190/FUWLEP240906037M

Original scientific paper

PROPOSAL OF THE RULE FOR RATING LEVELS OF INDUSTRIAL IMPULSIVE NOISE REGARDING THE RISK OF HEARING DAMAGE

UDC 613.644:616.21/.23

Jovan Miočinović

TEHPRO d.o.o., Belgrade, Serbia

ORCID iD: Jovan Miočinović N/A

Abstract. *Since the release of the core standards for determining occupational noise exposure, ISO 1999:2013 and ISO 9612:2009, adjustments for noise types that were previously thought to have additional damaging effects of noise uneven in the time and frequency domain have been left out when rating noise levels in the workplace. Recent literature as well as models of the effect of noise on hearing indicate a particularly damaging effect of impulsive noise. At the same time, the regulation requires consideration of the type of noise, including any exposure to impulsive noise. This paper proposes a rule for rating that would reduce the risk of hearing damage arising from disregarding the impulsive nature of noise.*

Key words: *industrial noise, impulsive noise, rating levels*

1. INTRODUCTION

In order for an effect to be well-founded, it is necessary to have proven empirical evidence, and a corresponding theoretical explanation — specifically, when considering the effect of a physical agent on a human, the connection of the physical phenomenon that causes it with the biological response — the effect on the organism.

1.1. Empirical evidence of the additional effect of occupational impulse noise on hearing

A number of studies on the effect of industrial impulsive noise on hearing carried out from the seventies to the 2020s show that exposure to impulsive noise among workers cause significant hearing loss compared to exposure to steady noise [1,2,3]. Studies carried out in several countries (US, Canada, Russia, Norway, Finland, Sweden) have shown that

Received September 6, 2024 / Accepted October 16, 2024
Corresponding author: Jovan Miočinović
TEHPRO d.o.o., Lole Ribara 120, 11250 Belgrade, Serbia
E-mail: jovan.miocinovic@tehpro.rs

most of the hearing loss was in the higher frequencies (3–8 kHz). The hearing loss at 4 kHz was approximately 5–10 dB for those under 30 and 35–40 dB for those between 50 and 60 years of age.

1.2. Two theories of mechanism of impact on hearing

Brüel (1976) explained how impulse noise can cause more damage than the amount of energy calculated would indicate, compared to continuous noise [4]. The averaging time of the brain is about 35 ms, and therefore these impulses are more intensive than they appear to be based on loudness, that is short impulses sound less loud than longer ones of the same intensity. The increased risk to hearing arises because, first of all, these impulses are transmitted with full force to the inner ear (the averaging times of the outer and middle ears being 50 and 35 ms, respectively). Short impulses with relatively high energy content around 4 kHz are almost always amplified by resonance in the outer and middle ear so that these impulses reach the inner ear with an amplitude of 10–12 dB higher than other types of noise. Given this amplification, certain loud sounds may damage the nerve ends of the inner ear producing permanent hearing loss, even though a sound level meter with a fast time constant would indicate that their level is lower than the danger level.

Clifford and Rogers (2009) provided a new explanation of the mechanism by which impulse noise may be more damaging than continuous sound [5]. As sound energy to the cell increases, the mechanism of cochlear damage shifts from biochemical injury to mechanical injury. Outer hair cells appear to be more sensitive than inner hair cells to impulse noise because of their energy requirements, which lead to increased production of reactive oxygen and nitrogen species and self-destruction by apoptosis.

From Brüel's theory, as an indicator of impulsivity a quantity with the same name as the phenomenon arises, impulsive noise. Impulsive noise is measured with sound level meter using exponential RMS integration for impulse exponential time constant, $\tau = 35$ ms, that is AI-weighted equivalent continuous sound pressure level, L_{pAIeq} comparing to linear RMS integration for fast time constant, $\tau = 125$ ms that is used for measuring A-weighted equivalent continuous sound pressure level, L_{pAeq}, that is time-weighting I specified in the well-known sound level meter's International Standard IEC 61672-1 (at least in previous updates as will be noted later).

As for Clifford and Rogers' theory statistical measurements such as kurtosis hold promise for the quantitative prediction of hearing loss. A basic form for noise metrics is designed by combining the equivalent sound pressure level and a temporal correction term defined as a function of kurtosis of the noise. Kurtosis is defined as the fourth standardized moment about the mean of the data, Eq. (1):

$$\frac{E\left(x-m\right)^4}{s^4}, \tag{1}$$

where s is the standard deviation of x, $E(x-m)$ represents the expected value of quantity, m is the mean of x. Kurtosis describes the peakedness of a distribution, which is independent of the overall level and was suggested as a metric of impulsiveness by Erdreich [6].

1.3. Study of the relation between the indicators of impulsiveness

In addition to the listed indicators of impulsivity supported by these two theories, many others appear in the literature, standards and national regulations: the highest peak in the series of successive peaks — peak level, A duration — a duration of the first overpressure, B duration — the duration from the highest peak level to a point of time when the envelope of pressure fluctuation stays within 20 dB of the peak pressure level, crest factor — the difference between peak and RMS level of the noise, C-weighted peak sound pressure level, number of impulses that overpass the given peak pressure during the working day [7,3]. In a recent study [8], the relationship of a number of these indicators (impulsive adjustment K_{I}, C-weighted peak sound pressure level $L_{\mathrm{p,Cpeak}}$, and crest factor) to kurtosis as a promising candidate for predicting the damaging effect of impulsivity was examined. Here impulsive adjustment for the impulsive noise is determined as the difference between the AI-weighted equivalent continuous sound pressure level L_{pAIeq} and A-weighted equivalent continuous sound pressure level L_{pAeq}, Eq. (2):

$$K_{\mathrm{I}} = L_{\mathrm{pAIeq}} - L_{\mathrm{pAeq}} \tag{2}$$

Since kurtosis was identified as a promising factor in an indicator based on a new model that is still being tested on animals (chinchillas) [9] and on certain groups of shipbuilding workers in China [10] in new approaches to the problem of the impact of impulsive noise on humans, the original idea was to find from the existing ones the indicators that correlate with kurtosis the best. It was shown on a sample of 140 various noise exposures measured in situ in the industry where impulsive noise occurs that Brüel's adjustment for impulsivity K_{I} strongly correlates with kurtosis at the significance level of 0.01, while other examined indicators of impulsivity do not correlate significantly. The correlation at the stated significance level means that there is a 99 % probability that measurands K_{I} and kurtosis are correlated, and therefore may be stated that they do measure the same quality, in contrast to others that are not significantly correlated to kurtosis and therefore it is very probable that they do not measure same quality.

As it appears, two theories give two measurements that equally well (or at least very similarly) predict the effect of impulsivity. A similar duality in prediction is also found in the evaluation of vibrations containing occasional shocks on humans. It turns out that the effect of that kind of vibration can be viewed in two different ways: by evaluating *MTVV* calculated by exponential RMS integration, similar to Brüel's impulsiveness for impulsive noise, and the fourth degree of vibration dose (*VDV*) [11], i.e. the sixth degree of vibration dose (ISO 2631-5 method [12]) which as statistical measures of vibration distribution in the time domain would correspond to kurtosis. Since noise and vibrations are physically the same (oscillations of the physical environment), they manifest themselves as one or the other depending on the environment (gas, liquid, solid body), and the biological individual on which they act is the same — a human being, one would expect a similar duality of theoretical explanation to be demonstrated for the case of impact of impulsive noise on humans.

1.4. Inconsistencies in existing regulations and available evaluation methods

The national Regulation [13] based on Directive 2003/10/EC of the European Parliament and of the Council [14] in Article 10 mandates the evaluation of noise, including the evaluation of different noises in the time (especially impulsive) and frequency domain (eg tonal noise). The mandatory method for the determination of occupational noise exposure

is the ISO 9612 method [15]. From this standard, since its 2009 update, the method of determination of rating level for the type of noise, which was previously provided in Annex C [16], has been removed. In the current ISO 9612 update is stated that this International Standard deals with A-weighted levels but is applicable also to C-weighted levels. As seen before, C-weighted peak sound pressure level is not a good predictor of the effect of impulsive noise on hearing, at least in the industry where impulsive noise appears (exposures to blasts are excluded). Exposures determined by the ISO 9612 method are to be compared to the limits set on the basis of the estimation of noise-induced hearing impairment that is given in ISO 1999 [17]. The current update states that the prediction method presented is based primarily on data collected with essentially broadband, steady, non-tonal noise. In the previous update, [18] further stated that users may wish to consider tonal noise and/or impulsive/impact noise as being about as harmful as a steady non-tonal noise that is approximately 5 dB higher in level due to the fact that the application of the database to tonal or impulsive/impact noise represents the best available extrapolation.

The campaign to remove the correction for noise types dates back to the 1980s and continues to the present day. By the update of IEC 61672-1:2013 [19] the technical specifications of time-weighting I have been removed. Finally, it was removed from ISO 7779 by the update ISO 7779:2018 [20].

Some explanations that, if any, are given for this would be that there are no confirmed effects of impulsivity that would further affect the human beyond the equivalent noise level (not true, there are and they are proven), the absence of an adequate theoretical model that would describe the eventual mechanism of additional effect of impulsivity (not true, there are at least two as shown before) and that there is simply no good argument for choosing the right one out of the multitude of impulsivity indicators. As for the last of these arguments recent research points to kurtosis, and there is also well-established Brüel's impulsivity as demonstrated in the correlation study mentioned before that equally well or very similarly predicts the effect.

2. Proposal of the Rule for Rating

For task-based measurement for the task where impulse noise occurs rating level is calculated according to Eq. (3):

$$L_{\mathrm{r}} = L_{\mathrm{pAeq}} + K, \tag{3}$$

where K is adjusted according to 2.1. or 2.2. depending on the choice.

Daily noise exposure level is calculated from the L_{pAeq}-s (where impulse noise doesn't occur) and from L_{r}-s (where impulse noise occurs) for each task and the duration of each of the tasks according to Clause 9 of ISO 9612.

For job-based measurement from the jobs identified, for each homogeneous noise exposure group and each sample taken among the members of the group for the sample where impulse noise occurs rating level is calculated according to Eq. (3).

Daily noise exposure levels for workers in a homogenous exposure group are calculated from the L_{pAeq}-s (where impulse noise doesn't occur) and from L_{r}-s (where impulse noise occurs) for each sample according to Clause 10 of ISO 9612.

For full-day measurement for each full-day measurement where impulse noise occurs rating level is calculated according to Eq. (3).

Daily noise exposure level is calculated from the L_{pAeq}-s (where impulse noise doesn't occur) and from L_r-s (where impulse noise occurs) according to Clause 10 of ISO 9612.

2.1. Rule based on impulsive adjustment K_I only

$$\begin{aligned} K &= 0 \text{ dB} \quad \text{if} \quad L_{pAIeq} - L_{pAeq} < 2 \text{ dB} \\ K &= L_{pAIeq} - L_{pAeq} \quad \text{if} \quad 2 \text{ dB} \le L_{pAIeq} - L_{pAeq} < 5 \text{ dB} \\ K &= 5 \text{ dB} \quad \text{if} \quad L_{pAIeq} - L_{pAeq} \ge 5 \text{ dB} \end{aligned} \tag{4}$$

In Eq. (1) rule based on impulsive adjustment K_I only is given. As may be seen it's practically the same rule given by the former update of ISO 9612 [16]. The advantages of choosing this rule would be well-established metrics of objective test method theoretically and empirically confirmed. Flaws may be seen when comparing K_I to kurtosis for different industrial impulsive noises [8]. Fig. 1 shows the correlation of K_I and kurtosis classified into distinctive zones according to impulsivity significance. Here K_I and kurtosis are to be considered significant when greater than 3 dB.

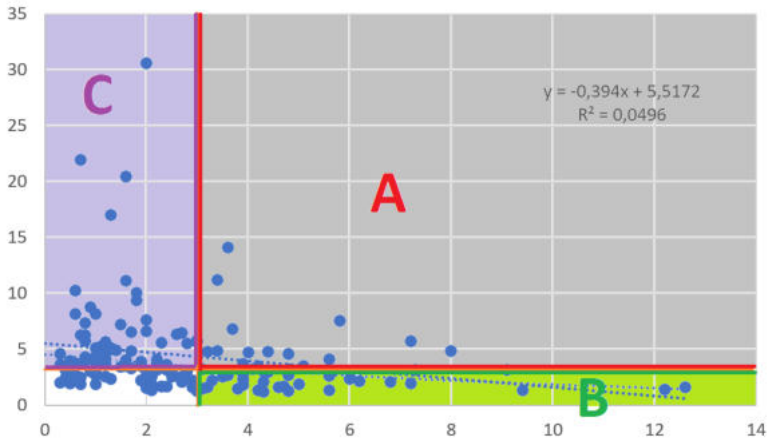

Fig. 1 Correlation plot for K_I and kurtosis classified into zones according to impulsivity significance [8]

Here in zone A are noises that have both impulsivity adjustments greater than 3 dB, in zone B noises whose K_I level is greater than 3 dB and kurtosis not, and in zone C noises whose kurtosis is greater than 3 dB but K_I not. Considering kurtosis as a promising basis for new metrics for noise impulsivity as recent research shows [5,9,10] by choosing this rating noises with high kurtosis and low K_I would be missed (e.g. some noises in in metal working industry, quasi-impulsive noises [8]).

2.2. Rule based on both impulsive adjustment K_I and kurtosis

$$K = \begin{cases} 0\,\text{dB} & \text{if} \quad L_{\text{pAIeq}} - L_{\text{pAeq}} < 2\,\text{dB}, \text{ and } kurtosis < 2\,\text{dB} \\ \dfrac{\left(L_{\text{pAIeq}} - L_{\text{pAeq}}\right) + kurtosis}{2} & \text{if} \quad 2\,\text{dB} \le \dfrac{\left(L_{\text{pAIeq}} - L_{\text{pAeq}}\right) + kurtosis}{2} < 5\,\text{dB} \\ 5\,\text{dB} & \text{if} \quad \dfrac{\left(L_{\text{pAIeq}} - L_{\text{pAeq}}\right) + kurtosis}{2} \ge 5\,\text{dB} \end{cases} \tag{5}$$

In Eq. (5) rule based on both impulsive adjustment K_I and kurtosis is given. This rule is balanced, on the one hand, there is metrologically well-based K_I, on the other kurtosis has a role in balancing for situations mentioned in 2.1. as flaws of choice of that rule. Adding kurtosis is problematic in the sense that the exact metric of the model based on it has not yet been developed (or at least published), namely theoretically it is evident that a true indicator of the damaging effect of temporally uneven noise (and impulsive) is some function of kurtosis, but for now, in the available literature, the authors have not come up with an exact formulation. On the other hand, the measured similarities in value and in the very order of values of impulsivity K_I and kurtosis would justify such averaging because this would increase the effect of impulsivity for statistically more uneven noise i.e. higher values of kurtosis (which effect is the basis of the theoretical explanation of the new model) and reduce it for impulsive noise statistically less uneven in time i.e. lower values of kurtosis (which is again in line with the new theoretical model). Therefore, the choice of this rating rule will ensure that some cases of harmful impulsivity are not omitted from consideration.

2.3. On the limits of adjustment

This rating is adapted to the national regulation. Namely, according to the Regulation [13], there are two action values and the limit value (80, 83 and 85 dB). The adjustment 2 to 5 dB stands for if the measured noise level is between two limits, say 80 and 83 dB, the adjustment of 2 dB would shift the level above the next limit for some values of the measured exposure. An adjustment greater than 5 dB is not required, because exposure to noise above 83 dB requires personal protective equipment by the Regulation. For regulations in other countries, e.g. taken from the Directive [14] (80 and 85 dB), it would make sense to take other limits of adjustment for the range of impulsivity, e.g. 3 and 6 dB. Here, values above 5 dB would make sense if the noise level is close to 80 dB, in which case a correction of 5 dB could leave the corrected value below 85 dB (the level that requires personal protective equipment by the Directive) and leave the worker unprotected.

3. CONCLUSION

Numerous studies on the effect of industrial impulsive noise on hearing conducted worldwide demonstrate that exposure to impulsive noise among workers causes significant hearing loss compared to steady noise exposure, due to the need for a proper assessment of the occupational risk of hearing damage on the one hand and the requirements of regulations on the other. Therefore, a rule for rating levels of industrial impulsive noise was proposed based on selected indicators of impulsivity. Of the multitude of indicators of

impulsivity present in the literature, primacy is given here to the impulsive adjustment which has been present in the literature since the 1970s and whose measurement represents an objective method of examination and kurtosis, the statistical measure, which is a promising candidate supported by recent theoretical research and experimental studies, and arguments for this choice are given.

REFERENCES

1. A. Lie et al. “Occupational noise exposure and hearing: a systematic review”, Int Arch Occup Environ Health 89:351-372, 2016.
2. Starck J, Toppila E, Pyykko I. “Impulse noise and risk criteria”, Noise Health 5:63-73, 2003.
3. Miočinović, J. and Beljić Durković, B. “Industrial impulsive noise and hearing: evaluation according to the regulations and applicable standards and possible additional risk on hearing comparing to the effect of steady noise”, 26th International Conference Noise and Vibration, Niš, 2018.
4. P.V. Brüel, "Do We Measure Damaging Noise Correctly?", B&K Technical Review, no. 1, pp. 3-32, 1976
5. R.E. Clifford and R.A.Rogers “Impulse noise: theoretical solutions to the quandary of cochlear protection”, Ann Otol Rhinol Laryngol 118(6):417–427, 2009.
6. J. Erdreich “Distribution based definition of impulse noise,” J. Acoust. Soc. Am. 77, S19–S19, 1985.
7. C. G. Rice and A. M. Martin “Impulse Noise Damage Risk Criteria”, Journal of Sound and Vibration 28(3), 359-367, 1973.
8. Miočinović, J. and Beljić Durković, B. “Industrial impulsive noise, practical study: from comparing the existing criteria to forming the novel evaluation model”, 27th International Conference Noise and Vibration, Niš, 2022.
9. R. P. Hamernik, W. Qiu and B. Davis “The effects of the amplitude distribution of equal energy exposures on noise-induced hearing loss: The kurtosis metric”, J. Acoust. Soc. Am. 114, 386–395, 2003.
10. Davis RI, Qiu W, Heyer NJ, Zhao Y, Qiuling Yang M S, Li N, Tao L, Zhu L, Zeng L, Yao D. “The use of the kurtosis metric in the evaluation of occupational hearing loss in workers in China: Implications for hearing risk assessment”, Noise Health 2012;14:330-42.
11. ISO 2631-1:1997+A1:2010, SRPS ISO 2631-1:2014 Mechanical vibration and shock — Evaluation of human exposure to whole-body vibration — Part 1: General requirements.
12. ISO 2631-5:2018 Mechanical vibration and shock — Evaluation of human exposure to whole-body vibration – Part 5: Method for evaluation of vibration containing multiple shocks.
13. Regulation on preventive measures for health and safety at work regarding noise exposure. Off. J. RS. 2011, 96, pp. 10-12, Off. J. RS. 2015, 78, p. 24, and Off. J. RS. 2019, 93, p. 270-271
14. Directive 2003/10/EC of the European Parliament and of the Council of 6 February 2003 on the minimum health and safety requirements regarding the exposure of workers to the risks arising from physical agents (noise). Off. J. Eur. Commun. L 42, 15.2.2003, p. 38
15. ISO 9612:2009, SRPS EN ISO 9612:2016 Acoustics — Determination of occupational noise exposure — Engineering method
16. ISO 9612:1997, SRPS ISO 9612:2008 Acoustics – Guidelines for the measurement and assessment of exposure to noise in a work environment
17. ISO 1999:2013 Acoustics – Determination of occupational noise exposure and estimation of noise-induced hearing impairment
18. ISO 1999:1990 Acoustics – Determination of occupational noise exposure and estimation of noise-induced hearing impairment
19. IEC 61672-1:2013 Electroacoustics - Sound level meters - Part 1: Specifications
20. ISO 7779:2018 Acoustics – Measurement of airborne noise emitted by information technology and telecommunications equipment

FACTA UNIVERSITATIS
Series: **Working and Living Environmental Protection** Vol. 21, Nº 4, Special Issue, 2024, pp. 401 - 408
https://doi.org/10.22190/FUWLEP240924038H

Original scientific paper

NONLINEAR VIBRATION OF A BEAM SUBJECTED TO MECHANICAL IMPACT AND WINKLER-PASTERNAK FOUNDATION

UDC 624.072.2:519.957

Nicolae Herisanu[1,2], Bogdan Marinca[1], Vasile Marinca[1,2]

[1]University Politehnica Timisoara, Romania
[2]Center for Advanced and Fundamental Technical Research,
Romanian Academy Branch of Timisoara, Romania

ORCID iDs: Nicolae Herisanu https://orcid.org/0000-0003-2968-5309
Bogdan Marinca https://orcid.org/0000-0003-2340-1280
Vasile Marinca https://orcid.org/0000-0002-0947-1322

Abstract. *The simultaneous effects of mechanical impact and Winkler-Pasternak foundation on the dynamic response of an Euler-Bernoulli beam are studied. By means of the Galerkin-Bubnov procedure, the governing equation with partial derivatives is reduced to an ordinary differential equation. This nonlinear equation is solved by means of the Optimal Homotopy Asymptotic Method (OHAM).*

Key words: *nonlinear vibration, OHAM, mechanical impact, Winkler-Pasternak foundation*

1. INTRODUCTION

Vibration of a beam under mechanical impact and resting on a nonlinear Winkler-Pasternak foundation is interesting as the basic research on vibration problems considering practical bridges. Some of the previous works have been the study of Ansari et al. [1]. They found the existence of the attractors at modest oscillation levels during investigations with realistic parameters. Abiala [2] used the finite element method and Neimark's integration to obtain the dynamic response of beams under uniformly distributed moving loads. The fourth-order Runge-Kutta method is applied by Ding et al. [3] to three types of conventional boundary conditions. The geometrical nonlinearities are considered by Nbendjo and Woafo [4], showing that the single-mode dynamic of the beam can be described by a Φ^6 potential with various configurations. Poorjamishidian et al. [5] analyzed the nonlinear vibration for a simply supported beam with a constant velocity carrying a moving mass.

Received September 24, 2024 / Accepted October 10, 2024
Corresponding author: Nicolae Herisanu
University Politehnica Timisoara, Bd. Mihai Viteazu 1, 300222 Timisoara, Romania
E-mail: nicolae.herisanu@upt.ro

Pirmoradian and Karinpour [6] explored dynamic stability in the Hamiltonian formulation. The vibration of viscoelastic axially moving Rayleigh and Euler-Bernoulli beam is investigated by Shariati et al. [7]. Herisanu and Marinca [8] studied the nonlinear vibration of a beam under mechanical impact in the presence of an electromagnetic actuator.

The present study is devoted to the nonlinear forced vibration of a beam resting on a nonlinear Winkler-Pasternak elastic foundation subjected to a mechanical impact. The time response of the beam has been obtained using the Optimal Homotopy Asymptotic Method (OHAM). The results show that the result of the analytical procedure has a very good correspondence with numerical integration results.

2. THE GOVERNING EQUATION

The physical model of a simply supported beam of length L subjected to a mechanical impact by the force F and resting on the Winkler-Pasternak foundation with linear and nonlinear springs K_1 and K_3 respectively is presented in Fig. 1.

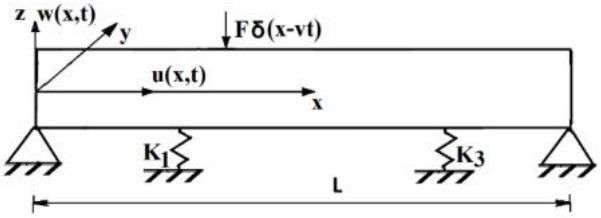

Fig. 1 Geometry of the beam under mechanical impact and elastic foundation

The Young's modulus E, a mass density ρ and the cross-sectional area A of the beam are supposed to be constants. The transverse and longitudinal displacements are w(x,t) and u(x,t), respectively.

The deflection of an element of length ds of the beam at rest is defined by

$$ds = \left[\left(1+\frac{\partial u}{\partial x}\right)^2 + \left(\frac{\partial w}{\partial x}\right)^2\right]^{1/2} dx \tag{1}$$

If the terms of the forms u_x^2, $u_x w_x^2$, u_x^3, $u_x^2 w_x^2$, u_x^4, where $u_x = \frac{\partial u}{\partial x}$, are neglected, from Eq.(1) one can get:

$$\frac{dx}{ds} = [(1+u_x)^2 + w_x^2]^{-\frac{1}{2}} \cong 1 - u_x - \frac{1}{2}w_x^2 + \frac{3}{8}w_x^4 \tag{2}$$

The unit vector parallel to the defined element (1) can be written in the form

$$\bar{k} = [(1+u_x)\bar{\imath} + w_k\bar{\jmath}]\frac{dx}{ds} \tag{3}$$

The tension in the beam is

$$T = -EAe \tag{4}$$

in which e is defined as

$$e = \frac{dx-ds}{dx} = 1 - \frac{ds}{dx} \cong u_x + \frac{1}{2}w_x^2 - \frac{3}{8}w_x^4 \tag{5}$$

The dynamics of the beam is defined by the equation [4]:

$$\rho A\frac{\partial^2 w}{\partial t^2}+EI\frac{\partial^4 w}{\partial x^4}=-\frac{\partial}{\partial x}\left(T\bar{k}\right)\bar{J}+F_{mi}+F_{wp} \tag{6}$$

where I is the moment of inertia of the beam cross-section, F_{mi} and F_{wp} are the impact force and nonlinear elastic foundation, respectively.

Substituting Eqs. (3)-(5) into Eq.(6), we obtain

$$\rho A\frac{\partial^2 w}{\partial t^2}+EI\frac{\partial^4 w}{\partial x^4}=-EA\frac{\partial}{\partial x}\left(e\frac{\partial w}{\partial x}\right)+F_{mi}+F_{wp} \tag{7}$$

It is known that the material term in Eq.(5) is small such that $\frac{d}{dx}(e)=0$.

It follows that

$$u_x+\frac{1}{2}w_x^2-\frac{3}{8}w_x^4=e=C \tag{8}$$

where C is a constant which can be determined by integrating the last equation

$$u(x)=u(0)+Cx-\frac{1}{2}\int_0^x\left(\frac{\partial w}{\partial x}\right)^2dx+\frac{3}{8}\int_0^x\left(\frac{\partial w}{\partial x}\right)^4dx \tag{9}$$

Using the boundary conditions for the longitudinal displacement: u(L,t)=u(0,t)=0, from Eq.(9) we have that

$$e=C=\frac{1}{2L}\int_0^L\left(\frac{\partial w}{\partial x}\right)^2dx-\frac{3}{8L}\int_0^L\left(\frac{\partial w}{\partial x}\right)^4dx \tag{10}$$

From Eqs. (7) and (10) one can get

$$\rho A\frac{\partial^2 w}{\partial t^2}+EI\frac{\partial^4 w}{\partial x^4}=\frac{EA}{2L}\frac{\partial^2 w}{\partial x^2}\left[\int_0^L\left(\frac{\partial w}{\partial x}\right)^2dx-\frac{3}{4}\int_0^L\left(\frac{\partial w}{\partial x}\right)^4dx\right]+F_{mi}+F_{wp}=0 \tag{11}$$

The term F_{mi} represents the mechanical impact of load F:

$$F_{mi}=F\delta(x-vt) \tag{12}$$

where v is the speed of the load and δ is the Dirac-delta function.

The nonlinear elastic medium of the Winkler-Pasternak type is given by

$$F_{wp}=-K_1w-K_3w^3 \tag{13}$$

Inserting Eqs. (12) and (13) into Eq. (11) one retrieves:

$$\rho A\frac{\partial^2 w}{\partial t^2}+EI\frac{\partial^4 w}{\partial x^4}-\frac{EA}{2L}\frac{\partial^2 w}{\partial x^2}\left[\int_0^L\left(\frac{\partial w}{\partial x}\right)^2dx-\frac{3}{4}\int_0^L\left(\frac{\partial w}{\partial x}\right)^4dx\right]-$$

$$-K_1w-K_3w^3=F\delta(x-vt) \tag{14}$$

with the simply supported beam, such that the boundary conditions are

$$w(0,t)=w(L,t)=\frac{\partial^2 w(0,t)}{\partial x^2}=\frac{\partial^2 w(L,t)}{\partial x^2}=0 \tag{15}$$

To express the governing Eqs. (14) and (15) in nondimensional form, the following parameters are defined:

$$\bar{w}=\frac{W}{L},\quad \bar{x}=\frac{x}{L},\quad \bar{t}=\frac{t}{L^2}\sqrt{\frac{EI}{\rho A}},\quad \bar{v}=vL\sqrt{\frac{\rho A}{EI}}$$

$$\tilde{\alpha}=\frac{L^2A}{2I},\quad \bar{K}_1=K_1\frac{L^4}{EI},\quad \bar{K}_3=K_3\frac{L^2}{EI}\quad \bar{f}_0=\frac{FL^4}{EI} \tag{16}$$

Omitting the bar, Eq. (14) can be rewritten in nondimensional form as

$$\frac{\partial^2 w}{\partial t^2}+\frac{\partial^4 w}{\partial x^4}-\alpha\frac{\partial^2 w}{\partial x^2}\left[\int_0^1\left(\frac{\partial w}{\partial x}\right)^2dx-\frac{3}{4}\int_0^L\left(\frac{\partial w}{\partial x}\right)^4dx\right]-$$
$$-K_1w-K_3w^3=f\delta(x-vt) \tag{17}$$

Using the Galerkin-Bubnov procedure, the solution of Eq.(17) can be assumed to be of the form

$$w(x,t)=X(x)T(t) \tag{18}$$

in which, taking into account the conditions (15), X(x) can be expressed as

$$X(x)=\sqrt{2}\sin\pi x \tag{19}$$

Inserting Eqs. (18) and (19) into Eq.(17) and multiplying this equation by X(x), and then integrating on the domain [0,1] it holds that

$$\ddot{T}+\omega^2T+aT^3+bT^5=f sin\pi vt \tag{20}$$

where the dot denotes the derivative with respect to time and

$$\omega^2=\int_0^1\frac{d^2X(x)}{dx^2}X(x)dx-K_1\int_0^1X^2(x)dx\,;$$
$$\text{a=-}\alpha\left[\int_0^1\left(\frac{dX(x)}{dx}\right)^2dx\right]\left[\int_0^1\frac{d^2X(x)}{dx^2}X(x)dx-K_3\int_0^1X^4(x)dx\right];$$
$$b=\frac{3}{4}\alpha\left[\int_0^1\left(\frac{dX(x)}{dx}\right)^4dx\right]\left[\int_0^1\frac{d^2X(x)}{dx^2}X(x)dx\right];f=\sqrt{2}f_0 \tag{21}$$

for the nonlinear differential Eq. (20), the initial conditions are

$$T(0)=A,\ \dot{T}(0)=0 \tag{22}$$

The Eqs. (20) and (22) are very difficult to be analytically solved to obtain exact solutions. In what follows, for Eqs. (20) and (22) we will apply the OHAM to obtain an analytical approximate solution.

3. The Optimal Homotopy Asymptotic Method

We will apply OHAM to the following nonlinear differential equation [9-11]:

$$L[T(t)]+N[T(t)]=0 \tag{23}$$

whose boundary conditions are

$$B\left(T(t),\frac{dT(t)}{dt}\right)=0 \tag{24}$$

In Eq.(23), L and N are linear operators and nonlinear operators, respectively. If $\bar{T}(t)$ is the unknown approximate solution of Eq. (23)-(24), then we can write that

$$\bar{T}(t)=T_0(t)+T_1(t) \tag{25}$$

where the initial approximation $T_0(t)$ can be evaluated from the linear equation

$$L[T_0(t)] = 0, \quad B\left(T_0(t), \frac{dT_0(t)}{dt}\right) = 0 \tag{26}$$

The first approximation $T_1(t)$ can be evaluated from the linear equation

$$L[T_1(t)] = H(t, C_1, C_2, \ldots, C_n)N[T_0(t)], \quad B\left(T_1(t), \frac{dT_1(t)}{dt}\right) = 0 \tag{27}$$

where $H(t,C_1,C_2,\ldots,C_n)$ is an arbitrary auxiliary function. This auxiliary function and $N[T_0(t)]$ should be of the same shape. The parameters C_1, C_2, …,C_n which appear on the first-order approximate solution obtained from Eq. (27) can be determined in many ways, using for example the least square method, the Galerkin method, the collocation method, the Ritz method or by minimizing the square residual error.

With these parameters known (namely the convergence-control parameters), the approximate solution (25) is well-determined.

4. Application of OHAM to the Nonlinear Vibration of the Beam

Making the transformations

$$\tau = \Omega t, T(t) = A\Psi(\tau) \tag{28}$$

in which Ω is the unknown natural frequency of the beam, Eq. (20) becomes

$$\Psi'' + \frac{\omega^2}{\Omega^2}\Psi + \frac{\alpha A^2}{\Omega^2}\Psi^3 + \frac{bA^4}{\Omega^2}\Psi^5 = \frac{f}{A\Omega^2} sin\frac{\pi v}{\Omega}\tau, \;\; \Psi(0) = 1, \Psi'(0) = 0 \tag{29}$$

where the prime denotes derivative with respect to τ.

The linear operator and nonlinear operator of Eq. (29) are respectively

$$L[\Psi(\tau)] = \Psi'' + \Psi\,; \;\; N[\Psi(\tau)] = \left(\frac{\omega^2}{\Omega^2} - 1\right)\Psi + \frac{\alpha A^2}{\Omega^2}\Psi^3 + \frac{bA^4}{\Omega^2}\Psi^5 - \frac{f}{A\Omega^2} sin\frac{\pi v\tau}{\Omega} \tag{30}$$

The initial approximation $\psi_0(\tau)$ is determined from Eqs. (26) and (30):

$$\Psi_0'' + \Psi_0 = 0, \;\; \Psi_0(0) = 1, \Psi_0'(0) = 0 \tag{31}$$

and has the solution

$$\Psi_0(\tau) = cos\tau \tag{32}$$

Substituting Eq. (32) into the nonlinear operator (30) one gets:

$$N[\Psi_0(\tau)] = M_1 cos\tau + M_3 cos3\tau + M_5 cos5\tau + Psin\frac{\pi v\tau}{\Omega} \tag{33}$$

where the constants M_i and P are given by

$$M_1 = \frac{\omega^2}{\Omega^2} - 1 + \frac{3aA^2}{4\Omega^2} + \frac{5bA^4}{8\Omega^2}\,; M_3 = \frac{aA^2}{4\Omega^2} + \frac{5bA^4}{16\Omega^2}; M_5 = \frac{bA^4}{16\Omega^2}\,; P = -\frac{f}{A\Omega^2} \tag{34}$$

The auxiliary function $H(\tau,C_1,C_2,\ldots,C_n)$ from Eq. (27) is chosen such that the product $H(\tau,C_1,C_2,\ldots,C_n)N[\psi_0(\tau)]$ and $N[\psi_0(\tau)]$ be of the same form. The auxiliary functions $H(\tau,C_1,C_2,\ldots,C_n)$ and the natural number n are not unique. For example, we can alternatively choose these auxiliary functions in the following expressions:

$$H_1(\tau, C_1, C_2, C_3, C_4) = C_1 + 2C_2 cos2\tau + 2C_3 cos4\tau + 2C_4 cos6\tau \tag{35}$$

$$H_2(\tau, C_1, C_2) = C_1 + 2C_2 cos2\tau \tag{36}$$

$$H_3(\tau, C_1, C_2, C_3) = C_1 + 2C_2 cos4\tau + 2C_3 cos6\tau \tag{37}$$

$$H_4(\tau, C_1, C_2, C_3) = C_1 + 2C_2 cos2\tau + 2C_3 cos4\tau \tag{38}$$

and so on. Using only the expression (35), Eq. (27) can be written as follows:

$$\Psi_1'' + \Psi_1 = [M_1(C_1 + C_2) + M_3(C_2 + C_3) + M_5(C_3 + C_4)]cos\tau +$$
$$[M_3(C_1 + C_4) + M_1(C_2 + C_3) + M_5C_2]cos3\tau +$$
$$[M_5C_1 + M_3C_2 + M_1(C_3 + C_4)]cos5\tau + [M_5C_2 + M_3C_3 + M_1C_4]cos7\tau,$$
$$\Psi_1(0) = \Psi_1'(0) = 0 \tag{39}$$

No secular terms into Eq. (39) require that the coefficient of τ be zero. From this condition, one can put the natural frequency:

$$\Omega^2 = \omega^2 + \frac{3}{4}aA^2 + \frac{5bA^4}{8} + \left(\frac{aA^2}{4} + \frac{5bA^4}{16}\right)\frac{C2+C3}{C1+C2} + \frac{bA^4}{16}\frac{C3+C4}{C1+C2} \tag{40}$$

The solution of Eq. (39) is

$$\Psi_1(\tau) = \frac{M_1(C_2+C_3)+M_3(C_1+C_4)+M_5C_2}{8}(cos\tau - cos3\tau) + \frac{M_1(C_3+C_4)+M_3C_2+M_5C_1}{24}(cos\tau - cos5\tau) + \frac{M_1C_1+M_3C_3+M_5C_2}{48}(cos\tau - cos7\tau) + \frac{M_3C_4+M_5C_3}{80}(cos\tau - cos9\tau) + \frac{M_3C_1}{120}(cos\tau - cos11\tau) \tag{41}$$

The approximate solution of Eqs. (20) and (22) are obtained from Eqs. (25), (28), (32) and (41) as:

$$\bar{T}(t) = Acos\Omega t + \frac{A[M_1(C_2+C_3)+M_3(C_1+C_4)+M_5C_2]}{8}(cos\Omega t - cos3\Omega t) + \frac{A[M_1(C_3+C_4)+M_3C_2+M_5C_1]}{24}(cos\Omega t - cos5\Omega t) + \frac{A[M_1C_1+M_3C_3+M_5C_2]}{48}(cos\Omega t - cos7\Omega t) + \frac{A[M_3C_4+M_5C_3]}{80}(cos\Omega t - cos9\Omega t) + \frac{AM_3C_1}{120}(cos\Omega t - cos11\Omega t) \tag{42}$$

in which Ω is evaluated from Eq. (40).

5. NUMERICAL RESULTS

To illustrate the accuracy of OHAM, we consider the parameters ω=1.3, A=0.5, a=0.24, b = 0.16, v = 0.414, f = 0.001.

Using a collocation approach, there are obtained the values C_1 = 0.092731330625, C_2= -1.2082598891606, C_3 =1.199106193799, C_4=-0.593752904778.

Figure 2 presents the solution (42) in comparison with the numerical integration results.

One can see that the error between the approximate solution and the numerical result is very small.

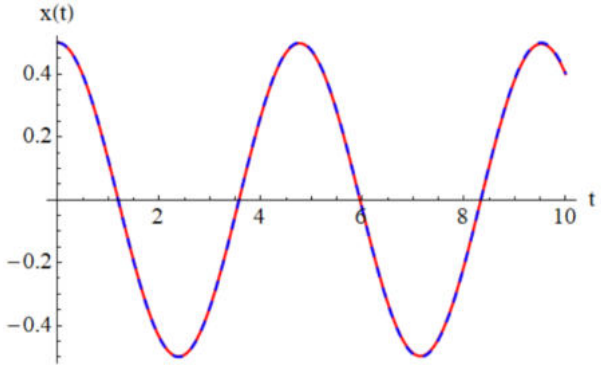

Fig. 2 Comparison between approximate solution (42) and numerical integration results: _ _ _ _ analytical; _____ numerical

6. Conclusions

In the present research, we propose the Optimal Homotopy Asymptotic Method (OHAM) to obtain an approximate analytical solution to the nonlinear differential equation of vibration of a beam subjected to mechanical impact and resting on the Winkler-Pasternak elastic nonlinear foundation. The validity of our procedure was demonstrated appropriately by choosing the linear operator and auxiliary function.

A numerical example is given and a very good agreement was found between the approximate analytical results and numerical simulation. Our proposed procedure is valid even if the nonlinear differential equation does not contain any small parameters.

References

1. Ansari M., Esmailzadeh E., Younesian D., Internal-external resonance of beams on nonlinear viscoelastic foundation traversed by moving load, *Nonlinear Dynamics,* 31, pp.1163-1182, doi:10.1007/s11071-009-9639-0, https://link.springer.com/article/10.1007/s11071-009-9639-0
2. Abiala I.O.: Finite element evaluation of the dynamic response of beams under uniformly distributed moving loads, *Journal of Natural Sciences, Engineering and Technology*, 8, pp. 95-105, doi:10.51406/jnset.v8i1.983, https://journal.funaab.edu.ng/index.php/JNSET/article/view/983
3. Ding H., Chen L.Q., Pyang S.: Convergence of Galekin truncation for dynamic response of finite beams on nonlinear foundations under a moving load, *Journal of Sound and Vibration*, 331, pp. 2426-2442, doi:10.1016/j.jsv.2011.12.036,https://www.sciencedirect.com/science/article/abs/pii/S0022460X12000041?via%3Dihub
4. Nbendjo B.R.N., Woafo P.: Modelling of the dynamic of Euler's beam by Φ^6 potential, *Mechanics Research Communications*, 38, pp.542-545, doi:10.1016/j.mechrescom.2011.07.010, https://www.sciencedirect.com/science/article/abs/pii/S0093641311001510?via%3Dihub
5. Poorjamshidian M., Sheikhi J., Moghadas S.M., Nakhaie M.: Nonlinear vibration analysis of the beam carrying a moving mass using modified homotopy, *Journal of Solid Mechanics*, 6, pp. 389-396, https://sanad.iau.ir/journal/jsm/Article/514611?jid=514611
6. Pirmoradian M., Karinpour H..: Parametric resonance and jump analysis of a beam subjected to a periodic mass transition, *Nonlinear Dynamics*, 89, pp. 2141-2154, doi:10.1007/s11071-017-3575-1, https://link.springer.com/article/10.1007/s11071-017-3575-1
7. Shariati A., Jung D.W., Sedighi H.M., Zur H.K., Habibi M., Safa M.: Stability and dynamic of viscoelastic moving Rayleigh beams with an asymmetrical distribution of material parameters, *Symmetry* 12, 586, doi:10.3390/sym12040586, https://www.mdpi.com/2073-8994/12/4/586

8. Herisanu N., Marinca V.: Effect of mechanical impact and electromagnetic actuation on the nonlinear vibration of a beam, *Springer Proceedings in Physics*, 302, pp. 19-28, doi:10.1007/978-3-031-48087-4, https://link.springer.com/chapter/10.1007/978-3-031-48087-4_3
9. Marinca V. and Herisanu N., *The Optimal Homotopy Asymptotic Method. Engineering Applications*, Springer, Cham 2015.
10. Marinca V., Herisanu N.: The Optimal Homotopy Asymptotic Method for solving Blasius equation, *Applied Mathematics and Computation*, 231, pp. 134-139, doi:10.1016/j.amc.2013.12.121, https://www.sciencedirect.com/science/article/abs/pii/S0096300313014112
11. Herisanu N., Marinca V.: Explicit analytical approximation to large amplitude nonlinear oscillations of an uniform cantilever beam carrying an intermediate lumped mass and rotary inertia, *Meccanica*, 45, pp. 847-855, doi:10.1007/s11012-010-9293-0, https://link.springer.com/article/10.1007/s11012-010-9293-0

FACTA UNIVERSITATIS
Series: **Working and Living Environmental Protection** Vol. 21, Nº 4, Special Issue, 2024, pp. 409 - 416
https://doi.org/10.22190/FUWLEP240924039M

Original scientific paper

DYNAMIC ANALYSIS OF A NANOBEAM UNDER THE INFLUENCE OF AN ELECTROMAGNETIC ACTUATOR AND A MECHANICAL IMPACT

UDC 534.01

Bogdan Marinca[1], Nicolae Herisanu[1,2], Vasile Marinca[1,2]

[1]University Politehnica Timisoara, Romania
[2]Center for Advanced and Fundamental Technical Research, Romanian Academy branch of Timisoara, Romania

ORCID iDs: Bogdan Marinca https://orcid.org/0000-0003-2340-1280
Nicolae Herisanu https://orcid.org/0000-0003-2968-5309
Vasile Marinca https://orcid.org/0000-0002-0947-1322

Abstract. *The Optimal Auxiliary Functions Method (OAFM) is applied in the study of nonlinear vibration of a nanobeam, considering the curvature of the beam, the presence of an electromagnetic actuator and a mechanical impact. Our procedure is based on the existence of some auxiliary functions which assure a fast convergence of the approximate solution. The convergence-control parameters present in the auxiliary functions are evaluated by rigorous mathematical procedures.*

Key words: *OAFM, electromagnetic actuator, mechanical impact, nonlinear forced vibration*

1. INTRODUCTION

The study of the vibration of a nanobeam under mechanical impact in the presence of an electromagnetic actuator accounting for the curvature of the beam is interesting for researchers because many structures include the nanobeam. Textile fibers, flexible satellites, paper sheets, oil pipelines, airplane wings, and so on. Nanobeams have attracted considerable attention in the literature. For example, Ghayesh [1] investigated the forced nonlinear vibrations of an axially moving beam fitted with an intra-span spring-support which is solved by the pseudoarclength continuation technique. The thermo-mechanical nonlinear vibration and stability of a hinged-hinged axially moving beam additionally supported by a nonlinear spring-mass support are examined by two numerical procedures

Received September 24, 2024 / Accepted October 10, 2024
Corresponding author: Nicolae Herisanu
University Politehnica Timisoara, Bd. Mihai Viteazu 1, 300222 Timisoara, Romania
E-mail: nicolae.herisanu@upt.ro

by Kazemirad et al. [2]. To obtain static pull-in voltage with fringing field effects in an electrostatically actuated cantilever and clamped-clamped microbeam, Rokni et al. [3] proposed a novel method for converting a governing fourth-order differential equation into a Fredholm integral equation. Peng et al. [4] presented a nonlinear electro-dynamic analysis for a size-dependent microbeam made of materials with nonlinear elasticity by employing the modified behavior of electrically actuated carbon nanotubes-based nano-actuator including the higher-order strain gradient deformation, the geometric nonlinearity, the slack effect and the temperature gradient effects.

The effect of a magnetic field on the nonlinear vibration response of single-walled carbon nanotubes based on nonlocal strain gradient theory is studied by Anh and Hieu [5]. Using the equivalent linearization method with weighted averaging value, expressions of the nonlinear frequencies are obtained in the analytical forms. Yinussa and Sobamovo [6] explored nonlinear internal flow-induced vibration and stability of a pre-tensioned nanotube that rests on an elastic foundation.

In the present work, the nonlinear forced vibration of a nanotube under the influence of mechanical impact and an electromagnetic actuator considering the curvature of the beam is investigated. The nonlinearity of the equation is caused by the curvature of the nanobeam and of the electromagnetic actuator. The governing equation is discretized using the Galerkin-Bubnov procedure. The obtained nonlinear differential equation is solved by using OAFM. A very accurate solution is obtained using a moderate number of convergence-control parameters via auxiliary functions.

2. FORMULATION OF THE PROBLEM

A simply supported nanobeam of length L subjected to a mechanical impact by force F and electromagnetic load V_{DC} is presented in Figure 1. The transverse and longitudinal displacements are w(x,t) and u(x,t) respectively.

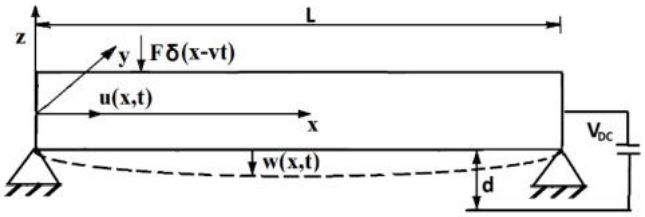

Fig. 1 A simply supported nanobeam subjected to impact force F and electromagnetic actuator

The Euler-Bernoulli beam theory proves that the displacement fields of any point are

$$u_x(x,z,t) = u(x,t) - z\frac{\partial w(x,t)}{\partial x}$$

$$u_y(x,z,t) = 0$$

$$u_z(x,z,t) = w(x,t) \tag{1}$$

The axial strain ε_{xx} and shear strain γ_{xz} of the beam, considering von Karman's nonlinear strain are

$$\varepsilon_{xx} = \frac{\partial u}{\partial x} + \frac{1}{2}\left(\frac{\partial w}{\partial x}\right)^2 - zk, \ \gamma_{xz} = \frac{\partial u_x}{\partial x} + \frac{\partial u_y}{\partial y} = 0 \tag{2}$$

where

$$k = \frac{\partial^2 w}{\partial x^2} \Big/ \left[1 + \left(\frac{\partial w}{\partial x}\right)^2\right]^{3/2} \tag{3}$$

is the curvature of the beam.

The kinetic energy of the beam is

$$K_e = \frac{1}{2}\rho A \int_0^1 \left[\left(\frac{\partial u}{\partial t}\right)^2 + \left(\frac{\partial w}{\partial t}\right)^2\right] dx \tag{4}$$

while the first variation of the strain energy is

$$\delta U_s = \int_V (\sigma_{xx}\delta\epsilon_{xx}) dV \tag{5}$$

where σ_{xx} is the stress: σ_{xx}=E ε_{xx}, E being the elasticity modulus.

Substituting Eq. (2) into Eq. (5) one can get

$$\delta U_s = \int_0^L \left[N\delta\left(\frac{\partial u}{\partial x} + \frac{1}{2}\left(\frac{\partial w}{\partial x}\right)^2\right) - M\delta\left(\frac{\partial^2 w}{\partial x^2}\right)\right] dx \tag{6}$$

in which N and M are the axial force and bending moment respectively. The stress resultants used in Eq. (6) are defined as

$$N = \int_A \sigma_{xx} dA \, , M = \int_A z\sigma_{xx} dA \tag{7}$$

where A is the area of the cross-section for the nanobeam.

The strain energy U_s can be written as

$$U_s = \frac{1}{2}\int_0^L \left[N\left(\frac{\partial u}{\partial x} + \frac{1}{2}\left(\frac{\partial w}{\partial x}\right)^2\right) - M\left(\frac{\partial^2 w}{\partial x^2}\right)\right] dx \tag{8}$$

The virtual work by the external mechanical impact and electromagnetic actuator is given by

$$\delta W = \int_0^L q\delta W dx \tag{9}$$

where

$$q = F\delta(x - vt) + \frac{1}{2}\frac{C_0 V_{DC}^2}{[d - w(x,t)]^2} - \frac{1}{2}\frac{C_0 V_{DC}^2}{[d + w(x,t)]^2} \tag{10}$$

in which C_0 is the capacitance of the actuator, d is the gap width and V_{DC} is the voltage. The expression of the electromagnetic actuation can be simplified as

$$\frac{1}{2}\frac{C_0 V_{DC}^2}{[d - w(x,t)]^2} - \frac{1}{2}\frac{C_0 V_{DC}^2}{[d + w(x,t)]^2} = \frac{2C_0 V_{DC}^2}{L}\left[\frac{W}{d} + 2\left(\frac{W}{d}\right)^3 + 3.0925\left(\frac{W}{d}\right)^5\right] \tag{11}$$

The variational form of the equation of motion can be obtained by Hamiltonian principle

$$\delta \int_{t_1}^{t_2} [K_e - U_s + W)]dt = 0 \tag{12}$$

From Eqs. (4), (8), (9) and (12) and integrating by parts, and then collecting the coefficients of δ_u and δ_w we obtain the following equations of motion

$$\frac{\partial N}{\partial x} - \rho A \frac{\partial^2 u}{\partial t^2} \tag{13}$$

$$\frac{\partial^2 M}{\partial x^2} - \frac{\partial}{\partial x}\left(N \frac{\partial w}{\partial x}\right) + \frac{2C_0 V_{DC}^2}{d^2}\left[\frac{W}{d} + 2\left(\frac{W}{d}\right)^3 + 3.0925\left(\frac{W}{d}\right)^5\right] + F\delta(x - vt) = \\ = \rho A \frac{\partial^2 w}{\partial t^2} - \rho I \frac{\partial^4 w}{\partial t^2 \partial x^2} \tag{14}$$

where N and M from Eq. (7), become by integration:

$$N = EA\left[\frac{\partial u}{\partial x} + \frac{1}{2}\left(\frac{\partial w}{\partial x}\right)^2\right] \tag{16}$$

$$M = -EI \frac{\partial^2 w}{\partial x^2} \Big/ \left[1 + \left(\frac{\partial w}{\partial x}\right)^2\right]^{3/2} \tag{17}$$

Usually, the longitudinal inertial term $\frac{\partial^2 u}{\partial t^2}$ into Eq. (13) can be neglected, such that from Eq. (13) it is clear that N is a constant N=C and therefore from Eq. (16) it holds that

$$\frac{\partial u}{\partial x} = \frac{C}{EA} - \frac{1}{2}\left(\frac{\partial w}{\partial x}\right)^2 \tag{18}$$

By integrating the last equation with the boundary conditions

$$u(0, t) = u(L, t) = 0 \tag{19}$$

the constant C is given by

$$C = N = -\frac{EA}{2L} \int_0^L \left(\frac{\partial w}{\partial x}\right)^2 dx \tag{20}$$

According to the Eq. (17), the term which defines the curvature of the beam can be written in the form:

$$\frac{\partial^2 w}{\partial x^2} \Big/ \left[1 + \left(\frac{\partial w}{\partial x}\right)^2\right]^{3/2} \cong \frac{\partial^2 w}{\partial x^2}\left[1 - \frac{3}{2}\left(\frac{\partial w}{\partial x}\right)^2\right] \tag{21}$$

such that the nonlinear equation of motion for the nanobeam can be obtained by substituting Eqs. (20), (21) and (17) into Eq. (14) as follows:

$$EI\left[\frac{\partial^4 w}{\partial x^4} - \frac{3}{2}\frac{\partial^4 w}{\partial x^4}\left(\frac{\partial w}{\partial x}\right)^2 - 3\left(\frac{\partial^2 w}{\partial x^2}\right)^3 - 9\frac{\partial w}{\partial x}\frac{\partial^2 w}{\partial x^2}\frac{\partial^3 w}{\partial x^3}\right] + \rho A \frac{\partial^2 w}{\partial t^2} + \frac{2C_0 V_{DC}^2}{d^2}\left[\frac{W}{d} + 2\left(\frac{W}{d}\right)^3 + \right. \\ \left. 3.0925\left(\frac{W}{d}\right)^5\right] + \rho I \frac{\partial^4 w}{\partial t^2 \partial x^2} - \frac{EA}{2L}\frac{\partial^2 w}{\partial x^2}\int_0^L \left(\frac{\partial w}{\partial x}\right)^2 dx = F\delta(x - vt) \tag{22}$$

The following nondimensional quantities are considered:

$$\bar{x} = \frac{x}{L}, \bar{w} = \frac{w}{d}, \bar{t} = \frac{t}{L^2}\sqrt{\frac{EI}{\rho A}}, \bar{\alpha} = \frac{I}{AL^2}, \bar{\beta} = \frac{2C_0 L^4 V_{DC}}{d^3 EI}, \bar{v} = vL\sqrt{\frac{\rho A}{EI}}, \bar{f} = \frac{FL^4}{EI} \tag{23}$$

Omitting the bars, the nondimensional form of the Eq. (22) can be written as

$$\frac{\partial^2 w}{\partial t^2}+\frac{\partial^4 w}{\partial x^4}-\frac{3}{2}\frac{\partial^4 w}{\partial x^4}\left(\frac{\partial w}{\partial x}\right)^2-3\left(\frac{\partial^2 w}{\partial x^2}\right)^3-9\frac{\partial w}{\partial x}\frac{\partial^2 w}{\partial x^2}\frac{\partial^3 w}{\partial x^3}+\beta(w+2w^3+3.0925w^5)-\frac{1}{\alpha}\frac{\partial^4 w}{\partial t^2\partial x^2}-\frac{\alpha}{2}\frac{\partial^2 w}{\partial x^2}\int_0^1\left(\frac{\partial w}{\partial x}\right)^2 dx=f\delta(x-vt) \quad (24)$$

The solution of Eq. (24) can be assumed, according to the Galerkin-Bubnov procedure to be of the form

$$w(x,t)=X(x)T(t) \quad (25)$$

By substitution of Eq. (25) into Eq. (24) and then multiplying Eq. (24) by X(x) and integrating on the domain [0,1], using the expression

$$\int_0^1 f(x)\delta(x-vt)dx=f(vt) \quad (26)$$

one can obtain the following nonlinear differential equation of motion

$$\ddot{T}+\omega^2 T+aT^3+bT^5=f_0(vt),\ f_0(vt)=fX(vt) \quad (27)$$

where the dot denotes the derivative with respect to time and the parameters which appear into Eq. (27) are

$$q=\int_0^1\left[X^2(x)dx+\alpha X(x)\frac{d^2X(x)}{dx^2}\right]dx$$

$$\omega^2=\frac{1}{q}\left[\int_0^1\frac{d^4X(x)}{dX^4}X(x)\,dx+\beta\int_0^1 X^2(x)dx\right]$$

$$a=-\frac{3}{q}\int_0^1\left[X(x)\frac{d^4X(x)}{dx^4}\left(\frac{dX(x)}{dx}\right)^2+X(x)\left(\frac{d^2X(x)}{dx^2}\right)^5+3X(x)\frac{dX(x)}{dx}\frac{d^2X(x)}{dx^2}\frac{d^3X(x)}{dx^3}\right]dx-\frac{1}{2\alpha q}\left[\int_0^1\frac{dX(x)}{dx}dx\right]\left[\int_0^1 X(x)\frac{d^2X(x)}{dx^2}dx\right]-\frac{\beta}{q}\int_0^1 X^4(x)dx,\quad b=3.0925\int_0^1 X^5(x)\,dx \quad (28)$$

In the present study, we consider the case of a simply supported beam, and therefore the boundary conditions are

$$w(0,t)=\frac{\partial^2 w(0,t)}{\partial x^2}=0,\ \ w(1,t)=\frac{\partial^2 w(1,t)}{\partial x^2}=0 \quad (29)$$

The eigenfunction X(x) can be expressed from Eq. (29) as

$$X(x)=sin\pi x \quad (30)$$

For the nonlinear differential Eq. (27), where $f_0(t)=fsin\pi vt$, the initial conditions are

$$T(0)=A,\ \dot{T}(0)=0 \quad (31)$$

For nonlinear Eq. (27) and (31) we will apply OAFM [7-11].

3. APPLICATION OF OAFM TO THE NONLINEAR EQUATION OF NANOBEAM

To find an analytical approximate solution for nonlinear differential Eq. (27) and (31) near the primary resonance $\omega \approx \pi\nu$, we make the transformation

$$\tau = \Omega t, \;\; T(t) = A\theta(\tau) \tag{32}$$

Eqs. (27) and (31) can be rewritten as

$$\theta'' + \left(\frac{\omega}{\Omega}\right)\theta + \frac{aA^2}{\Omega^2}\theta^3 + \frac{bA^4}{\Omega^2}\theta^5 = \frac{f_0}{A\Omega^2} sin\frac{\omega\tau}{\Omega}\,, \;\; \theta(0) = 1, \theta'(0) = 0 \tag{33}$$

where the prime denotes the derivative with respect to τ and Ω is the frequency of the system. The linear and nonlinear operators corresponding to Eq. (33) are respectively:

$$L[\theta(\tau)] = \theta'' + \theta \;\; , N[\theta(\tau)] = \left(\frac{\omega^2}{\Omega^2} - 1\right)\theta + \frac{aA^2}{\Omega^2}\theta^3 + \frac{bA^4}{\Omega^2}\theta^5 - \frac{f_0}{A\Omega^2} sin\frac{\omega\tau}{\Omega} \tag{34}$$

The approximate solution of Eq.(34) can be written as

$$\bar{\theta}(\tau) = \theta_0(\tau) + \theta_1(\tau) \tag{35}$$

The initial approximate solution $\theta_0(\tau)$ is determined from the linear differential equation

$$\theta_0''(\tau) + \theta_0(\tau) = 0, \quad \theta_0(0) = 1, \theta_0'(0) = 0 \tag{36}$$

whose solution is

$$\theta_0(\tau) = cos\tau \tag{37}$$

Inserting Eq. (37) into the second expression of Eq. (34), it holds that

$$N[\theta_0] = N_1 cos\tau + N_3 cos3\tau + N_5 cos5\tau - N_6 sin\frac{\omega\tau}{\Omega} \tag{38}$$

where

$$N_1 = \frac{\omega^2}{\Omega^2} - 1 + \frac{3aA^2}{4\Omega^2} + \frac{5bA^4}{8\Omega^2}, \;\; N_2 = \frac{aA^2}{4\Omega^2} + \frac{5bA^4}{46\Omega^2}, N_5 = \frac{bA^4}{16\Omega^2} \;\; N_6 = -\frac{f_0}{A\Omega^2} \tag{39}$$

From Eq. (38) we propose the following linear equation for the first approximation:

$$\Theta_1'' + \theta_1 = (C_1 + 2C_2 cos2\tau + 2C_3 cos4\tau)(N_1 cos\tau + N_3 cos3\tau),$$
$$\theta_1(0) = \theta_1'(0) = 0 \tag{40}$$

After some manipulations, Eq. (40) can be written as

$$\theta_1'' + \theta_1 = [(C_1 + C_2)N_1 + (C_2 + C_3)N_3]cos\tau + [(C_2 + C_3)N_1 + C_1N_3]cos3\tau + [C_2N_3 + C_3N_1]cos5\tau + C_3N_3\, cos7\tau \tag{41}$$

Avoiding the secular term in the last equation, we can find the frequency of the system:

$$\Omega^2 = \omega^2 + \frac{3aA^2}{4} + \frac{aA^2}{4}\frac{C_2+C_3}{C_1+C_2} \tag{42}$$

The solution of Eq. (40) becomes

$$\Theta_1(\tau) = \frac{(C_2+C_3)N_1+C_1N_3}{8}(cos\tau - cos3\tau) + \frac{C_2N_3+C_3N_1}{24}(cos\tau - cos5\tau)$$

$$\frac{C_3N_3}{48}(cos\tau - cos7\tau) \tag{43}$$

The approximate solution of Eqs. (27) and (31) becomes:

$$\bar{T}(t) = Acos\Omega t + \frac{A[(C_2+C_3)N_1+C_1N_3}{8}(cos\Omega t - cos3\Omega t) + \frac{A[C_2N_3+C_3N_1}{24}(cos\Omega t - cos5\Omega t) + \frac{AC_3N_3}{48}(cos\Omega t - cos7\Omega t) \tag{44}$$

where Ω is given by Eq. (42). The convergence control parameters are determined by minimizing the residual of the initial equation.

4. Numerical Application

The efficiency of OAFM can be proved through the following particular case: ω= 1.5, A = 1, a = 0.88, b = 1.23, f = 0.001, v = 0.478.

The obtained values of the convergence-control parameters are: C_1 = 0.750030876926, C_2 = -1.069177153794, C_3 = 0.013599617044

Fig.2 shows the comparison between the approximate solution (44) and the numerical solution obtained by a fourth-order Runge-Kutta approach.

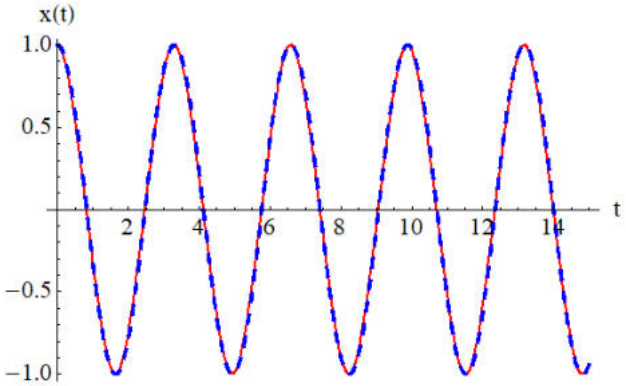

Fig. 2 Comparison between the analytical solution (44) and numerical integration results for Eqs. (27) and (31), numerical; _ _ _ _ Eq.(44)

It can be observed that our approximate solution for the nanobeam obtained through OAFM is nearly identical to the numerical integration results, which proves the efficiency of our analytical technique.

4. Conclusions

According to the present results, the oscillatory behavior of simply supported uniform nanobeam, taking into consideration the curvature of the beam, is studied. The Bernoulli-Euler beam is subjected to a mechanical impact using the Dirac-delta function and the electromagnetic actuation. The OAFM procedure was applied to solve the complex nonlinear differential equation introducing so-called auxiliary functions and some

convergence-control parameters, without supplementary hypothesis. These parameters are optimally determined by rigorous mathematical procedures. Our technique leads to a very accurate solution using only one iteration. It should be emphasized that any nonlinear dynamical system is reduced to only two linear differential equations.

REFERENCES

1. Ghayesh M., Stability and bifurcation of an axially moving beasm with an intermediate spring support, *Nonlinear Dynamics*, 69, pp.193-200, doi:10.1007/s11071-011-0257-2, https://link.springer.com/ article/10.1007/s11071-011-0257-2
2. Kazemirad S., Ghayesh M., Amabili M., Thermal effects on nonlinear vibration of an axially moving beam with an intermediate spring-mass support, *Shock and Vibration*, 20, pp.387-399, doi:10.1155/2013/621295, https://onlinelibrary.wiley.com/doi/10.3233/SAV-120752
3. Rokni H., Seethaler R.J., Milani A.S., Hashemi S.H., Li X.F., Analytical closed-form solutions for size-dependent pull-in behavior in electrostatic micro-actuators via Fredholm integral equation, *Sensors and Actuators A: Physical*, 190, pp.32-43, doi:10.1016/j.sna.2012.10.035, https://www.sciencedirect.com /science/article/abs/pii/S0924424712006528?via%3Dihub
4. Peng J., Yang L., Lin F., Yang J., Dynamic analysis of size-dependent microbeams with nonlinear elasticity under electrical actuation, *Applied Mathematical Modeling,* 43, pp.441-453, doi: 10.1016/j.apm.2016.11.025, https://www.sciencedirect.com/science/article/pii/S0307904X16306308
5. Ahn N.D., Hieu D.V., Nonlinear vibration of nonlocal strain gradient nanotubes under longitudinal magnetic field, *Vietnam Journal of Mechanics*, 43, pp.55-77, doi:10.15625/0866-7136/15467, https://vjs.ac.vn/index.php/vjmech/article/view/15467
6. Yinusa A.A., Sobamowo M.G., Mechanics of nonlinear internal flow-induced vibration and stability analysis of a pre-tensioned single-walled carbon nanotube using classical differential transformation method with CAT and SAT after-treatment techniques, *Forces in Mechanics*, 7, 100083 doi:10.1016/j.finmec.2022.100083,https://ww.sciencedirect.com/science/article/pii/S2666359722000130
7. Marinca V., Herisanu N., Marinca B., *Optimal Auxiliary Functions Method for Nonlinear Dynamical Systems*, Springer, Cham, 2021
8. Herisanu N., Marinca V., An efficient analytical approach to investigate the dynamics of a misalignment multirotor system, Mathematics, 8, 1083, doi:10.3390/math8071083, https://www.mdpi.com/2227-7390/8/7/1083
9. Marinca B., Bogdan C., Marinca V., Dynamical SEIR epidemic model by OAFM, *Chaos, Solitons,Fractals* 14, 2020, 110949, doi:10.1016/j.chaos.2021.11094, https://www.sciencedirect.com/science/article/pii/S0960077921003039?via%3Dihub
10. Herisanu N., Marinca V., A solution procedure combining analytical and numerical approach to investigate a two degree of freedom vibroimpact oscillator, *Mathematics*, 9, 1374, doi:10.3390/math9121374, https://www.mdpi.com/2227-7390/9/12/1374
11. Herisanu N., Marinca B., Marinca V., Nonlinear vibration of double walled carbon nanotubes subjected to mechanical impact and embedded on Winkler-Pasternak foundation, *Materials* 15, 8599, 10.3390/ma15238599, https://www.mdpi.com/1996-1944/15/23/8599

FACTA UNIVERSITATIS
Series: **Working and Living Environmental Protection** Vol. 21, Nº 4, Special Issue, 2024, pp. 417 - 425
https://doi.org/10.22190/FUWLEP240910040J

Original scientific paper

VIBRATIONS MEASUREMENTS IN INDUSTRIAL PLANTS AND THEIR INFLUENCE ON MACHINES

UDC 534.13:621-1/-9

Dragan Jovanović[1], Milena Mančić[2], Milena Medenica[2], Miomir Raos[2], Marjan Popović[3]

[1]University of Niš, Faculty of Mechanical Engineering, Niš, Serbia
[2]University of Niš, Faculty of Occupational Safety in Niš, Serbia
[3]Miphem, Beograd, Serbia

ORCID iDs:	Dragan Jovanović	https://orcid.org/0009-0005-2060-1297
	Milena Mančić	https://orcid.org/0000-0002-6181-2286
	Milena Medenica	https://orcid.org/0000-0001-6561-5696
	Miomir Raos	https://orcid.org/0000-0001-5586-0276
	Marjan Popović	N/A

Abstract. *In the field of industrial machinery condition monitoring, vibration analysis is a vital technique that helps engineers and maintenance specialists identify possible problems in intricate systems before they become expensive failures. Ensuring the best performance and longevity of industrial gear is crucial, especially in sectors that largely depend on intricate machinery. The proper selection and application of measurement tools and methodologies is one of the most important components of an efficient vibration analysis. This research analyzes the impact of vibrations on the performance of two distinct machines, as well as the different methods employed by the machine manufacturers in interpreting the vibration measurements.*

Key words: *vibration measurements, industrial machines, vibration impact*

1. INTRODUCTION

Vibration analysis has become a critical tool in the field of industrial machinery condition monitoring, enabling engineers and maintenance professionals to detect and diagnose potential issues within complex systems before they escalate into costly breakdowns. Maintaining the optimal performance and longevity of industrial equipment is of paramount importance, particularly in industries that rely heavily on complex machinery, such as automotive manufacturing, cement production, and petrochemicals [1].

Received September 10, 2024 / Accepted November 21, 2024
Corresponding author: Milena Mančić
University of Niš, Faculty of Occupational Safety, Čarnojevića 10a, 18000 Niš, Serbia
E-mail: milena.mancic@znrfak.ni.ac.rs

One of the key aspects of effective vibration analysis is the selection and use of appropriate measurement techniques and equipment. Sophisticated vibration measurement devices with advanced signal processing capabilities are now widely available, allowing for the precise quantification and characterization of vibration patterns in industrial machines. These devices typically offer features such as multi-channel data acquisition, high sampling rates, and the ability to simultaneously measure overall vibration values, spectra, and time-domain signals across multiple axes.

The choice of measurement method and equipment is largely dependent on the specific application and the characteristics of the equipment under investigation. For example, in the case of NEMA AC induction motors commonly used in the petrochemical industry, the most common vibration measurement techniques include overall vibration levels, frequency-domain analysis, and time-domain waveform analysis [3].

Vibration analysis has proven to be a valuable tool for the diagnosis of a wide range of machinery issues, including bearing defects, unbalance, misalignment, and other mechanical faults [4]. By carefully analyzing the vibration signatures of industrial equipment, maintenance professionals can often identify the root cause of a problem and take appropriate corrective action before the issue leads to a failure or costly downtime.

The power of vibration analysis lies in its ability to provide early warning signs of impending problems, enabling proactive maintenance strategies that can significantly extend the useful life of industrial equipment [2-4].

By leveraging the insights gained through vibration analysis, plant operators and maintenance teams can optimize the performance and reliability of their machinery, ultimately contributing to improved productivity, reduced maintenance costs, and enhanced overall plant efficiency [2-4].

Devices and machines in operating conditions cause vibrations in the working environment in which they are located as part of the system along with other machines and the construction itself on which they are located. The impact of vibrations can be viewed from different aspects, and most often the focus is on the harmful impact on the worker, unsafe work and the impact on the building structure on which the machine is located. The measurement and analysis of vibrations have a significant role in the protection of workers who are in the environment and under the influence of vibrations and are subject to constant improvement with the aim of protecting people's health. However, there are other aspects of the impact of vibrations that are significant for industry, primarily the impact on precision machines that cannot work in the nominal mode of operation for which they were designed, precisely because of the existence of vibrations originating from devices and machines located in the immediate industrial environment. This paper will present the results of measuring the impact of vibrations on precision machines and objects in such a working environment.

2. VIBRATIONS MEASUREMENTS

The diagnosis and correction of motor vibration problems are of paramount importance in avoiding costly downtime and ensuring the efficient operation of industrial plants. Since vibration analysis can provide information about the underlying causes of vibrations, such as imbalance, misalignment, bearing problems, or other mechanical faults, it is a useful technique for identifying and diagnosing early machine and equipment failures [4].

Various methods and types of vibration measurement are employed in the industry, with sophisticated devices and analysis techniques being widely available [3]. The proper selection and application of these methods can significantly improve the accuracy and reliability of vibration measurements, leading to more effective diagnostics and condition monitoring [4].

One of the key aspects of vibration measurement in industrial plants is the understanding of the different sources of vibration and their influence on machine performance. Factors such as motor speed, load, and environmental conditions can all contribute to the observed vibration patterns, and a comprehensive analysis is necessary to identify the root causes of the observed vibrations.

In a study on motor vibration problems, it was found that the proper data collection and analysis techniques can accurately determine the true source of the vibration, allowing for the implementation of appropriate corrective measures [7-10].

We notice that it is important to look at the operation of the surrounding devices, as well as the base on which it is placed, when the location of the machine is being installed [11].

In this paper, we consider the effects of vibrations on two different types of machines, the measuring machine HEXAGON type GLOBAL S and the production machine META V1800, the recommended and measured values of vibrations in its working environment, as well as their influence on the operation of that machine. Measuring machine "HEXAGON" type GLOBAL S has specified requirements regarding vibrations at the place of installation in order to be able to achieve the declared accuracy. The manufacturer, taking into account the technical solutions applied in the construction of the machine, defined the criteria that the machine's base should meet and submitted it as a condition for the customer to fulfill as an element of the contract declaring the machine's performance.

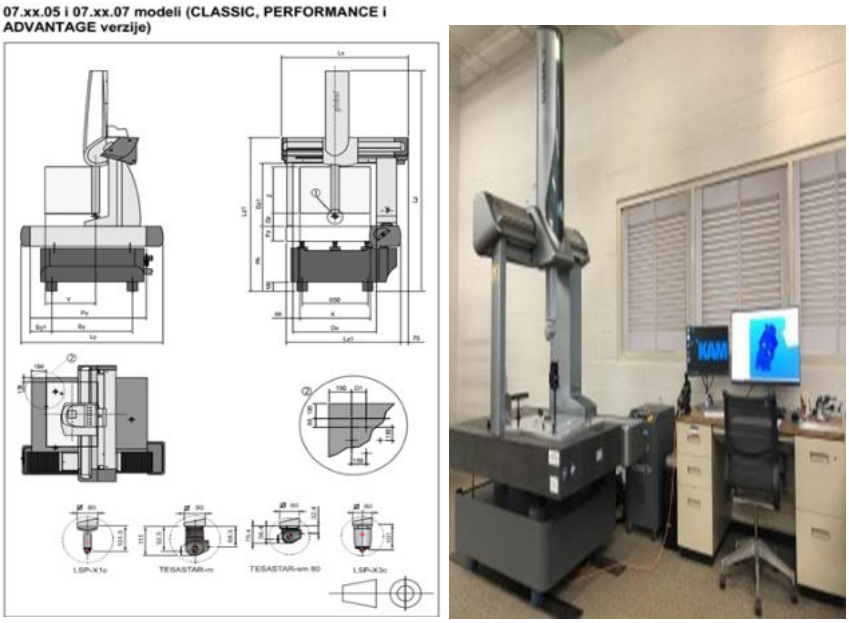

Fig. 1 a) Dimensions of the Hexagon Global S machine, b) appearance of the measuring machine in real space

Figure 1 presents the dimensions, functional schematics and representation in the real working environment of the analyzed machine. The manufacturer has fully defined the measuring points, the type and range of the measuring device that should be used to control vibrations, as well as the criteria that the substrate should meet at the place where the machine is installed.

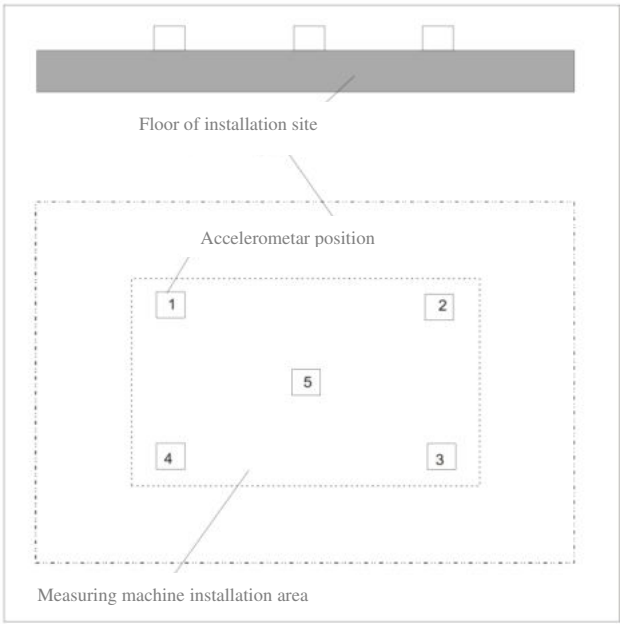

Fig. 2 Arrangement of measuring points for the installed machine

Figure 2 shows the arrangement of accelerators and measuring points for a machine placed on the floor without an anti-vibration pad in a real environment. It is noted that measurements are taken at five characteristic points on the substrate, according to the manufacturer's instructions.

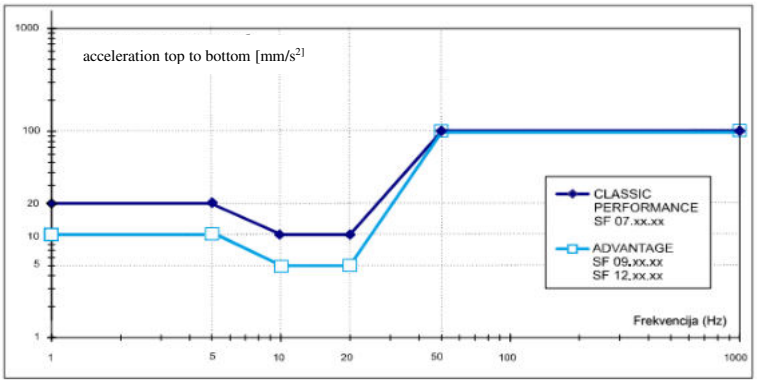

Fig. 3 Maximum vibrations allowed at the installation site (Passive anti-vibration support)

Figure 3 shows the maximum permissible vibrations at the characteristic points, given by the manufacturer, the first line represents the values for optimal operation in real conditions when classic accuracy of the machine is necessary, and when increased accuracy of the machine is required, the recommended values are read on the bottom line. By issuing detailed instructions on vibration measurement points on the base, the machine manufacturer protects himself from possible misunderstandings in the use of the machine and has prepared technical solutions for the operation of the machine in an environment that does not meet his requirements from the point of view of vibrations, so in those cases, anti-vibration support is used and other technologically available solutions.

Fig. 4. Bruel&Kjaer Vibroport 80 with piezoelectric acceleration measuring cell AS-063

For the purposes of writing this paper, the vibration of the substrate was measured at the place of installation of the machine, using the Bruel&Kjaer Vibroport 80 device with piezoelectric acceleration measuring cell AS-063, which is shown in Figure 4. The results were processed in the REO software of the same manufacturer. In order to avoid drilling the industrial floor at the installation site, an inertial weight (large mass) was used, to which the measuring cell was attached. The measurement results are tabulated according to the measurement scheme provided by the machine manufacturer.

According to the detailed instructions of the machine manufacturer, all filters and measurement ranges were set with the REO software, which was highlighted by the machine manufacturer in their request.

Table 1 Measured values in measuring points

Measuring point	v_{pp} [mm/s]	a_{pp} [m/s^2]	g_{pp} [m/s^2]	FFT [peack]	f [Hz]
MT1V	14.55	0.154	0.0688g	0.010 [m /s^2]	0.60
MT1H	8.60	0.303	0.0186g	0.014 [m /s^2]	3.70
MT2V	15.86	0.358	0.0822g	0.302 [m /s^2]	50
MT2H	98.37	0.456	0.0542g	0.136 [m /s^2]	50
MT3V	17.61	0.387	0.0260g	0.245 [m /s^2]	50
MT3H	55.03	0.313	0.0308g	0.247 [m /s^2]	50
MT4V	7.41	0.280	0.0288g	0.265 [m /s^2]	50
MT4H	5.35	0.305	0.0925g	0.282 [m /s^2]	50
MT5V	12.75	0.926	0.116g	0.295 [m /s^2]	50
MT5H	11.63	0.599	0.0541g	0.288 [m /s^2]	50

The measured values, in the measurement points shown in Fig. 2, are given in Tab. 1 and represent measurements in all 5 characteristic points in two axes, vertical and horizontal, due to the operation of the surrounding machines in operation. All values are below the permissible for the "classic" and "advantage" operation of the machine, while at point MT2H, a slightly increased value appears compared to the remaining measured values. At the frequency of 50 Hz, at which the measurement was performed, the permissible vibration level is 100 [mm/s], and at this point, the value was measured at 98.37 [mm/s].

In addition to this approach to machine vibration measurements where the manufacturer declares its requirements, there is also a different approach by machine manufacturers. Namely, they ask to establish the impact on the surface where the machine is placed, and the manufacturer's design team decides whether and to what extent the measured vibrations affect the operation of their machine. Although such an approach is different, it actually contains the need to protect certain technical solutions of very expensive and unique machines. Thus, the impact of the machine's operation with shock effects on the base where the machine is installed was measured.

Fig. 5 Considered production machine in operating condition

The operational state of the manufacturing machine META V1800 is depicted in Fig. 5, which was analyzed in terms of the vibration level and the effect of its operation mode. Unlike the first case, where the manufacturer defined the required operating conditions, with this type of machine, the measurement results, shown in Tab. 2, were submitted to the machine manufacturer to assess whether the measured vibration levels would have an impact on the operation of this production machine.

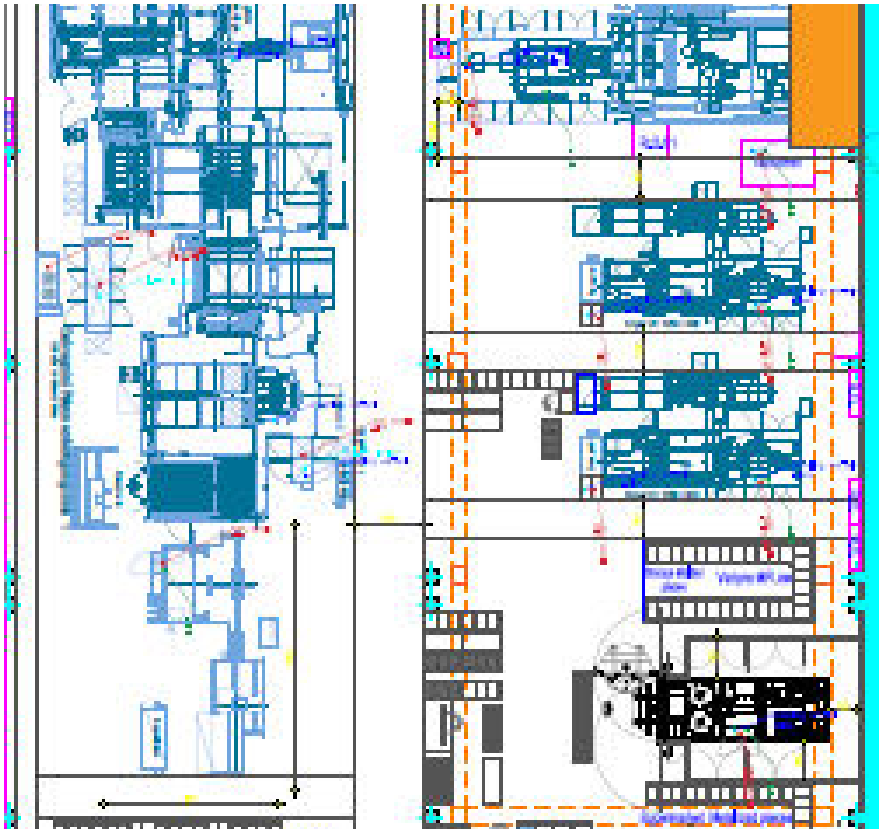

Fig. 6 Display of the arrangement of machines in the production plant

Figure 6 shows the layout of the machines that influence the production machine, where analyzed production machine is shown in black and researched the influence of the rest of the production plant on its operation.

Measurements were made at 24 measuring points in a grid around the machine and it was concluded with the consultation of the manufacturer that the values obtained from the measurement did not affect the operation of this machine, therefore further exploitation of the machine was started. In the first example, we had only 10 measuring points instead of 24 in the second example, and the main reason is that for the first we had recommendations and given measured values for non-obstructed work whereas the second manufacturer insisted that we measure in every point given in the instructions.

Table 2 Results of floor vibration speed measurements in the vertical direction

Measuring point	Vibration rate RMS (mm/s)	Vibration rate Peak-Peak (mm/s)
MT1	0.23	0.59
MT2	0.13	0.81
MT3	0.44	0.58
MT4	0.14	0.89
MT5	0.56	0.58
MT6	0.19	0.72
MT7	0.36	0.76
MT8	0.17	0.67
MT9	0.38	0.75
MT10	0.31	0.56
MT11	0.18	0.83
MT12	0.33	0.66
MT13	0.29	0.54
MT14	0.38	1.12
MT15	0.28	1.19
MT16	0.31	0.78
MT17	0.32	1.38
MT18	0.51	1.48
MT19	0.38	0.64
MT20	0.22	0.73
MT21	0.42	0.75
MT22	0.65	1.49
MT23	0.69	1.38
MT24	0.63	1.67

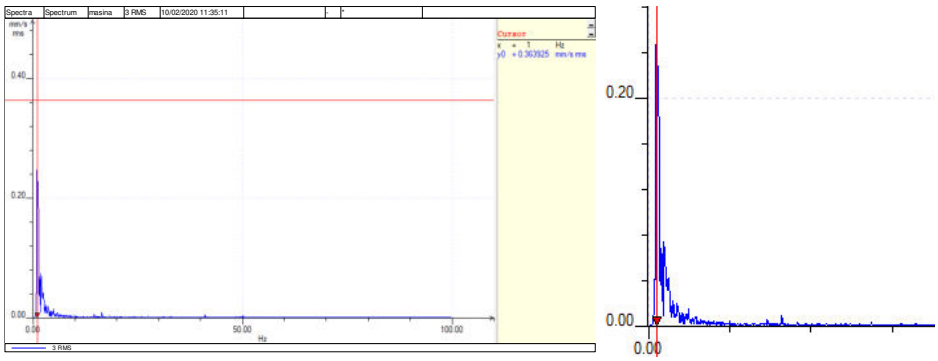

Fig. 7 Frequency diagram and enlarged part of the diagram from 0-30Hz, at one measurement point

Figure 7 shows a characteristic frequency diagram of measurements at one measuring point. Results and frequency diagrams were given to the machine manufacturer, who used them to determine that the operation of one production line did not affect the machine's operation so the machine was installed as intended and has been working for a long time without technical problems.

3. CONCLUSION

There are standards and norms for many aspects of the effect of vibrations, but they are mainly concentrated on the effect on the environment: servers or man as a working environment and construction objects as a working environment. In this paper, the machine is viewed as a working environment because it can only function under the conditions set by the manufacturer and according to the requirements regarding vibrations transmitted by the foundation. Manufacturers have different business policies to define what kind of vibrations are allowed for the operation of their machines or to ask for a vibration measurement to be performed and to conclude for themselves whether the vibrations present in the environment affect the operation of their machine. But in any case, modern and expensive machines also represent objects on which vibrations have a significant impact, and it is necessary to normalize the level of vibrations acting on the machines.

It is the fact that in addition to the workers who work on certain machines and the impact on the foundations of buildings, vibrations also affect the work of other machines and devices that are in the immediate environment, and this influence is absolutely important for precision and production machines with high-level accuracy.

Acknowledgement: *This research was financially supported by the Ministry of Education, Science and Technological Development of the Republic of Serbia, according to contract No.451-03-47/2023-01/ 200148.*

REFERENCES

1. Vulcu, O I., & Arghir, M. (2016, August 1). Impact of maintenance in the automotive field. Experimental study of mechanical vibration. IOP Publishing, 147, 012056-012056. https://doi.org/10.1088/1757-899x/147/1/012056
2. Alkaya, H Ç., & Görgülü, S. (2023, January 15). Investigation of Static and Dynamic Analysis of Asynchronous Motors in the Cement Industry. , 13(1), 7-11. https://doi.org/10.36222/ejt.1223666
3. Davis, J., & Bryant, R A. (2002, December 30). NEMA induction motor vibration measurement: a comparison of methods with analysis. https://doi.org/10.1109/pcicon.1993.337401
4. Gupta, K. (1997, June 1). Vibration — A tool for machine diagnostics and condition monitoring. Springer Science+Business Media, 22(3), 393-410. https://doi.org/10.1007/bf02744480
5. Au-Yang, M K. (1985, November 1). Flow-Induced Vibration: Guidelines for Design, Diagnosis, and Troubleshooting of Common Power Plant Components. ASM International, 107(4), 326-334. https://doi.org/10.1115/1.3264460
6. Davis, J., & Bryant, R A. (2002, December 30). NEMA induction motor vibration measurement: a comparison of methods with analysis. https://doi.org/10.1109/pcicon.1993.337401
7. Finley, W., Sauer, B J., & Loutfi, M Y. (2015, November 1). Motor Vibration Problems: How to Diagnose and Correct Vibration Errors. Institute of Electrical and Electronics Engineers, 21(6), 14-28. https://doi.org/10.1109/mias.2014.2345811
8. Urrea, C., Cisterna, R., & Kern, J. (2016, July 7). Virtual Instrument for the Analysis of Vibrations in Rotary Machines. https://doi.org/10.5772/63736
9. P. Girdhar and C. Scheffer, ''Practical Machinery Vibration Analysis and Predictive Maintenance'', ISBN 0 7506 6275 1, Elsevier.
10. D. Jovanović, N. Živković, M. Raos, Lj. Živković, M. Jovanović, M. Prašćević, ''Testing of level of vibration and parameters of bearings in industrial fan'', Applied Mechanics and Materials, Vol. 430, DOI 10.4028/www.scientific.net/AMM.430.118, pp 118-122, 2013.
11. ISO 10816-1 - Mechanical vibration -- Evaluation of machine vibration by measurements onnon-rotating parts -- Part 1: General guidelines

FACTA UNIVERSITATIS
Series: **Working and Living Environmental Protection** Vol. 21, Nº 4, Special Issue, 2024, pp. 427 - 433
https://doi.org/10.22190/FUWLEP241004041T

Original scientific paper

ADVANTAGES AND DISADVANTAGES OF VECTOR SENSORS COMPARED TO CLASSICAL ACOUSTIC SENSORS AND ACOUSTIC ANTENNAS

UDC 623.46:534

Tihomir Trifonov[1], Yavor Boychev[2], Ivan Ivanov[2]

[1]Vasil Levski National Military University, Veliko Tarnovo, Bulgaria
[2]Institute of Metal Science, Equipment and Technologies with Hydro- and Aerodynamics Centre "Acad. A. Balevski", Bulgarian Academy of Sciences, Sofia, Bulgaria

ORCID iDs: Tihomir Trifonov https://orcid.org/0000-0002-9649-4396
Yavor Boychev https://orcid.org/0009-0009-7681-8398
Ivan Ivanov N/A

Abstract. *The report examines the characteristics, advantages and disadvantages of vector acoustic sensors used in recent years in civil and military information systems for the detection, localization and classification of various types of targets and noise sources with high dynamics of emitted signals. A comparison with classical acoustic sensors and discrete acoustic antennas is given. Conclusions and recommendations are made. They are based on a review of publications and experiments.*

Key words: *acoustic sensors, weapon systems, battlefield detection*

1. INTRODUCTION

Increasing the efficiency of all acoustic systems is directly related to improving the signal/noise ratio [1,2]. In this regard, one of the most important elements of these systems is the acoustic sensor, which perceives and converts information. It can be a single sensor or a group of sensors constructed as an antenna array. In some cases, groups of sensors located at long distances are also grouped to obtain as large a base as possible. All subsequent processing of the signals and ultimately the adoption of one or another solution depends on the characteristics of the sensor.

It is clear that obtaining as much information as possible about the acoustic field at any set spatial volumes can be done by the optimal placement and increase in the number of

Received October 4, 2024 / Accepted November 7, 2024
Corresponding author: Tihomir Trifonov
Vasil Levski National Military University, Veliko Tarnovo, 76, Bulgaria Blvd., 5000, Veliko Tarnovo
E-mail: TihomirTrifonov@ieee.org

pressure sensors or by additionally placing receivers of the first or higher order. This allows us to obtain both the sound pressures and their gradients, bi-gradients, etc.

A few decades ago, sound pressure gradient receivers were used for the first time in certain acoustic equipment in a one-dimensional, two-dimensional and three-dimensional version. The three-component sound pressure gradient receiver whose sensors are located along the three orthogonal axes with one phase center is commonly referred to as the vector receiver [3,4].

The main advantage of a vector receiver is that it can determine the location of the sound source from a point without the need for an antenna configuration from multiple pressure receivers. This is particularly important for acoustic signals and noises in the low-frequency audible and near and far infrasonic ranges. If a classic discrete antenna array is used, the antenna aperture would be extremely large. In some cases, as in sound-ranging systems, it is necessary to use acoustic groups of sensors spread in space at a distance of hundreds of meters [5] or even kilometers with additional time delay processing and other characteristics of the received signals (most often pulsed).

2. Classical Antenna Systems

One way to improve the signal/noise ratio is to use acoustic antennas, most often in the form of antenna arrays. It is generally known that when hypothetical point acoustic transducers are located at a distance of less than or equal to half a wavelength $d \leq \lambda/2$, the directivity characteristic is equivalent to that of a continuous antenna with the same aperture. It is important to note that the directivity diagram is obtained for the far field of the antenna, where the intensity of the sound drops inversely with the square of the distance, that is, by a spherical law. The district is called the Fraunhofer zone. For a flat emitter, the distance r to its near limit is determined by the formula [1,2]:

$$r \sim \frac{d^2}{\lambda} \tag{1}$$

where λ is a wavelength in meters, d is the largest linear emitter size.

One of the most important parameters of the antenna is the normalized directivity diagram, which is found as the ratio of the spatial directivity diagram A (α, φ) to its meaning in the direction of maximum pressure A (0.0):

$$R(\alpha, \varphi) = \frac{A(\alpha,\varphi)}{A(0,0)} \tag{2}$$

It is obvious that the meaning of the normed directivity diagram is always less than or equal to one.

The concentration coefficient is another very important parameter. It is obtained as a ratio of the intensity of the axis of the antenna to the intensity at the same point of a non-directional emitter at the same power of the two instruments. Its approximate meaning can be determined by the formula:

$$\gamma = \frac{4\pi S}{\lambda^2} \tag{3}$$

From the above ratios, it can be concluded that as the frequency of the sound wave decreases, the dimensions of the antenna at the same set directionality increase. The

problem is particularly large with low sound and infrasonic frequencies. As is known, the absorption of the energy of acoustic waves is proportional to the square of their frequency [1]. For example, a sound wave with a frequency of 1000 Hz loses 90 % of its energy at a distance of 7 kilometers at sea level, if the frequency is 1 Hz, this distance is 3000 kilometers [5]. In addition, firing conventional fire systems creates extremely wide-spectrum noise that contains infrasound, sound and ultrasound. Therefore, acoustic direction finders built according to the classic scheme use a measuring base with a length of several hundred meters and pressure sensors. Different types of antenna arrays are commonly used to study battlefield acoustics in modern acoustic information systems [5,6,7]. They must form a directional beam over a wide frequency range. In principle, two sound receivers are required to determine the direction of the sounding target. However, two more receivers are needed to determine the coordinates of the target (classical principle of triangulation). A third pair of receivers is used for greater accuracy. A third receiver (microphone) can be placed in the center of the acoustic base. Accuracy increases even more.

3. Vector Receivers

The one-dimensional velocity sensor measures the speed of air movement through two small, resistive strips of platinum that heat up to 220°C [8,9], Fig. 1. In acoustics, this movement of air is called the oscillation velocity of particles. When the air passes through the strips, the first strip cools a little and therefore the air is heated. The second strip is therefore cooled with slightly heated air and cooled less than the first conductor. A temperature difference occurs in the wires and causes a difference in their electrical resistance. This results in a voltage difference that is proportional to the particle velocity and the effect is directional: when the direction of the airflow changes, the temperature difference will also change. In the case of a sound wave, the airflow through the strips alternates depending on the waveform and thus the direction can be determined. In Fig.1, a three-dimensional vector sensor is shown. For comparison, a match was photographed together with him. The right panel shows a similar sensor mounted on the Colt C8 along with a miniature microphone, as well as a Microflown-Avisa shot detection system.

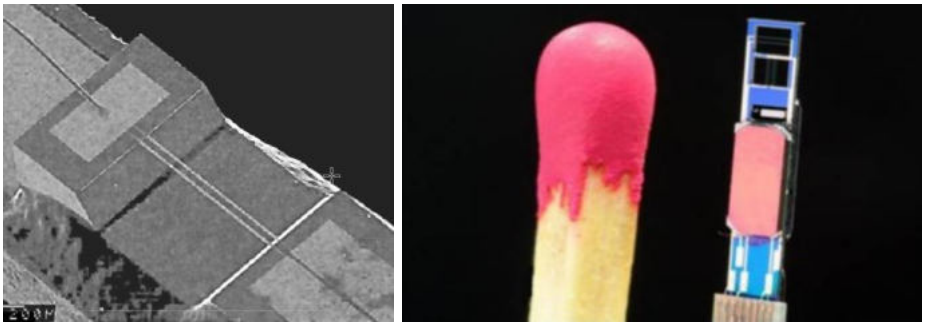

Fig. 1 One-dimensional vector sensor (particle velocity sensor) - the left panel. A three-dimensional vector sensor was photographed on the right panel. In comparison, a match was photographed with him

Fig. 2 A three-dimensional vector sensor mounted on the Colt C8 along with a miniature microphone [7] is shown on the left panel. On the right panel is the Ground-Based Gunshot Localization System – GBGLS, http://microflown-avisa.com/products/ground-based-gunshot-localisation/, equipped with a similar sensor [8]

4. Some Results and Conclusions

Over the past year, our team has taken acoustic measurements of various types of conventional weapon systems. The experiments were conducted at the Belyakovets shooting range, near the city of Veliko Tarnovo in June and at the Markovo training ground, near the city of Shumen, in September.

To obtain the raw acoustic signal, a Type 4193 wideband measuring microphone, combined with a classic Type 2669 low noise preamplifier and a compact 35608 Bruel&Kjaer data acquisition module, was used. In addition, an acoustic antenna array with 30 microphones of the same company was also used - Figs. 3 and 4.

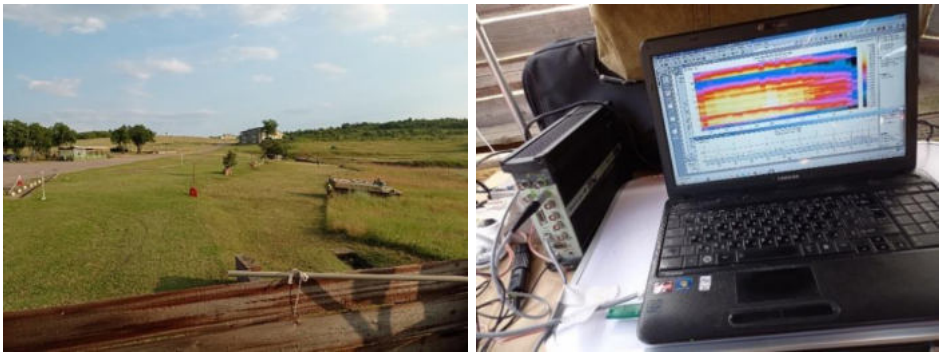

Fig. 3 On the left panel: Belyakovets shooting range; on the right panel: a typical measurement screen with a compact data collection module 35608 Bruel&Kjaer

Fig. 4 Conducting measurements during a complex tactical exercise in the village of Belyakovets. The antenna array of a Bruel&Kaer acoustic camera is visible

Fig. 5 Conducting demonstration shootings at the range in the village of Markovo, 24-26.09.2024. On the left panel 152 mm howitzer D20, on the right panel 122 mm SAU Gvozdika

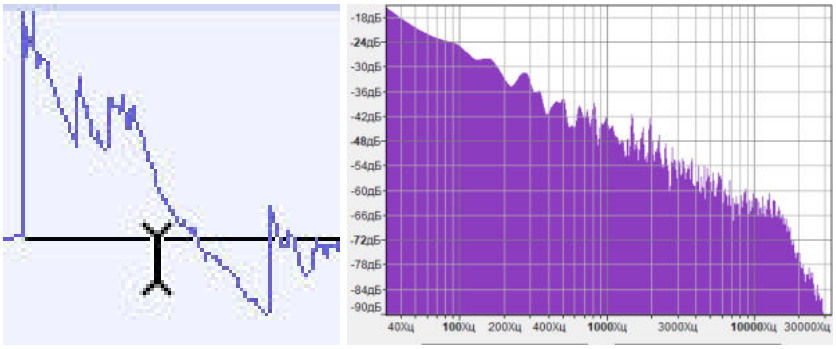

Fig. 6 Conducting demonstration shootings at the range in the village of Markovo, 24-26.09.2024. On the left panel, a recording of the muzzle wave of the 122 mm Gvozdika self-propelled gun, on the right panel, the spectrum of the shot

Explosive propelled weapons produce their characteristic sound as a result of the rapid expansion of gases at the end of their barrel, formally known as muzzle blast. The second component is the shock wave created by supersonic projectiles. It is commonly called N-wave due to its characteristic geometry and, unlike the muzzle blast, it has a local influence since it only appears at distances close enough to the trajectory of the projectile. In close-range recordings, ground reflections from both muzzle blasts and shock waves, along with the sound produced by the firing mechanism of the weapon, are most likely overlapped with the direct signal. From the spectrum of the shot shown in Fig.6 it is seen that, as might be expected, the acoustic energy is concentrated in the region of the low and infrasonic frequencies.

The acoustic situation on the battlefield has extreme, complex and multifaceted parameters. Different weapon systems, vehicles and the human factor create high-intensity noises and sounds, a large dynamic and frequency range. In addition, they are of different duration, directionality and spectral composition. The frequency range extends from infrasound at near zero frequency to ultrasound of several tens of kilohertz. This necessitates the use of complex acoustic and seismic systems for the detection, localization and classification of sources.

As emphasized above, the expertise of the authors who for many years designed, constructed and analyzed acoustic and hydroacoustic equipment allows us to draw the following important conclusions:

- acoustic sensors are at the beginning of the signal processing system. Therefore, the quality of the entire system depends on its parameters;
- sensors must have a maximally simplified construction, small dimensions and mass and be resistant to climatic and other effects;
- sensors must be easily maskable;
- the main advantage of acoustic detection systems is that they are passive;
- modern technologies make it possible to construct microphones with a sufficiently wide bandwidth - from infrasonic to ultrasonic frequencies;
- recent technological advances allow the creation of miniature acoustic vector sensors that make it possible to replace discrete acoustic antenna arrays that take up a lot of space and are easily detectable by the potential opponent.

Acknowledgement: *This report is supported by the National Scientific Program "Security and Defense", approved by Decision № 171/21.10.2021 of the Council of Ministers of the Republic of Bulgaria.*

REFERENCES

1. Trifonov T., Foundations of Audio Engineering, Publ. of Ministry of Defense, " St. George the Victorious", Sofia, 1995, p.198
2. Dragan Cvetkovic, Momir Prascevic, Noise and Vibration, Nis, 2005, ISBN 86-80261-45-9, p.293
3. Trifonov T., I. Ivanov, N. Iordanov, Overview of acoustic sensor systems for obtaining and analyzing information from the battlefield, In Proceedings of the Annual University Scientific Conference on 08-09 June 2023, Publ. by NMU "Vasil Levski", Veliko Tarnovo, ISSN 2367-7481, pp.1483-1490
4. Trifonov T., I. Ivanov, Modern Acoustic Sensors Used for Battlefield Detection, Acoustics, year XXV, vol. 25, July 2024, ISSN 1312-4897, pp.72-79
5. Tihomir Trifonov, Nonstandard Applications of the Infrasonic and Hydroacoustic Components of the International Monitoring System of Nuclear Explosions, In Proceedings of the 14th International Engineering Conference on Communications, Electromagnetics and Medical Applications CEMA'21, 2021, pp. 15-19, ISSN: 1314-2100
6. Brüel & Kjær, Knowledge-center, https://www.bksv.com/en/Knowledge-center
7. Tactical Infrasound, Study Leader: Christopher Stubbs, JASON, The MITRE Corporation, 2005, p.73
8. https://www.microflown.com
9. D.R. Yntema, J.W. van Honschoten, H.-E. de Bree, R.J. Wiegerink, M. Elwenspoek, A Tree Dimensional Microflown, In Proceedings of the IEEE International Conference on Micro Electro Mechanical Systems (MEMS), January 2006, pp.654-657, DOI: 10.1109/MEMSYS.2006.1627884

FACTA UNIVERSITATIS
Series: **Working and Living Environmental Protection** Vol. 21, Nº 4, Special Issue, 2024, pp. 435 - 446
https://doi.org/10.22190/FUWLEP241028042L

Review paper

SENSING WITH SOUND: IMPROVING GASES AND SOLID ANALYSIS BY PHOTOACOUSTIC SPECTROSCOPY

UDC 534.42

Mladena Lukić[1], Katarina Đorđević[2], Žarko Ćojbašić[3], Dragan Markushev[4]

[1]University of Niš, Faculty of Occupational Safety in Niš, Niš, Serbia
[2]University of Belgrade, Vinča Institute of Nuclear Sciences, Belgrade, Serbia
[3]University of Niš, Faculty of Mechanical Engineering, Niš, Serbia
[4]University of Belgrade, Institute of Physics, Belgrade, Serbia

ORCID iDs:	Mladena Lukić	https://orcid.org/0000-0003-1105-3637
	Katarina Đorđević	https://orcid.org/0000-0002-1397-8011
	Žarko Ćojbašić	https://orcid.org/0000-0002-4581-1048
	Dragan Markushev	https://orcid.org/0000-0002-0330-3600

Abstract. *The development of photoacoustic spectroscopy is being driven by the growing demand for precise, efficient, and reliable detection methods that can be used for in situ measurements and real-time monitoring. Along with rapid technological progress, photoacoustic spectroscopy became an ultra-sensitive, selective, cost-effective technique that can meet the demanding requirements for environmental monitoring, industrial safety, and medical diagnostics. This paper highlights how continuous improvements in photoacoustic technologies, including the use of appropriate laser sources as well as sensing elements, and machine learning methods, are pushing the limits of gases and solid analysis and providing critical tools for addressing modern scientific and industrial challenges.*

Key words: *photoacoustic spectroscopy, trace gases analysis, material characterization, photoacoustic imaging, machine learning*

1. INTRODUCTION

To meet the evolving demands for detecting and monitoring of a variety of phenomena regarding environmental pollution and climate change, industrial process control and workplace safety, agriculture and food industry, as well as medical diagnostic, modern detection techniques should fulfill very stringent criteria. Greenhouse gases, ozone, and toxic and flammable gases, known as trace gases, usually have concentrations in the range

Received October 28, 2024 / Accepted December 4, 2024
Corresponding author: Mladena Lukić
University of Niš, Faculty of Occupational Safety, Čarnojevića 10a, 18000 Niš, Serbia
E-mail: mladena.lukic@znrfak.ni.ac.rs

of ppm (parts per million)[1]. Traditionally, non-optical and optical methods have been used for concentration measurement. Non-optical methods (chromatography and mass spectrometry) regardless of high sensitivity, can be time-demanding and inappropriate for real time and field measurements or can suffer from stability and sensitivity (electrochemical and semiconductor sensors). Optical gas sensing methods stand out as highly sensitive and selective, with fast response time, allowing real time in situ measurement.

Over the years, photoacoustic spectroscopy (PAS) as an optical, laser-based detection technique, has evolved into a powerful, highly sensitive (from ppm to ppt range of concentration), selective, robust, cost-effective, and easy handling technique with large dynamic range (several orders of magnitude in concentration) [1].

PAS combines optical and acoustic phenomena, converting optical into acoustic energy. Photoacoustic (PA) effect occurs when a sample (gas, liquid, or solid) absorbs modulated or pulsed laser radiation. Localized sample heating led to generations of pressure (acoustic) waves, which are typically detected by appropriate detectors (usually microphones). PAS enables non-invasive, sensitive investigations of samples. Along with rapid technological progress and the development of lasers and sensors, PAS has been recognized as impactful in many areas: trace gas detection, industrial process control, chemical reaction dynamics, monitoring of deexcitation processes, investigation of thermoelastic and other physical properties of materials, acoustic-electronic properties of semiconductors, medical imaging, human breath diagnosis, and many others. This paper provides a brief review of some modern PA applications in gaseous, solid sample analysis, and medical diagnostics, to highlight the versatility and huge potential of PA application. Also, a review of some machine learning implementations in PAS analysis has been given.

Trace gas detection by PAS offers multi-component and real-time, in situ detection with no need for sample preparation. Industrial applications of PAS provide continuous monitoring and detection of toxic, flammable gases, hazardous gas leaks, emissions control and workplace safety. PA technique is suitable for the study of thermal and optical characterization of a wide range of liquids (from optically transparent to opaque), measurement of pollutant concentration, etc. Material characterization by PAS provides detailed insights into mechanical, thermal, and structural properties. The propagation of PA waves is influenced by the material's characteristics, allowing precise analysis of its physical features [2]. This technique is especially beneficial for opaque, nontransparent materials where traditional optical methods are not applicable. Novel PAS applications are focused on medical diagnostics, offering non-invasive, non-ionization accurate, and fast analysis [3]. Photoacoustic imaging (PAI) is used to visualize the mechanical and optical properties of soft tissues. Utilizing the acoustic waves generated by light absorption in tissues, PAI provides high-resolution images of biological structures.

2. TRACE GASES ANALYSIS BY PHOTOACOUSTICS

The PA effect was discovered by Alexander Graham Bell in 1880. He found that a solid sample can generate sound when it is illuminated by an interrupted beam of sunlight. The discovery was neglected for years due to the lack of suitable light sources and detectors. After the laser invention, PA effect has sparked a keen interest and its widespread use has started. The high spectral brightness of the laser, and appropriate techniques for acoustic

[1] Concentrations are expressed as parts per million 10^6 (ppm), billion 10^9 (ppb) or trillion 10^{12} (ppt), by volume.

signal amplification enable the determination of low concentrations of air pollutants. Inspired by the encouraging results of Kreutzer's measurements of methane (CH_4) concentration in the ppb range (1971.), many researchers started to apply PAS in various scientific fields [4].

A PA signal is generated by the absorption of laser radiation in a sample. To achieve high sensitivity in trace gas detection, laser radiation must coincide with the absorption lines of the measured gas species. Photon energy in the infrared (IR) spectral region (called molecular fingerprint region, from 3 to 12 μm), excited molecule's rotational and vibrational energy state. Absorbed energy release via molecule collisions. The fastest relaxation type of absorbed IR energy is transfer from vibrational to translational modes of colliding molecules (V-T relaxation). Energy is released via V-T relaxation type heating the sample. Localized heat increasing the temperature causes pressure to rise. Since laser excitation can be continuous (modulated) and pulse, temperature and pressure vary periodically generating thermal and acoustic waves (Fig. 1).

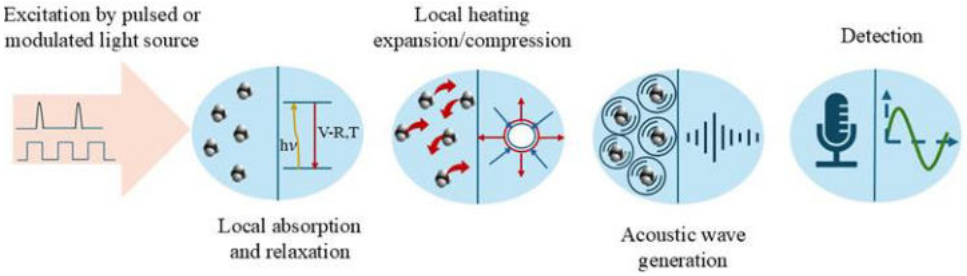

Fig. 1 Typical scheme for PA wave generation in a gas sample

Experimental arrangement for PAS measurement typically consists of a laser as a light source, a PA cell (for signal generation) and a detector (pressure sensing devices for sound detection). The commonly used light source in trace gas measurement is a laser with a narrow bandwidth, and wavelength that matches the absorption lines of investigated molecule species. PAS is an appropriate technique for trace gas concentration measurement, due to the proportionality between the intensity of the PA signal, absorbed energy and concentration of absorbing species [1,5]. This proportionality is valid for a wide range of concentration, (ranging from high concentrations in urban to small concentrations in rural environments). High-power lasers (CO_2, and CO lasers) are preferred sources in trace gas measurements, providing high sensitivity (in the sub-ppb range) and high selectivity. They are mainly used for laboratory experiments due to their cumbersomeness and complexity. Nowadays, more compact and appropriate forms for in situ measurements are available. In various areas of PAS application, different laser sources have been applied: diode laser, quantum cascade laser, Nd: YAG laser, light-emitting diode (increasingly used in PA applications in medicine), and many others.

The sensitivity of PA detection depends on the sensitivity of acoustic detectors, geometry and design of PA cells. Depending on operation (at an acoustic resonance or not) the PA cell can be described as resonant or nonresonant [5]. Sound waves in PA cells are detected by microphones (capacitive microphones are the widely used microphones for sound detection). To enhance the sensitivity of PA measurement and signal-to-noise ratio, different modifications of typical PAS arrangement have been designed.

To advance detection of trace gases by PAS quartz-enhanced photoacoustic spectroscopy (QEPAS) has been proposed [6]. The sensing element in the QEPAS setup is a quartz tuning fork (QTF), an efficient acoustic resonator that increases weak PA signals. QTF effectiveness has been proved in the detection of numerous gases at concentrations ranging from ppm to ppt. A recent review by Sampaolo et al. [6], emphasizes QEPAS's versatility in multi-gas detection including CH_4, nitrous oxide (N_2O), and carbon monoxide (CO). De Palo et al. [7] proposed QEPAS for the detection of eight air pollutants (CH_4, N_2O, CO, nitrogen dioxide - NO_2, carbon dioxide - CO_2, nitric oxide - NO, sulfur dioxide SO_2, and ammonia - NH_3), in the ppb concentration range underlining its ability for urban air quality monitoring. Lin et al. [8] introduced an all-optical off-beam QEPAS spectrophone based on double-pass acoustic microresonators, demonstrating advanced detection efficiency of CH_4 (2.41 ppm), and applicability in harsh environments and under strong electromagnetic interference. To achieve sub-ppb detection (of 54 ppt) of NO_2 (which is essential for controlling ozone formation), Yin et al. [9] developed a PA system with a differential PA cell and multimode diode laser. Further applications of QEPAS are explored in methane-based gas leaks, demonstrating hydrogen sulfide (H_2S) detection (of 2.5 ppm) in mixed gas environments [10]. The simultaneous detection of pollutants with overlapping spectra such as H_2S and CH_4 (from oil wells and refineries) is of key importance, due to potential environmental and health risks. A portable QEPAS sensor for real-time CO monitoring in urban areas, developed by Sgobba et al. [11] highlights the field-deployment potential of modern PAS systems. Zheng et al. [12] utilized near-IR telecommunication diode lasers for CO_2 detection in atmospheric conditions. A wide dynamic range of PAS detection of several orders of magnitude is an especially important feature for long-time monitoring in the chemical industry, warfare agents and explosives. For example, atmospheric NH_3 concentrations can range from a few ppb to hundreds of ppb in polluted areas, and up to hundreds of ppm in industrial plants following leaks [13].

Trace gas detection of volatile organic compounds (VOCs) emitted mainly from transportation, engine exhaust, and refineries, including benzene, toluene, ethylbenzene, and xylene, are of great importance due to their health impact, even at ppb levels. Advanced methods for detecting VOCs using long-wavelength quantum cascade lasers have been investigated by Kinjalk et al. [14]. Further improvement of PAS sensitivity (more than one order of magnitude) is achieved using a micromechanical cantilever as a sensing element in the cantilever-enhanced PAS proposed in [15].

The main advantages of PAS are adaptability and the capability to satisfy specific measurement requirements for sensitive and selective detection of various gas species, by replacing laser source, cell or sensing element with a suitable one.

3. Material Characterization by Photoacoustics

The underlying mechanism of PA generation in solid and liquid samples has some common characteristics. The dominant mechanism of PA wave generation in liquids is thermoelastic mechanisms. Laser radiation heated a limited volume of liquid causing a temperature gradient which leads to the strain and PA wave formation. Using this mechanism, the optical and thermal properties of liquids can be measured, Also, flow speed and liquid viscosity measurement by PA technique are very important in medical diagnostics.

PA signal in a solid sample is created after complex thermomechanical processes. As a result, the PA signal provides valuable information of the thermal, optical, and elastic

characteristics of the sample. Accordingly, the PA technique has been widely applied for the study of sound velocity, temperature, thermal diffusivity, thermal conductivity elasticity, flow velocity, specific heat, thickness, subsurface defects, material discontinuities, crystallinity, phase transition and many others [2]. Nowadays, along with the rapid development of renewable and sustainable energy technologies, thermal conductivity and diffusivity measurements are crucial for the selection of materials that can be used in thermoelectric energy conversion, thermal energy storage, sensors, etc. Some applications require materials with low thermal conductivity (to minimize heat leakage), while other high thermal conductivity is needed to enhance heat transfer and energy efficiency [16]. Measurements of the thermal properties of materials, especially those with nanoscale dimensions (e.g., thin films, nanowires), are very demanding. PAS is a contactless, non-destructive technique, applicable for in situ measurement. The PA method has proved to be very successful for the study of totally opaque materials, and light scattering materials (powders), where conventional spectroscopy is not usable or provides inadequate results.

PA signals can be generated directly in a sample that absorbs light energy. Otherwise, it is generated indirectly within a medium adjacent to the sample, such as a solid-gas-microphone configuration (mostly used in the thermal, optical and mechanical study of solids). After absorption of electromagnetic energy, thermal diffusion takes place, leading to elastic stress as a result of thermal expansion. Theoretical explanation of PA signal generation in solids was developed by Rosencwaig and Gersho [17] and extended by McDonald and Wetsel which include thermally induced mechanical vibration of the sample surface [18]. Based on the underlying processes of the PA generation, two components can be distinguished: a thermodiffusion (caused by thermal diffusion mechanism dominating at a low frequency), and thermoelastic (caused by thermoelastic expansion and bending, dominating at high frequency). In semiconductors, the PA signal has an additional plasmaelastic component (originates from mechanical strain due to carrier recombination) [19]. Important information about the thermophysical and optical characteristics of the sample can be obtained by analyzing PA signal amplitude and phase dependency on frequency [20]. Thermal conductivity and diffusivity are important characteristics of semiconductors, polymers, ceramics, and composites. Also, PA can be used to evaluate the elastic properties of a material, especially in thin films [21,22,23]. Acoustic waves generated by the PA effect carry information about the thickness of each layer and any imperfections at the interfaces. This makes PA ideal for characterizing materials in microelectronics and coatings [24]. PA technique has been applied in determining the reflection coefficient and thermal diffusivity of a specific metal mirror, characterized by high reflection coefficient [25].

The possibility to develop a PA experimental setup according to specific measurement requirements is a considerable advantage of the PA technique (open or closed PA system configuration, depending on sample properties to be measured) [21,22,23]. Commonly used acoustic detectors are microphones for pressure variation detection (condenser or electret microphone) or piezoelectric devices more suitable for PA detection in solids. Although there are many different sensors for PA detection such as fiber optics, electromagnetic acoustic transducers, the Michelson interferometric system, etc. Also, PA configuration for solids can be adjusted to in situ measurements [26].

It is interesting to note that PAS can play a significant role in fundamental research in physics. Extremely fast relaxation phenomena and nonequilibrium processes have not been well described up until now, because orders of magnitude for relaxation times of various subsystems in condensed matter are unknown (even approximately). The theoretical

prediction ranges from 10^{-14} s (for metals and superconductors) to 10 s (for biological tissues) [27]. According to theoretical predictions in complex systems such as noncrystalline solids, polymeric materials, or biological tissues, the influence of these relaxations could be expected in simple experimental setups, while, in crystals and 2D crystals relaxations impact could be expected in the nanosecond range or shorter. The development of modern detectors, ultra-fast electronics, pico- and attosecond lasers have accelerated the enhancement of experimental PAS setups which could detect relaxation phenomena even in highly ordered interior structures of condensed matter. However, one of the obstacles to characterizing relaxation phenomena by PAS or other methods is the lack of a theoretical model which is essential for the analysis and interpretation of experimental results. Most models of PAS signals are based on classical Fourier heat conduction theory, which is inherently approximative and established at the phenomenological constitutive relation (Fourier's constitutive relation) [28]. Nowadays, in scientific literature for modeling PAS signals generalized theories of heat conduction have been increasingly used: from hyperbolic theories [29,30,31,32], and the dual-phase lag theory [33], to fractional theories of anomalous diffusion [34,35,36]. Using a highly sophisticated PAS experimental setup and the hyperbolic heat conduction theory thermal relaxation time (in the nanosecond range) is measured in 2D graphene lattice at temperatures above 100 K and 200 K [37, 38].

4. Medical Application of Photoacoustics

PAS has been used as a promising tool in a various medical application: qualitative and quantitative analysis of pharmaceutical drugs, human breath diagnosis, breast cancer diagnosis, detection of cardiovascular disease, blood oxygenation levels monitoring, and others. The medical use of the PA technique is mainly focused on photoacoustic imaging (PAI) [3,39,40]. Imaging biological tissues plays a crucial role in diagnostics of diseases. Commonly used techniques include magnetic resonance imaging (MRI), X-ray computed tomography (CT), and positron emission tomography (PET). While these techniques are widely used, they have drawbacks such as potential health risks from ionizing radiation, limited mobility, and high costs. In contrast, PAI offers a noninvasive, nonionizing alternative, leveraging the PA effect. In PAI short laser pulses (in the nanosecond range) irradiate biological tissues whose components absorb photons, and subsequent localized heating and thermoelastic expansion occur. This process generates megahertz-range ultrasound (US) waves that can be detected and used to reconstruct images. PAI stands out because of its ability to provide high-resolution and deep-tissue imaging, outperforming purely optical techniques, which suffer from significant scattering with increasing depth. Compared to optical scattering in soft tissues, which greatly reduces spatial resolution with depth, US scattering in biological tissues is two to three orders of magnitude weaker, allowing clearer imaging at greater depths [41]. However, PA wave propagation is influenced by both scattering and absorption within the tissue, and attenuation varies based on tissue type and frequency. PA signal is determined by energy deposited in a tissue, scattering characteristics, thermal properties (thermal diffusivity and thermal expansion coefficient), and the elastic features of the tissue.

Frequently used excitation source in PAI is a pulsed Q-switched Nd: YAG laser. Recently, more economical, low-cost laser sources such as laser diode and LED have been used as suitable for portable PA sensing and imaging systems [42,39]. PA signals are detected by a US sensor placed around the sample surface [39]. The commonly used sensor

for US detection is piezoelectric crystal, which converts pressure change to an electrical signal. Also, optical detectors with wide bandwidth can be used for sensitive US detection. Numerous novel technical solutions of PA are developed into various imaging modalities [39]. PA signal analysis can generally be performed in both the time and frequency domains. In the time domain, key characteristics of the sample - such as optical absorption, absorber position, and absorber size - can be inferred from four main parameters of the PA signal: amplitude, time delay, signal width, and relaxation time. Different optical absorption properties between normal and pathological tissues result in variations in PA signal amplitude, providing high contrast and aiding in tissue differentiation. The time delay offers critical information about the depth of the absorber and, together with the PA signal, is crucial for accurate image reconstruction [3]. Various algorithms have been developed to solve inverse problems in PA image reconstruction (backpropagation, iterative reconstruction methods, and others) [40,41]. The choice of algorithm is the trade-off between image reconstruction accuracy and computational efficiency. To improve PAI contrast and sensitivity, reference [43] suggests using plasmonic hetero-nanoparticle with broadband transient responses and wavelength tunability, for precise control of light absorption and heat conversion. Those characteristics could be crucial for high-resolution imaging applications in biomedical imaging and diagnostics.

Unlike traditional US diagnostics, PAI provides valuable information about tissue composition by exploiting the wavelength-dependent absorption of optical energy. Tissue chromophores - such as hemoglobin, lipids, proteins, water, and melanin - absorb light at specific wavelengths, which enables targeted imaging for various medical conditions. By selecting appropriate excitation wavelengths, PAI enhances the detection and diagnosis of cancers and hematological disorders. Major biomedical applications of PAI include brain imaging, arthritis detection, arterial plaque identification, and diagnostics for hematological diseases and cancers [39].

Human breath analysis represents another important medical application of the PA technique. It has been established that many exhaled compounds can reflect both physiological and pathophysiological states, offering diagnosis of various diseases [44]. Compounds such as NH_3, NO, H_2S, and VOCs are byproducts of normal metabolism, while others may be caused by different reasons. PA sensing offers a noninvasive, real-time, sensitive detection in the ppm to ppb range [44,45]. Additionally, using the PA technique for breath analysis it is possible to detect bacterial infections [45].

5. Intelligent Photoacoustics

In the realm of PA analysis, one of the key challenges is the inverse problem - reconstructing the physical properties of a sample, such as gas concentration, material and tissue characteristics, from the measured PA signals [46]. The complexities of PA analysis, including multiparameter function, nonlinearity, and noise, along with the need for real-time processing, pattern recognition, classification, and optimization, make AI and machine learning - ML (as a subcategory of AI) a highly suitable tool for PA applications. AI's adaptability allows it to handle nonlinear, ill-defined, incomplete, and noisy data while offering rapid signal processing, real-time operation, and high accuracy and sensitivity.

In trace gas analysis, the complexity of multi-gas mixtures, potential interferences between components, noise, and variations in experimental parameters often affect the precision of PA

detection. The generated PA signal depends on numerous factors, including the sample's absorption properties, laser parameters (wavelength, modulation frequency, fluence), detector characteristics, temperature, pressure, and others. Variations in these parameters during experiments can influence the PA signal. Solving the inverse problem by extracting gas sample characteristics (such as concentration, relaxation time, and optical absorption coefficient) and experimental parameters (such as the spatial profile of the laser beam) have traditionally relied on algorithms that are time-consuming and sensitive to initial parameter selection [47,48]. Artificial neural networks (ANNs), highly parallel connectionist systems, offer a faster alternative, enabling real-time analysis by processing data more efficiently than traditional methods. As adaptive systems, ML algorithms improve performance over time, refining estimations and accuracy without relying on exact mathematical models. ANNs have been successfully applied for simultaneous estimation of PA signal parameters, such as the spatial profile of the laser beam and the V-T relaxation time of molecular species [49]. Real-time, and accurate estimation of parameters by ANNs allows correction of laser parameter variations during experiments, preventing overlaps in absorption efficiencies among different gases.

To address fluence variation based on PA signal analysis, Lukic et al. applied another technique designed for dealing with imprecise or fuzzy data: the adaptive-network-based fuzzy inference system (ANFIS) [50]. In practical applications of PAS for trace gas analysis, an optimization procedure is required to calibrate and fit the measured PA spectrum with a reference spectrum. As an effective method for function optimization metaheuristic algorithms have been applied to resolve challenges in determining optimal values and multiple PA signal parameters. The effectiveness of several metaheuristic algorithms including genetic algorithms (GA), particle swarm optimization (PSO), artificial bee colony (ABC), and simulated annealing (SA) in simultaneous determination of PA signal parameters has been compared in studies [51,52].

In material characterization, ML can be applied to solve inverse problems and predict key mechanical, thermal, and optical properties, thereby facilitating the characterization of complex materials, composites, semiconductors, and thin layers. ML-driven models can handle large datasets in real time, making the characterization process faster and more efficient. Semiconductors and thin layers, which play a crucial role in modern advanced electronic devices, particularly benefit from such approaches. Djordjevic et al. employed ANNs to simultaneously determine thermal diffusivity, thermal expansion coefficient, and thickness from the transmission and frequency-modulated PA response of a sample. Their results demonstrate that ANNs are an effective tool for the precise, real-time characterization of plasma-thick semiconductors [53]. In related work [54,55], researchers applied ANNs to characterize the thermoelastic and geometric properties of aluminum and thin aluminum samples, crucial for applications in thin films, micro- and nanostructures, polymers, and composite materials. Further studies have shown that ANNs are highly effective in estimating the thermal, elastic, and geometric properties of a thin TiO_2 film deposited on a silicon substrate [56]. ANNs combined with reverse-back procedures for analyzing the optical properties of semiconductors (such as absorption coefficient and reflection) enable the detection of light source variations and changes in the sample surface, as discussed in [57]. Additionally, ANNs can be trained to recognize microphone characteristics, preventing PA signal distortion during measurements [58].

PAI combines optical and ultrasound characteristics to provide high-resolution, spatially resolved images of optical tissue properties. However, determining key tissue parameters requires solving inverse image reconstruction problems. Traditional iterative techniques for

solving inverse problems are computationally costly and sensitive to the selection of initial parameters. To address these challenges, ML-powered image reconstruction algorithms, such as deep learning (DL), have been developed to enhance the spatial resolution and contrast of PA images. These algorithms learn from large datasets of medical images, enabling them to improve image quality even in difficult conditions, such as deep tissue imaging, where signal attenuation occurs. DL models can enhance image clarity, improving the visualization of small anatomical structures and early disease markers, such as tumors or vascular abnormalities [59,60]. For diagnostic purposes, ML, particularly DL techniques like convolutional neural networks (CNNs), can automatically segment and classify PA images, distinguishing between healthy and pathological tissues. This is particularly useful in oncology, where ML can aid in tumor detection and monitor disease progression. Moreover, ML algorithms can predict physiological parameters, such as blood oxygenation and hemoglobin concentration, from PA signals, contributing to non-invasive diagnostic assessments [55].

The successful application of ML techniques relies heavily on the availability of valid and extensive training data that accurately represents the problem at hand. Collecting such representative data often requires numerous experiments, which can be challenging and time-consuming. Additionally, neural network limitations can be slow and demanding training processes and the selection of appropriate datasets for training. Choosing the optimal network topology can also be demanding. On the other hand, metaheuristic methods are robust and reliable, capable of exploring a wide solution space and effectively handling noisy data. However, they also have their own limitations, such as the need to adapt to specific problems and the requirement for parameter tuning to achieve optimal results.

6. CONCLUSION

The growing applications of the PA technique in gas sensing, material characterization, and medical diagnostics highlight its significant potential as a versatile tool. In trace gases analysis, the PA technique provides highly sensitive and selective detection, enabling measurements of various trace gases with applications ranging from environmental monitoring to industrial safety. In solid-state analysis, PA offers valuable insights into mechanical properties, structural characteristics, and composition, supporting non-destructive testing with high precision. Moreover, PA has revolutionized medical diagnostics, facilitating early cancer detection and cardiovascular monitoring. However, some challenges in PA applications include the selection of a suitable experimental setup, calibration, high-power laser control, the complexity of PA signal generation, and solving the inverse problem. Since ML continues to develop as a robust, efficient, and precise tool, its role in optimizing PA technique is likely to expand. The main challenge in the future can be the practical implementation of ML software tailored by PA experimental setup.

Acknowledgement: *This research has been supported by the Ministry of Science, Technological Development and Innovation of the Republic of Serbia [Contract No. 451-03-65/2024-03/200148, Contract No. 451-03-66/2024-03/200017, and Contract No. 451-03-65/2024-03/200109].*

REFERENCES

1. Sigrist M.W. Bartlome R. Marinov D., et al. (2008). Trace gas monitoring with infrared laser-based detection schemes. *Applied Physics B*, 90, 289–300. DOI: 10.1007/s00340-007-2875-4. https://doi.org/10.1007/s00340-007-2875-4 .
2. Tam, A. C. (1986). Applications of photoacoustic sensing techniques. *Reviews of Modern Physics*, 58, pp. 381 - 431, DOI:10.1103/RevModPhys.58.381. https://doi.org/10.1103/RevModPhys.58.381
3. Biswas, D., Roy, S., Vasudevan, S., (2022). Biomedical Application of Photoacoustics: A Plethora of Opportunities. *Micromachines*, 13, p. 1900. DOI:10.3390/mi13111900. https://doi.org/10.3390/mi13111900
4. L. B. Kreuzer, (1971). Ultralow gas concentration infrared absorption spectroscopy, *Journal of Applied Physics*, 42, pp. 2934–2943. https://doi.org/10.1063/1.1660651
5. Miklós, A., Hess, P., Bozóki, Z., (2001). Application of acoustic resonators in photoacoustic trace gas analysis and metrology. *Review of Scientific Instruments*, 72, pp. 1937-1955, DOI:10.1063/1.1353198. https://doi.org/10.1063/1.1353198
6. Sampaolo, A., Patimisco, P., Giglio, M. et al. (2022). Quartz-enhanced photoacoustic spectroscopy for multi-gas detection: A review. *Analytica Chimica Acta*, 1202, p. 338894. DOI: 10.1016/j.aca.2021.338894. https://doi.org/10.1016/j.aca.2021.338894
7. De Palo, R., Elefante, A., Biagi, G. et al., (2023). Quartz-Enhanced Photoacoustic Sensors for Detection of Eight Air Pollutants. *Advanced Photonics Research*, 4, p. 2200353. DOI:10.1002/adpr.202200353. https://doi.org/10.1002/adpr.202200353
8. Lin, C., Yan, X., Huang. Y. (2022). An all-optical off-beam quartz-enhanced photoacoustic spectroscopy employing double-pass acoustic microresonators. *Optics Communications*, 503, p. 127447. DOI: 10.1016/j.optcom.2021.127447. https://doi.org/10.1016/j.optcom.2021.127447
9. Yin, X., Dong L., Wu, H. et al., (2017). Sub-ppb nitrogen dioxide detection with a large linear dynamic range by use of a differential photoacoustic cell and a 3.5W blue multimode diode laser. *Sensors and Actuators B*: *Chemical*, 247, pp. 329-335. DOI:10.1016/j.snb.2017.03.058. https://doi.org/10.1016/j.snb.2017.03.058
10. Olivieri, M.; Menduni, G.; Giglio, M. et al., (2023). Characterization of H2S QEPAS detection in methane-based gas leaks dispersed into environment, *Photoacoustics*, 29, p. 100438, DOI:10.1016/j.pacs.2022.100438. https://doi.org/10.1016/j.pacs.2022.100438
11. Sgobba, F., Sampaolo, A., Patimisco, P. et al. (2022). Compact and portable quartz-enhanced photoacoustic spectroscopy sensor for carbon monoxide environmental monitoring in urban areas, *Photoacoustics*, 25, p. 100318. DOI:10.1016/j.pacs.2021.100318. https://doi.org/10.1016/j.pacs.2021.100318
12. Zheng, H., Dong, L., Liu, X. et al., (2015). Near-IR telecommunication diode laser based double-pass QEPAS sensor for atmospheric CO2 detection. *Laser Physics*, 25, p.125601, DOI:10.1088/1054-660X/25/12/125601. https://dx.doi.org/10.1088/1054-660X/25/12/125601.
13. Pushkarsky, M., Webber, M., Baghdassarian, O., Narasimhan L.R., Patel. C.K.N. (2002). Laser-based photoacoustic ammonia sensors for industrial applications. *Applied Physics B*, 75, pp. 391–396. DOI:10.1007/s00340-002-0967-8. https://doi.org/10.1007/s00340-002-0967-8
14. Kinjalk, K., Paciolla, P., Sun B. et al., (2024). Highly selective and sensitive detection of volatile organic compounds using long wavelength InAs-based quantum cascade lasers through quartz-enhanced photoacoustic spectroscopy. *Applied Physics Reviews*, 11, p. 021427, DOI:10.1063/5.0189501. https://doi.org/10.1063/5.0189501
15. Wilcken, K., Kauppinen, J. (2003). Optimization of a microphone for photoacoustic spectroscopy. *Applied Spectroscopy* 57, pp. 1087–1092. DOI:10.1366/00037020360695946. https://doi.org/10.1366/00037020360695946
16. Abad, B., Borca-Tasciuc D.-A., Martin-Gonzalez M.S., (2017). Non-contact methods for thermal properties measurement, *Renewable and Sustainable Energy Reviews*, 76, pp. 1348-1370. DOI:10.1016/j.rser.2017.03.027. https://doi.org/10.1016/j.rser.2017.03.027
17. Rosencwaig, A., Gersho, A. (1976). Theory of the photoacoustic effect with solids, *Journal of Applied Physics*, 47, pp. 64-69. DOI: 10.1063/1.322296. https://doi.org/10.1063/1.322296
18. McDonald, F. A., Wetsel Jr, G. C., (1978). Generalized theory of the photoacoustic effect, *Journal of Applied Physics*, 49, pp. 2313-2322. DOI:10.1063/1.325116. https://doi.org/10.1063/1.325116
19. Nikolić, P.M., Todorović, D.M, (1989). Photoacoustic and electroacoustic properties of semiconductors. *Progress in Quantum Electronics*, 13, pp. 107-189, DOI:10.1016/0079-6727(89)90006-2. https://doi.org/10.1016/0079-6727(89)90006-2
20. Todorovic, D.M., Rabasovic, M.D., Markushev, D.D. et al. (2015). Photoacoustic Elastic Bending Method: Characterization of Thin Films on Silicon Membranes, *International Journal of Thermophysics*, 36, pp. 1016–1028. DOI:10.1007/s10765-014-1801-3. https://doi.org/10.1007/s10765-014-1801-3

21. Markushev, D. K., Markushev, D. D., Aleksić, S. M. et al. (2022). Enhancement of the thermoelastic component of the photoacoustic signal of silicon membranes coated with a thin TiO2 film, *Journal of Applied Physics*, 131, p. 085105. DOI:10.1063/5.0079902. https://doi.org/10.1063/5.0079902
22. Todorović, D. M., Rabasović, M. D., Markushev, D. D., Sarajlić M., (2014). Photoacoustic elastic bending in thin film–substrate system: Experimental determination of the thin film parameters, *Journal of Applied Physics* 116, p. 053506. DOI:10.1063/1.4890346. https://doi.org/10.1063/1.4890346
23. Galovic, S.P., Stanimirovic, Z., Stanimirovic, I., et al. (2024). Time-resolved photoacoustic response of thin solids measured using minimal volume cell, *International Communications in Heat and Mass Transfer*, 155, p. 107574. DOI:10.1016/j.icheatmasstransfer.2024.107574 https://doi.org/10.1016/j.icheatmasstransfer.2024.107574
24. Krishnaswamy, S. (2008). Photoacoustic Characterization of Materials. Springer Handbook of Experimental Solid Mechanics. Springer, 769-800. ISBN 978-0-387-26883-5 https://doi.org/10.1007/978-0-387-30877-7_27
25. Swapna, M.S., Sankararaman, S., Korte, D. (2024). Thermal lensing and photoacoustics as potential tools for nanomaterial characterization: a review. *Journal of Material Science* 59, pp. 10140–10168. DOI:10.1007/s10853-024-09773-4. https://doi.org/10.1007/s10853-024-09773-4
26. Rabasović, D.M., Nikolić, G.M., Dramićanin, D.M., et al. (2009). Low-cost, portable photoacoustic setup for solid samples, *Measurement Science and Technology* 20, 095902. DOI:10.1088/0957-0233/20/9/095902. https://dx.doi.org/10.1088/0957-0233/20/9/095902
27. Galovic, S., Kostoski, D. (2003). Photothermal wave propagation in media with thermal memory, *Journal of Applied Physics*, 93, pp. 3063–3071. https://doi.org/10.1063/1.1540741
28. Joseph, D.D., Preciozi, L. (1989). Heat wave, *Review of Modern Physics*, 61, 41. https://doi.org/10.1103/RevModPhys.61.41
29. Jou, D., Casas-Vazquez, J., and Lebon, G. (1988). Extendid Irreversible Thermodynamics, *Reports on Progress in Physics*, 51, pp. 1105-1179. DOI:10.1088/0034-4885/51/8/002. https://dx.doi.org/10.1088/0034-4885/51/8/002
30. Galovic, S., Soskic, Z., Popovic, M., et al. (2014). Theory of photoacoustic effect in media with thermal memory, *Journal of Applied Physics*, 116, p. 02491. DOI: 10.1063/1.4885458. https://doi.org/10.1063/1.4885458
31. Popovic, M.N., Markushev, D.D., Nesic, et al. (2021). Optically induced temperature variations in a two-layer volume absorber including thermal memory effects. Journal of Applied Physics, 129, p. 015104 https://doi.org/10.1063/5.0015898
32. Miletic, V. V., Popovic, M. N., Galovic, S. P., D. D. Markushev, et al. (2023). Photothermally induced temperature variations in a low-absorption sample via backside absorption. *Journal of Applied Physics*, 133, p. 075101. DOI: 10.1063/5.0134313. https://doi.org/10.1063/5.0134313
33. Djordjevic, K. Lj., Milicevic S.P., Galovic, E., et al. (2022). Photothermal Response of Polymeric Materials Including Complex Heat Capacity. *International Journal of Thermophysics*, 43, p. 68. https://doi.org/10.1007/s10765-022-02985-3
34. Korabel, N., Klages, R., Chechkin, A.V., et al., (2007). Fractal properties of anomalous diffusion in intermittent maps. *Physical Review E*, 75, p. 036213, https://doi.org/10.1103/PhysRevE.75.036213
35. Somer, A., Popovic, M.N., da Cruz, G.K. et al. (2022). Anomalous thermal diffusion in two-layer system: The temperature profile and photoacoustic signal for rear light incidence. *International journal of thermal sciences*, 179, p.107661. https://doi.org/10.1016/j.ijthermalsci.2022.107661
36. Somer, A., Galovic, S., Lenzi, E.K. et al., (2023) Temperature profile and thermal piston component of photoacoustic response calculated by the fractional dual-phase-lag heat conduction theory. *International Journal of Heat and Mass Transfer*, 203, p. 123801. https://doi.org/10.1016/j.ijheatmasstransfer.2022.123801
37. Ding, Z., Chen, K., Song, B. et al. (2022). Observation of second sound in graphite over 200 K. *Nature Communications* 13, p. 285. https://doi.org/10.1038/s41467-021-27907-z
38. Huberman, S., Duncan, R.A., Chen, K., et al. (2019). Observation of second sound in graphite at temperatures above 100 K. *Science*, 364,6438, pp. 375-379. https://doi.org/10.1126/science.aav3548
39. Neprokin, A., Broadway, C., Myllylä, T., et al. (2022). Photoacoustic Imaging in Biomedicine and Life Sciences. *Life*, 12, p. 588. https://doi.org/10.3390/life12040588
40. Liu, H., Teng, X., Yu, S., et al. (2024). Recent Advances in Photoacoustic Imaging: Current Status and Future Perspectives. *Micromachines*, 15(8), 1007. DOI:10.3390/mi15081007. https://doi.org/10.3390/mi15081007
41. Xu, M., Wang, V. L., (2006) Photoacoustic imaging in biomedicine. *Review of Scientific Instruments* 77, 041101. DOI:10.1063/1.2195024. https://doi.org/10.1063/1.2195024
42. Zhong, H., Duan, T., Lan, H., et al. (2018). Review of Low-Cost Photoacoustic Sensing and Imaging Based on Laser Diode and Light-Emitting Diode. *Sensors*, 18, p. 2264. https://doi.org/10.3390/s18072264
43. Bykov, A. Y., Xie, Y., Krasavin, A. V., Zayats, A.V., (2023). Nano Letters 23 (7), pp. 2786-2791. https://doi.org/10.1021/acs.nanolett.3c00063?urlappend=%3Fref%3DPDF&jav=VoR&rel=cite-as

44. Dumitras, D.C., Petrus, M., Bratu, A-M, et al., (2020). Applications of Near Infrared Photoacoustic Spectroscopy for Analysis of Human Respiration: A Review. *Molecules*. 25(7) 1728. DOI:10.3390/molecules25071728. https://doi.org/10.3390/molecules25071728
45. Henderson, B., Khodabakhsh, A., Metsälä, M. et al. (2018). Laser spectroscopy for breath analysis: towards clinical implementation. *Applied Physics B* 124, 161. DOI:10.1007/s00340-018-7030-x. https://doi.org/10.1007/s00340-018-7030-x
46. Djordjevic, K. Lj., Markushev, D. D., Ćojbašić, Ž. M., (2020). Inverse problem solving in semiconductor photoacoustics by neural networks. *Inverse Problems in Science and Engineering*, 29 (2), pp. 248–262. DOI:10.1080/17415977.2020.1787405. https://doi.org/10.1080/17415977.2020.1787405
47. Moeckli, M., Hilbes, C., Sigrist, M. (1998). Photoacoustic multicomponent gas analysis using a Levenberg–Marquardt fitting algorithm. *Applied Physics B*, 67, 449–458. DOI:10.1007/s003400050529. https://doi.org/10.1007/s003400050529
48. Rabasović, M. D., Nikolić, J. D., Markushev, D. D., (2007). Simultaneous determination of the spatial profile of the laser beam and vibrational-to-translational relaxation time by pulsed photoacoustics. *Applied Physics B*, 88, 309-315 (2007). DOI:10.1007/s00340-007-2697-4. https://doi.org/10.1007/s00340-007-2697-4
49. Lukić, M., Ćojbašić, Ž., Rabasović, M. D., et al., (2014) Computationally intelligent pulsed photoacoustics. *Measurement Science and Technology* 25, 125203. DOI:10.1088/0957-0233/25/12/125203.
50. Lukić, M., Ćojbašić, Ž., Markushev, D. (2023). Neuro fuzzy prediction of laser fluence based on photoacoustic signal analysis in different gas mixtures. *Measurement*, 210, p. 112533. DOI:10.1016/j.measurement.2023.112533.
51. Lukić, M., Ćojbašić, Ž. Markushev, D. (2021). Simulated Annealing Optimization for Inverse Problem Solving of Trace Gasses Detection by Infrared Pulsed Photoacoustic, *Proceedings of 15 International conference on applied electromagnetics*, ПЕС 2021, 121-124, Niš, Serbia ISBN:978-86-6125-241-9.
52. Lukić, M. Ćojbašić, Ž., Markushev, D. (2022). Trace gases analysis in pulsed photoacoustics based on swarm intelligence optimization. *Optical and Quantum Electronics* 54, p. 674. DOI:10.1007/s11082-022-04059-y. https://doi.org/10.1007/s11082-022-04059-y
53. Djordjevic, K.Lj., Markushev, D.D., Ćojbašić, Ž.M. et al. (2020). Photoacoustic Measurements of the Thermal and Elastic Properties of n-Type Silicon Using Neural Networks. *Silicon* 12, pp.1289–1300. DOI:10.1007/s12633-019-00213-6. https://doi.org/10.1007/s12633-019-00213-6
54. Djordjević, K.Lj., Galović, S.P., Popović, M.N. et al. (2022). Use neural network in photoacoustic measurement of thermoelastic properties of aluminum foil. *Measurement*, 199, 111537. DOI:10.1016/j.measurement.2022.111537. https://doi.org/10.1016/j.measurement.2022.111537
55. Djordjević, K.Lj., Stoisavljević, Z.Z., Dragaš, M.A.,et al., (2024). Application of neural network to study of frequency range effect to photoacoustic measurement of thermoelastic properties of thin aluminum samples. *Measurement*, 236, p. 115043. DOI:10.1016/j.measurement.2024.115043. https://doi.org/10.1016/j.measurement.2024.115043
56. Djordjević, K.L.; Markushev, D.K.; Popović, et al. (2023). Photoacoustic Characterization of TiO2 Thin-Films Deposited on Silicon Substrate Using Neural Networks. *Materials* 16, p. 2865. DOI:10.3390/ma16072865. https://doi.org/10.3390/ma16072865
57. Djordjevic, K.L., Galovic, S.P., Jordovic-Pavlovic, M.I. et al. (2020). Photoacoustic optical semiconductor characterization based on machine learning and reverse-back procedure. *Optical and Quantum Electronics* 52, 247. DOI:10.1007/s11082-020-02373-x. https://doi.org/10.1007/s11082-020-02373-x
58. Jordović-Pavlović, M.I., Stanković, M.M., Popović, M.N. et al. (2020) The application of artificial neural networks in solid-state photoacoustics for the recognition of microphone response effects in the frequency domain. *Journal of Computational Electronics*, 19, pp. 1268–1280. DOI:10.1007/s10825-020-01507-4. https://doi.org/10.1007/s10825-020-01507-4
59. Gröhl, J., Schellenberg,M., Dreher, K., et al., (2021) Deep learning for biomedical photoacoustic imaging: A review. *Photoacoustics*, 22, p. 100241. DOI:10.1016/j.pacs.2021.100241. https://doi.org/10.1016/j.pacs.2021.100241
60. Kim, M., Jeng, G., Pelivanov I. S., et al. (2020). Deep-Learning Image Reconstruction for Real-Time Photoacoustic System. *IEEE Transactions on Medical Imaging*. 39 (11) pp. 3379-3390. DOI: 10.1109/TMI.2020.2993835

FACTA UNIVERSITATIS
Series: **Working and Living Environmental Protection** Vol. 21, Nº 4, Special Issue, 2024, pp. 447 - 454
https://doi.org/10.22190/FUWLEP240924043B

Original scientific paper

ENSURING AN ACOUSTICALLY UNPOLLUTED LIVING ENVIRONMENT

UDC 534.321.9

Vasile Bacria, Nicolae Herisanu

University Politehnica Timisoara, Timisoara, Romania

ORCID iDs: Vasile Bacria N/A
Nicolae Herisanu https://orcid.org/0000-0003-2968-5309

Abstract. *Human beings are always concerned with living in an unpolluted environment. Noise pollution is one type of pollution that can arise. To address this issue, the acoustic properties of the environment are studied. This is done through periodic measurements, identifying the sources of pollution at the same time. The impact on the environment is then evaluated based on the collected data. Based on this, pollution reduction measures are established, and measures to reduce pollution are implemented accordingly. The methodology, measurement procedures, development of reduction strategies, and their effectiveness are thoroughly outlined.*

Key words: *environmental pollution, noise reduction*

1. INTRODUCTION

In the urban environment, human life and activity are constantly affected by noise and vibrations. These are mostly generated by means of transport participating in road, rail, and air traffic. This is a very actual and important research direction, and many researchers were recently concerned with investigating specific problems [1-5]. In this sense, we focused on the identification of the most important sources of noise from transportation means, specifying the harmful effects, the admissible limits, and the way of propagation. Starting from the results of the performed measurements and their analysis, some methods of achieving acoustic comfort were established, and following their implementation, the obtained effect was researched.

Received September 24, 2024 / Accepted November 7, 2024
Corresponding author: Nicolae Herisanu
University Politehnica Timisoara, Bd. Mihai Viteazu 1, 300222 Timisoara, Romania
E-mail: nicolae.herisanu@upt.ro

2. Noise Sources of Vehicles

The noise generated by means of transport in the urban environment is characterized by specific frequency spectra, acoustic pressure levels, and their variation over time. This can also be seen in Fig. 1, which shows the average spectra of the noise generated by different categories of means of transport: 1 - trucks with diesel engines; 2 - trucks with gasoline engines; 3 - trams; 4 - buses; 5 - cars; 6 - trolleybuses; 7 - motorcycles.

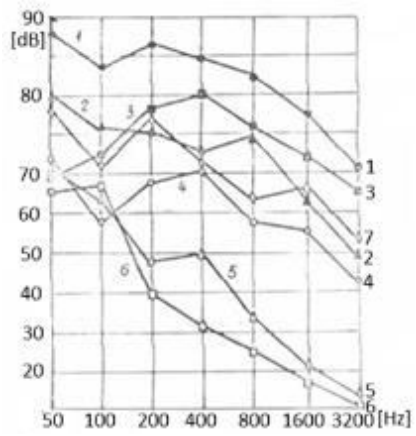

Fig. 1 Average spectra of noise generated by different transportation means [6]

In general, it can be said that the means of transport in road traffic have a low-frequency and partially medium-frequency character. Noise depends on the intensity and composition of the traffic, as well as the speed of travel, and is generated by three important sources: the engine, the transmission system, and the contact between the wheel and the track.

The means of railway transport generate noise and vibrations due to the variation of the movement speed, the play at the ends of the rails (joints), the unevenness, the curves, and the elasticity of the tracks, the conicity, the eccentricity, and the deviations from the proper shape of the tires, the guidance of the rolling wheel on the rail through the lip of the bandage, and the jerks during the maneuver during braking and acceleration.

The most important sources of noise and vibrations in air traffic are the explosion engine, the propeller, and, in the case of modern aircraft, jet engines, turboprops, or stators.

3. The Harmful Effects of Noise

Noise is extremely harmful to human life and activity. Thus, in the case of noise with the equivalent level of 70 dB, during the day, 60 % of the population is disturbed.

Noise affects the human nervous system, producing psycho-physiological changes, blood circulation, and sleep disorders, negatively influencing the visual function and endocrine glands, and producing biochemical disorders. Noise also causes hearing fatigue and sound trauma.

In order to reduce the effects of noise, limit values were provided, exceeding which is prohibited. The equivalent acoustic level and noise curves (Cz) are used as elements to

characterize these limits. The equivalent continuous acoustic level corresponds to an equivalent intensity over a time interval considered T and is defined by the relation

$$L_{ech} = 10 \lg \left[\frac{1}{T} \int_0^T 10^{0,1L(t)} dt \right] \quad (1)$$

where L(t) is the instantaneous sound level.

Noise curves (Cz) define the relationship between the characteristic frequency of a sound and the corresponding level of acoustic pressure under the conditions of an equivalent subjective sensation [7,8].

In this sense, according to SR 10009, "Urban Acoustics", admissible limits of the noise level in the urban environment were established, differentiated by zones and functional equipment by technical categories of streets, established on the basis of the specific technical regulations in force regarding environmental protection surrounding.

Table 1 Admissible limits for noise

Street type (STAS 10144/1-90)	Leq [dB]	Cz [dB]	L10 [dB]
type I – thoroughfare	75-85	70-80	85-95
type II – street of connection	70	65	75
type III – street of collection	65	60	75
type IV – street of local service	60	55	70

Admissible limits have been established for the noise level on the streets (Tab. 1). At the same time, the location of residential buildings on streets of different technical categories or the border of functional zones or facilities, as well as the organization of traffic, will be done in such a way as to ensure the value of 50 dB(A) of the noise level outside the building, measured at 2 m from the front of the building, respectively, the noise curve Cz45.

In the same way, to avoid the effects of the noise produced by the railway traffic in the urban environment, it was established that it should not exceed 70 dB at the limit of the railway zone, respectively the noise curve Cz65. Also, in order to limit the noise generated by air traffic, it is recommended that its level during the day between 7.00 and 19.00 should not exceed 90 dB, 85 dB in the evening between 19.00 and 23.00, and 80 dB during the night between 23.00 and 7.00.

The noise generated by means of transport affects both their drivers and passengers and people in the surrounding environment.

4. Study of the Acoustic Field

During the operation of the various sources, their vibrations propagate in the surrounding environment in the form of spherical waves and cylindrical waves, and at a great distance from the source, as plane waves. If the environment in which the waves propagate is considered to be perfectly elastic, homogeneous, and isotropic, choosing as a parameter the potential velocity Φ, the equation of the spherical wave, in the case of a harmonic disturbance, considering the movement only along the vector radius is

$$\phi = \frac{A_c}{r} e^{jk(ct-r)} \tag{2}$$

where A_c is the complex amplitude of the wave, having the frequency $f = \frac{\omega}{2\pi}$, c is its propagation speed, and $k = \frac{\omega}{c}$ is the wave number. If it is considered, $A_c = Ae^{j\alpha}$ then the pressure at a point of the acoustic field is determined by the relation

$$p = \rho_0 \omega \frac{A}{r} \sin(\omega t - kr + \alpha) \tag{3}$$

At the same time, if the vibrations of the sources produce cylindrical waves, considering that all points of the environment move in a direction perpendicular to the source, the equation of such a wave is:

$$\phi = \left[AJ_m(kr) + jBY_m(kr)\right] e^{-jm\varphi} e^{-j\omega t}, \tag{4}$$

where r and φ are the cylindrical coordinates of the volume element, and A and B are constants of integration, J_m is the Bessel function of the first kind and order m, and Y_m is the Bessel-Neumann function of the second kind and order m.

Considering that the waves are produced due to radial and uniform vibrations of the source, the expression of the acoustic pressure at a point of the medium can be written

$$p = A\left[J_0(kr) + jY_0(kr)\right] e^{-j\omega t}, \tag{5}$$

where J_0 and Y_0 are respectively the zero-order Bessel and Neumann functions.

Taking into account the approximation of the functions J_0 and Y_0 for small values of the variable r, expression (5) becomes

$$p = j\left(\frac{2A}{\pi}\right) \ln(kr) e^{-j\omega t} \tag{6}$$

and at a great distance from the source

$$p = A\sqrt{\frac{2}{\pi kr}} e^{j\left[k(r-ct)-\frac{\pi}{4}\right]} \tag{7}$$

The pressure variation at a point of the acoustic field is due to the propagation of both spherical and cylindrical waves and plane waves at a large distance from the source.

If the pressure at a certain time during wave propagation is p, then the sound pressure level is

$$L = 20 \lg \frac{p}{p_0}, \tag{8}$$

where $p_0 = 2 \cdot 10^{-5}$ [N/m2] is the reference sound pressure.

In the case of the propagation of acoustic waves in closed spaces, considering the case of real rooms, the delimiting surfaces are not perfectly reflective, but when they are hit by the acoustic waves, a certain energy dissipation occurs, and the waves that are formed in the closed space will be damped. The damping term $e^{-\delta t}$ can be introduced into the standing

wave equation by replacing the wave number k with a propagation constant, a complex quantity of the form $k + j\frac{\delta}{c}$, where δ is the wave-damping constant [9].

In the wave equation, the phase angles (φ_x, φ_y, φ_z) will also have to be introduced because they are different from zero, as a result of the fact that the bounding surfaces of the closed space are not rigid and perfectly reflective. In this way, the damped standing wave equation, choosing pressure as a parameter, is

$$p = Pch\left[(\delta_x - j\omega_x)\frac{x}{c} + \phi_x\right] ch\left[(\delta_y - j\omega_y)\frac{y}{c} + \phi_y\right] ch\left[(\delta_z - j\omega_z)\frac{z}{c} + \phi_z\right] e^{(j\omega-\delta)t} \quad (9)$$

The phase constants φ_x, φ_y, φ_z are determined by the boundary conditions x=0, y=0, z=0 that must be satisfied. Using this expression of the acoustic pressure, the acoustic pressure level at a point of the acoustic field can be determined using relation (8).

At the same time, it must be taken into account that in the case of noise propagation in closed spaces, the reflected ones are superimposed on the direct acoustic waves.

5. Performing of Measurements

Taking into account the multitude and diversity of the sources that generate noise in the urban environment as well as the nature of the acoustic waves produced by them, the acoustic field is very complex, and its investigation is indicated to be done experimentally.

In this sense, noise level measurements were made using the Bruel & Kjaer 2250 investigator. Noise level measurements were carried out in 119 measurement points that were established in the most important intersections of traffic arteries in Timisoara. For the measurements of the noise generated by the railway traffic, the microphone was positioned at the limit of the railway zone, and for that generated by the air traffic in the area of the Timisoara Airport.

The measuring devices used allowed the recording and automatic calculation of the main physical noise indicators: L_{eq} (equivalent noise level), SEL (Sound Exposure Level), L_{max} (maximum noise level), L_{min} (minimum noise level), L_5, L_{10}, L_{50}, L_{90}, and L_{95} (percentage noise levels). These parameters were determined over a continuous period of 8 hours (7.30 - 15.30), divided into time intervals of one hour.

Using these measured parameters, other physical indicators characterizing the effect of noise were calculated, such as:

- the Noise Climate

$$N.C. = L_{10} - L_{90} \quad (10)$$

- the Traffic Noise Index

$$T.N.I. = 4(L_{10} - L_{90}) + L_{90} - 30 \quad (11)$$

- the Level of Noise Pollution

$$L.N.P. = L_{eq} + L_{10} - L_{90} \quad (12)$$

For measurements, the microphone was mounted on the edge of the sidewalk at 7.5 m from the axis of the first traffic lane, at a height of 1.3 m from the ground. Simultaneously with the recording of the noise levels, the intensity and composition of the traffic and the speed of the means of transport were determined.

Measurements of the noise level inside different types of vehicles were also carried out. The noise level inside trams, buses, trolleybuses, and cars during a complete route was measured. For this, the microphone was mounted near the passenger's ear at 0.6 m from the vehicle wall.

6. Analysis of Measurement Results

The values of the measured noise levels, those of the intensity and the composition of the traffic, were centralized in a database for the study of noise pollution in Timisoara.

Following the obtained data, the equivalent noise level at 95 of the 119 measurement points (79.85 %) exceeds the maximum value allowed by the SR 10009 standard on "Urban acoustics." The exceedances recorded values between 0.1 and 15.5 dB.

The intensity of road traffic had values between 9 veh/h and 2681 veh/h, and the travel speed was 50 – 60 km/h. The highest percentage of vehicles present in traffic at the measurement points was that of passenger cars, between 34.2 % and 95.87 %.

The presence of traffic of many trams, trucks, trains, and tractors contributed to the increase in the noise level. The damaged condition and the nature of the roadway superstructure favor the increase of the noise level values produced by different types of vehicles depending on the speed.

In most measurement points, the peak noise level was generally exceeded by 1 – 9.5 dB. The noise level of 50 dB allowed at 2 m from the wall of buildings was generally exceeded by 1.3 – 32.9 dB.

The results of measurements carried out inside different types of vehicles are presented in Tab. 2.

Table 2 Noise levels [dB]

Type of vehicles	Leq	SEL	L_{max}	L_{min}	L_5	L_{10}	L_{50}	L_{90}	L_{95}
Trams	68.1-75.3	95.9-104.2	83.2-90.1	43.1-61.4	73.1-80.7	72.2-78.7	64.3-78.2	49.5-70.0	47.9-69.1
Buses	70.9-73.0	100.4-100.8	82.0-89.5	49.4-68.1	76.9-77.8	76.0-76.7	70.0-71.6	65.6-70.0	60.7-69.8
Trolleys	71.0-73.8	98.0-101.3	85.0-88.2	44.0-45.7	75.0-80.7	74.0-78.7	65.1-66.8	57.1-61.0	58.1-60.2
Cars	64.1-68.2	91.2-93.5	88.2-90.1	42.5-45.1	71.6-73.2	69.1-71.3	63.2-65.4	53.4-55.2	50.2-53.4

The noise level generated by trains measured at the border of the railway zone exceeded the allowed value by 2.2 – 12.7 dB.

The increase in the noise level is mainly due to the traffic of cars, trains, and planes, changing the direction of travel, passing over the running path of trams, accelerations, and braking. During the movement of vehicles on corridor streets, the increase in noise level is also produced by the overlap of the reflected waves over the direct ones. Also, the high degree of damage to some vehicles is an important factor that contributes to the increase in the level of traffic noise.

The noise inside the means of transport is also largely influenced by the operations of closing and opening the doors, driving maneuvers, the unevenness of the roadway, the conversation of passengers, etc.

7. Methods of Achieving Acoustic Comfort

Since in most of the points where measurements were made the permitted limits of the noise levels were exceeded, some noise reduction measures were required to achieve acoustic comfort. These measures would consist of organizing and systematizing traffic, improving or changing the superstructure of the roadway for vehicles, limiting travel speed, replacing some trams, improving the technical condition of vehicles and trains, applying a cushioning layer between the running line of the tram and sleepers, the construction of a bypass belt of the municipality of Timisoara, and the elimination of railway traffic from the city.

In order to reduce the noise generated by cars and trains, as well as by airplanes at Timişoara Airport, it is necessary to create acoustic screens and green areas near residential areas. An appropriate attenuation of the noise and the achievement of acoustic comfort inside the vehicles can be obtained by covering the ceiling and floor walls with sound-absorbing materials. At the same time, the drivers of the means of transport must drive them quietly.

Following these recommendations, the local public authorities of the municipality of Timisoara undertook an important program to reduce noise in the urban environment. In this sense, the old system of tram lines was completely replaced with a new one, quieter, with better insulation properties. The old Romanian trams have been replaced by a modern generation of trams. On many streets, the superstructure of the vehicle carriageway was improved or changed. Many intersections have been modernized, geometrically modified, and traffic lights introduced. On many streets one way was introduced, and speed was limited. The presence of large vehicles in the central area of the city was eliminated. On the other hand, in order to eliminate from the urban environment vehicles with a large mass in transit, the construction of the bypass belt of the municipality of Timişoara has begun.

To reduce the noise generated by railway traffic, new, quieter trains were introduced, many were also modernized between the tracks and residential areas, or acoustic screens and green areas were created.

The effects of these measures were evaluated through new measurements carried out in 46 measurement points that were established near the intersections where they were implemented.

From the obtained data, it follows that the equivalent noise level was reduced by 0.1 – 10.5 dB, and in 32 measurement points (69.56 %), the noise level does not exceed the maximum value allowed by SR 10009.

At the same time, in the 10 measurement points located at the border of the railway zone, the equivalent noise level was reduced by 0.1 – 9.3 dB, and in 6 of them (60 %) the noise level did not exceed the limit value allowed by the standard. The traffic intensity had values between 96 veh/h and 2822 veh/h, the travel speed was 50-60 km/h, and the highest percentage presence in the traffic was that of cars (66.65 % – 94.65 %).

8. CONCLUSIONS

The established noise reduction methods and their implementation have proven to be effective in contributing to the achievement of acoustic comfort in the urban environment. They can be applied in any situation regarding traffic or industrial noise.

REFERENCES

1. Bacria V., Herisanu N., Chilibaru-Opritescu C., Protecting residential areas against noise generated by car wash units. A case study, *Springer Proceedings in Physics,* 274, 127-138, doi:10.1007/978-3-030-96787-1_15, https://link.springer.com/chapter/10.1007/978-3-030-96787-1_15
2. Bacria V., Ghita E., Herisanu N., On acoustic comfort in urban transport on rails, *Springer Proceedings in Physics,* 274, 127-138, doi:10.1007/978-3-319-69823-6_10, https://link.springer.com/chapter /10.1007/978-3-319-69823-6_10
3. Praščević M., Mihajlov D., Gajicki A., Measurement and prediction of highway noise—Case study from Serbia, *Springer Proceedings in Physics,* 302, 89-97, doi:10.1007/978-3-031-48087-4_10, https://link.springer.com/chapter/10.1007/978-3-031-48087-4_10
4. Mihajlov D., Praščevič M., Ličanin M., Raos M., Reliability of Different Environmental Noise Monitoring Programs in Serbia, *Tehnicki Vjesnik,* 29, 114-120, doi:10.17559/TV-20210209123431, https://hrcak.srce.hr/en/269490
5. Mihajlov D., Praščevič M., Ličanin M., Raos M., Radičević B., A rational approach to determining environmental noise indicators, *Tehnicki Vjesnik,* 29, 553-560, doi:10.17559/TV-20210226134508, https://hrcak.srce.hr/en/272607
6. Iudin E.Ia. *Izolarea împotriva zgomotelor*, Editura Tehnică, Bucureşti 1968
7. Grumăzescu M., Stan A., Wegner W., Marinescu V., *Combaterea zgomotului şi vibraţiilor*, Ed. Tehnică, Bucureşti 1964.
8. Pupăzan C., *Acustica în construcţii. Propagarea zgomotului şi izolarea fonică*, Ed. Academiei Române, Bucureşti 1970
9. Enescu N., Magheţi I., Sârbu M.A., *Acustica tehnică*, Ed. ICPE, Bucureşti 1998

FACTA UNIVERSITATIS
Series: **Working and Living Environmental Protection** Vol. 21, Nº 4, Special Issue, 2024, pp. 455 - 463
https://doi.org/10.22190/FUWLEP240928044I

Original scientific paper

APPLICATION OF ULTRASOUND FOR DIFFERENT PURPOSES WITH EXAMPLES

UDC 534.321.9

Milica Ivić Nikolić[1], Snežana Jovanović[1], Branislav Đorđević[2], Aleksandar Sedmak[3]

[1]Technical Test Center, Military Scientific Research Institution of the Serbian Army, Belgrade, Serbia
[2]University of Belgrade, Innovation Centre of the Faculty of Mechanical Engineering, Belgrade, Serbia
[3]University of Belgrade, Faculty of Mechanical Engineering, Belgrade, Serbia

ORCID iDs: Milica Ivić Nikolić https://orcid.org/0009-0007-6217-4929
Snežana Jovanović https://orcid.org/0009-0004-6468-7726
Branislav Đorđević N/A
Aleksandar Sedmak https://orcid.org/0000-0002-5438-1895

Abstract. *In the last decade application of ultrasound has been increasing. The reason for this is that a wide range of frequencies can be utilized for various purposes. Different scientific fields describe ultrasound in their own way, and from an engineering point of view, the use of ultrasound is quite interesting. The purpose of this paper is to provide an overview of how ultrasound can be applied in diagnostics and welding, including practical examples. Also, during this research dependency between the measured echo of ultrasound wave and depth of founded irregularity is given.*

Key words: *ultrasound, ultrasound diagnostics, ultrasound welding, echo, depth, wires and welded joint*

1. INTRODUCTION

Ultrasonic represents vibrations of frequencies greater than the upper limit of audible range for humans, greater than 20 kHz. Ultrasound waves of very high amplitudes define the term sonic, which is applied to ultrasound [1]. Ultrasound is used in many different fields in order to detect objects and measure distances and more. The first article on the history of ultrasound was written in 1948 [2]. In ordinary daily communication, people are

Received September 28, 2024 / Accepted November 29, 2024
Corresponding author: Milica Ivić Nikolić
Technical Test Center, Military Scientific Research Institution of the Serbian Army, Vojvode Stepe 445, 11000 Belgrade, Serbia
E-mail: milicaivicnikolic@gmail.com

familiar with the fact that ultrasound is mostly used in medicine but this powerful method is used in a variety of different fields. Non-destructive testing (NDT) or Ultrasonic diagnostics (UD) represent a way to inspect and monitor the conditions of parts or equipment ensuring that cannot be damaging of components or materials. The application of ultrasound can be in many different fields such as: medicine, industrial processing, robotics, bioacoustics, etc. In the field of industrial processing can be used for cutting, welding, drilling, monitoring liquid flows, etc. In the field of welding, UD has a huge purpose as a method that can ensure the quality and integrity of weld joints. This means that this method allows the detection of defects and irregularities with welds mostly in order to prevent potential failures that could have serious consequences during exploitation. Inside defects of welded joints or defects somewhere near the weld zone must be inspected, and it's often used in practice for different types of industries. The main principles of UD are introduced, including air-coupled ultrasonic testing, electromagnetic ultrasonic testing, laser ultrasonic testing and so on in [3]. NDT can detect defects inside industrial materials, such as cracks, corrosion and voids by analyzing the characteristics of the signal, such as amplitude, time delay and frequency [4,5,6,7]. A group of authors in [8] present research about the propagation of ultrasonic waves in ultrasonically welded thermoplastics composite joints. One part of this paper will represent an ultrasonic diagnostic of welded joints. In the paper [9], a method for evaluating spot-welded joints using ultrasonic surface waves was proposed. The study employed ultrasonic transducers operating at a frequency of 10 MHz, along with a specialized testing setup, to analyze a range of spot-welded samples with different welding process parameters. The macrostructure from the defect indication site was evaluated and assigned using ultrasound indication [10], where the aim of the article was to check the internal defects in the butt welded joints. An ultrasonic detection method for weld defects based on neural network (NN) architecture is presented in [11], where including NN new scientific field is open.

The second part of this paper will be dedicated to showing the usage of ultrasound in the field of ultrasonic welding. Following the new standard in the solderless connection part of IEC 60352-9 [12] covers ultrasonically welded connections and includes requirements, tests and practical guidance information. This presents the modern way how to use ultrasound. A central focus in [13] was to investigate the weldability of Al-wires and flat flexible copper cables using ultrasonic welding. In the manufacturing industry, ultrasonic welding can be used on many different materials including plastics, rubbers, metals, textiles and components. It has become a very popular manufacturing process such as the automotive industry, electronics industry, medical device production and even the production of furniture. The authors of this paper want to explain how sound, as one of the basic physical units, can have huge practical usage in different industries and different methods of how to use sound, in this case, ultrasound. It's very important to mention that two big industries, the automotive industry and electronic industry, have deeply integrated the use of ultrasound in their manufacturing processes. Advances in technology, rapid technological development, low cost, and practical usage are some of the top targets in the future in mentioning industry. This means that ultrasonic welding will continue to be used, and we can expect many more innovations in this field, along with new standards set by leaders in the industry.

2. Overview of the Application of Ultrasound with Examples

2.1. Application of ultrasound in diagnostic

The basic principle of the ultrasonic method involves the transitions of ultrasonic pulses generated by a piezoelectric transducer through the material. When the waves encounter a region with an acoustic impedance value different than the host material, they are reflected and scattered [14]. Simply said UD is a technique that sends ultrasonic waves through an object or material. High-frequency of sound waves are transmitted into materials. The frequency range of 0.1 ÷ 15 MHz represents a range for short pulse waves, in some cases frequencies above 50 MHz also can be used. The basic methods of ultrasonic diagnostics can be carried out using the pulse-echo technique, although through transmission is also an available option. If ultrasonic diagnostic equipment (ultrasonic defectoscope for example) uses pulse-echo testing this means that the ultrasonic defectoscope produces short electrical impulses of pointed or square shape. These electrical impulses travel from the ultrasonic defectoscope, through the probe and finally to the transducer. Transducer are mostly piezo-electrical and convert electrical impulses to mechanical oscillations. The frequency of the transducer is above 20 kHz. Oscillation from the transducer, with the help of ultrasonic gel, travels through material like ultrasonic waves. Ultrasonic waves that travel through the object have a start value of acoustic (sound) pressure. During the propagation of ultrasound waves, through the material, sound pressure decreases with increasing traveled path of ultrasonic waves. After the emission of ultrasonic waves, the ultrasonic defectoscope starts to measure how much time is necessary for ultrasonic waves to come to some irregularities in the materials. Those irregularities can be named “reflectors” because they have acoustic features to reflect ultrasonic waves. Reflected ultrasonic waves represent echo. Reflected ultrasonic waves that return to the probe trigger the transducer's oscillations, which are then converted into low-voltage impulses. Those electric voltages travel through to defectoscope where can be filtered, processed and amplified. Signals on the screen of the ultrasonic defectoscope represent indications of reflections in material [15]. There are two types of ultrasound waves; it can be longitudinal waves or transverse waves. In the first part, authors will give practical examples of ultrasonic diagnostics (UD).

In this paper examinations that were performed were related to the ultrasonic testing of the welded joints of the supports of the harbor pontoon access bridge. For this testing, four pieces of the supports were inspected. This paper will present the results of one study to demonstrate the applicability of ultrasonic testing (UT) as a technique for inspecting welded joints. The material from which the supports are made is steel. Dimensions of the supports are 900 × 300 × 10 mm. The type of welded joint is angle T welded joint with K weld. Welding procedure was done with CO_2. Figure 1 shows one of the four inspected supports, labeled as number 4.

Fig. 1 Steel support No.4 of the harbor pontoon access bridge

The scope of this investigation was completed at 100 %, with a surface temperature of 26°C, which was also the ambient temperature. The used

device for the UD of material is USM 36 GE and the ultrasound probe is MWB 70 4 MHz, as shown in Fig. 2. Amplification was 48,3 dB, type of ultrasonic waves was transverse. Ultrasonic gel was used as a contact medium. Acceptance criteria are defined by the level of quality described in SRPS EN ISO 5817 "B" and the level of acceptability is defined in SRPS EN ISO 11666 "2".

Fig. 2 USM 36 GE Devices

The supports of the access bridge are located on the port side deck of the port pontoon; the supports are numbered 1 to 4 running from bow to stern. A drawing of support No.4 with found irregularities is shown in Fig. 3. In this case 5 irregularities were found on support No. 4.

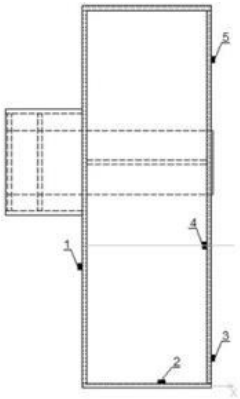

Fig. 3 Drawing of support No. 4 with irregularities

Repairs and re-testing were carried out in places where, during the first test pass, irregularities greater than those allowed by the standard defining the levels of acceptance of welded joints (SRPS EN ISO 11666) were measured. All tested welded joints are of the prescribed quality level. Table 1 gives the measuring results from support No. 4 with all detected irregularities. During this examination, the dependency between the echo of ultrasound waves and the depth of detected irregularity was found. Figure 4 shows that with the increase of depth, echo sound is decreasing. Inversely proportional dependency between the echo of ultrasound wave and depth of found defect exists. The overall conclusion from this practical example is that ultrasonic diagnostics were used to inspect the welded joints, and all of them exhibited a high level of quality.

Table 1 The measured results and important data of welded joint

Type of welded joint	Number of findings	Parameters of detected findings					Status OK	Status NOK
		Echo Height*)	Distance from "zero point"**)	Length	Depth	Position		
		dB	mm	mm	mm	***)		
T	1	4.5	X= 0 Y=280	1	4.6	MWJ	X	-
T	2	5	X= 180 Y=0	1	3	MWJ	X	-
T	3	0.8	X= 300 Y=65	6	8.7	RW	X	-
T	4	5	X= 300 Y=330	1	2	MWJ	X	-
T	5	0.4	X= 300 Y=378	10	9.3	RW	X	-

*) Above the reference level
**) „Zero point" and direction of detection
***) BM – Base Material, MWJ – Metal Welded Joint, HAZ – Heat Affected Zone, RW – Root of the weld, N – Welded layer

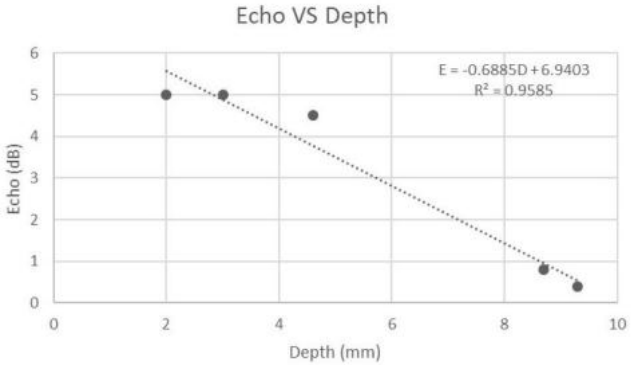

Fig. 4 Dependency between the echo of ultrasound waves and depth of detected irregularity in welded joint

2.2. Application of ultrasound in welding

Ultrasonic welding (USW) represents currently the fastest known welding technique. Speaking about ultrasonic metal welding (USMW) this technology receives widespread attention because of its advantages of environmental protection, high efficiency, etc. The core of the USMW is ultrasonic vibration. This process uses vibrations to the acoustic softening of materials during welding. High frequencies somewhere between 15 ÷ 70 kHz generate vibrations. These vibrations generate enough heat which melts the material and welds two parts together creating a strong bond. In the second part of this paper main goal is to show how ultrasound is used in wiring technology (for example, automobile industry). In general, the wires and cables industry rests on ultrasonic welding. The goal of this method is to connect the conductors between themselves or to connect them with the

contactors. Figure 5 shows an ultrasonic welded splice between two wires protected with a shrink tube as an example of ultrasonic welding. Here, A represents the length of the splice, B is the wire overhang at the splice's end, C is the distance between the insulation and the splice, and D is the overlapping length of the shrink tube and wire insulation. [12].

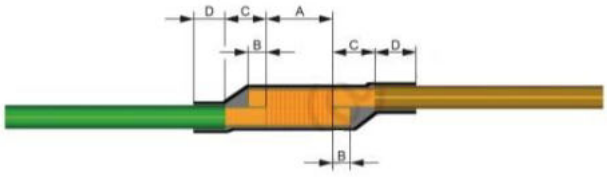

[12]

Fig. 5 Ultrasonic welded splice of two wires protected by a shrink tube

Figure 6 shows visual inspection of each ultrasonic splice weld (inline or end splice). These examples are done with error and splices in that condition cannot be accepted. In row (a) wires are too far outside, (b) wires are too far inside position, (c) single loose strands are detected and (d) insulation is in the weld splice. These examples of ultrasonic welding are unacceptable and those splices must be returned to rework. In Fig 7 a good example of correct ultrasonic welding is shown. Visually both splices are done perfectly [12].

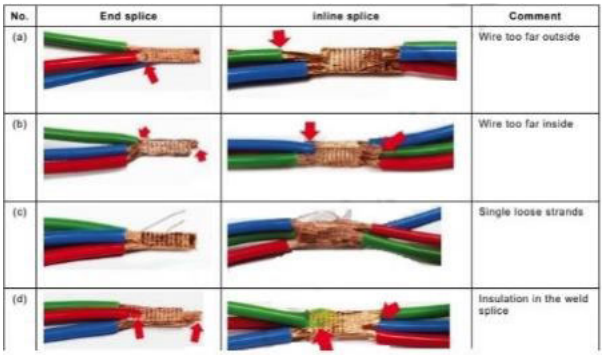

[12]

Fig. 6 Error characteristics for end splices and inline splices

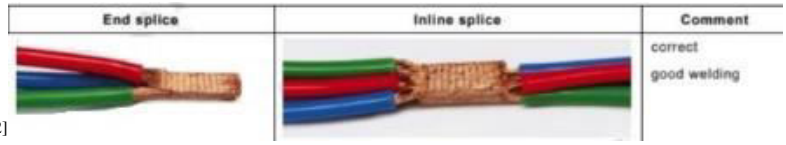

[12]

Fig. 7 Good welds for end splice and inline splice

It is familiar that ultrasound is above the human hearing range, greater than 20 kHz. When it comes to comparing the range between those two ultrasound applications, it can be said that the range of frequency for USW (or USMW) is below the range of UD. USW

(USMW) vibrations work on a lower frequency and it overlaps with the human hearing area. In the range of frequency for UD propagation of waves through the material space is on higher frequency. Figure 8 shows a diagram of the frequency range for USW, UD and hearing range.

Fig. 8 Diagram of the frequency range for USW, UD and hearing range

3. CONCLUSION

In this paper, the focus was to show two different ways to use the ultrasound field. One way shows how ultrasonic diagnostics is a necessary tool in measuring all irregularities, which is unavoidable in the welding process. Ultrasonic diagnostic is a non-destructive type of examination, becoming a more and more popular method in the field of engineering. UD advantages can be described through the following conclusion: Modern devices enable the visual display of results, signal recording, and real-time monitoring and UD devices are mostly portable. Handling this type of weld testing equipment is safe for the user. Also, the UD technique can detect surface and subsurface defects and provide instant results. UD can detect more than 50 % of irregularity, for some new equipment on the market, that number is over 85 %, in some cases even 90 %. The disadvantages of UD techniques are that information about materials and parts must be known in order to have reference to calibrate equipment set-up, difficult to use on thin materials and most important above all disadvantages is expensive training for UD which implicates the high price of the UD service. This example demonstrates the use of ultrasonic diagnostics (UD) and explains how the ultrasonic equipment operates. The most important conclusion from this paper is that with the increase of measured echo of ultrasonic waves, the depth of detected irregularity is decreasing. The used UD on the welded joint confirmed a good level of quality. The second example of the usage of ultrasound is ultrasonic welding. A new standard from IEC 60352 covers this topic where ultrasound can connect wires of copper or copper alloy, as well as aluminum or aluminum alloy. There are many reasons why ultrasonic welding may be preferable as compared to other welding and joining techniques. Some of these advantages of ultrasonic welding: Safety - USW (USMW) equipment is extremely safe compared to other welding techniques. The ultrasonic energy is highly targeted, reducing the risk of dangers due to excess electrical energy the heat produced is minimal, localized and quickly dissipated, minimizing the thermal impact on the material and human also; Speed - it is an fast process, the welding process takes a few seconds at most, high-frequency ultrasonic acoustic vibrations allows the material to heat, weld and cool very quickly; Joint quality - Ultrasonic welding equipment produces no deformation, resulting in a clean, nearly invisible seam that requires no touch-up work, ultrasonic

welding produces a very clean and precise joint; Reliability **-** The process can even be automated so that thousands of parts can be welded reliably with minimal human intervention; Flexibility - Ultrasonic welding can be applied to a variety of materials and parts; Reduced material costs - USW is very cost-effective in terms of material usage, because of the highly precise and high-quality joints, part scrapping is kept to a minimum. Ultrasonic welding is not an ideal welding technique and has some negativity such as: Joint type limitations- this type of welding can only be used on specifically designed joints, called lap joints, where parts directly overlap one another with a flat surface (Corner, butt, tee, and edge joints cannot be effectively welded using this technique); Material limitations - Materials with high moisture content require vibration welding, which is an entirely different technique; Size limitations **-** ultrasonic welding is highly useful for many thermoplastics and specific types of metals, it is not appropriate for all applications involving these materials (ultrasonic energy is not enough to produce large joints greater than 250 mm in length); High investment - ultrasonic welding equipment is significantly more expensive than traditional welding equipment, and the costs only increase with the introduction of automation [13]. In the Republic of Serbia, there are several manufacturing facilities of large companies from the automotive industry. All of these companies use ultrasonic welding (USW or USMW) in their production for renowned customers who have very strict standards. A lot of people are trained to work on ultrasound machines, and in the future accent must be on ultrasound welding. Future research will focus on developing new procedures, methods, and methodologies for applying ultrasound in this field. Automotive industries are moving fast into electromobility and ultrasound will be a topic of interest in many different fields.

REFERENCES

1. Berg, Richard E., (2024), *Ultrasonic,* Encyclopedia Britannica, 12 Jul.2024, https://www.britannica.com/science/ultrasonics.
2. Klein E., (1948), *Some background history of ultrasonic*, Journal of the Acoustical Society of America, Vol.20, Issue 5, pp. 601-604, doi 10.1121/1.1906413.
3. Fan, Z., Bai, K. & Chen, C., (2024), *Ultrasonic testing in the field of engineering joining*. Int J Adv Manuf Technol 132, pp. 4135-4160, doi.org/10/1007/s00170-024-13569-w.
4. Carvalho A.A, Rebello J.M.A, Souza M.P.V., Sagrilo L.V.S, Soarez S.D., (2008), *Reliability of Non-destructive Test Techniques in the Inspections of Pipelines Used in the Oil Industry*, Int. J. Press. Vessel. Pip. 2008, 85, pp. 745-751.
5. Stavridis J., Papacharalampopoulos A., Stavropoulos P., (2017), *Quality Assessment in Laser Welding: A Critical Review*, Int. J. Adv. Manuf. Technol., 2017, 94, pp. 1825-1847.
6. Tanaka T., Izawa Y., (2001), *Nondestructive Detection of Small Internal Defects in Carbon Steel by Laser Ultrasonic*, Jpn. J. Appl. Phys. 2001, 40, 1477 .
7. Zhang J., Wedge S., Rogerson A., Drinwater B., (2015), *Comparison of Ultrasonic Imag Features with Echodynamic Curves for Defect Classification and Categorization*, AIP Conf. Proc. 2015, 1650, pp. 970-977.
8. Ochôa P., Villegas F. I., Groves M.R., Benedictus R., (2019), *Diagnostic of manufacturing defects in ultrasonically welded thermoplastics composite joints using ultrasonic guided waves*, NDT & E International, Volume 107, 2019, pp. 102-126, ISSN 0963-8695, doi.org/10.1016/j.ndteint.2019.102126 .
9. Ulbrich, D., Psuj, G., Wypych, A., Bartkowski, D., Bartkowska, A., Stachowiak, A., Kowalczyk, J.,(2023), *Inspection of Spot Welded Joints with the Use of the Ultrasonic Surface Wave.,* Materials 2023, 16, 7029. https://doi.org/10.3390/ma16217029
10. Boháčik M., Mičian M., Koňár R., Hlavatý I., (2017), *Ultrasonic Testing of Butt Weld Joint by TOFD Technique*, Manufacturing Technology. 17. 842-847. 10.21062/ujep/x.2017/a/1213-2489/MT/17/6/842.
11. Rui Zhang, Mei-Rong Gao, Peng-Yun Zhang, Yong-Mei Zhang, Liu-Hu Fu, Yan-Feng Chai, Research on an ultrasonic detection method for weld defects based on neural network architecture search, Measurement,Volume 221, 2023, 113483, ISSN 02632241, https://doi.org/10.1016/j.measurement.2023.113483. (https://www.sciencedirect.com/science/article/pii/S0263224123010473)

12. International Standard, IEC 60352-9, (2024), *Solderless connections - Part 9: Ultrasonically welded connections – General requirements, test methods and practical guidance*, Edition 1.0, 2024, ISBN 978-8322-8261-8.
13. Heinz S., Wagner G. & Eifle D., (2012), *Ultrasonic Welding of Wires and Cables*, JOM 64, pp. 421-426 (2012), doi.org/10.1007/s11837-012-0266-8.
14. Adrian P. Mourtiez, (2012), *Nondestructive inspections and structural health monitoring of aerospace materials*", Introductions to Aerospace Materials, Woodhead Publishing, 2012, pp. 534-557, ISBN 9781855739468, doi.org/10.1533/9780857095152.534.
15. Opačić M., (2023), *Integrity assessment of welded joints with unacceptable defects*, Doctoral dissertation, University of Belgrade, Faculty of Mechanical Engineering, pp.27-32
16. https://gesrepair.com/ultrasonic-welding-advantages-disadvantages/

FACTA UNIVERSITATIS
Series: **Working and Living Environmental Protection** Vol. 21, Nº 4, Special Issue, 2024, pp. 465 - 476
https://doi.org/10.22190/FUWLEP241028045G

Original scientific paper

VIBRATION PHENOMENA INDUCED BY PULSED LASER HEATING OF MICROMECHANICAL CANTILEVER: INFLUENCE OF LASER-PULSE TEMPORAL SHAPE

UDC 534.23:772.96

Slobodanka Galović[1], Katarina Đorđević[1], Mladena Lukić[2], Dalibor Chevizovich[1]

[1]University of Belgrade, Vinča Institute of Nuclear Sciences, Belgrade, Serbia
[2]University of Nis, Faculty of Occupational Safety in Niš, Serbia

ORCID iDs: Slobodanka Galović https://orcid.org/0000-0002-6728-8868
Katarina Đorđević https://orcid.org/0000-0002-1397-8011
Mladena Lukić https://orcid.org/0000-0003-1105-3637
Dalibor Chevizovich https://orcid.org/0000-0001-7688-3792

Abstract. *Illumination-induced vibrational phenomena can significantly affect the mechanical behavior of micro-mechanical sensors (MEMS) and, consequently, the noise performance of detectors based on these sensors. In this paper, we study thermoelastic deflection induced by photothermal heating of a solid micro-mechanical cantilever illuminated by a short square laser pulse. An analytical-numerical technique based on the Laplace transform is employed to calculate the spectral function of lateral deflection. The results indicate that the profile of laser-induced vibrations depends on the temporal shape of the excitation optical pulse. The square pulse enhances the increasing trend of the high-frequency lateral vibration amplitude peak if cantilever thickness increases suggesting the possibility of size-dependent engineering of the properties of detectors utilizing micro-mechanical cantilevers.*

Key words: *photothermal effect, generalized thermoelasticity, cantilever, micro resonator, nano electro-mechanical systems*

1. INTRODUCTION

Laser-induced heating of a solid, also known as the photothermal (PT) effect [1–3], causes a temperature gradient within the illuminated sample, altering the temperature profile and, consequently, generating expansions and contractions in the optically excited sample [4–6]. This mechanism has attracted considerable attention due to the extensive application of lasers

Received October 28, 2024 / Accepted December 4, 2024
Corresponding author: Mladena Lukić
University of Niš, Faculty of Occupational Safety, Čarnojevića 10a, 18000 Niš, Serbia
E-mail: mladena.lukic@znrfak.ni.ac.rs

in material processing and the non-destructive detection and characterization of various materials and devices, including biomedical diagnostics [7–13]. Laser-induced vibrations of thin cantilevers have also gained significant attention because of their technological applications in Micro-Electro-Mechanical Systems (MEMS) and Nano-Electro-Mechanical Systems (NEMS) [14–17].

The analysis of thermoelastic displacements requires examining the coupled temperature and deformation fields [5]. In the case of ultra-short-pulsed laser heating, the high-intensity energy flux and ultra-short laser beam duration create situations where very large thermal gradients or ultra-high heating speeds may occur at the boundaries. In such cases, as noted by many investigators, the classical Fourier model, which implies an infinite propagation speed of thermal energy, is no longer valid [17–23]. The non-Fourier effect of heat conduction accounts for thermal relaxation time in the relationship between heat flux and the temperature gradient, thereby resolving this contradiction. For this reason, a generalized model of the thermoelastic problem, known as the Lord-Shulman model, was proposed. It introduces a hyperbolic theory of heat conduction that incorporates the non-Fourier effect [24]. This model has been applied in many studies of thermoelastic deformation induced by modulated laser beams or pulsed laser irradiation [25–27].

In the literature, one can find studies addressing optically generated vibrations of a thin cantilever of finite length illuminated by pulses with smooth rising and falling edges, such as Gaussian and non-Gaussian time profiles of short duration [16,27]. However, in many applications of semiconducting micro-mechanical devices, the time dependence of the excitation beam is better described by short square pulses or a series of such pulses [28–31]. Therefore, this paper derives a model of thermoelastic vibrations in a micro-mechanical cantilever, assuming that the time dependence of the optical excitation can be described by a short square pulse.

Based on the derived model, the spectral function of the lateral displacement profile for low and high harmonics is calculated and analyzed. The dependence of the high-frequency amplitude peak of midpoint deflection on the cantilever thickness is also investigated. Finally, the most important conclusions are presented.

2. MATHEMATICAL FORMULATION OF THE PROBLEM

We consider the micro-mechanical resonator (MMR) illustrated in Fig. 1, whose length is denoted as L, and whose cross-section is rectangular, with linear dimensions b and h that are much smaller than the sample length L.

The initial temperature distribution $T(x, y, z, t = 0)$ is assumed to be equal to the environmental temperature T_0. From the moment $t = 0$, the upper surface of the resonator ($z = h/2$) is uniformly irradiated by a short laser pulse.

$$S(t) = S_0 f(t) = S_0(h(t) - h(t - t_p)) \tag{1}$$

where t_p is the duration of a laser pulse and S_0 is the laser irradiance (total energy carried by a laser pulse per unit of cross section of the sample per unit of time).

Absorbed electromagnetic energy generates thermal source along the $z-$ axis (photothermal effect) $Q(z,t)$ [27]:

$$Q(z,t) = S_0 R_a e^{\frac{z-\frac{h}{2}}{\delta}} f(t) \tag{2}$$

where δ is the absorption depth of electromagnetic energy (inverse coefficient of optical absorption) and R_a is the coefficient of optical reflection of irradiated surface.

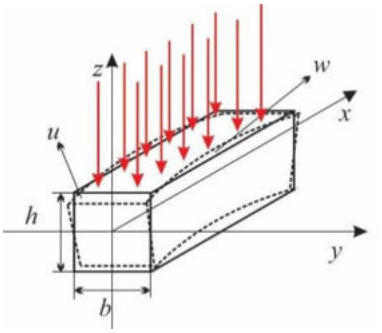

Fig.1 Geometry of the problem

Since the heat source depends on only one spatial coordinate ($z$coordinate), the photothermally induced heat transfer within the micro-mechanical resonator (MMR) can be described as a one-dimensional problem. In this case, the non-Fourier thermal conduction that includes the thermoelastic coupling term has the following form [24]:

$$\rho c_v \frac{\partial \vartheta}{\partial t} + \tau_0 \rho c_v \frac{\partial^2 \vartheta}{\partial t^2} + \beta \tau_0 \frac{\partial e}{\partial t} + \tau_0 \beta T_0 \frac{\partial^2 e}{\partial t^2} - k \frac{\partial^2 \vartheta}{\partial z^2} = Q + \tau_0 \frac{\partial Q}{\partial t}, \tag{3}$$

where $\vartheta(x,z,t) = T(x,z,t) - T_0$ is the temperature increment, $e = \frac{\partial u}{\partial x} + \frac{\partial v}{\partial y} + \frac{\partial w}{\partial z}$ is volumetric strain, coefficient β is defined by $\beta = E\alpha_T(1-2\nu)$ in which ν is Poisson's ratio, E is Young's modulus, and α_T is coefficient of linear expansion of the sample, c_v is the heat capacity, ρ is the mass density of the sample, k is heat conductivity, and τ_0 is the thermal relaxation time (this parameter has not yet been measured in any material at room temperature, and estimates of its value for semiconductors and dielectrics range from the order of magnitude of microseconds to the order of picoseconds [27,32,33], meaning that the influence of this parameter should be taken into account for laser pulses of picosecond duration.) In Eq. 3, we neglected the influence of photogenerated electrons and electron-phonon interactions on sample heating [34–37]. With u, v, w are denoted the displacements in the direction of x, y, and z-axis, respectively, Fig. 1.

By considering that there is no heat flow across the upper and lower surfaces of MMR, the following boundary conditions can be defined:

$$\frac{\partial \vartheta(x,z,t)}{\partial z}\Big|_{z=h/2} = 0 \tag{4}$$

the photothermally generated displacement of MMR is described by using the usual Euler-Bernoulli assumption [27]:

$$u = -z\frac{\partial w}{\partial x},\ v = 0\ ,\ w(x,y,z,t) = w(x,t)\,, \tag{5}$$

where w the lateral deflection (see Fig. 1).

The differential equation of thermally induced lateral deflection w of the sample can be written in the form:

$$EI\frac{\partial^4 w}{\partial x^4} + \rho bh\frac{\partial^2 w}{\partial t^2} + EI\alpha_T\frac{\partial^2 M_T}{\partial x^2} = 0\,, \tag{6}$$

where M_T is thermal moment, which is defined as:

$$M_T = \frac{12}{h^3}\int_{-h/2}^{h/2} z\vartheta(x,z,t)dz \tag{7}$$

and I is the moment of inertia for the structure illustrated in Fig. 1, $I = bh^3/12$.

For a very thin resonator, Eq. 7, can be reduced to [27]:

$$M_T = -\frac{1}{p^2}\int_{-h/2}^{h/2}\frac{12}{h^3}\frac{\partial^2\vartheta}{\partial z^2}zdz\,, \tag{8}$$

where $p = \pi / h$.

By using Eqs. 2, 3 and 6, 8, the generating equations for the coupled thermoelastic problem can be obtained as follows:

$$EI\frac{\partial^2 w}{\partial x^4} + \rho bh\frac{\partial^2 w}{\partial t^2} + EI\alpha_T\frac{\partial^2 M_T}{\partial x^2} = 0 \tag{9}$$

$$k\left(\frac{\partial^2 M_T}{\partial x^2} - p^2 M_T\right) - C_v\frac{\partial M_T}{\partial t} + T_\beta\frac{\partial^3 w}{\partial x^2\partial t} - \tau_0 C_v\frac{\partial^2 M_T}{\partial t^2} + \tau_0 T_\beta\frac{\partial^4 w}{\partial x^2\partial t^2} + \frac{6R_a S_0 a_\delta\Gamma(t)}{h^2} = 0 \tag{10}$$

where: $C_v = \rho c_v$, $T_\beta = T_0\beta$, $a_\delta = \dfrac{(1+2a)+(1-2a)e^{\frac{1}{a}}}{e^{\frac{1}{a}}}$, $a = \delta / h$, and

$$\Gamma(t) = f(t) + \tau_0\frac{\partial f(t)}{\partial t}\,. \tag{11}$$

The problem described by Eqs. 3, 8, and 9-11 with zero initial conditions is a standard problem, the solution of which, for different methods of strengthening a thin micro-cantilever (Fig. 1), describes the lateral deflection profile and its dependence on time. The temporal shape of the excitation pulse $f(t)$ affects the lateral deflection through the function $\Gamma(t)$ in Eq. 10. In the literature, a similar description of the problem can be found for optical

excitation in the form of an asymmetric Gaussian function [27]. The problem described in this section is more general because it includes any time dependence of the excitation pulse.

In this paper, the problem of lateral deflection is solved under the assumption that the sample is clamped on both sides:

$$\frac{\partial w(x,z,t)}{\partial x}\Big|_{x=0} = \frac{\partial w(x,z,t)}{\partial x}\Big|_{x=L} = 0\,, \quad w(x=0,z,t) = w(x=L,z,t) = 0\,, \tag{12}$$

and that the moment of temperature is equal to zero in the places where the sample is clamped:

$$M_T(x=0,t) = M_T(x=L,t) = 0\,. \tag{13}$$

We did the calculation by introducing dimensionless coordinates

$$\zeta = \frac{x}{L}\,,\ \tau = \frac{vt}{L}\,, \tag{14}$$

where $v = \sqrt{\frac{E}{\rho}}$ is the longitudinal speed of propagation of elastic deformation.

We also introduced two dimensionless variables: dimensionless deflection $W(\zeta,\tau)$ and dimensionless thermal moment, $\Theta(\zeta,\tau)$:

$$W(\zeta,\tau) = \frac{w(x,t)}{L}\,,\ \Theta(\zeta,\tau) = \alpha L M_T(x,t)\,. \tag{15}$$

Since the problem described by Eqs. 3, 8, 9, and 11 is linear in time, it can be solved by the application of Laplace transform on time dependence variables. This transform, as well as dimensionless coordinates and considered variables, reduce the problem to two ordinary differential equations in a complex domain:

$$\frac{d^4\bar{W}(\xi)}{d\xi^4} + \bar{A}_1\bar{W}(\xi) + \frac{d^2\bar{\Theta}(\xi)}{d\xi^2} = 0\,, \tag{16}$$

$$\frac{d^2\bar{\Theta}(\xi)}{d\xi^2} - \bar{A}_2\bar{\Theta}(\xi) + \bar{A}_3\frac{d^2\bar{W}(\xi)}{d\xi^2} = -A_4\bar{G}(s)\,, \tag{17}$$

with zero boundary conditions (see Eqs. 12 and 13). In the above equations, the bar above symbols is introduced to denote variables and coefficients dependent on the complex frequency s, and $G(s)$ denotes the Laplace transformation (spectral function) of the function $\Gamma(t)$, which depends on the temporal shape of the optical excitation (Eq. 11).

Coefficients $\bar{A}_1 - \bar{A}_3$ are complex quantities that depend on the dimensions and properties of the sample:

$$\bar{A}_1 = \frac{12L^2}{h^2}s^2\,,\ \bar{A}_2 = \frac{\tau_0 c_v E}{k}s^2 + \frac{c_v\rho v L}{k}s + p^2 L\,,$$

$$\bar{A}_3 = \frac{\tau_0\alpha_T T_0\beta E}{\rho k}s^2 + \frac{\alpha_T T_0\beta v L}{k}s\,, \tag{18}$$

while the coefficient A_4 is real and equal to:

$$A_4 = \frac{6R_a S_0 \alpha_T L^3 \tau_0 a_\delta}{kh^2}. \tag{19}$$

If the second derivative of the dimensionless moment from Eq. 16 is replaced in Eq. 17, the expression for the generalized moment is obtained:

$$\bar{\Theta}(\xi) = -\frac{1}{\bar{A}_2}\frac{d^4\bar{W}(\xi)}{d\xi^4} - \frac{\bar{A}_1}{\bar{A}_2}\bar{W}(\xi) + \frac{\bar{A}_3}{\bar{A}_2}\frac{d^2\bar{W}(\xi)}{d\xi^2} + \frac{A_4}{\bar{A}_2}\bar{G}(s), \tag{20}$$

which, by double differentiation and substitution in Eq.16, gives the differential equation that describes the lateral deflection along the dimensionless axis ξ (in the *x*-axis direction, Fig. 1):

$$\frac{d^6\bar{W}(\xi)}{d\xi^6} + \bar{a}\frac{d^4\bar{W}(\xi)}{d\xi^4} + \bar{b}\frac{d^2\bar{W}(\xi)}{d\xi^2} + \bar{c}\bar{W}(\xi) = 0 \tag{21}$$

where the coefficients in differential equation Eq. 21 are defined by the following expressions:

$$\bar{a} = -(\bar{A}_2 + \bar{A}_3)\ ,\ \bar{b} = \bar{A}_1\ ,\ \bar{c} = -\bar{A}_1\bar{A}_2. \tag{22}$$

From Eqs. 21 and 22, one could mistakenly conclude that the lateral deflection does not depend on the irradiance, the temporal shape, and the duration of the excitation optical pulse, because neither the coefficient A_4 nor the function $G(s)$ appears anywhere. However, the resulting differential equation indicates that only the form of the fundamental solutions will be the same for any irradiance and for any time-dependent form of excitation, including a simple periodic modulated optical beam. The total solution, which represents a linear combination of the fundamental solutions, depends on the coefficients by which the fundamental solutions are multiplied. These coefficients, through the boundary conditions, depend on the irradiance, the temporal shape of the optical excitation, and the length of its duration.

The solution of linear homogeneous differential equation of the sixth order Eq. 21 can be found in the literature [27,38] and the solution procedure will not be presented here. This solution is given by a linear combination of fundamental solutions:

$$\bar{W}(\xi) = \sum_{j=1}^{3}(C_j e^{-\lambda_j \xi} + C_{j+3}e^{\lambda_j \xi}) \tag{23}$$

where λ_j are roots of characteristic equation for differential equation Eq. 21:

$$\lambda_1^2 = -P\eta - Q\eta^2 - \frac{\bar{a}}{3}\ ,\quad \lambda_2^2 = -Q\eta - P\eta^2 - \frac{\bar{a}}{3}\ ,\quad \lambda_3^2 = -P - Q - \frac{\bar{a}}{3} \tag{24}$$

Parameters *A*, *P*, *Q*, and η are related with complex coefficients of Eq.21 as follows:

$$P = \left[\frac{1}{2}\left(\bar{q} + \sqrt{\bar{q}^2 + 4\bar{p}^3}\right)\right]^{1/3}\ ,\quad Q = \left[\frac{1}{2}\left(\bar{q} - \sqrt{\bar{q}^2 + 4\bar{p}^3}\right)\right]^{1/3},$$

$$\bar{p} = \frac{\bar{b} - \bar{a}^2/3}{3}\ ,\ \bar{q} = \bar{c} - \frac{\bar{a}\,\bar{b}}{3} + \frac{2}{27}\bar{a}^3\ ,\ \eta = (-1 + i\sqrt{3})/2. \tag{25}$$

By replacing Eq. 23 in 20, the solution for the dimensionless moment is also obtained:

$$\bar{\Theta}(\xi) = -\frac{1}{\bar{A}_2}\left[\sum_{j=1}^{3} \bar{K}_j(\bar{C}_j e^{-\lambda_j \xi} + \bar{C}_{j+3} e^{\lambda_j \xi}) - A_4 \bar{G}(s)\right] \tag{26}$$

Where constants K_j are defined by the following expression:

$$K_j = \lambda_j^4 - \bar{A}_3 \lambda_j^2 + \bar{A}_1 \tag{27}$$

As can be seen from the Eq. 26, the thermal moment depends on the irradiance, temporal shape, and duration of optical excitation directly, through the particular solution, but also indirectly, through the constants C_j.

The constants C_j can be determined by substituting Eqs. 23 and 26 into zero boundary conditions and solving the following matrix equation:

$$\begin{bmatrix} C_1 \\ C_2 \\ C_3 \\ C_4 \\ C_5 \\ C_6 \end{bmatrix} = \begin{bmatrix} 1 & 1 & 1 & 1 & 1 & 1 \\ e^{-\lambda_1} & e^{-\lambda_2} & e^{-\lambda_3} & e^{\lambda_1} & e^{\lambda_2} & e^{\lambda_3} \\ -\lambda_1 & -\lambda_2 & -\lambda_3 & \lambda_1 & \lambda_2 & \lambda_3 \\ -\lambda_1 e^{-\lambda_1} & -\lambda_2 e^{-\lambda_2} & -\lambda_3 e^{-\lambda_3} & \lambda_1 e^{\lambda_1} & \lambda_2 e^{\lambda_2} & \lambda_3 e^{\lambda_3} \\ K_1 & K_2 & K_3 & K_1 & K_2 & K_3 \\ K_1 e^{-\lambda_1} & K_2 e^{-\lambda_2} & K_3 e^{-\lambda_3} & K_1 e^{\lambda_1} & K_2 e^{\lambda_2} & K_3 e^{\lambda_3} \end{bmatrix}^{-1} \begin{bmatrix} 0 \\ 0 \\ 0 \\ 0 \\ A_4 \bar{G}(s) \\ A_4 \bar{G}(s) \end{bmatrix} \tag{28}$$

By numerical solving Eq. 28 and replacing the obtained constants in Eq. 23, we obtained the spectral functions of lateral displacement for short square optical pulse.

3. Results and Discussions

We analyze the thermoelastic displacement excited by a square laser pulse of short duration for MMR made of silicon. The material parameters are given in Tab. 1 [27]. We take, as it was done in [27], that the aspect ratios of MMR are fixed as $L/h = 10$ and $b/h = 0.5$. The time duration of laser pulse is $t_p = 2$ps and the intensity of laser pulse is $S_0 = 10^{11}$ W/m^2. Parameter R_a depends on the material of the resonator and wavelength of laser beam. We take that $R_a = 0.5$.

Table 1 Material parameters used in calculation

Properties	Denotations	Value
Young modul	E	169 GPa
Mass density	ρ	2330 kg/m^3
Heat capacity	c_v	713 J/kgK
Coefficient of linear expansion	α_T	2.59 x10^{-6} 1/K
Poisson's ratio	v	0.22
Thermal conduction	k	156 W/mK

The Laplace transform of time dependence of heat source in Eq. 1 generated by square pulse is given by [40]:

$$G(s) = L\{\Gamma(t)\} = \left(\frac{1}{s} + \tau_0\right)(1 - e^{-st_p}) \tag{28}$$

The calculated distribution of spectral function of dimensionless lateral deflection along the dimensionless axis normal to the direction of optical excitation (Eqs. 23, 27, 28) is illustrated in Fig. 2 for a few harmonics.

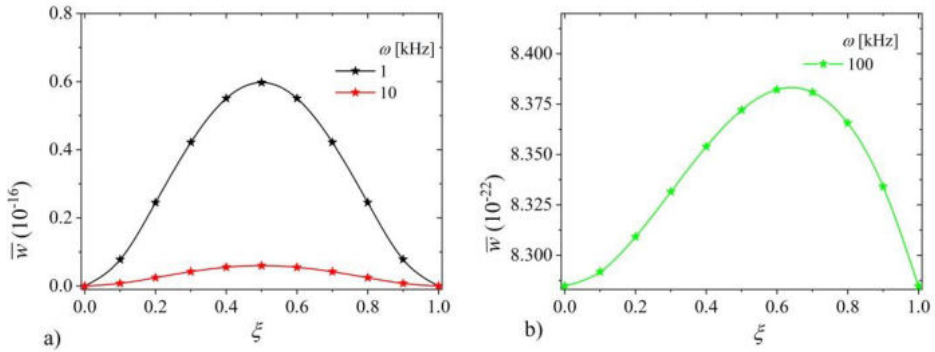

Fig. 2 a) The distribution of lateral deflection along the axis normal to the direction of optical excitation for following harmonics $f = 1$ kHz (black line), $f = 10$ kHz (red line), and b) $f = 100$ kHz (green line)

As can be seen from Figs. 2a and 2b, the maximum deflection (deflection peak) appears at the midpoint of the micro-cantilever for all harmonic excitation. This peak decreases when the frequency of harmonic increases. The form of lateral deflection depends on the frequency of harmonics: for lower harmonics, this form is symmetric in relation to the midpoint ($\xi = 0.5$, $x = L/2$) but for higher harmonic, this form becomes asymmetric due to the influence of spectral function of heat source induced by optical excitation, Eq. 28. It means that the temporal shape of optical excitation influences to distribution of lateral deflection.

High-frequency micro-cantilever vibrations are utilized in various types of oscillators and the development of different methods for non-destructive testing of materials [28,39]. Figure 3 shows the dependence of the midpoint amplitude of lateral vibrations (amplitude peak) on the frequency of the excitation harmonics.

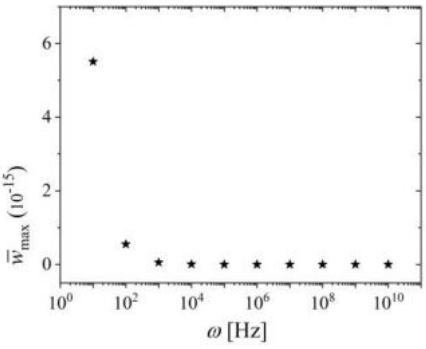

Fig. 3 The spectral function of midpoint lateral deflection

As shown in Fig. 3, the deflection peaks decrease rapidly with an increase in the frequency of the excitation harmonics, indicating that high-frequency vibrations generated by short optical excitation can be neglected.

Based on the derived model for the spectral function of the sample deflection (Eq. 23) the height of maximal deflection amplitude (peak of deflection) is calculated $f = 100$ kHz and its dependence on sample thickness h is shown in Fig. 4.

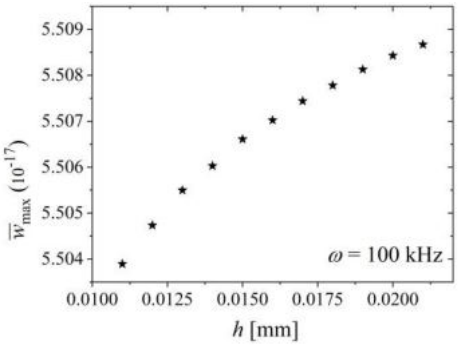

Fig. 4 The peak of deflection for samples of different thicknesses

Figure 4 shows a trend of increasing amplitude of the high-frequency peak of lateral deflection with increasing sample thickness, consistent with the model presented in [39] for a thin semiconducting disk excited by a high-frequency square pulse train, and contrary to the results presented in [27] for a micro-cantilever excited by a short non-Gaussian pulse. This indicates that the temporal shape of the excitation pulse affects this trend.

By applying the numerical inverse Laplace transform to the spectral function of dimensionless lateral displacement in Eq. 23, one can obtain the time-domain displacement for various temporal shapes of optical excitation. We attempted to solve the inverse Laplace transform for a square laser pulse of duration t_p (Eq. 1) numerically, using the MATLAB function INVLAP. However, this function did not yield good results for high-resolution changes in the dimensionless time coordinate because the sharp optical profile causes a steep wavefront of thermo-elastic deformation [41].

A detailed analysis of the impact of the square optical pulse on the time-dependent behavior of the temperature moment and lateral deflection requires the development of a numerical algorithm for solving the inverse Laplace transform for functions with sharp fronts [41], which is the subject of our further research.

4. Conclusions

In this paper, the model of photothermally induced vibration of lateral deflection is derived. The model is based on the Lord-Shulman theory of thermoelastic vibrations with the Euler-Bernoulli approximation. The derived model is more general than those in the literature because it includes any time-dependent optical excitation, enabling the study of the influence of the temporal shape of optical excitation on the vibrational characteristics of the deflection of micro-cantilevers.

Based on the derived model, the vibrational characteristics of the deflection of an Euler-Bernoulli micro-cantilever induced by a short square laser pulse are analyzed. The obtained results indicate that the spatial profile of laser-induced vibrations depends on the frequency spectrum of the excitation and, consequently, on the temporal shape of the laser pulse. The lateral vibrational peaks are scale-dependent, independent of the temporal shape of the laser pulse, but this shape influences the trend of either increase or decrease. For a square laser pulse, as the sample thickness increases, the peak deflection increases, indicating the possibility of size-dependent engineering of the high-frequency properties of various detectors that utilize micro-mechanical cantilevers.

Both the analysis of the frequency spectrum of the temperature moment based on the derived model and the time-domain analysis of lateral vibrations for various temporal shapes of the laser pulse are subjects of our ongoing investigations.

Acknowledgement: *The authors are grateful to the Ministry of Science, Technological Development and Innovations of the Republic of Serbia [Contract No. 451-03-66/2024-03/200017 and Contract No. 451-03-65/2024-03/200148].*

REFERENCES

1. Rosencwaig, A., Gerscho, A. Theory of the photoacoustic effect with solids. J. Appl. Phys., 47(1); 64–69, (1976). https://doi.org/10.1063/1.322296
2. Vargas, H., Miranda, L.C.M. Photoacoustic and related photothermal techniques. Phys. Rep., 161(2); 43–101, (1988). https://doi.org/10.1016/0370-1573(88)90100-7
3. Bialkowski, S. Photothermal Spectroscopy Methods for Chemical Analysis (New York: John Wiley 1996). ISBN: 978-0-471-57467-5
4. Rousset, G., Lepoutre, F., Bertrand, L. Influence of thermoelastic bending on photoacoustic experiments related to measurements of thermal diffusivity of metals. J. Appl. Phys, 54(5) 2383–2391, (1983). https://doi.org/10.1063/1.332352
5. Todorovic D.M., Nikolic P.M., Carrier transport contribution to thermoelastic and electronic deformation in semiconductors, Chapter 9 in Mandelis A. P. Hess, ed. Semiconductors and Electronic Materials, SPIE Opt.Eng .Press, Belingham,Washington, (2000). ISBN: 9780819435064
6. Todorović, D.M., Galović, S., Popović, M. Optically excited plasmaelastic waves in semiconductor plate-coupled plasma and elastic phenomena. J. Phys.: Conf. Ser 214, 012106, (2010). https://doi.org/10.1088/1742-6596/214/1/012106
7. Galović, S., Popović, M., Todorović, D.M. Photothermal dynamic elastic bending in a semiconductor circular plate induced by a focused laser beam. Journal of Physics: Conference Series, 214, 012113. (2010) https://doi.org/10.1088/1742-6596/214/1/012113
8. Wang, X., Xu, X., Thermoelastic wave induced by pulsed laser heating. Appl. Phys. A 73, 107–114, (2001). https://doi.org/10.1007/s003390000593
9. Wang, X., Xu, X.,Thermoelastic wave in metal induced by ultrafast laser pulses. J. Therm. Stresses 25, 457–473, (2002). https://doi.org/10.1080/01495730252890186
10. Todorović, D.M., Cretin, B., Vairac, P., Song, Y.Q., Rabasović, M.D., Markushev, D.D, Laser-Excited Electronic and Thermal Elastic Vibrations in a Semiconductor Rectangular Plate. Int J Thermophys., 34(8-9); 1712–1720, (2013) https://doi.org/10.1007/s10765-013-1461-8
11. Nesic, M.V., Popovic, M.N., Galovic, S.P., Djordjevic, K.Lj., Jordovic-Pavlovic, M.I., Miletic, V.V., Markushev, D.D., Estimation of linear expansion coefficient and thermal diffusivity by photoacoustic numerical self-consistent procedure. J. Appl. Phys. 131(10); 105104, (2022) https://doi.org/10.1063/5.0075979
12. Wang, X., Pang, Y., Ku, G., Xie, X., Stoica, G., Wang, L.V. Noninvasive laser-induced photoacoustic tomography for structural and functional in vivo imaging of the brain. Nat. Biotechnol., 21(7); 803–806, (2003) https://doi.org/10.1038/nbt839
13. Xu, M., Wang, L.V. Photoacoustic imaging in biomedicine. Rev. Sci. Instrum., 77(4); 041101, (2006) http://dx.doi.org/10.1063/1.2195024

14. Todorovi D.M., Cretin B., Song Y.Q., Vairac P. Photothermal elastic vibration method: Investigation of the micro-electro-mechanicalsystems, J. Phys.: Conf. Ser. 214 012105 15th International Conference on Photoacoustic and Photothermal Phenomena (ICPPP15) (2010). https://doi.org/10.1088/1742-6596/214/1/012105
15. Cyr B., Sumaria V., Long Y., Tadigadapa S., Sugawara T., Fu K., How Lasers Exploit Photoacoustic and PhotoelectricPhenomena to Inject Signals into MEMS Microphones, (2024). https://doi.org/10.21203/rs.3.rs-4197809/v1
16. Fang, D.N., Sun, Y.X., Soh, A.K., Advances in thermoelastic damping in micro- and nano- mechanical resonators: a review. J. Solid Mech. Mate. Eng. 1 (1), 18–34, (2007). https://doi.org/10.1299/jmmp.1.18
17. Joseph, D.D., Preziosi, L. Heat waves. Rev. Mod. Phys., 61(1); 41–73, (1989). https://doi.org/10.1103/RevModPhys.61.41
18. Tang, D.W., Araki, N., Wavy, wavelike, diffusive thermal responses of finite rigid slabs to high-speed heating of laser-pulses. Int. J. Heat Mass Trans. 42, 855–860, (1999). https://doi.org/10.1016/s0017-9310(98)00244-0
19. Tang, D.W., Araki, N., The wave characteristics of thermal conduction in metallic films irradiated by ultra-short laser pulses. J. Phys. D: Appl. Phys. 29, 2527–2533, (1996). https://doi.org/10.1088/0022-3727/29/10/001
20. Tzou, D.Y., Macro- to Micro-scale Heat Transfer: The Lagging Behavior. Taylor & Francis, Bristol, (1997). ISBN:9781118818220, https://doi.org/10.1002/9781118818275
21. Ozisik, M.N., Tzou, D.Y., On the wave theory in heat-conduction. J. Heat Transfer ASME 116, 526–535, (1994). https://doi.org/10.1115/1.2910903
22. Novikov, A., Harmonic thermal waves in materials with thermal memory. J. Appl. Phys., 81(3); 1067–1072, (1997). https://doi.org/10.1063/1.363849
23. S. Galovic, D. Kostoski. Photothermal wave propagation in media with thermal memory. J. App. Phys. 93(5); 3063-3070, (2003). https://doi.org/10.1063/1.1540741
24. Lord, H.W., Shulman, Y., A generalized dynamical theory of thermoelasticity. J. Mech. Phys. Solids 15, 299–309, (1067). https://doi.org/10.1016/0022-5096(67)90024-5
25. Sherief, H.H., Anwar, M.N., Problem in generalized thermoelasticity. J. Therm. Stresses 9, 165–181, (1986). https://doi.org/10.1080/01495738608961895
26. Sun, Y.X., Fang, D.N., Soh, A.K., Thermoelastic damping in micro-beam resonators. Int. J. Solids Struct. 43, 3213–3229, (2006). https://doi.org/10.1016/j.ijsolstr.2005.08.011
27. Sun, Y.; Fang, D.; Saka, M.; Soh, A.K. Laser-induced vibrations of micro-beams under different boundary conditions. Int. J. Solids Struct. 45, 1993–2013, (2008). https://doi.org/10.1016/j.ijsolstr.2007.11.006
28. Stanimirović, Z., Stanimirović, I., Galović, S., Djordjević, K., Suljovrujić, E. Transmission pulse photoacoustic response of thin semiconductor plate, J. Appl. Phys. 133,195701 (2023). https://doi.org/10.1063/5.0152714
29. Galovic, S.P., Stanimirovic, Z., Stanimirovic, I., Djordjevic, K.L., Milicevic, D., Suljovrujic, E. Time-resolved photoacoustic response of thin solids measured using minimal volume cell. Int. Commun. Heat Mass Transf. 155, 107574, (2024). https://doi.org/10.1016/j.icheatmasstransfer.2024.107574
30. Djordjevic, K.Lj., Galovic, S.P., Nesic, M.V., Todorovic, D.M., Popovic, M.N., Markushev, D.D., Markushev, D.K. Transmission pulse photoacoustic set-up for characterization of solids, in 21st International Symposium INFOTEH-JAHORINA, 16-18 (March 2022). https://infoteh.etf.ues.rs.ba/zbornik/2022/radovi/O-8-3.pdf
31. Galovic, S.P., Djordjevic, K.Lj, Nesic, M.V., Popovic, MN, Markushev, DD Markushev, DK, Todorovic, DM, Time-domain minimum-volume cell photoacoustic of thin semiconductor layer. I. Theory, J. Appl. Phys. 133,245701, (2023) https://doi.org/10.1063/5.0152519
32. Galovic, S., Soskic, Z., Popovic, M.,Cevizovic, D., Stojanovic, Z., Theory of photoacoustic effect in media with thermal memory, J. Appl. Phys. 116(2),024901,2014 https://doi.org/10.1063/1.4885458
33. Mitra, K., Kumar, S., Vedavarez, A., Moallemi. M.K., Experimental Evidence of Hyperbolic Heat Conduction in Processed Meat. J. Heat Transfer, 117(3); 568-573, (1995) https://doi.org/10.1115/1.2822615
34. Stanimirović, I., Markushev, D., Stanimirović, Z, Galović, S, Djordjević, K. Analysis of plasma-elastic component of time-domain photoacoustic response, J. Appl. Phys. 133, 235701, (2023). https://doi.org/10.1063/5.0152713
35. Lashkevych I., Titov O., Gurevich Y.G. Recombination and temperature distribution in semiconductors, IOP Publishing Ltd, Semicond. Sci. Technol. 27, 055014, (2012). https://doi.org/10.1088/0268-1242/27/5/055014
36. Mandelis A. Laser infrared photothermal radiometry of semiconductors: principles and applications to solid state electronics. Solid-State Electronics, 42(1), 1–15, (1998). https://doi.org/10.1016/s0038-1101(97)00238-4
37. Rojas-Trigos J.B., Calderón A., Marín E. A practical model for the determination of transport parameters in semiconductors. Journal of Materials Science, 46(24), 7799–7805 (2011), https://doi.org/10.1007/s10853-011-5760-9
38. Belajcic, D. Differential equation (in Serbian), Naucna knjiga, Belgrade, (1989)

39. Todorovi D.M., Nikolic P.M., Carrier transport contribution to thermoelastic and electronic deformation in semiconductors, Chapter 9 in Mandelis A. P. Hess, ed. Semiconductors and Electronic Materials, SPIE Opt.Eng .Press, Belingham,Washington, 2000. ISBN: 9780819435064
40. Stojic, M., Continuous System of Automatic Control (in Serbian), (Naucna knjiga, Belgrade, 1991.)
41. Stanimirovic, Z., Stanimirovic, I., Galovic, S., Djordjevic, K., Suljovrujic, E. Haar wavelet operational matrix based numerical inversion of Laplace transform for irrational and transcendental transfer functions. Facta universitatis - series: Electronics and Energetics. 2023, 3, Issue 3, 395-410. https://doi.org/10.2298/FUEE2303395S

FACTA UNIVERSITATIS Series: Working and Living Environmental Protection would like to acknowledge the expertise of the following reviewers, which has helped to set the standard of the journal in 2024

Aleksandar Cvjetić, Ph.D., Full Professor, University of Belgrade, Faculty of Mining and Geology in Belgrade, Serbia
Aleksandar Miltenović, Ph.D., Associate Professor, University of Niš, Faculty of Mechanical Engineering in Niš, Serbia
Atanas Ivanov Nachev, Ph.D., Full Professor, University of Library Studies and Information Technologies in Sofia, Bulgaria
Biljana Vranješ, Ph.D., Assistant Professor, Faculty of Mechanical Engineering, University of Banja Luka
Bojan Krstić, Ph.D., Full Professor, University of Niš, Serbia, Faculty of Economics,
Bojana Petković, Dr.-Ing, Postdoctoral Fellow, Technische Universität Ilmenau, Germany
Branko Radičević, Ph.D., Associate Professor, University of Kragujevac, Faculty of Mechanical and Civil Engineering in Kraljevo, Serbia
Darko Zigar, Ph.D., Assistant Professor, University of Niš, Faculty of Occupational Safety in Niš, Serbia
Darko Mihajlov, Ph.D., Associate Professor, University of Niš, Faculty of Occupational Safety in Niš, Serbia
Dejan Jovanović, Ph.D., Assistant Professor, University of Niš, Faculty of Electronic Engineering in Niš, Serbia
Dejan Milićević, Ph.D., Senior Research Associate, University of Belgrade, Institute of Nuclear Sciences "Vinča", Serbia
Dejan Vasović, Ph.D., Associate Professor, University of Niš, Faculty of Occupational Safety in Niš, Serbia
Dragan Cvetković, Ph.D., Full Professor in retirement, University of Niš, Faculty of Occupational Safety in Niš, Serbia
Dušan Ranđelović, Ph.D., Assistant Professor, University of Niš, Faculty of Civil Engineering and Architecture in Niš,Serbia
Dušica Pešić, Ph.D., Full Professor, University of Niš, Faculty of Occupational Safety in Niš, Serbia
Đorđe Damjanović, Ph.D., Assistant Professor, University of Kragujevac, Faculty of Technical Sciences Čačak, Serbia
Emir Ganić, Ph.D., Senior Research Associate, Ph. D., University of Belgrade, Faculty of Transport and Traffic Engineering in Belgrade, Serbia
Filip Pantelić, Ph.D, Senior Lecturer, Academy of Technical and Art Applied Studies, School of Electrical and Computer Engineering, Belgrade, Serbia
Ivanka Stanimirović, Ph.D., Senior Research Associate, University of Belgrade, Institute of Nuclear Sciences "Vinča", Serbia
Jelena Savić, Ph.D., Assistant Professor, University of Niš, Faculty of Civil Engineering and Architecture in Niš, Serbia
Jurica Ivošević, PhD, Assistant Professor, University of Zagreb, Faculty of Transport and Traffic Sciences, Croatia
Ljiljana Vasilevska, Ph.D., Full Professor, University of Niš, Faculty of Civil Engineering and Architecture in Niš, Serbia

CIP - Каталогизација у публикацији
Народна библиотека Србије, Београд

502/504

FACTA Universitatis. Series, Working and Living Environmental Protection / editor in chief Nenad Živković. - [Štampano izd.]. - Vol. 1, no. 1 (1996)- . - Niš : University of Niš, 1996- (Niš : Atlantis). - 24 cm

Dostupno i na:
http://casopisi.junis.ni.ac.rs/index.php/FUWorkLivEnvProt. - Tri puta godišnje. - Drugo izdanje na drugom medijumu: Facta Universitatis. Series: Working and Living Environmental Protection (Online) = ISSN 2406-0534
ISSN 0354-804X = Facta Universitatis. Series: Working and Living Environmental Protection
COBISS.SR-ID 72210956